Editor’s Round One Decision Letter

Subject: [Seismica] Editor Decision

Dear Daisuke Ishimura, Naoya O Takahashi, Hiroyuki Tsutsumi, Shin’ichi Homma, Sakae Mukoyama, Toshihiko Ichihara:

I hope this email finds you well. I have reached a decision regarding your submission to Seismica, "Paleoseismic trenching on slip-partitioned surface ruptures associated with the 2016 Kumamoto earthquake: Implications for simultaneous rupturing of the primary, subsidiary, and secondary active faults ". Thank you once again for submitting your work to Seismica.

I have now received two detailed and thorough reviews of your manuscript. Based on the comments in those reviews, it seems that your manuscript may be suitable for publication after some revisions. Although the reviewers raise a variety of issues of varying severity, I would describe the two most consistent and significant criticisms as follows: 1) The exact event chronology documented from the trench analysis is somewhat questionable, largely because the supporting evidence has not been clearly presented and/or linked with the primary interpretations. The second reviewer similarly remarks on a lack of consideration for possible alternative interpretations in the discussion when the results seem to make clear that such alternatives are at least permissible. and 2) Significant issues related to English language usage, clarity, and grammar. Both reviewers acknowledge and appreciate that language barriers are difficult and English is likely not the first language of the authors. They recommend, however, that a more detailed review of the manuscript's writing be conducted to address these issues before resubmission. The reviewers do seem to be in agreement that the data set (and the illustrations used to convey it) are of high quality, and that the science is meaningful and likely to make a contribution to the general field. I agree with the reviewers on all of these points, so I would like to further consider your manuscript for publication after you have had a chance to address the comments provided.

When you are ready to resubmit the revised version of your manuscript, please upload

- A 'cleaned' version of the revised manuscript, without any markup/changes highlighted.
- A pdf version of the revised manuscript clearly highlighting changes/markup/edits.
- A 'response-to-reviewers' letter that shows your response to each of the reviewers' points, together with a summary of the resulting changes made to the manuscript.

If you deem it appropriate, please check that the revised version of your manuscript recognises the work of the reviewers in the Acknowledgements section. I do intend to send the manuscript back to the reviewers for additional examination once a revised version is submitted.

Please note that Seismica does not have any strict deadlines for submitting revisions, but naturally, it is likely to be in your best interest to submit these fairly promptly, and please let me know of any expected delays.

I wish you the best with working on the revisions. Please don't hesitate to contact me with any questions or comments about your submission, or if you have any feedback about your experience with Seismica.

Kind regards,

Randy Williams

Reviewer 1 Round 1 Comments:

Please see review letter.

In general, I find this paper really interesting and important. It does need some revisions on organization, writing, and the event chronology. Suggestions to help with this are provided in the review letter.

Reviewer 2 Round 1 Comments:

In this study, Ishimura et al present 3D lidar differencing and trench logs focused on a section of the 2016 Kumamoto earthquake where surface rupture occurred on both the primary Futagawa and secondary Idenokuchi faults. In this region, slip was partioned between the faults such that the Futagawa fault accommodated mostly dextral displacement and the Idenokuchi fault recorded vertical (normal) and minor sinistral displacement. Using a new trench on the Idenokuchi fault and prior work on the Futagawa and other secondary faults, the authors suggest that the Idenokuchi and Futagawa faults are linked at depth, with overlapping paleoseismic histories and a history of simultaneous ruptures. The study helps to understand deformation that occurred in the 2016 Kumamoto earthquake, in addition to being one of the few studies with unequivocal evidence of slip

partitioning in a single earthquake. The data suggesting that there is a history of similar slip partitioning between the Idenokuchi and Futagawa faults will also be important for understanding slip partitioning in general.

Line comments are included in the attached PDF since the manuscript lacked continuous line numbers.

General comments:

The text needs significant review and editing for English language and grammar. I've noted many places in the line comments in the attached PDF.

There are some places with incomplete reasoning or statements that are made without references or evidence in this work to back them up, which I've noted in the line comments in the attached PDF. Some of these are likely due to the authors writing in a second language with minor editing to fix; others will require more thorough citations.

It is difficult to follow the evidence that supports the rich earthquake history described in section 6.2. A table or a section in the results describing the evidence used to interpret each earthquake would be useful.

Additionally, the authors present a single version of the earthquake history from the trench. However, their interpretations seem to support the option that earthquakes 5 and 6 were one earthquake. While this would not change the conclusions of the study, it would be good to acknowledge more of the uncertainty in the interpreted earthquake history in the text and perhaps offer another version(s) of earthquake history that are is supported by the data.

The interpretation of Trace 2 as a surface rupture trace does not seem supported by the horizontal differencing (vectors seem continuous across it in Figure 4). I cannot tell if there is vertical across it because it is difficult to see the vertical differencing results in Figure 4 (see comment in the attached PDF for Figure 4). The vertical difference across it shown in Figure 5, line A-A' is minimal, and could be interpreted as noise, so more evidence is likely necessary to include it as a surface rupture trace.

Review of Ishimura et al:

Paleoseismic trenching on slip-partitioned surface ruptures associated with the 2016 Kumamoto earthquake: Implications for simultaneous rupturing of the primary, subsidiary, and secondary active faults

Overall review summary

This paper provides data on the surface ruptures of the 2016 Kumamoto earthquake, the patterns of displacement and amounts of slip partitioning inferred from lidar differencing, and a record of past events inferred from a paleoseismic trench. The differencing data is used to show that the Futagawa and Idenokuchi faults are likely connected at depth and have ruptured together in the past. The trench data is nicely compared to other sites in the region and appears to be in agreement with the timing of the last several events. The information is important for local seismic hazard assessments as well as understanding the interaction of primary and secondary faults elsewhere. I commend the authors for beautiful and appropriate figures. I have one primary reservation on the interpretation of the number of events and the general lack of specific stratigraphic evidence to support the event chronology. I encourage the authors to reconsider the number of events reported and better describe the evidence for them. Once a revised event chronology is assessed, that information can be propagated through the second half of the paper. More information on this topic is described in the comments that follow. I have also provided a significant number of text suggestions for the author to consider on the attached annotated pdf. These are primarily aimed at making the text more concise and clear. I am happy to discuss my comments with the authors and be recognized for this review.

Sincerely,

Rich Koehler

More salient comments pertain to:

- Introduction: Could be made more concise and focus more clearly on the questions and main points.
- Regional Setting: The broader regional geologic setting of Kyushu could be better described in the context of Japan. Suggest a separate new paragraph on this topic to start the section. Addition of a subsection on previous paleoseismic studies would be helpful, briefly summarizing some of the earthquake chronologies. This would help set the stage for comparison of this study's results later in the paper.
- Misuse of the word conjugate in describing faults. None of the fault traces have geometric characteristics consistent with 'conjugate geometry'. They are more parallel branches, secondary faults, etc. suggest removing conjugate fault terminology throughout.
- Event evidence: This is currently presented in the discussion section. I suggest moving it the end of the Results section. Present the evidence for each event clearly. New subsection could be called 'Evidence for earthquakes'. Focus on the stratigraphic evidence (i.e. buried soils and fault terminations).

- Number of events: It is difficult to verify the number of events described inspecting the logs and the text. Seems like some of the events shown as individual earthquakes in the retrodeformation figure could be related to the same event. In normal faults one of the primary lines of evidence is the downdropping of paleosols on the hanging wall. From that line of reasoning I see 3 paleosols (units S20, S31, and S50). If the paleosols are buried after downdropping that suggests 3 events. Adding in the 2016 event gives 4 events. That is what is clear with the stratigraphy. The lower part of the exposure gets more complicated and it can be inferred that at least one more event occurred to create the accommodation space for the S50 deposits to accumulate. There is clear evidence for at least 5 events which is less than the eight events reported. The authors should reevaluate the number of events and more clearly describe the stratigraphic evidence for each event. See comments on line 465 for more details.
- Discussion: The comparison to other trench chronologies in the region is very good and the supporting figure is excellent. The slip partitioning section is good but could be made a bit more consice. I did not spend as much time editing the sentence structure in this section as earlier in the paper. I encourage the authors to spend a bit of time cleaning up the sentence structure to proper English. I understand this a challenge for non-english writers, however getting a little feedback prior to resubmission is encouraged.

Additional comments by section and line numbers.

Non-technical summary

This reads as almost a verbatum repeat of the abstract. Please simplify using more general terms. Perhaps a list of bullets.

Introduction

The introduction is currently a bit rambling and wordy. I have added suggestions to the annotated pdf in areas where I feel like the text could be shortened and made more concise. I suggest the authors re write some of the introduction and focus on the main points more clearly. Basically, the main points to introduce are, 1) InSAR allows the detection of small offsets off the primary fault on secondary faults during complex ruptures 2) understanding them and their synchroneity is important for displacement hazard assessment, 3) relationship of the Idenokuchi and Miyaji faults to the Futagawa fault, 4) and finally what was done in this study.

Supplementary materials.

The supplementary tables are all nice and necessary. The figures are also nice. Thanks for including the oxcal code. Please add a summary paragraph at the beginning of the Supplement to summarize what is contained in the materials. Some sort of Table of Contents would help readers. Also make sure to add the Supplementary tables to the pdf so that everything is in one Supplementary Materials document. Should there be a sample name for the second line of table S2?

General comments by line number

Line 0: Title. Seems like the title can be shortened a bit. See suggestion.

Line 41: Convention today is to spell 'lidar' with lower case letters. This comment should be applied throughout the manuscript.

Lines 86-95. This part of the introduction can be shortened and made more clear and concise. Suggest less emphasis on the terminology and more emphasis on recognizing the relationship of various faults and their synchroneity. Suggest something like this.

"Such complex ruptures have involved contemporaneous slip on primary faults and other related faults variably referred to in the literature as secondary, subsidiary, sympathetic, and distributed faults (e.g. Numinen et al., 2020; 2022). Understanding the history and distribution of complex ruptures is important for assessment of displacement hazards, however few studies have evaluated the relative synchroneity of past ruptures along primary faults and nearby associated faults".

Line 99-100. Add the magnitude to each of these events (prior to the year).

Lines 125-134. This can be made more concise. Just point out how good site conditions on the crater rim allowed for a robust earthquake chronology and helped motivate you to find additional sites to examine synchronous rupture with the Futagawa fault. See suggestion on the annotated pdf.

Line 137. Specify what type of data was used to generate the DTM's. Is this the lidar or some other type of remote data?

Line 140-150. This can be simplified and made more concise. See suggestion on annotated pdf. Report the synchronous rupture result and what the implications are.

Lines 153-168. Is this section necessary? Seems like it is not discussed later in the paper very much. I would delete it unless it can be simplified.

Line 170. Regional Setting: Adde a new paragraph at the beginning. this section should start with a paragraph describing the broader tectonics of southern Japan and the general location of Kyushu from a geologic perspective. Many readers will not be familiar with Japan tectonics, so a brief paragraph to bring readers up to speed is warranted. Then move on into the tectonics of Central Kyushu (currently first paragraph) as a second paragraph.

Line 183-185. Slight rewrite of this sentence is suggested.

Line 192. What is meant by the word conjugate? Seems like it may be misused in this case. Conjugate has a very specific meaning (two planes two planes are oriented for equal resolved shear stress (e.g. at 60° angle if friction is byerlee) and the maximum principal stress bisects the acute angle. If these conditions are not met then 'conjugate' should not be used. There are other terms that can be used to describe multiple ruptures along a fault including, high angle splays, branching splays, orthogonal faults, secondary or subsidiary faults. From inspection of fig 1 it looks like secondary or subsidiary faults is probably best.

Line 194-198. This sentence is rather long. Suggest simplifying. Something like "Toda et al (2016) inferred that the vertical slip on the Idenokuchi fault was related to slip partitioning with the oblique lateral slip on the Futagawa fault".

Line 199. Seems like a section describing previous paleoseismic work is needed here because this data is used later in the paper. This should not be a long section. Just a summary of previous trenching and general results from the previous work. Start with something like, "Extensive paleoseismic trenching has been conducted along the Futagawa fault". Then briefly describe some of the more important results from the previous work.

Line 200-209. This text seems out of place here. Not really related to regional setting. However this text is good. Suggest moving to the introduction perhaps after the description of previous trenching (line 135) prior to the paragraph on what was done in this study.

Line 213. Seems like there should be some statement on how the DTM's were generated in this paragraph prior to describing how they were used to do the differencing. I now see this in the second paragraph (line 233-239), so maybe just move this paragraph to before line 213.

Line 282. Some statement on how many tephra samples were analyzed and reference to the supplementary tables is needed.

Lines 350-386. Numerous text suggestions were added to the annotated pdf for the authors consideration. Tried to make it read more clearly.

Line 351. This paragraph should start with a more general statement on the stratigraphy exposed in the trench. That sets the stage for the more detailed description of the individual units that follows. Something like "In general, the trench exposed a package of silts, clays and paleosols separated from gravely clays and bedrock across a primary normal fault"

Line 387. A better introductory statement to this paragraph is needed. See addition on annotated pdf.

Line 419. Good place to introduce where the samples were from. See addition on annotated pdf.

Line 451 and 452. Please indicate the sample number and age in the text everywhere C14 ages are reported.

Line 465. Add a section on evidence for earthquakes. Much of this info is currently in the discussion between lines 517 and 571. From my inspection it looks like E0 is 2016. E1 postdates S20 and predates S10, and was associated with a fissure fill and warping of S20. Looking at the east wall all of the upward fault terminations occur near the top of unit S20 which also supports the occurrence of E1. E2 postdates S30 and predates S20. E3 postdates S50 and predates S40 or during deposition of S30 lower part.. At least one older event is required to downdrop the lower stratigraphy to allow the S50 marsh deposits to accumulate. I see at least 5 defensible events. I encourage the authors to better describe the additional events if they believe that they are real.

Figures

Figure 1. Nice figure. It would be helpful to number each previous paleoseismic site and add those numbers with their respective reference at the end of the caption. I now see that this is done for figure 10. Thus, maybe just mention in the caption that the paleoseismic sites and their respective references are shown on Figure 10.

Figure 2. Suggest using a more contrasting color for indistinct rupture traces. It is hard to tell where they are as the current color is similar to the red for surface rupture traces. A bit more information could be provided in the caption to describe the different lidar surveys (even though it is in the legend). For example: 'Lidar survey areas including post Kumamoto earthquake (black polygon) and pre-Kumamoto earthquake (blue polygon)'. Add a star or other symbol for the epicenters of the earthquakes (in addition to the tag line). Add this symbol to the legend and also mention in caption. Also a few latitude and longitude ticks would be helpful.

Figure 3. It would be nice to show where this is on another figure. Perhaps on figure 2. And/or add latitude and longitude ticks to figure 3a.

Figure 4. Add location of KMR trench to figure 4b, like in figure 4a.

Figure 5. Nice figure.

Figure 6. It would help the reader to label which wall is which on the logs. I.e. West wall, East wall, and North wall. Labeled clearly on the top of each log. Radio carbon dates are hard to read. Suggest giving them a larger font. Also indicate on the logs where the event horizons are for the various earthquakes. A label like E1 and an arrow that points to the event horizon.

Figure 10. Excellent figure. Needs a description of the map shown in the upper panel. Something like 'Map in upper panel shows previous paleoseismic trenching sites from which earthquake chronologies have been determined'. Lower panel needs some more detailed description of what is shown. What is K-Ah, ACP1, and N2S? What does the yellow, blue, and pink shading represent? Assuming that they represent the best correlation of events through all sites, but this needs to be clearly stated in caption. Also need to describe the red horizontal lines (age range of interpreted events?), and what is meant by the red arrows (event happened before a certain time?).

Paleoseismic trenching on slip-partitioned surface ruptures associated with the 2016 Kumamoto earthquake: Implications for ~~simultaneous rupturing of the primary, subsidiary, and secondary active faults~~

Daisuke Ishimura [1,*], Naoya O Takahashi [2], Hiroyuki Tsutsumi[3], Shin'ichi Homma[4], Sakae Mukoyama[4], and Toshihiko Ichihara[5]

[1] Department of Earth Sciences, Chiba University, 1-33 Yayoi-cho, Inage-ku, Chiba 263-8522, Japan
[2] Department of Earth Science, Tohoku University, 6-3 Aoba, Aoba-ku, Sendai 980-8578, Japan
[3] Department of Environmental Systems Science, Doshisha University, 1-3 Tataramiyakodani, Kyotanabe, Kyoto 610-0394, Japan
[4] Department of Research & Development of Kokusai Kogyo Co., Ltd., 2-24-1 Harumi-cho, Fuchu, Tokyo 183-0057, Japan
[5] Department of Disaster Prevention & Geology of Hopedesign Co., Ltd., 3-5 Shuri-Akatacho, Naha, Okinawa 903-0813, Japan
[*]Corresponding author: ishimura@chiba-u.jp

Author ORCIDs

Daisuke Ishimura: 0000-0002-4798-3425
Naoya Takahashi: 0000-0003-4196-1409

Author contributions

Conceptualization: D. Ishimura
Data Curation: N. Takahashi, S. Homma, S. Mukoyama
Formal Analysis: D. Ishimura, S. Homma, S. Mukoyama
Funding Acquisition: D. Ishimura
Investigation: D. Ishimura, N. Takahashi, H. Tsutsumi, T. Ichihara
Methodology: D. Ishimura, S. Homma, S. Mukoyama
Project Administration: D. Ishimura
Resources: D. Ishimura
Software: S. Homma, S. Mukoyama
Supervision: H. Tsutsumi
Validation: D. Ishimura
Visualization: D. Ishimura, N. Takahashi
Writing – original draft: D. Ishimura
Writing – review & editing: N. Takahashi, H. Tsutsumi, S. Homma, S. Mukoyama

Abstract

Surface ruptures appear over a wide area in addition to the primary fault during a Large earthquake like the 2016 Kumamoto earthquake. Although the displacement of such distributed surface ruptures is small, information on their paleo activities provides clues for evaluating displacement hazard risk and whether they can be used as a paleoseismic history of the primary fault. We conducted LiDAR differencing analysis and trench excavation on the Idenokuchi fault, which was activated simultaneously with the primary Futagawa fault, during the 2016 Kumamoto earthquake, and where a slip partition occurred. First, we clarified the 3D displacement field by LiDAR differencing and discussed quantitatively how the slip partition occurred on both faults. We found that deep oblique slip is completely split into horizontal and vertical components at the ground surface and inferred that the Idenokuchi fault is structurally connected to the Futagawa fault. Then, we excavated a trench on the ~~conjugate~~ surface rupture of the Idenokuchi fault and identified eight faulting events since 15 ka. Finally, we revealed a reliable activity history since 7.3 ka. Our results indicate that the Futagawa fault has ruptured relatively periodically and many surface ruptures have appeared in the last few events, like the 2016 event.

Second language abstract: 要旨 (日本語)

2016 年熊本地震のような大地震の際に主断層周辺に加えて幅広い範囲に断層が出現することがある．そのような断層の変位は小さいが，その過去の活動の情報は変位ハザードリスクや主断層の活動履歴の復元に有用かどうかの評価に関して手がかりを与えてくれる．そこで我々は LiDAR 差分解析とトレンチ掘削調査を 2016 年熊本地震の際に布田川断層と同時に活動しスリップパーティションが生じたとされた出ノ口断層で実施した．まず，LiDAR 差分により 3 次元変位場を求め，定量的に両断層でスリップパーティションが生じたかどうかを議論した．その結果，深部の斜めすべりが地表では完全に水平と鉛直成分に分割されたことが明らかとなり，出ノ口断層は構造的に布田川断層と地下でつながっていることが推定された．また，出ノ口断層の共役断層上でトレンチ掘削した結果，15 ka 以降に 8 回のイベントを推定し，最終的に 7.3 ka 以降の信頼たる活動時期を明らかにした．この結果は布田川断層が比較的周期的に活動したことと，最近数回のイベントでは 2016 年同様に多くの断層が地表に出現したことを示唆する．

Third language abstract: NA

Non-technical summary

We conducted a geomorphological differencing analysis using pre- and post-earthquake topography and trench excavation on the Idenokuchi fault, which was activated simultaneously with the primary Futagawa fault, during the 2016 Kumamoto earthquake, Japan. First, we clarified the 3D displacement field by geomorphological differencing and quantitatively discussed how displacement was partitioned on active faults. We found that deep oblique slip is completely split into horizontal and vertical components at the ground surface and inferred that the Idenokuchi fault is structurally connected downdip to the Futagawa fault. Second, we excavated a trench on the surface rupture of the Idenokuchi fault and identified eight faulting events since about 15,000 years ago. Our results indicate that the Futagawa fault has ruptured relatively periodically and many surface ruptures have appeared in the last few events.

1. Introduction

Recent developments in remote sensing technology (e.g., SAR and optical correlation) have enabled the distribution and amount of ground surface displacement associated with earthquakes to be captured with high resolution and precision. As a result, it has become clear that the distribution of surface ruptures ~~by earthquakes~~ is not simple but complex when viewed in detail, and in some cases, ~~they appeared~~ over ~~an~~ extensive area (e.g., 2016 Kumamoto earthquake, 2016 Kaikoura earthquake, and 2019 Ridgecrest earthquake). Various terms, such as primary, secondary, and subsidiary surface ruptures/faults, have been used to describe such complex surface ruptures in previous studies. Recently, Nurminen et al. (2020, 2022) categorized principal, distributed, and sympathetic faults for hazard assessment. However, it is difficult to adopt the classification, and there are many cases in which it is not unambiguously determined. In any case, a hierarchical relationship between primary and secondary surface ruptures/faults (in the broader sense of the term) has been recognized in surface ruptures and active faults. While surface ruptures and active faults in such a secondary relationship are also important for evaluation when considering displacement hazard, it has not been sufficiently verified whether such surface ruptures and faults have repeatedly occurred in the past due to the activity of the primary fault.

InSAR ~~analysis indicated~~ that surface ruptures ~~appeared over a wide area~~ around the main (primary) fault in the 2016 Kumamoto earthquake (Fujiwara et al., 2016) as well as the 2016 Kaikoura earthquake (e.g., Hamling et al., 2017) and 2019 Ridgecrest earthquake (e.g., Barnhart et al., 2019; Xu et al., 2020). In ~~Kumamoto's case~~, field surveys confirmed surface displacements and/or deformations at the InSAR

~~discontinuities~~ (Goto et al., 2017; Ishimura et al., 2017; Okamura et al., 2018; Sato et al., 2021). The Idenokuchi and Miyaji faults ~~especially represent such characteristics of surface ruptures.~~ The Idenokuchi fault ~~runs~~ parallel to the Futagawa fault. Along this parallel ~~running~~ section, right-lateral displacement occurred on the Futagawa fault and vertical displacement occurred on the Idenokuchi fault, which Toda et al. (2016) inferred that ~~the dextral and vertical components of the fault~~ slip ~~were~~ partitioned ~~into~~ the two faults. ~~Therefore~~, the Futagawa and Idenokuchi faults ~~are considered to~~ merge at the ~~deeper part; that is, the Idenokuchi fault is structurally related to the Futagawa fault.~~ On the other hand, the Miyaji faults (Fig. 1; Ishimura et al., 2021) have the same strike and displacement sense as the Futagawa fault but are not connected to the Futagawa fault according to the fault model inferred from the InSAR analysis (Fukushima and Ishimura, 2020), and are considered surface ruptures caused by triggered slip. This indicates that various ~~factors~~ may have contributed to the surface ruptures around the Futagawa fault during the 2016 Kumamoto earthquake.

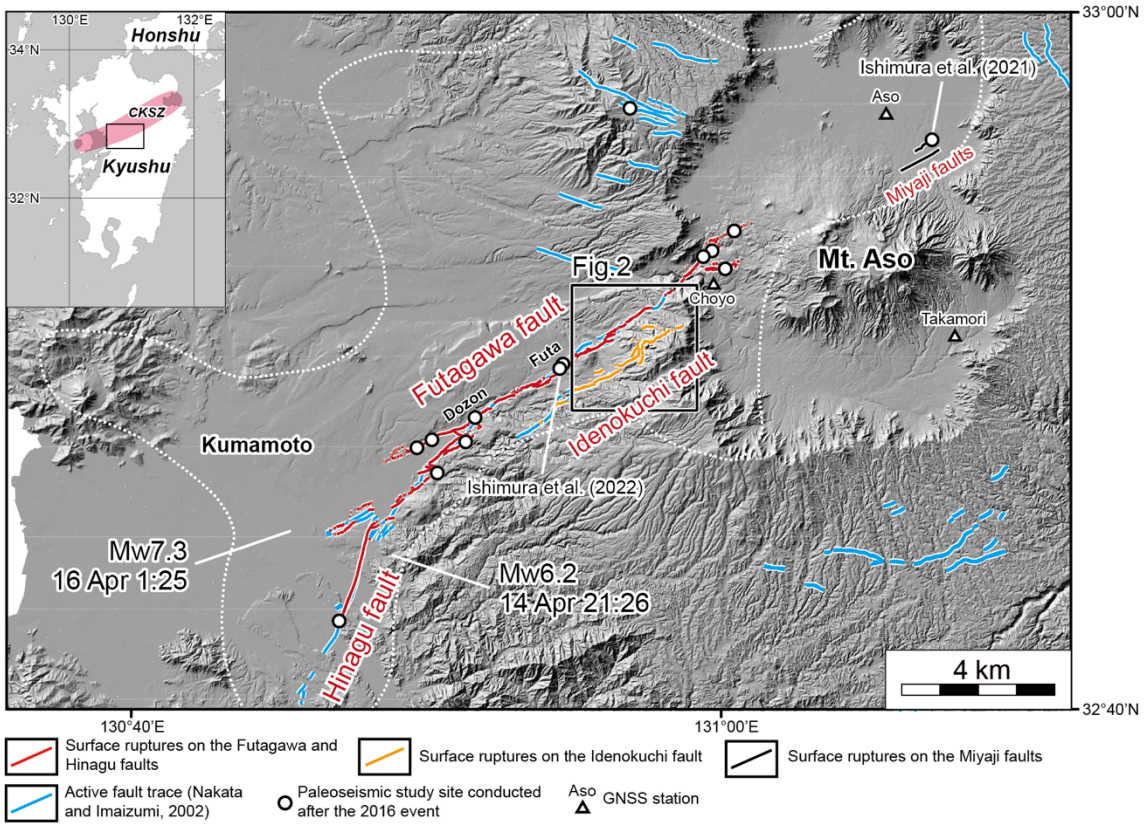

Figure 1. Spatial relationships among the primary Futagawa–Hinagu rupture zones and previously mapped active fault traces. Locations of the surface ruptures along the Futagawa, Hinagu, Idenokuchi, and Miyaji faults are from Kumahara et al. (2022). Previously mapped active fault traces are from Nakata and Imaizumi (2002). Red and orange lines indicate primary and subsidiary surface ruptures as defined in this study. The dotted line encloses the area where lineaments indicating secondary surface ruptures were identified by InSAR (Fujiwara et al., 2016). The Miyaji faults (Ishimura et al., 2021) are examples of the many secondary surface ruptures associated with the 2016 event. In this study, we defined the Kiyama, Futagawa, and Kitamukiyama faults, previously mapped by the Research Group for Active Faults of Japan (1991), as the Futagawa fault. CKSZ, Central Kyushu Shear Zone (Oohashi et al., 2020).

A paleoseismic survey conducted on the Miyaji faults revealed that the fault moved about 2,000 years ago, which coincides with the previous activity of the Futagawa fault (Ishimura et al., 2021). Their results suggest that the slip on the Miyaji faults was repeatedly triggered by the Futagawa fault in the past. In addition, trenching surveys on surface ruptures in the outer rim of the Aso caldera and on other short surface ruptures

also showed activity preceding the 2016 event (Inoue et al., 2020; Sato et al., 2021), suggesting ~~that these surface ruptures appeared not only during the 2016 event but appeared repeatedly. Because the smaller displacement of such surface ruptures compared to that of the primary surface ruptures does not displace sediments much, they are expected to record paleoseismic history more clearly and for a more extended period in trench walls and outcrops if the sedimentation rate is sufficiently fast. In fact, on the Miyaji faults, the fast sedimentation rate and multiple tephra layers of distinct age and lithology due to its location downwind of the Aso volcano have allowed us to reveal the amount and timing of past vertical displacement of about 15 cm with high accuracy (Ishimura et al., 2021). Therefore, paleoseismic investigations on such surface ruptures could provide long-term and more accurate paleoseismic history information than on the primary fault and enable us to examine their simultaneity with it.~~

In this study, we conducted a paleoseismic trenching of the Idenokuchi fault, which has a strong structural relationship with the primary Futagawa fault. Using digital terrain models (DTMs) before and after the earthquake, we calculated the three-dimensional displacement across the Futagawa and Idenokuchi faults ~~and examined whether slip partitioning occurred and, if so, what the distribution of displacement partitioning was like.~~ We then discussed the slip partition on the Idenokuchi fault, clarified the relationship between the Futagawa and Idenokuchi faults, and revealed the paleofaulting history of the Idenokuchi fault. Finally, we compared the paleofaulting history of the Idenokuchi fault with that of the Futagawa and Miyaji faults and discussed the simultaneity of these faults' activity. This study would provide important insights into the past activities of secondary faults visualized by recent technological improvements

(especially relative to the activities of the primary fault) and their value as new paleoseismic survey sites and displacement hazards on secondary faults. In addition, there are few examples of slip partitions occurring in a single earthquake on inland active faults (King et al., 2005), and this study can provide a valuable case study on such a relationship on the faults.

2. Definition of primary, subsidiary, and secondary surface ruptures/faults in the 2016 Kumamoto earthquake

In this study, we defined primary, subsidiary, and secondary surface ruptures/faults in the 2016 Kumamoto earthquake according to the criteria by Ishimura et al. (2022). A surface rupture or fault that is clearly a branch of the primary fault (e.g., a surface rupture that occurs locally around the primary surface rupture) or that has been pointed out to be a branch of the primary fault (e.g., Idenokuchi fault; Toda et al., 2016) is defined as a subsidiary surface rupture/fault (Fig. 1). A surface rupture or fault that is located away from the primary and subsidiary surface ruptures is defined as a secondary surface rupture/fault (e.g., Miyaji faults, black lines in Fig. 1; Ishimura et al., 2021). Although it is difficult to define the threshold of distance from the primary and subsidiary surface ruptures for a fault to be considered secondary, most of the surface ruptures detected by InSAR (distributed within the area enclosed by the white dotted line in Fig. 1) are likely to be defined as secondary surface ruptures (Fujiwara et al., 2016), except those on the Futagawa, Hinagu, and Idenokuchi faults. These secondary surface ruptures characterized the 2016 Kumamoto earthquake. Some of them have also been confirmed in the field (Goto et al., 2017; Ishimura et al., 2017; Okamura et al., 2018; Sato et al., 2021).

3. Regional Settings

Central Kyushu, where a north-south extension has been ongoing since 6 Ma (Kamata and Kodama, 1994), is structurally characterized by the Beppu-Shimabara graben (Matsumoto, 1979). This area is characterized by many east-west-striking normal faults (Research Group for Active Faults of Japan, 1991) and high levels of volcanic activity. According to Oohashi et al. (2020), central Kyushu has been a transtensional tectonic zone, which they call the Central Kyushu Shear Zone, since 1 Ma (Fig. 1), characterized by dextral faults, rift zones, and volcanism.

The Futagawa fault (Fig. 1) is a ca. 25-km-long active dextral strike-slip fault (Watanabe and Ono, 1969; Research Group for Active Faults of Japan, 1980, 1991; Nakata and Imaizumi, 2002; Kumahara et al., 2017a; Suzuki et al., 2017) and generated the mainshock (Mw 7.0) of the 2016 Kumamoto earthquake sequence on April 16, 2016. Primary surface ruptures appeared during the mainshock along the previously mapped active fault traces (Fig. 1; Kumahara et al., 2022). A large dextral displacement (~2 m) was observed from Dozon to Futa along the central part of the Futagawa fault, and a maximum dextral displacement of 2.5 m was observed at Dozon (Fig. 1; Shirahama et al., 2016; Okamura et al., 2018; Kumahara et al., 2022). The slip rate of the Futagawa fault for the area around Futa is 1.5–3.7 mm/yr for the right lateral slip and 0.9–1.1 mm/yr for the vertical slip (Ishimura, 2019).

The Idenokuchi fault is a 10-km-long active dip-slip fault mainly up on the south (Research Group for Active Faults of Japan, 1980, 1991; Nakata and Imaizumi, 2002),

and ~~moved~~ during the mainshock of the 2016 Kumamoto earthquake (Fig. 1; Kumahara et al., 2022). Multiple surface ruptures, including conjugate faults, appeared along the fault. The maximum vertical displacement was 2 m (south up), and the average vertical displacement was about 1 m (Kaneda et al., 2022). Toda et al. (2016) assumed that the slip-partition was caused by the oblique slip on the deep part of the Futagawa fault between the parallel running section of the Futagawa and Idenokuchi faults because horizontal displacement occurred on the Futagawa fault and the vertical displacement occurred on the Idenokuchi fault. The slip rate of the Idenokuchi fault has not been determined.

The three-dimensional deformation caused by the 2016 event has been revealed by InSAR and differential light detection and ranging (~~LiDAR~~) analyses (Moya et al., 2017; Scott et al., 2018; He et al., 2019; Himematsu and Furuya, 2020; Aoyagi et al., 2021; Muroi et al., 2024). In particular, ~~LiDAR~~ differencing provides higher resolution and more accurate displacement information in areas with larger displacements than InSAR analysis. Although ~~it has been conducted by~~ Scott et al. (2018), Aoyagi et al. (2021), and Muroi et al. (2024) ~~along the portion and extension of the Futagawa fault, it has not been obtained in the area where the slip partition occurred, which is the focus of this study, and how the amount of displacement due to the slip partition is distributed has not been obtained until now in the world.~~

4. Methods and Data

4.1 LiDAR differencing

We applied 3D-Geomorphic Image Velocimetry method (Kokusai Kogyo Co., Ltd., 2010) for LiDAR differencing. In this method, the particle image velocimetry method and pre- and post-event DTMs (Fig. 2) were used to calculate the surface displacement vectors according to Mukoyama (2011) and Ishimura et al. (2019). Aoyagi et al. (2021) and Muroi et al. (2024) used this method for the eastern extension of the Futagawa fault inside the Aso caldera. The method procedure is as follows. First, we prepared slope-shaded images using pre- and post-event DTMs. Next, we carried out a grid search by moving a pre-event image in a pixel-by-pixel manner in the scanning area on the post-event image and estimated the position that exhibits the highest value of the coefficient of correlation using subpixel interpolation. Additionally, we calculated the horizontal component of displacement ~~and estimated the vertical component~~ using the elevation values from DTMs with interpolation calculation around the head and tail of each horizontal vector. Subsequently, we slid the search area in steps and repeated the image matching and calculation of the 3D displacement. Finally, we plotted the complete 3D vectors on maps. In this study, the search area size, search area step size, and output grid size were set to be 64 x 64 pixels (128 x 128 m), 5 m, and 5 x 5 m, respectively. Additionally, the theoretical error of this analysis is 0.1 pixel (0.2 m) due to subpixel interpolation in the displacement calculation.

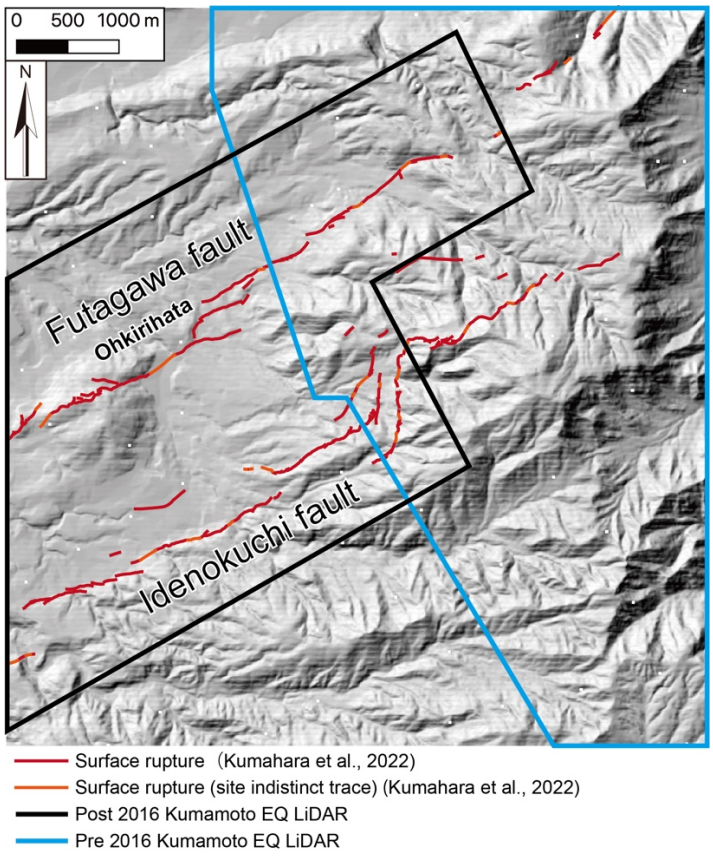

Figure 2. LiDAR measurement areas.

The DTMs we used were 2-m grid DTM taken from January 2013 to February 2014 and 2-m grid DTM taken on 8 May 2016. Although we do not possess the original point cloud data of pre- and post-earthquake datasets, nor have the details for constructing the DTMs from the original point cloud data, all the DTMs were tested and examined under the regulations required for a public LiDAR survey in Japan. We used the Japan plane rectangular coordinate system II (in meters) for the horizontal data and as the coordinate system for all data.

The expected ground motions during the measurement period are as follows: (1) the deformation associated with the 2016 Kumamoto earthquake, (2) the postseismic deformation (e.g., aftershocks and afterslip), (3) the background tectonic deformation, and (4) the artificial modification and present-day surface processes. We evaluate the deformation of items 2 and 3 using the GNSS observations in the study area. Based on the GNSS stations at the Choyo (960701), Aso (960703), and Takamori (960704) of GeoNET, the postseismic and background deformations (vertical, north-south, and east-west components) from April 2010 to May 2016 are nearly equal of the theoretical error level (0.2 m). Thus, the deformations associated with items 2 and 3 are negligible.

4.2 Trench survey

We looked for an appropriate site for a paleoseismic excavation ~~survey~~ along the Idenokuchi fault (Fig. 2). We selected possible ~~survey~~ sites based on the following criteria: 1) little artificial modification, 2) clear surface rupture traces, and 3) stable and continuous soil deposition. As a result, we selected a trench excavation site on a gentle slope ~~between conjugate surface ruptures~~ of the Idenokuchi fault, expecting trapped sediment and stable and continuous soil deposition (Fig. 3). The trench site is on a clear single surface rupture (north-up normal fault), and another surface rupture (south-up normal fault) runs parallel at its southeast side. Currently, the fields are cow ranches with ~~few~~ artificial modification~~s~~.

We excavated a 13-m-long, 5-m-wide, and 3.5-m-deep trench (Fig. 3; KMR trench) and established a grid system on the trench walls. We logged the walls and collected samples for tephra analyses and radiocarbon dating. To further examine the subsurface geology, we used a handy corer 50 cm long and 4 cm wide to obtain seven cores from the trench floor and upthrown side (Fig. S1). The Nikon Nivo5.SC total station was used to map the locations of surface ruptures, trench, and coring sites (Fig. 3b).

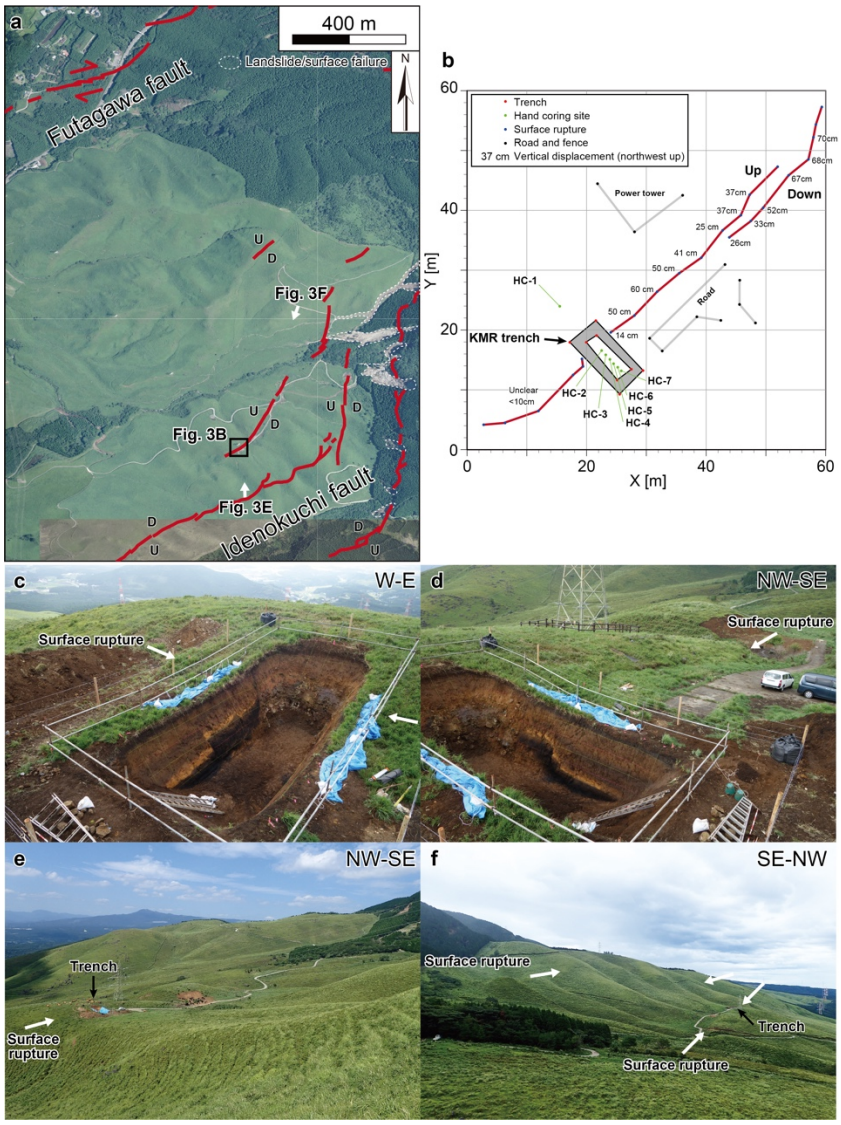

Figure 3. Geomorphic map and photographs around the trench site. (a) Red lines show the 2016 surface ruptures (Kumahara et al., 2022). Aerial photographs ~~are~~ from the Geospatial Information Authority of Japan. (b) Location map of the trench and surface ruptures. (c) West wall of the trench. (d) East wall of the trench. (e) (f) ~~Geomorphology~~ around the Idenokuchi fault. Photo locations are shown in Fig. 3a.

4.3 Laboratory analysis

We determined refractive indices and major element compositions of volcanic glass shards in sampled tephras. First, we sieved the samples with water through a 62-μm nylon mesh. Then, we oven-dried the samples at 50 °C and sieved the dried samples through a 120-μm nylon mesh. The refractive index of volcanic glass shards in the 62–120 μm fraction of each sample was measured with a RIMS 2000 refractive index measuring system (Kyoto Fission Track Co., Ltd.) with an accuracy of ±0.0002 (Danhara et al., 1992). The major element composition of volcanic glass shards was measured by energy-dispersive X-ray spectrometry (EDAX Genesis APEX2 and JEOL JSM-6390) following the method and analysis conditions described by Suzuki et al. (2014). Volcanic glass shards of the AT tephra sampled at Chigaki, Toyama Prefecture (Machida and Arai, 2003) were used as a working standard to check data reproducibility and instrument stability.

A total of 26 radiocarbon samples of charcoal and organic sediment were dated by accelerator mass spectrometry at the Laboratory of Radiocarbon Dating, the University Museum, the University of Tokyo, and the Institute of Accelerator Analysis Ltd., Japan. The obtained age data were calibrated using the OxCal 4.4 software (Bronk Ramsey, 2009) with the IntCal20 dataset (Reimer et al., 2020). The ages of paleofaulting events were calculated in the OxCal program by Bayesian analysis (Bronk Ramsey, 2008).

5. Results

5.1 3D displacement

Figure 4 shows the distribution of 3D displacement, and Figure 5 shows ~~the cross-sections of the A-D lines.~~ In the cross-sections (Fig. 5), the horizontal component is divided into two components: one parallel to the general strike of the Futagawa fault (N57°E) and the other perpendicular to it. The vertical component (Figs. 4B and 5) shows a displacement of 1.0–2.5 m at the southernmost part of the Idenokuchi fault and a vertical displacement of several tens of centimeters at the northern part of the fault. Compared to field measurements (Kaneda et al., 2022), a similar displacement was measured along the southernmost branch of the Idenokuchi fault, where a 2 m vertical displacement was observed. However, the amount of vertical displacement along the fault is noisy and subject to uncertainty because of slope failures in the surrounding area. Along the ~~conjugate fault~~ of the Idenokuchi fault, where we excavated the KMR trench, there is no significant difference between the calculated and field-measured displacements ~~in the field.~~ On the other hand, on the Futagawa fault, the amount of local vertical displacement associated with the dextral displacement is observed in a narrow section about 200 m wide. ~~Still, almost no vertical displacement is observed~~ when viewed over 200–400 m wide from the fault, virtually no vertical displacement is observed. The vertical displacement along the long baseline (> 3 km) ~~between~~ both the Futagawa and Idenokuchi faults is south-up of about 1 m (Lines A and B in Fig. 5).

Regarding the fault-parallel component (Figs. 4B and 5), a large displacement was observed on the Futagawa fault, and 1.8–3.1 m of dextral displacement occurred on the

western part of the calculated area. Since the displacement measured in the field was about 1.5–2.0 m (Shirahama et al., 2016; Kumahara et al., 2022), the 3D displacement data can be used to determine the amount of off-fault displacement in addition to the on-fault displacement. This trend has also been discussed by Scott et al. (2018), and in the western part of the Futagawa fault, larger dextral displacements were obtained for the long baseline (1 km) than for the short baseline (35 m and 100 m). Although it is difficult to read from the 3D displacement distribution map (Fig. 4B), a slight sinistral displacement occurred on the Idenokuchi fault, which is consistent with the field measurements (Toda et al., 2016; Shirahama et al., 2016; Kaneda et al., 2022). In the eastern half of the calculation area, the contrast in displacement is smaller, the amount of displacement decreases, and there is greater variability because surface failures and other factors may have also occurred. The dextral displacement along the long baseline (> 3 km) between both faults is about 2–2.5 m.

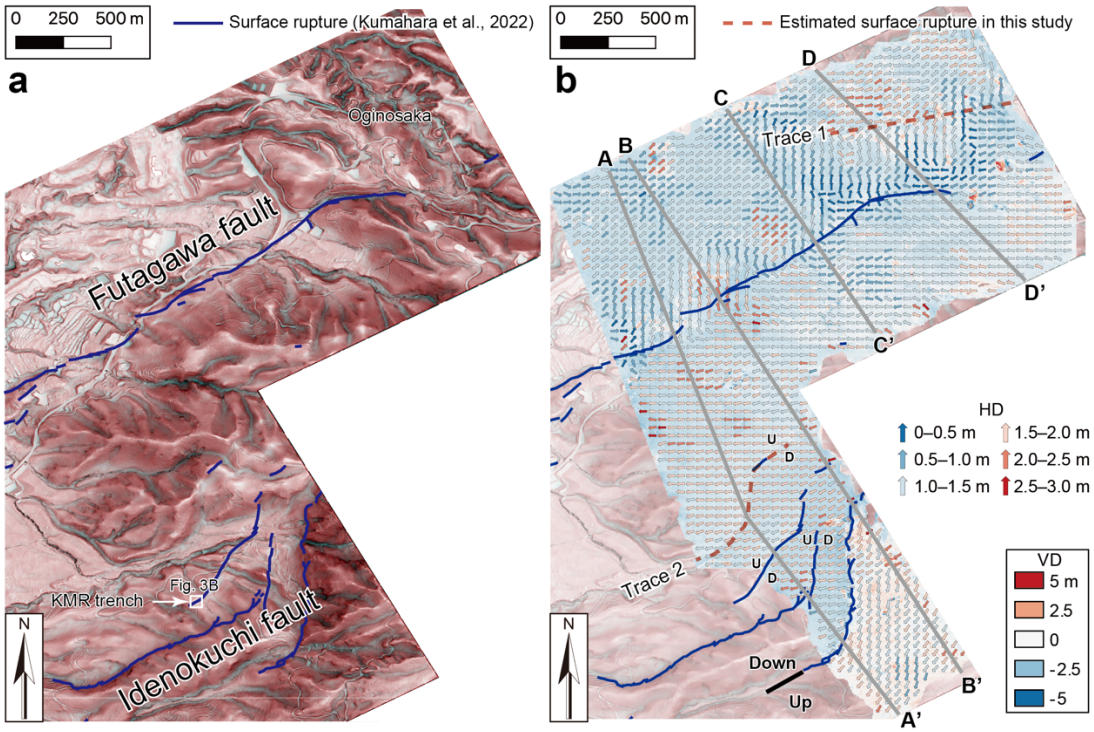

Figure 4. Results of the differential LiDAR analysis. (a) Red relief image map around the study area. The map was created based on Kaneda and Chiba (2019). Surface ruptures are after Kumahara et al. (2022). (b) 3D displacement fields. Vertical displacement is shown by the color map. Horizontal displacement is indicated by the arrow and color. HD: horizontal displacement, VD: vertical displacement.

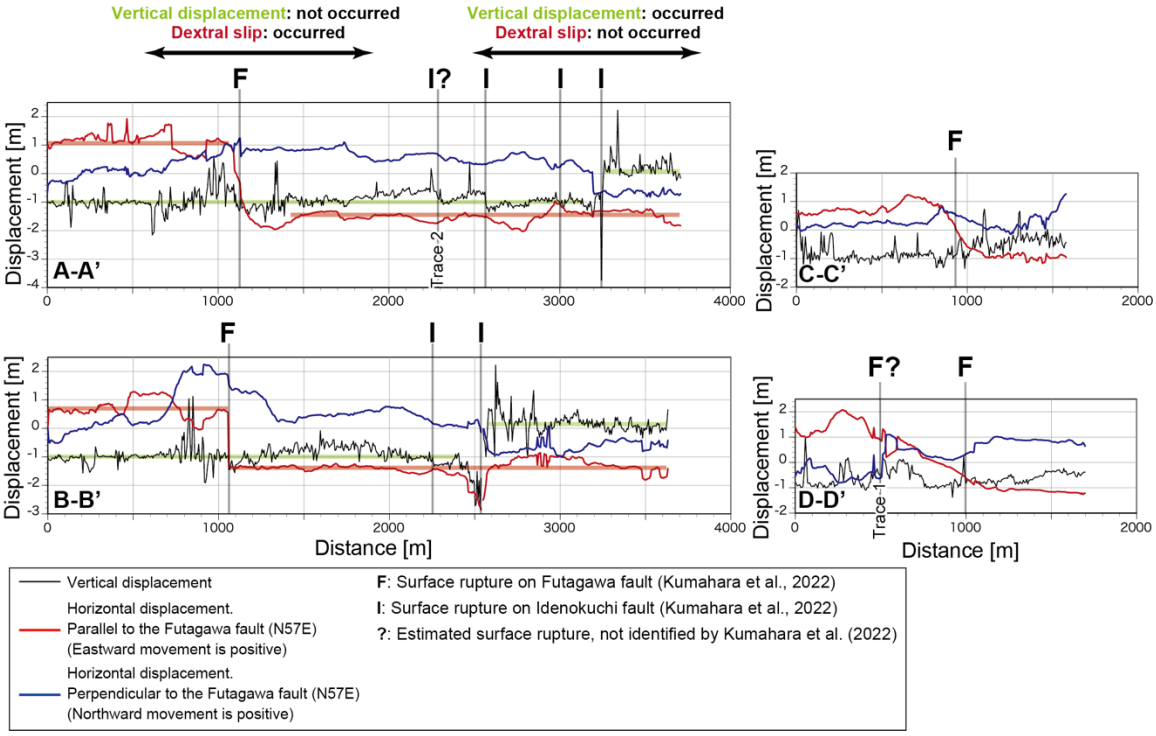

Figure 5. Vertical and horizontal displacement profiles. The profile lines are shown in Figure 4b.

Regarding the fault-perpendicular component (Figs. 4B and 5), ~~an~~ extension occurred locally on the Idenokuchi fault, and ~~a~~ contraction occurred locally on the Futagawa fault. The extension is large at the southernmost part of the Idenokuchi fault, with a displacement of about 1–1.5 m. ~~The~~ contraction of about <1 m occurred on the Futagawa fault. The displacement in the perpendicular direction of the fault along the long baseline (> 3 km) across both faults is about 1 m of extension.

The 3D displacement and field measurements generally agreed regarding the locations of surface ruptures and the amount and sense of displacements. ~~On the other hand~~, two locations ~~where~~ surface ruptures were ~~deduced~~ in areas not confirmed in the field ~~were recognized, and each trace was named~~ Trace 1 and Trace 2 (Fig. 4B). Trace 1 ~~is the eastern part of~~ the Futagawa fault in the calculated area. Here, contrasts in fault parallel and perpendicular components are observed, ~~although they are indistinct~~. Although it is unclear whether a well-defined fault ~~has appeared~~, ~~this eastern extension is connected to~~ a surface rupture that continues into the caldera (Kumahara et al., 2022). It is also ~~consistent~~ with ~~the~~ 2 m shortening identified ~~abutments in the bridge at~~ Oginosaka (Fig. 4) (Shirahama et al., 2016). Trace 2 is an extension of the short displacement recognized ~~at the northernmost part~~ of the Idenokuchi fault. Here, a discontinuity in vertical displacement is recognized. However, it ~~is consistent~~ with the present valley topography and may have been affected by fluvial erosion and other factors during the DTM measurement period.

5.2 Trench

5.2.1 ~~Sediments description~~ (including tephra analysis)

Figure 6 shows photomosaics and sketches of the west, east, and north walls. In this trench, sediments with different sedimentary facies and ages are distributed on the north (up-thrown side) and south (down-thrown side) sides across the primary normal fault at W9/E9. For this reason, the ~~north and south sides~~ are assigned different unit numbers except for the topsoil (unit 00). ~~The following scribes the sediments from the upper part on the south side.~~

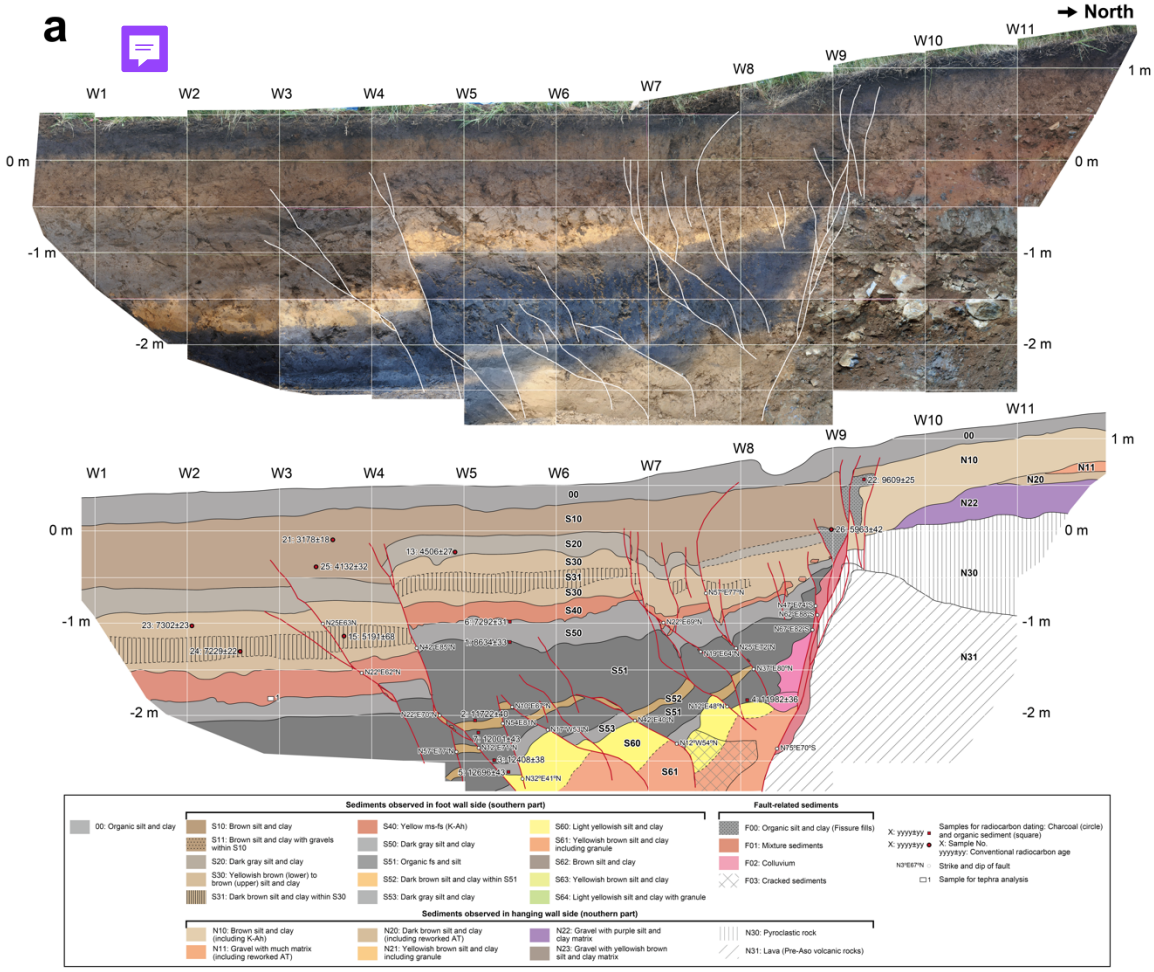
a
North
W1
W2
W3
W4
W5
W6
W7
W8
W9
W10
W11
1 m
0 m
-1 m
-2 m
00
S10
S20
S30
S31
S40
S50
S51
S52
S53
S60
S61
N10
N11
N20
N22
N30
N31
21 3178±18
13 4506±27
25 4132±32
23 7302±23
24 7229±22
15 5197±68
6 7292±31
1 8634±33
22 9609±25
26 5863±42
4 11082±36
Sediments observed in foot wall side (southern part)
00: Organic silt and clay
S10: Brown silt and clay
S11: Brown silt and clay with gravels within S10
S20: Dark gray silt and clay
S30: Yellowish brown (lower) to brown (upper) silt and clay
S31: Dark brown silt and clay within S30
S40: Yellow ms-fs (K-Ah)
S50: Dark gray silt and clay
S51: Organic fs and silt
S52: Dark brown silt and clay within S51
S53: Dark gray silt and clay
S60: Light yellowish silt and clay
S61: Yellowish brown silt and clay including granule
S62: Brown silt and clay
S63: Yellowish brown silt and clay
S64: Light yellowish silt and clay with granule
Fault-related sediments
F00: Organic silt and clay (Fissure fills)
F01: Mixture sediments
F02: Colluvium
F03: Cracked sediments
Sediments observed in hanging wall side (nouthern part)
N10: Brown silt and clay (including K-Ah)
N11: Gravel with much matrix (including reworked AT)
N20: Dark brown silt and clay (including reworked AT)
N21: Yellowish brown silt and clay including granule
N22: Gravel with purple silt and clay matrix
N23: Gravel with yellowish brown silt and clay matrix
N30: Pyroclastic rock
N31: Lava (Pre-Aso volcanic rocks)
X: yyyyyyy Samples for radiocarbon dating: Charcoal (circle) and organic sediment (square)
X: yyyyyyy X: Sample No. yyyyyyy: Conventional radiocarbon age
N3°E67°N Strike and dip of fault
1 Sample for tephra analysis

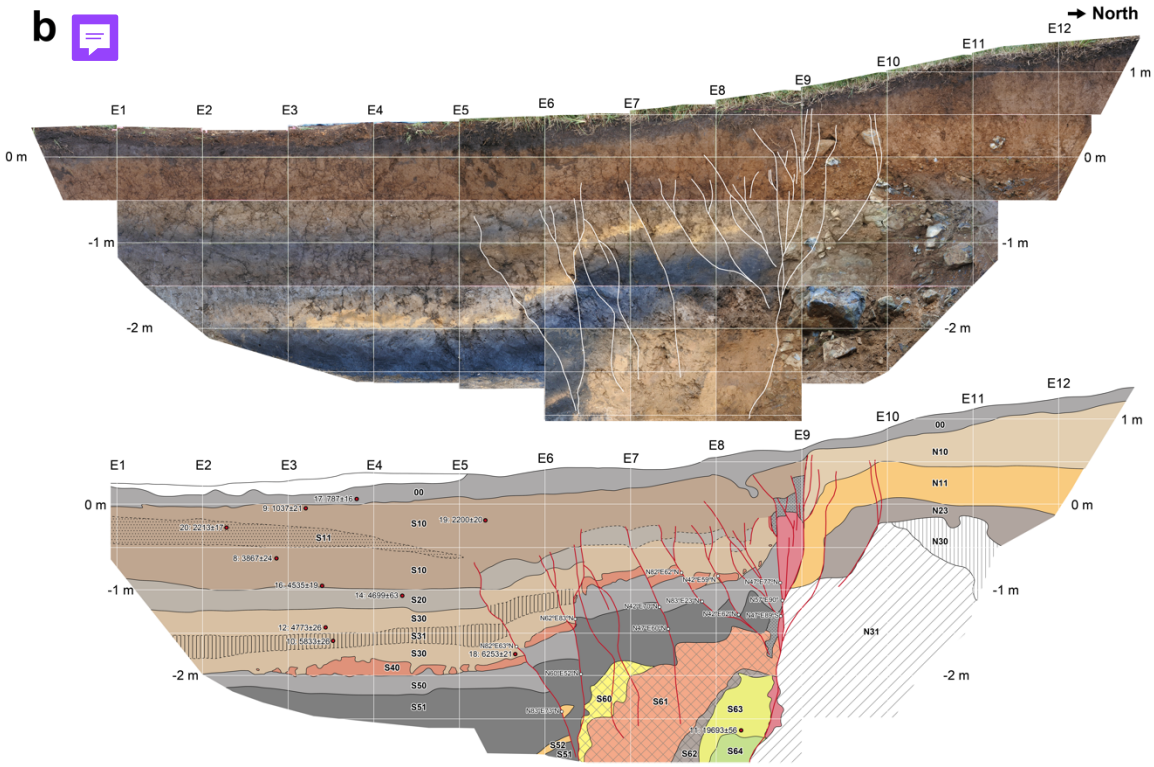
b
North
E1
E2
E3
E4
E5
E6
E7
E8
E9
E10
E11
E12
1 m
0 m
-1 m
-2 m
00
N10
N11
N23
N30
N31
S10
S11
S20
S30
S31
S40
S50
S51
S52
S60
S61
S62
S63
S64

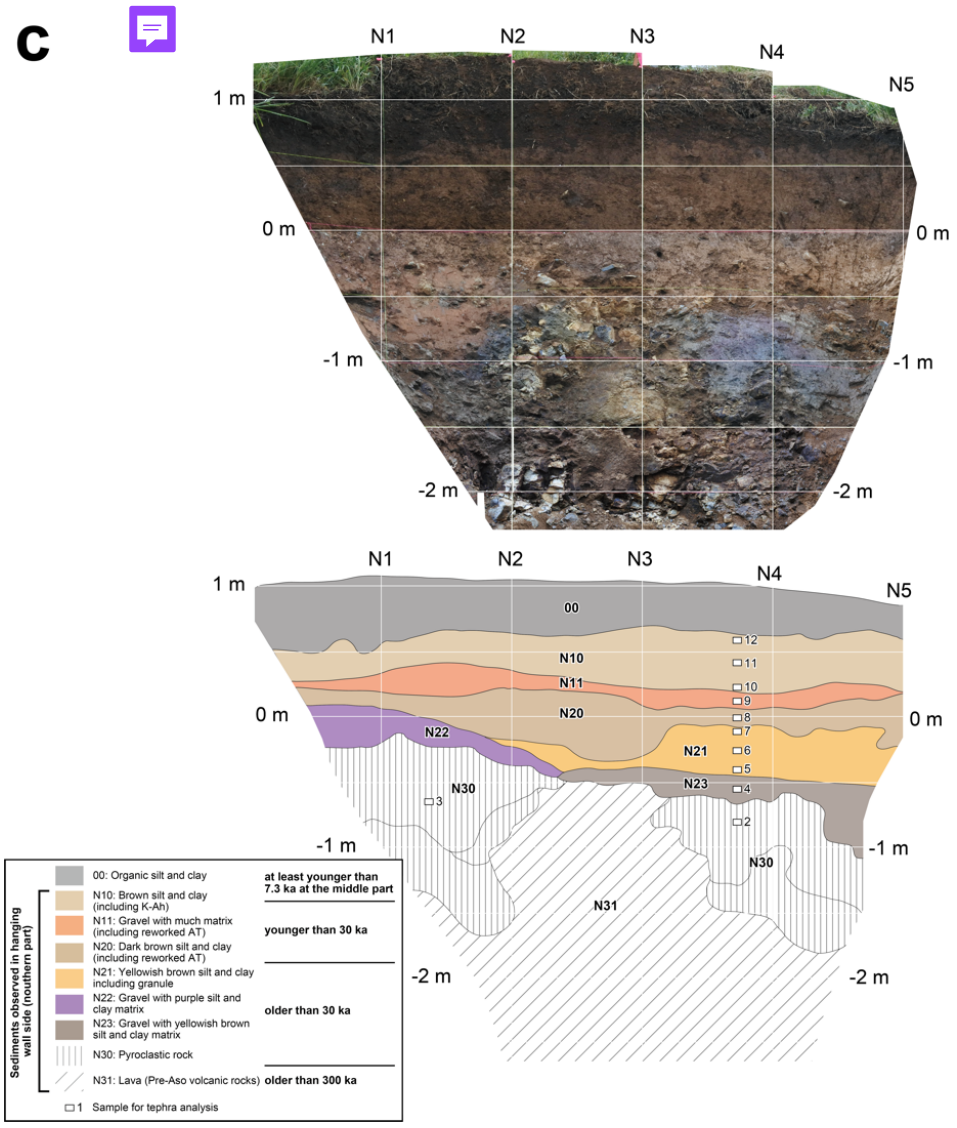

Figure 6. Photomosaics and sketches of the KMR trench walls. (a) West wall. The sketch of the west wall is flipped. (b) East wall. (c) North wall.

~~On the south side, the~~ sediments were deposited continuously, ~~mainly because it is on the down-thrown side of the fault~~ (Fig. 6). Unit 00 is the topsoil and consists of black organic silt and clay. Unit S10 is a thick, brown silt and clay below unit 00. On the east wall, an ~~unclear layer containing gravel~~ within unit S10 was classified as unit S11. Unit S20 is a dark gray silt and clay and is considered an organic-rich paleosol. Unit S30 is a

yellowish brown to brown silt and clay with a slightly darker unit S31 ~~within the thicker portion of unit S30 at the south side of the trench walls. Unit S31 is also considered an organic-rich paleosol like unit S20.~~ Unit S40 is yellow fine to medium sand, mainly composed of volcanic glass. Unit S50 is dark gray silt and clay, and unit S51 is organic silt and fine sand, with unit S50 slightly lighter than unit S51. Unit S52 is yellowish brown to brown silt and clay~~, partially observed on the south side of the thicker part of unit S51.~~ Unit S53, which is observed only in the west wall, is a slightly lighter gray silt and clay similar to unit S50. The base of unit S53 is undulating, ~~and a time gap is inferred~~ between units S53 and S60. Unit S60 is a bright yellowish silt and clay, and unit S61 is a yellowish brown silt and clay with granules. In the west wall, unit S61 is the lowest (oldest) ~~sediments. Unit S62 is brown silt and clay, unit S63 is yellowish brown silt and clay, and unit S64 is~~ light yellowish silt and clay with granules ~~on the east wall.~~

~~On the north side, the~~ sediments are thinner than ~~on~~ the ~~south side~~ and are composed of gravel and rock (Fig. 6). Unit N10, consisting of brown silt and clay, ~~shows a time gap~~ with unit N11 and lower units (see west wall in Fig. 6a). Unit N11 is a matrix~~-rich~~ gravel bed. Units N20 and N21 are dark brown and yellowish brown silt and clay, respectively. Both units N22 and N23 are ~~gravel beds containing a lot of matrix with different c~~rs. Unit N30 is pyroclastic rock, and its base shows undulating contact. Unit N31 is fragmented lava ~~and is considered to be~~ pre-Aso volcanic rock that forms the basement rock of the surrounding area (Hoshizumi et al., 2004).

~~The coring results (Fig. S1) showed that on the upthrown side (HC-1), the same stratigraphy is recognized at almost the same depth as on the north wall. Therefore,~~ the sediments ~~on~~ the north wall are ~~considered to be~~ distributed widely and uniformly on the

northern side of the fault. On the downthrown side (HC-2 to HC-7), the black silt and clay and yellowish brown to brown silt and clay, corresponding to unit S51 and lower, were ~~also~~ observed ~~as well as on the trench walls~~. No black soil, corresponding to units S51 to S53, was observed at depths greater than 1 m from the trench floor. Gravel and sand beds, not recognized in trench walls, were observed in some cores. However, no tephra layers were identified. On the other hand, sediments were in contact with high angles, and voids were observed in some cores, where we inferred faults. The primary normal fault was considered the boundary with the basement rock, so we inferred the normal fault at a depth where drilling was no longer possible.

5.2.2 Faults

In this trench, the primary normal fault is observed at W9/E9, and many other faults were rootless with bending in the lower part. Faults extending down to the trench bottom are the north-up normal faults at W9/E9 and the reverse faults at W3-W5 and E5-E6. Normal fault groups that form grabens develop at W7-W9 and E7-E10. The 2016 displacement was an open crack near W9/E9, which was already filled with sediments. ~~Such 2016~~ open cracks and fissure fill sediments have ~~also~~ been identified in the Futa trench at Futa (Fig. 1; Ishimura et al., 2022). However, no other distinct 2016 displacement (e.g., apparent vertical displacement) was observed in the trench walls. This is likely because the trench is located in an area of decreasing vertical displacement from northeast to southwest (Fig. 3b), where the 2016 displacement is small and indistinct. Other fissure-fill sediments that may have b~~een~~ formed ~~by the~~ pre-2016 a~~ctivity~~ ~~are~~ also identified below the 2016 fissure-fill sediments. Measurements of the strike and dip of faults on the trench walls

indicate that the main strike is northeast to southwest, but some are north to south or east-northeast to west-southwest (Fig. 6). The northeast-southwest strike is consistent with the surface ruptures (Fig. 3b). The other strike directions suggest that subsidiary surface ruptures to the primary normal fault ~~were present~~ in ~~the~~ past events.

5.2.3 Tephra analysis

The results of the tephra analysis are shown in Table S1, and the major element composition of volcanic glass shards is shown in Tables S2 and S3. The results show that unit S40 is composed almost entirely of volcanic glass, with a refractive index of 1.510-1.512 (mode: 1.511), suggesting that it correlates with the widespread tephra, Kikai-Akahoya (K-Ah), by the eruption of southern Kyushu at 7.3 ka (Machida and Arai, 2003; Smith et al., 2013). The chemical compositions confirmed this correlation (Table S2), consistent with the existing studies in the vicinity (e.g., Ishimura et al., 2022). Volcanic ash analysis of the samples from the north wall revealed no tephra layers. Therefore, we examined the volcanic glass content and ~~its~~ refractive ~~index~~ to determine if the samples contain volcanic glass shards from Aira-Tn (AT) (30 ka; Smith et al., 2013) and K-Ah tephras, which are commonly identified ~~widespread~~ tephras in this area (Machida and Arai, 2003). The results show almost no volcanic glass below unit N21, while units N20 and N11 show very low volcanic glass content (2%). The refractive indices of volcanic glass are mainly 1.495-1.500, which correlates with AT tephra. In contrast, the volcanic glass content increases from the lower to the upper part of unit N10. The refractive indices show that while unit N10 contains 1.497-1.500 of AT origin, the percentage of volcanic glass of 1.508-1.512 of K-Ah origin increases toward the upper part of unit N10.

This suggests that the age of the middle part of unit N10 is after the K-Ah tephra. This mixing of AT and K-Ah volcanic glass is also observed in soils in other regions, and the K-Ah ash fall horizon is roughly estimated at the peak of K-Ah volcanic glass shard content (Ishimura and Kakiuchi, 2011). Such distribution of volcanic glass shard content may be due to bioturbation and secondary deposition of tephra-origin particles. Based on the presence of AT volcanic glass, unit N20 is at least younger than 30 ka, and unit N21 and below are older than 30 ka. Based on the K-Ah glass content, the upper to middle part of unit N10 is interpreted to be at least younger than 7.3 ka. The fact that K-Ah tephra is ~~visible on the south side~~ indicates that ~~the sediments' deposition rate and preservation potential differ from north to south across the primary normal fault, as already mentioned.~~

5.2.4 Radiocarbon dating

Because the faulting events described below were identified on the down-thrown side of the primary normal fault, radiocarbon dating of samples collected from the south side of the trench walls was performed (Table S4). The youngest age was 7[illegible] ± 16 yr BP (charcoal) from unit 00, and the oldest was [illegible]93 ± 56 yr BP (charcoal) from unit S63. For sediments older than unit S50, bulk samples (organic sediments) were used except for the sample from unit S63. As Ishimura et al. (2022) pointed out, the ages of ~~the~~ bulk samples in this region sometimes ~~show~~ younger than the actual ages. In this trench, we compared the bulk sample ages with the ages of the K-Ah tephra and the charcoal from unit S63. As a result, the bulk sample ages were consistent with the tephra and charcoal age, and there was no contradiction between the stratigraphy and age. Because we used

charcoal samples for radiocarbon dating to determine the ages above unit S30, it is possible that older charcoals were included by reworking, resulting in older ages. In such cases, charcoals with younger ages in the same unit were employed for further analyses. As a result, we did not use the ages ~~of Nos. 23 and 24~~ samples (Table S4). Additionally, the ages of the open cracks were determined from the bulk samples, which are older than the surroundings. Therefore, the ages of these fissure-fill sediments are also not used.

6. Discussions

6.1 Slip partition based on 3D displacements

In this section, we discuss how the displacement is divided on both faults for the slip partition with line A (Fig. 5), where the influence of surface failure is small, and the Futagawa fault appeared as a single trace (Fig. 4). First, dextral displacement occurred only on the Futagawa fault, and local sinistral displacement is observed along the Idenokuchi fault. However, along the long baseline (> 3 km), no lateral displacement occurred on the Idenokuchi fault. On the other hand, the vertical displacement is the opposite of the lateral displacement. Vertical displacement of 1 m occurred only in the southernmost trace of the Idenokuchi fault along the long baseline, and little vertical displacement occurred in the 1 km width across the Futagawa fault. Vertical displacement of several tens of centimeters occurred on the conjugate faults of the Idenokuchi fault, but that decreased with distance from the fault. These suggest that extensional deformation and block rotation cause apparent vertical displacement on the conjugate faults.

Based on these observations, the slip partition on the Futagawa and Idenokuchi faults is considered to be the result of oblique lateral displacement at depth, which is

almost completely split into dextral and vertical displacement near the surface and accommodated by both faults, respectively, as shown schematically by Toda et al. (2016). In addition, our results show that the displacement is completely split, as mentioned in King et al. (2005). This may provide an important insight into the geometry (dip angle, distance of two faults, and amount of oblique displacement) of faults where slip partitioning can occur. In other words, the deeper part of the Idenokuchi fault is connected to the deeper part of the Futagawa fault, and the Idenokuchi fault is a branch fault of the Futagawa fault. The estimated depth at which they merge may be several kilometers, as shown by Toda et al. (2016), although it depends on their dip angles. This means that the two faults can be treated as a single source fault when assessing seismic hazards of active faults. Therefore, the paleoseismic history of the Idenokuchi fault should be consistent with that of the Futagawa fault, given its subsurface structure. In Scott et al. (2018) and Himematsu and Furuya (2020), large vertical displacement (1-2 m south-up) was observed on the Futagawa fault on the west side of the parallel section of the Futagawa and Idenokuchi faults. This indicates that the Futagawa fault has accommodated oblique slip on the west side of the Idenokuchi fault's parallel section. In addition, Himematsu and Furuya (2020) showed a sharp decrease in vertical displacement and nearly unchanged right lateral displacement along the Futagawa fault at the parallel section of the Idenokuchi fault, which is consistent with our results.

We discuss the relationship between slip partition and geology. King et al. (2005) mentioned the relationship between the slip partition and geology; the depth at which the fault branches into two could coincide with the bottom of surface sediments. Aoyagi et al. (2024) reported another slip partition on the western part of the Futagawa fault based on

the surface rupture distribution of the 2016 event, drilling cores, and seismic reflection survey. They reported that the subparallel surface ruptures/faults consumed oblique slip in the deeper part in the 2016 Kumamoto earthquake and converged at a depth of 350 m. The depth corresponds to that of the pre-Aso volcanic rocks and/or Kiyama metamorphic rocks (Kumamoto Prefecture Geological Map Compilation Committee, 2008) and there are unconsolidated sediments, including pyroclastic flow deposits from middle to late Pleistocene above these rocks. Thus, the upper end depth (convergent depth of both faults) of oblique slip faults seems to correspond to some geological (physical property) difference. In our study area, unlike the study area of Aoyagi et al. (2024), pre-Aso volcanic rocks are exposed on the surface around the Idenokuchi fault, deeper geology (e.g., Kiyama metamorphic rocks) may constrain the convergent depth of both faults.

6.2 Paleofaulting events on the Idenokuchi fault

We interpreted faulting events since unit S53 ~~deposition~~ by retrodeformation (Fig. 7 and S2) ~~because soils develop continuously~~ (Table S4). Ev0 is the 2016 event, and an open crack occurred directly above the primary normal fault near W9 (Fig. 6a). In the 2016 event, a further open crack was formed in the open crack formed by Ev1, which is described below, and was already filled with the deposit. Although no vertical displacement can be identified on the trench walls, it is clear from the mapping of surface ruptures that vertical displacement occurred here. Similarly, an open crack directly above the primary normal fault near E9 is recognized on the east wall (Fig. 6b).

Ev1, like Ev0, developed an open crack directly above the primary normal fault near W9 and was filled by fissure-fill deposits. This event is considered to have occurred during the deposition of unit S10. The bulk of this fissure-fill deposit was dated (Sample No. 22 (9609 ± 25 yr BP)), but this age is not used to estimate the age of the Ev1 because it is older than its surroundings.

In Ev2, an open crack, normal fault displacements near the primary normal fault (W7-W9), and reverse fault displacements on the southern faults (W3-W4) occurred. This event occurred after the deposition of unit S20 paleosol and during the deposition of unit S10. Similarly, on the east wall, normal fault displacements were observed near the primary normal fault (E7-E9), and the faults in the south (E5-E6) show reverse fault displacements. In addition, a gravel-rich unit S11 is recognized in unit S10 on the east wall, which is wedge-shaped and may be a deposit supplied from the southern slope due to surface failures. Therefore, unit S11 may be a post-earthquake deposit related to Ev2. Thus, the event horizon of Ev2 is estimated to be after unit S20 and before unit S11. This also confirms that the age of Ev1 is after unit S11 and during unit S10.

Ev3, like Ev2, shows normal fault displacements near the primary normal fault (W7-W9) and reverse fault displacements on the southern faults (W3-W4). The east wall similarly shows normal fault displacements at (E7-E9) and reverse fault displacements at the southern faults (E5-E6). The event horizon of Ev3 is estimated to be between units S20 and S31 since the fault at W3 displaces unit S31 but does not displace unit S20.

Ev4 is indistinct in the west wall, while it is distinct in the east wall, with reverse fault displacement on the lower surface of unit S50 near E6 and normal fault

displacements at E8-E9 (Fig. S2). The event horizon of Ev4 is estimated to be during the deposition of unit S50.

Ev5 and Ev6 are estimated after unit S52 deposition while the upper part of unit S51 is being deposited. During this period, reverse and normal fault displacements are observed in W4-W8. The reverse fault displacements occurred in Ev2-Ev4, and normal fault displacements occurred in Ev7, as described below. Considering the similarity of the displacement patterns, reverse fault motion was grouped as Ev5 and normal fault motion was grouped as Ev6. These normal and reverse fault displacements are considered to have occurred separately rather than simultaneously. Therefore, we interpreted that at least two events occurred during this period. Since the ages of Ev5 and Ev6 cannot be distinguished, both events are only constrained after unit S52 and during unit S51 deposition.

In Ev7, normal fault displacement at W7-W8 occurred at the lowest part of the soil deposits in this trench. Its age is between unit S52 and S53 deposition.

From these interpretations, eight faulting events (including the 2016 event) were recognized in this study since unit S53 deposition. The ages of the faulting events were obtained using OxCal (Fig. S4). The results show that Ev1: 2190–940 cal BP, Ev2: 4760–4250 cal BP, Ev3: 6040–5360 cal BP, Ev4: 9550–7280 cal BP, Ev5-Ev6: 13500–9680 cal BP, Ev7: 14700–13840 cal BP in the 2σ range. The average recurrence interval is 1990–2110 years. Unit S53 is buried 4.5–5 m below the present ground surface, indicating that the average buried amount is about 0.6 m per event. This value is roughly consistent with a representative coseismic displacement of 60 cm along the surface rupture in the 2016

event in case the downthrown side is buried by the same amount as the coseismic vertical displacement in each event.

We also examined why the reverse fault displacement was observed in this normal fault trench. Such subsidiary reverse faults in the primary normal fault displacements are generally considered "pseudreverse faults" (McCalpin, 2009), and it is considered to be an apparent reverse fault when the normal fault exceeds 90°, that is, “overturns,” near the ground surface. In this study, such a reverse fault is also apparent, with little compression, and gravity is considered a contributing factor. A similar one is recognized in Ev0 (2016 event) in the west wall. However, deformation at Ev2-Ev4 is characterized by the formation of graben near the primary normal fault and the southern reverse faults, which differs from the aforementioned explanation by McCalpin (2009). Therefore, we attempted to explain the deformation by assuming a block diagram shown in Figure 8.

The 3D displacement results show that the displacement around the trench indicates that the ratio of vertical to extensional displacement is 2:1. Therefore, we considered this ratio of fault displacement and displaced blocks 1 to 3 (Fig. 8). We assumed the displacement of each block like this; The block 1 was displaced 100%, block 2 was displaced 50%, and Block 3 was displaced 0%. Then, block 2 collapses to the downthrown side, as shown in Fig. 8b. Block 3 then falls between Block 2 and the primary normal fault. This causes graben-like displacement near the primary normal fault and an apparent reverse fault between blocks 2 and 3. Furthermore, in this trench, some rootless faults are bent at depth, and this kind of bending can also be explained by this block model. In reality, the red area in Figure 8 is not void, so the fault bends, and the displacement is distributed by minor faults. A similar displacement was described in the

trench on the Wasatch fault (Machette et al., 1992). Their trench was excavated to a greater depth (8 m) than ours and showed a reverse fault branching from the primary normal fault to the downthrown side. This reverse fault is behind the primary normal fault and is different from an apparent reverse fault, which is the normal fault exceeding 90° near the ground surface, as suggested by McCalpin (2009).

Then, we considered why such displacement occurs and suggested that tephric soil and sediments may be a factor. Because soil and sediments near the ground surface including many tephric particles (e.g., volcanic glass and clay minerals) are very sticky, when normal fault displacement occurs, the shallow part (blocks 2 and 3) cannot fall as far as the deep part along the fault plane.

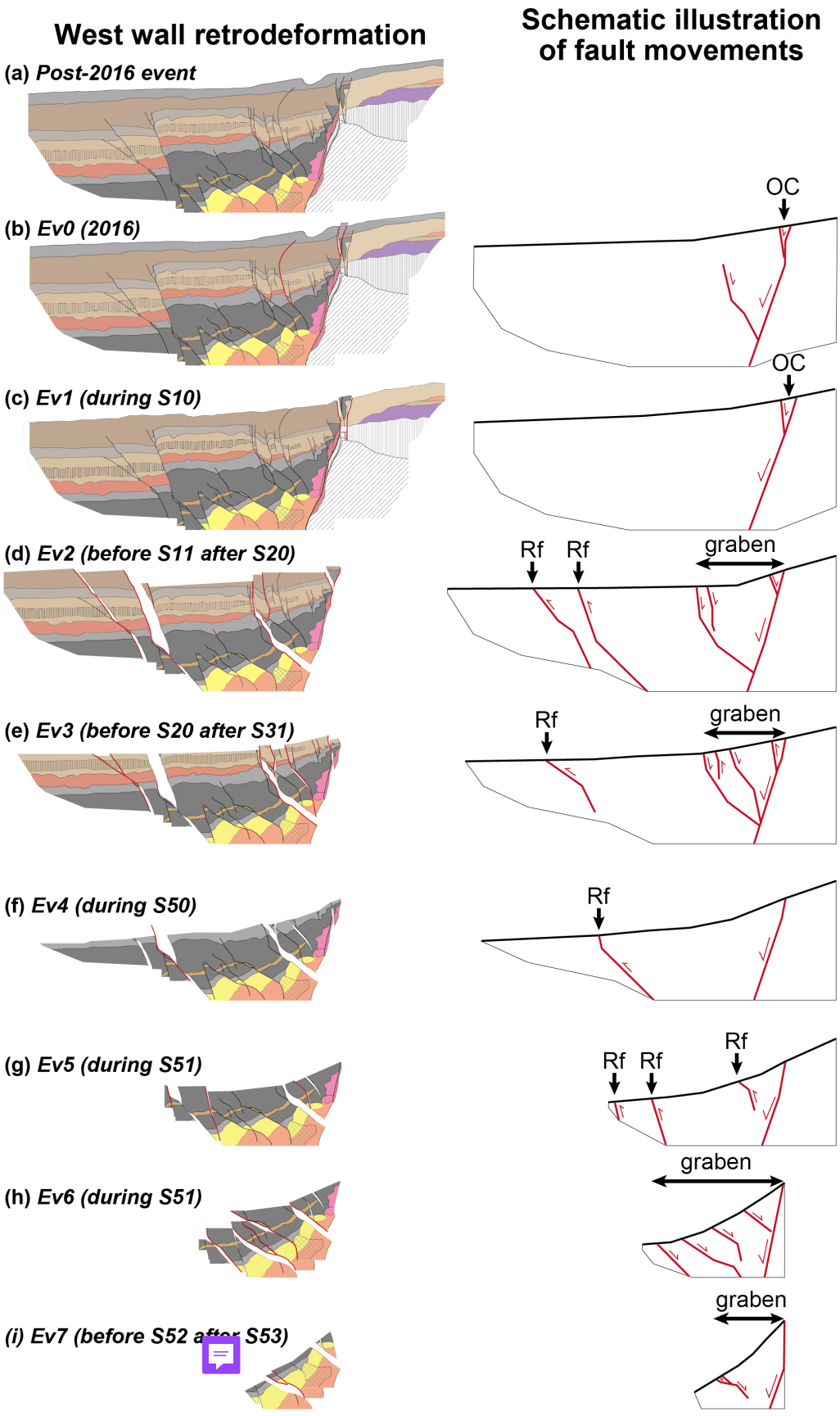
West wall retrodeformation
Schematic illustration of fault movements
(a) Post-2016 event
(b) Ev0 (2016)
(c) Ev1 (during S10)
(d) Ev2 (before S11 after S20)
(e) Ev3 (before S20 after S31)
(f) Ev4 (during S50)
(g) Ev5 (during S51)
(h) Ev6 (during S51)
(i) Ev7 (before S52 after S53)
OC
OC
Rf
Rf
graben
Rf
graben
Rf
Rf
Rf
graben
graben

Figure 7. Retrodeformation of the faults and schematic illustration of fault movements on the west wall. The left figures show reconstructions of the displacement for each event, and the right figures show the faults that were active during that event. Rf: reverse fault, OC: open crack.

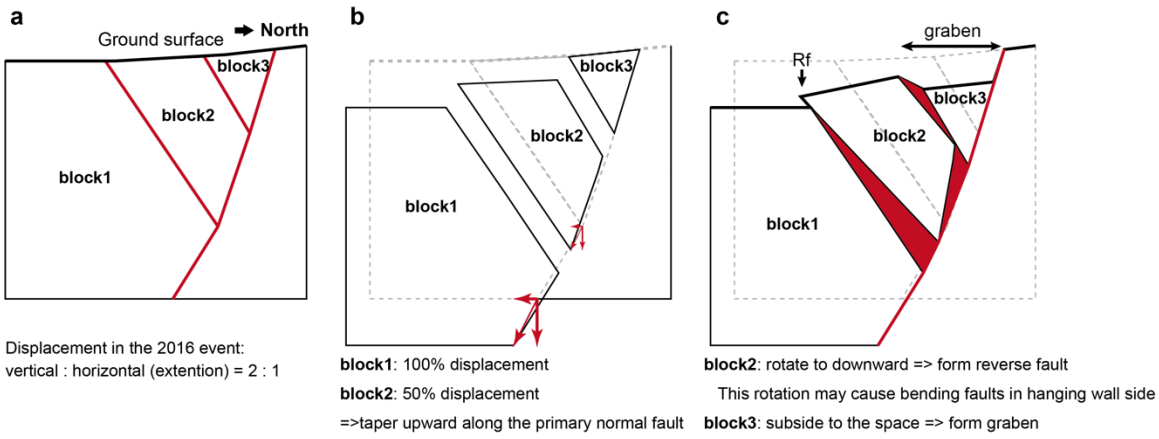

Figure 8. Schematic illustration explaining how the graben and apparent reverse faults were formed in the trench.

6.2 Comparison of paleoseismic events between the Futagawa and other faults

A summary of the paleofaulting history by the author's group (Fig. 9) shows that the ages of faulting events after the K-Ah tephra all overlap. This suggests that the Futagawa fault (Ishimura et al., 2022), Miyaji faults (Ishimura et al., 2021), and Idenokuchi fault have all moved simultaneously at least in the ~~recent~~ past. In particular, as shown in section 6.1, the Idenokuchi fault accommodates the vertical component of oblique slip in the deep part of the Futagawa fault, and the subsurface structure suggests that the Futagawa and Idenokuchi faults moved at the same time. The Miyaji faults that produced the 2016 surface rupture, which is distant from the Futagawa fault and seems structurally discontinuous (Fukushima and Ishimura, 2020), are also presumed to have been active in the past with the Futagawa fault. ~~The relationship between the primary and secondary~~

~~faults has not been sufficiently discussed in paleoseismological studies for simultaneity.~~

To analyze rupture process scenarios seen in the interlocking ruptures such as the 2016 Kaikoura earthquake and induced displacements such as the 2019 Ridgecrest earthquake, paleoseismic investigations focusing on such secondary and small displacements are also necessary.

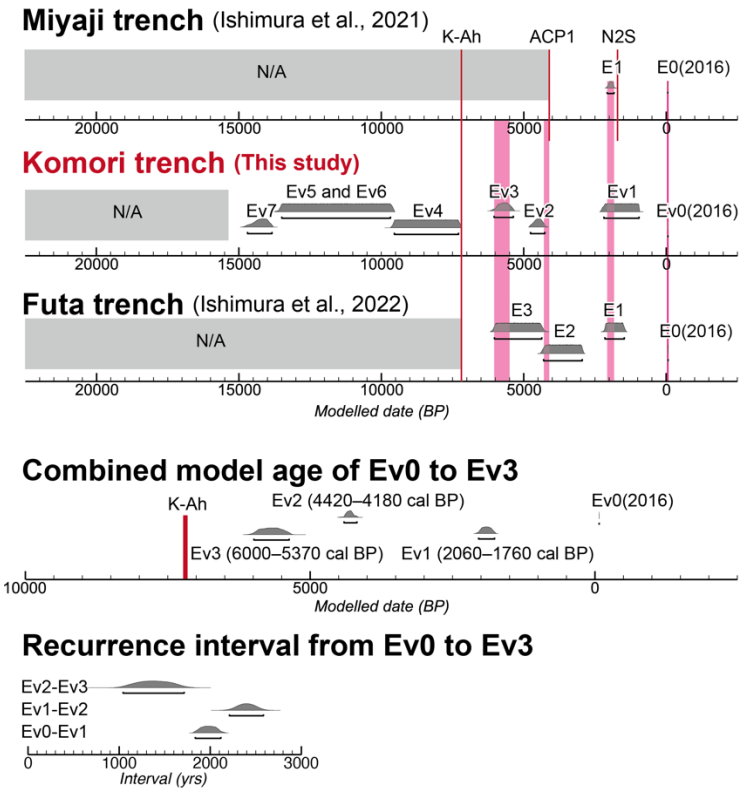

Figure 9. Modeled event ages and comparison to the author's previous paleoseismic studies. The underbars show the 2σ probability distribution ranges of the modeled ages. ACP1 and N2S are local tephras from the Aso volcano (Miyabuchi, 2009). ACP1 is Aso central cone pumice and its age is 4.1 ka (Miyabuchi, 2009). N2S is Nakadake N2 scoria and its age is 1490–1470 cal BP (68.2%) (Yamada et al., 2017).

Furthermore, assuming that the faulting events from Ev0 to Ev3 are the same among our three trenches, the calculated ages in OxCal modeling are Ev1: 2060–1760 cal

BP, Ev2: 4420–4180 cal BP, and Ev3: 6000–5370 cal BP (Fig. 9). Each recurrence intervals are Ev0/Ev1: 1830–2120 years, Ev1/Ev2: 2210–2590 years, and Ev2/Ev3: 1040–1720 years in the 2σ range. Based on the trench results, the average recurrence interval from Ev0 to Ev7 is 1990–2110 years, consistent with the interval from Ev0 to Ev3 mentioned above. This indicates that the Futagawa fault has ruptured relatively periodically. Despite the shallow depth of the trench, we could identify seven events, which were greater than those identified in trenches excavated on the primary Futagawa fault. This result emphasizes the importance of selecting a site with small displacement per event and relatively fast and continuous deposition.

The dextral slip rate from the recurrence interval (1990–2110 years) and single displacement (1.8–3.1 m) obtained in this study is 0.9–1.5 mm/yr for the Futagawa fault. For the Idenokuchi fault, vertical displacement is 1.0–2.5 m, so the vertical slip rate is estimated to be 0.5–1.3 mm/yr. On the west of this study area (Futa to Ohkirihata), across only the Futagawa fault, Ishimura (2019) calculated 0.9–1.1 mm/yr vertical slip rate and 1.5–3.7 mm/yr dextral slip rate from the vertical and dextral displacements of Takayubaru lava (K–Ar ages 81 ± 4 ka and 98 ± 18 ka; Miyoshi et al., 2013). The Idenokuchi fault runs parallel to the Futagawa fault, where these slip rates, i.e., the west of the study area, were calculated. However, the vertical displacement on the Idenokuchi fault in the 2016 event west of the study area is small (Kaneda et al., 2022). Therefore, the long-term slip rates can be regarded as representative values when oblique slip is accommodated only by the Futagawa fault. In considering this way, the long-term dextral and vertical slip rates are consistent with the results of this study. Oohashi (2020) pointed out that normal fault displacement was predominant on the Futagawa fault before Aso-4 pyroclastic flow

deposits (87 ka; Aoki, 2008), and dextral displacement became apparent later. Oohashi (2020) proposed the following possibilities for this change: 1) The stress field changed from a normal fault type with north-south extension to a dextral strike-slip fault type with predominant east-west compression, and 2) the normal fault component of the Futagawa fault was replaced by Idenokuchi fault and off-fault displacements, and the dextral displacement of the Futagawa fault became apparent. The fact that the long-term vertical slip rate coincides with that of the Idenokuchi fault from this study agrees with the second explanation. Therefore, the slip partition on the Idenokuchi fault must have occurred after the Aso-4 event.

Figure 10 summarizes the paleofaulting history since 7.3 ka based on the previous paleoseismic results, including archeological information, which is consistent with this study. The number of activities since 7.3 ka (including 2016) on the Futagawa fault is estimated to be four with considerable accuracy and precision based on the results of multiple trenches along the Futagawa fault and its vicinity. We believe that a series of studies by our group has provided highly accurate ages for the past three events because we studied the sites where minor artificial disturbance, continuous sediments, and good age markers (tephras). In addition, the paleofaulting history at the northwestern Aso caldera (Sato et al., 2021) and the western part of the Futagawa fault (Inoue et al., 2020), which are at secondary surface ruptures, indicate one of their events coincides with Ev1 in this study. Therefore, it is highly likely that the secondary faults were active simultaneously during at least the penultimate event of the Futagawa fault. Lateral spreading recognized at archaeological sites in the caldera (Kumamoto Prefectural Board of Education, 2010; Aso City Board of Education, 2011) was also approximately 2000

years ago, which also supports that secondary phenomena caused by earthquake similar to the 2016 event that occurred in the caldera. Thus, it is inferred that similar phenomena in the 2016 event (e.g., secondary surface rupture, liquefaction, and lateral spreading) also occurred during the previous activity. However, the age of the antepenultimate event in the northwestern part of the caldera does not match that of the Futagawa fault (Sato et al., 2021). In addition, no other secondary surface ruptures have been identified as having fault events older than the antepenultimate event, so it is unclear how the secondary fault behaved during the older events. Future accumulation of information on the presence or absence of older activities on such secondary faults and their histories will help us to better understand the secondary faults.

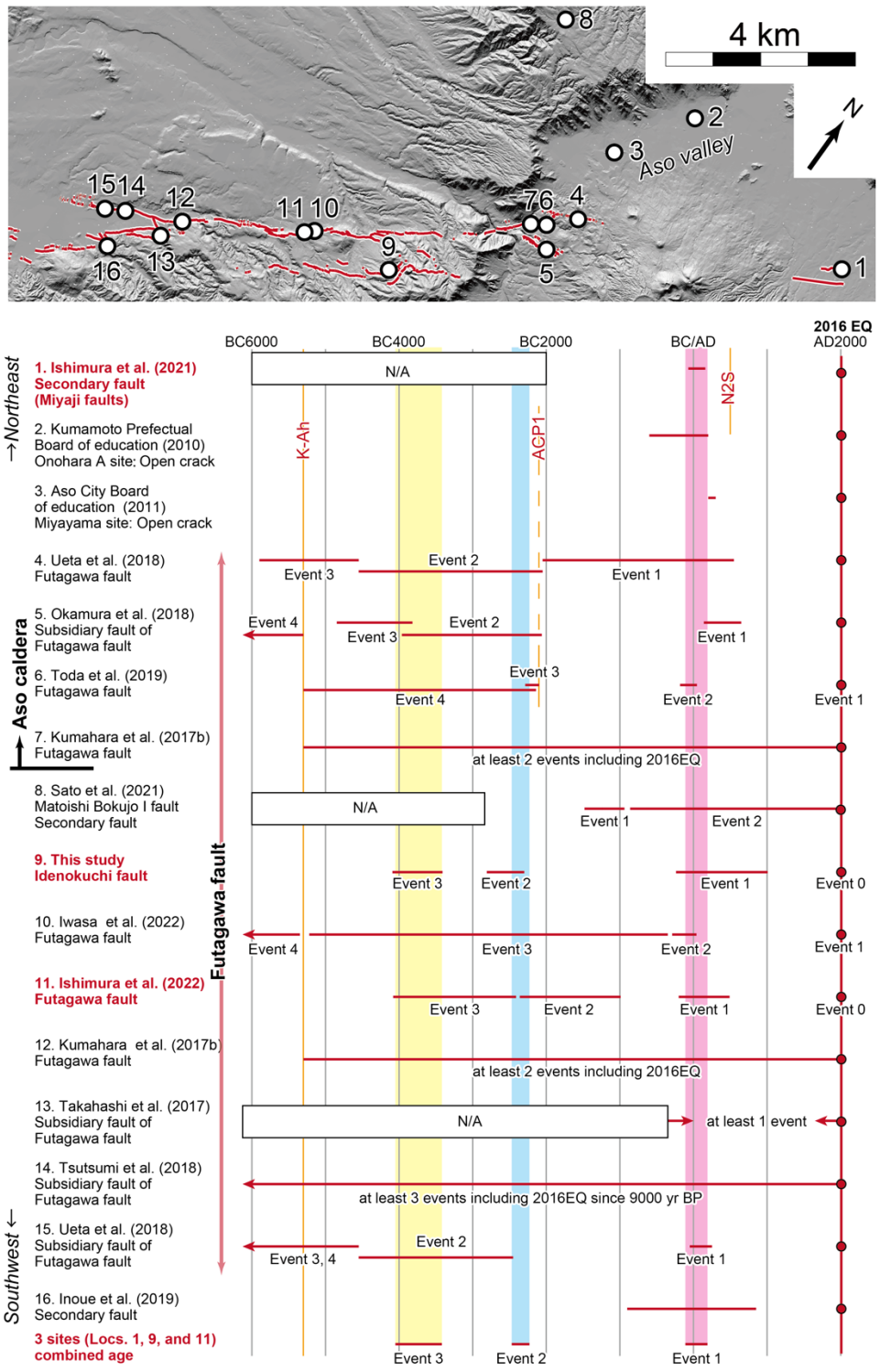

Figure 10. Compiled spatial-temporal age distribution of the paleofaulting events along the Futagawa and its subsidiary and secondary faults.

7. Conclusions

Using the 2016 Kumamoto earthquake as an example, we performed a DTM difference analysis in the area crossing the Futagawa and Idenokuchi faults where the slip partition occurred and conducted an excavation survey on the Idenokuchi fault. Based on the 3D displacement distribution, we discussed how the slip partition occurred on them and found that the oblique slip at depth was split entirely into vertical and horizontal displacements on the ground surface. This indicates that the Idenokuchi fault is structurally related to the Futagawa fault and that the paleofaulting history of the Idenokuchi fault is likely to correspond to that of the Futagawa fault.

The KMR trench at the Idenokuchi fault revealed continuous deposition of soil and tephra since 15 ka, and retrodeformation of the trench walls revealed at least eight faulting events (including 2016) during this period. Among them, the faulting events after I[illegible]h are consistent with paleoseismic surveys on the Futagawa fault (primary fault) and Miyaji faults (a secondary fault in the Aso caldera). This indicates that at least some surface ruptures that appeared around the Futagawa fault in the 2016 event are likely to have been active at the same time as the past activities of the Futagawa fault. The activity histories since 7.3 ka with the author's three trenches on the Futagawa, Miyaji, and Idenokuchi faults are E1: 2060–1760 cal BP, E2: 4420–4180 cal BP, and E3: 6000–5370 cal BP, indicating that they occurred relatively periodically. The mean recurrence interval since 15 ka is about 2000 years, supporting the periodic activity. The results of this study are also consistent with other trench investigations conducted after 2016. It is important to improve the accuracy and precision of the activity history of the Futagawa fault before 7.3 ka and to investigate the activity history of the Hinagu fault zone in the southern part

of the Futagawa fault zone to consider future seismic hazard and interlocking rupture. In addition, it will be important to clarify the subsurface structure and activity history of secondary faults in other earthquakes involving large amounts of surface ruptures, as well, to consider displacement hazards.

Acknowledgements

We thank Yasuhiro Kumahara, Ryuhei Oda, Jun Matsukaze, Motoya Kobayashi, Makoto Kobayashi, Yoshiya Iwasa, and Daichi Tomita for their help during the trench survey. We also thank Shinji Toda, Heitaro Kaneda, and Yasuo Miyabuchi for their discussions and constructive comments. This work was supported by KAKENHI Grant Number JP17H04730 from the Japan Society for the Promotion of Science.

Data and code availability

Supplementary figures (S1 to S2) and tables (S1 to S4) are available in the supplement material.

OxCal model codes are listed in the supplementary material.

Pre- and post-event DTMs used in this study were provided from Geospatial Information Authority of Japan (https://www.gsi.go.jp/ENGLISH/index.html).

Competing interests

The authors have no competing interests.

References

Aoki, K. (2008) Revised age and distribution of ca. 87 ka Aso-4 tephra based on new evidence from the Northwest Pacific Ocean. Quaternary International, 178, 100–118. doi: 10.1016/j.quaint.2007.02.005.

Aoyagi, Y., Higashi, S., Homma, S., Mukoyama S., Sugiyama, M., and Hijikata, K. (2021) Surface ruptures in the Aso campus of Tokai University caused by the 2016 Kumamoto Earthquake. Active Fault Research, 55, 1–18. (in Japanese with English abstract)

Aoyagi, Y., Ueta, K., Takemoto, T., Suehiro, M.,and Miyawaki, R. (2024) Seismic constraints on the subsurface extent of subparallel surface ruptures in Mashiki Town, Japan, associated with the 2016 Kumamoto Earthquake. Journal of the Seismological Society of Japan. 2nd ser., 77, 5–19. (in Japanese with English abstract)

Aso City Board of Education (2011) Miyayama ruinsII, Cultural Property Investigation Report of Aso City 2. Aso City Board of Education, Aso City. (in Japanese)

Barnhart, W.D., Hayes, G.P., and Gold, R.D. (2019) The July 2019 Ridgecrest, California, earthquake sequence: Kinematics of slip and stressing in cross-fault ruptures. Geophysical Research Letters, 46, 11859–11867. doi: 10.1029/2019GL084741.

Bronk Ramsey, C. (2008) Deposition models for chronological records. Quaternary Science Reviews, 27, 42–60. doi: 10.1016/j.quascirev.2007.01.019.

Bronk Ramsey, C. (2009) Bayesian analysis of radiocarbon dates. Radiocarbon, 51, 337–360. doi: 10.2458/azu_js_rc.v51i1.3494.

Danhara, T., Yamashita, T., Iwano, H., and Kasuya, M. (1992) An improved system for measuring refractive index using the thermal immersion method. Quaternary International, 13–14, 89–91. doi: 10.1016/1040-6182(92)90013-R.

Fujiwara, S., Yarai, H., Kobayashi, T., Morishita, Y., Nakano, T., Miyahara, B., Nakai, H., Miura, Y., Ueshiba, H., Kakiage, Y., and Une, H. (2016) Small-displacement linear surface ruptures of the 2016 Kumamoto earthquake sequence detected by ALOS-2 SAR interferometry. Earth, Planets and Space, 68, 160. doi: 10.1186/s40623-016-0534-x.

Fukushima, Y., and Ishimura, D. (2020) Characteristics of secondary-ruptured faults in the Aso Caldera triggered by the 2016 Mw 7.0 Kumamoto earthquake. Earth, Planets and Space, 72, 175. doi: 10.1186/s40623-020-01306-y.

Goto, H., Tsutsumi, H., Toda, S., and Kumahara, Y. (2017) Geomorphic features of surface ruptures associated with the 2016 Kumamoto earthquake in and around the downtown of Kumamoto City, and implications on triggered slip along active faults. Earth, Planets and Space, 69, 26. doi: 10.1186/s40623-017-0603-9.

Hamling, I.J., Hreinsdóttir, S., Clark, K., Elliott, J., Liang, C., Fielding, E., Litchfield, N., Villamor, P., Wallace, L., Wright, T.J., D'Anastasio, E., Bannister, S., Burbidge, D., Denys, P., Gentle, P., Howarth, J., Mueller, C., Palmer, N., Pearson, C., Power, W., Barnes, P., Barrell, D.J.A., Van Dissen, R., Langridge, R., Little, T., Nicol, A., Pettinga, J., Rowland, J., and Stirling, M. (2017). Complex multifault rupture during the 2016 Mw 7.8 Kaikōura earthquake, New Zealand. Science, 356, 6334. doi: 10.1126/science.aam7194.

He, P., Wen, Y., Xu, C., and Chen, Y. (2019) Complete three-dimensional near-field surface displacements from imaging geodesy techniques applied to the 2016 Kumamoto earthquake. Remote Sensing of Environment, 232, 111321. doi: 10.1016/j.rse.2019.111321.

Himematsu, Y., and Furuya, M. (2020) Coseismic and postseismic crustal deformation associated with the 2016 Kumamoto earthquake sequence revealed by PALSAR-2 pixel tracking and InSAR. Earth, Planets and Space, 7, 1–19. doi: 10.1029/2020EA001200.

Hoshizumi, H., Ozaki, M., Miyazaki, K., Matsuura, H., Toshimitsu, S., Uto, K., Uchiumi, S., Komazawa, M., Hiroshima, T., and Sudo, S. (2004) Geological Map of Japan 1:200,000, Kumamoto. Geological Survey of Japan, AIST.

Inoue, N., Kitada, N., Shibuya, N., Omata, M., Takahama, T., Tonagi, M., and Irikura, K. (2020) Probabilistic Evaluation of Off-Fault Displacements of the 2016 Kumamoto Earthquake. Pure and Applied Geophysics, 177, 2007–2019. doi: 10.1007/s00024-019-02345-7.

Ishimura, D., and Kakiuchi, Y. (2011) Chronology and processes of fluvial terrace formation in northeastern Kinki district, southwest Japan, based on cryptotephra analysis. Quaternary International, 246, 190–202. doi: 10.1016/j.quaint.2011.08.039.

Ishimura, D. (2019) Co-seismic vertical displacement associated with the 2016 Kumamoto earthquake (Mw7.0) and activity of the Futagawa fault around Futa, Nishihara Village, Kumamoto prefecture. Active Fault Resarch, 50, 33–32. (in Japanese with English abstract)

Ishimura, D., Toda, S., Ichihara, T., Takahashi, N., Konno, A., and Sato, H. (2017) A study on surface ruptures around Miyaji, Aso City, Kumamoto Prefecture, associated with the 2016 Kumamoto earthquake sequence and upward slip tapering on pit excavation walls. Active Fault Research, 47, 9–16. (in Japanese with English abstract)

Ishimura, D., Toda, S., Mukoyama, S., Homma, S., Yamaguchi, K., and Takahashi, N. (2019) 3D surface displacement and surface ruptures associated with the 2014 Mw 6.2 Nagano earthquake using differential lidar. Bulletin of the Seismological Society of America, 109, 780–796. doi: 10.1785/0120180020.

Ishimura, D., Tsutsumi, H., Toda, S., Fukushima, Y., Kumahara, Y., Takahashi, N., Ichihara, T., and Takada, K. (2021) Repeated triggered ruptures on a distributed secondary fault system: an example from the 2016 Kumamoto earthquake, Southwest Japan. Earth, Planets and Space, 73 doi: 10.1186/s40623-021-01371-x.

Ishimura, D., Iwasa, Y., Takahashi, N., Tadokoro, R. and Oda, R. (2022) Paleoseismic events and shallow subsurface structure of the central part of the Futagawa fault, which generated the 2016 Mw 7.0 Kumamoto earthquake. Geomorphology, 414, 108387. doi: 10.1016/j.geomorph.2022.108387.

Iwasa, Y., Kumahara, Y., Goto, H., Ishimura, D., and Hosoya, T. (2022) Faulting history of the Futagawa fault zone based on trenching survey at Komori, Nishihara Village, Kumamoto Prefecture. Active Fault Research, 56, 47–58. (in Japanese with English abstract)

Kamata, H., and Kodama, K. (1994) Tectonics of an arc-arc junction: an example from Kyushu Island at the junction of the Southwest Japan Arc and the Ryukyu Arc. Tectonophysics, 233, 69–81. doi: 10.1016/0040-1951(94)90220-8.

Kaneda, H., and Chiba, T. (2019) Stereopaired morphometric protection index red relief image maps (Stereo MPI-RRIMs): Effective visualization of high-resolution digital elevation models for interpreting and mapping small tectonic geomorphic features. Bulletin of the Seismological Society of America, 109, 99–109. doi: 10.1785/0120180166.

Kaneda, H., Toda, S., Ishimura, D., Kumahara, Y., Goto, H., Okada, S., and Kobayashi, M. (2022) Surface Ruptures and Tectonic Geomorphology Along and Around the Idenokuchi Fault. In: Kumahara, Y., Kaneda, H., Tsutsumi, H. (eds) Surface Ruptures Associated with the 2016 Kumamoto Earthquake Sequence in Southwest Japan. Advances in Geological Science. Springer, Singapore. doi: 10.1007/978-981-19-1150-7_12.

King, G., Klinger, Y., Bowman, D., and Tapponnier, P. (2005) Slip-Partitioned Surface Breaks for the Mw 7.8 2001 Kokoxili Earthquake, China. Bulletin of the Seismological Society of America, 95 (2), 731–738. doi: 10.1785/0120040101.

Kokusai Kogyo C o.,Ltd. (2010) 3D-Geomorphic Image Velocimetry. JP Patent No. 4545219.

Kumahara, Y., Okada, S., Kagohara, K., Kaneda, H., Goto, H., and Tsutsumi, H. (2017a) 1:25,000 Active Fault Map, Futagawa-Hinagu Fault Zone and its Vicinity “Kumamoto (Revision)”. Geospatial Information Authority of Japan, Ibaraki. (in Japanese)

Kumahara, Y., Torii, M., Nakata, T., Goto, H., Iwasa, Y., Suzuki, Y., Watanabe, M., Toda, S., Takahashi, N., and Okuno, M. (2017b) Fault History of the Northern Part of Futagawa-Hinagu Fault Zone Based on Trench Survey at Dozon, Mashiki Town and at Kawayo, Minami-Aso Village, Programme and Abstracts JSAF 2017 Fall Meeting, 24–25. (in Japanese)

Kumahara, Y., Kaneda, H., and Tsutsumi, H. (2022) Surface Ruptures Associated with the 2016 Kumamoto Earthquake Sequence in Southwest Japan. Advances in Geological Science. Springer, Singapore. doi: 10.1007/978-981-19-1150-7.

Kumamoto Prefectural Board of Education (2010) Earthquake traces in Onobaru-A site. Onobaru ruins group. In: Cultural Property Investigation Report of Kumamoto Prefecture, 257 (2), 147–149. (in Japanese)

Kumamoto Prefecture Geological Map Compilation Committee (2008) Geological Map of the Kumamoto Prefecture (1:100,000). Kumamoto Prefecture Geotechnical Consultants Association, Kumamoto.

Machette, M.N., Personius, S.F., and Nelson, A.R. (1992) Paleoseismology of the Wasatch fault zone: a summary of recent investigations, interpretations, and conclusions. in Gori, P.L., and Hays, W.W., eds., Assessment of Regional Earthquake Hazards and

Risk Along the Wasatch Front, Utah: U.S. Geological Survey Professional Paper 1500, A1–A71.

Machida, H., and Arai, F. (2003) Atlas of Tephra in and around Japan [revised edition]. University of Tokyo Press, Tokyo.

Matsumoto, Y. (1979) Some problems on volcanic activities and depression structures in Kyushu, Japan. Memoirs of the Geological Society of Japan, 16, 127–139. (in Japanese with English abstract)

McCalpin, J.P. (2009) Paleoseismology. 2nd Edition, Academic Press, Amsterdam-London.

Miyabuchi, Y. (2009) A 90,000-year tephrostratigraphic framework of Aso Volcano, Japan. Sedimentary Geology, 220, 169–189. doi: 10.1016/j.sedgeo.2009.04.018.

Miyoshi, M., Shinmura, T., Sumino, H., Sano, T., Miyabuchi, Y., Mori, Y., Inakura, H., Furukawa, K., Uno, K., Hasenaka, T., Nagao, K., Arakawa, Y., and Yamamoto, J. (2013) Lateral magma intrusion from a caldera-forming magma chamber: Constraints from geochronology and geochemistry of volcanic products from lateral cones around the Aso caldera, SW Japan. Chemical Geology, 352, 202–210. doi: 10.1016/j.chemgeo.2013.06.003.

Moya, L., Yamazaki, F., Liu, W., and Chiba, T. (2017) Calculation of coseismic displacement from lidar data in the 2016 Kumamoto, Japan, earthquake. Natural Hazards and Earth System Sciences, 17, 143–156. doi: 10.5194/nhess-17-143-2017.

Nakata, T., and Imaizumi, T. (2002) Digital Active Fault Map of Japan. University of Tokyo Press, Tokyo. (in Japanese)

Mukoyama, S. (2011) Estimation of ground deformation caused by the earthquake (M 7.2) in Japan, 2008, from the geomorphic image analysis of high resolution LiDAR DEMs. Journal of Mountain Science, 8, 239–245. doi: 10.1007/s11629-011-2106-7.

Muroi, S., Suzuki, Y., Mukoyama, S., Iwasa, Y., Yamashita, H., Muraki, M., Yamashita, K., Fukuba, T. (2024) Surface displacement vector discontinuity in the easternmost part of the Futagawa-Hinagu fault zone analyzed by using airborne laser scanning data at two different timings. Active Fault Research, 60, 11–25. (in Japanese with English abstract)

Nurminen, F., Baize, S., Boncio, P., Blumetti, A.M., Cinti, F.R., Civico, R., and Guerrieri, L. (2022) SURE 2.0 – New release of the worldwide database of surface ruptures for fault displacement hazard analyses. Scientific Data 9, 729. doi: 10.1038/s41597-022-01835-z.

Nurminen, F., Boncio, P., Visini, F., Pace, B., Valentini, A., Baize, S., and Scotti, O. (2020) Probability of Occurrence and Displacement Regression of Distributed Surface Rupturing for Reverse Earthquakes. Frontiers in Earth Science, 8, 581605. doi: 10.3389/feart.2020.581605.

Okamura, Y., Abe, S., Miyashita, Y., Azuma, T., Togo, T., Shirahama, Y., Awata, Y., Maruyama, T., Ogami, T., Imura, R., Tsutsumi, H., Goto, H., and Kumahara, Y. (2018) 3.1 Survey of detailed position and shape of active faults to understand the fault segments and observation to reveal the paleoseismic history and slip rates. In: Research Report of a

Comprehensive Active Fault Survey After the 2016 Kumamoto Earthquake, 2017 Fiscal Year. Ministry of Education, Culture, Sports, Science and Technology and Kyushu University. (in Japanese)

Oohashi, K., Otsubo, M., Matsumoto, S., Kobayashi, K., Sato, K., and Nishimura, T. (2020) The Quaternary tectonics of Central Kyushu and the 2016 Kumamoto Earthquake: from a multifaceted viewpoint combining geology, seismology, and geodesy. Journal of the Geological Society of Japan, 129, 565–589. (in Japanese with English abstract)

Reimer, P.J., Austin, W.E.N., Bard, E., Bayliss, A., Blackwell, P.G., Bronk Ramsey, C., Butzin, M., Cheng, H., Edwards, R.L., Friedrich, M., Grootes, P.M., Guilderson, T.P., Hajdas, I., Heaton, T.J., Hogg, A.G., Hughen, K.A., Kromer, B., Manning, S.W., Muscheler, R., Palmer, J.G., Pearson, C., Van Der Plicht, J., Reimer, R.W., Richards, D.A., Scott, E.M., Southon, J.R., Turney, C.S.M., Wacker, L., Adolphi, F., Büntgen, U., Capano, M., Fahrni, S.M., Fogtmann-Schulz, A., Friedrich, R., K¨ohler, P., Kudsk, S., Miyake, F., Olsen, J., Reinig, F., Sakamoto, M., Sookdeo, A., and Talamo, S. (2020) The IntCal20 Northern Hemisphere radiocarbon age calibration curve (0–55 cal kBP). Radiocarbon, 62, 725–757. doi: 10.1017/RDC.2020.41.

Research Group for Active Faults of Japan, 1980. Active Faults in Japan, Sheet Maps and Inventories. University of Tokyo Press, Tokyo. (in Japanese)

Research Group for Active Faults of Japan, 1991. Active Faults in Japan, Sheet Maps and Inventories, Rev. Ed. University of Tokyo Press, Tokyo. (in Japanese)

Sato, P.H., Komura, K., Une, H., Nakano, T., and Yagi, K. (2021) Study on Cumulative Activities of Passively Ruptured Faults through a Trenching Survey at the Matoishi Bokujo I Fault, Northwest Side of the Aso Caldera, Southwestern Japan. Geographical Review of Japan Series A, 94, 250–264. doi: 10.4157/grj.94.250. (in Japanese with English abstract)

Scott, C.P., Arrowsmith, J.R., Nissen, E., Lajoie, L., Maruyama, T., and Chiba, T. (2018) The M7 2016 Kumamoto, Japan, earthquake: 3-D Deformation along the Fault and within the damage Zone Constrained from Differential Lidar Topography. Journal of Geophysical Research: Solid Earth, 123, 6138–6155. doi: 10.1029/2018JB015581.

Shirahama, Y., Yoshimi, M., Awata, Y., Maruyama, T., Azuma, T., Miyashita, Y., Mori, H., Imanishi, K., Takeda, N., Ochi, T., Otsubo, M., Asahina, D., and Miyakawa, A. (2016) Characteristics of the surface ruptures associated with the 2016 Kumamoto earthquake sequence, Central Kyushu, Japan. Earth, Planets and Space, 68, 191. doi: 10.1186/s40623-016-0559-1.

Smith, V.C., Staff, R.A., Blockley, S.P.E., Bronk Ramsey, C., Nakagawa, T., Mark, D.F., Takemura, K., and Danhara, T. (2013) Identification and correlation of visible tephras in the Lake Suigetsu SG06 sedimentary archive, Japan: chronostratigraphic markers for synchronising of east Asian/west Pacific palaeoclimatic records across the last 150 ka. Quaternary Science Reviews, 67, 121–137. doi: 10.1016/j.quascirev.2013.01.026.

Suzuki, T., Kasahara, A., Nishizawa, F., and Saito, H. (2014) Chemical characterization of volcanic glass shards by energy dispersive X-ray spectrometry with EDAX Genesis

APEX2 and JEOL JSM-6390. Geographical reports of Tokyo Metropolitan University, 49, 1–12.

Suzuki, Y., Ishimura, D., Kumaki, Y., Kumahara, Y., Chida, N., Nakata, T., and Nakano, T. (2017) 1:25,000 Active Fault Map, Futagawa-Hinagu Fault Zone and its Vicinity "Aso". Geospatial Information Authority of Japan, Ibaraki. (in Japanese)

Takahashi, N., Ishimura, D., Toda, S., Nakata, T., and Watanabe, M. (2017) Vertical slip rate on a normal fault co-ruptured with the Futagawa fault at the 2016 Kumamoto earthquake. Active Fault Research, 46, 27–32. (in Japanese with English abstract).

Toda, S., Kaneda, H., Okada, S., Ishimura, D., and Mildon, Z.K. (2016) Slip-partitioned surface ruptures for the Mw 7.0 16 April 2016 Kumamoto, Japan, earthquake. Earth, Planets and Space, 68, 188. doi: 10.1186/s40623-016-0560-8.

Toda, S., Torii, M., Okuno, M., Konno, A., Ono, H., and Takahashi, N. (2019) Evidence for Holocene paleoseismic events on the 2016 Kumamoto earthquake rupture zone within the Aso caldera: a trench excavation survey at Kurokawa, the town of Minami-Aso, Southwest Japan. Active Fault Research, 51, 13–25. (in Japanese with English abstract)

Tsutsumi, H., Toda, S., Goto, H., Kumahara, Y., Ishimura, D., Takahashi, N., Taniguchi, K., Omata, M., Kohriya, Y., Gomi, M., Asano, K., and Iwata, T. (2018) Paleoseismic trenching across the surface rupture of the 2016 Kumamoto earthquake at Jichu, Mashiki Town, Kumamoto Prefecture. Active Fault Research, 49, 31–39. (in Japanese with English abstract)

Ueta, K., Miyawaki, R., Iemura, K., Yokoyama, T., and Miyawaki, A. (2018) Paleoseismological study on surface fault ruptures produced by the 2016 Kumamoto earthquake. In: Abstracts of Japan Geoscience Union Meeting 2018, Makuhari Messe, Chiba. (in Japanese with English abstract).

Watanabe, K. and Ono, K. (1969) Geology of the vicinity of Omine on the western flank of the Aso caldera. Journal of the Geological Society of Japan, 75, 365–374. (in Japanese with English abstract)

Xu, X., Sandwell, D.T., and Smith-Konter, B. (2020) Coseismic Displacements and Surface Fractures from Sentinel-1 InSAR: 2019 Ridgecrest Earthquakes. Seismological Research Letters, 91, 1979–1985. doi: 10.1785/0220190275.

Yamada, K., Takemura, K., Kuwae, M., Yamamoto, M., and Danhara, T. (2017) Revised ages of late Holocene tephras in Beppu Bay, central Kyushu, southwest Japan. Quaternary International, 452, 33–42. doi: 10.1016/j.quain t.2017.01.024.

Paleoseismic trenching on slip-partitioned surface ruptures associated with the 2016 Kumamoto earthquake: Implications for simultaneous rupturing of the primary, subsidiary, and secondary active faults

Daisuke Ishimura [1,*], Naoya O Takahashi [2], Hiroyuki Tsutsumi[3], Shin'ichi Homma[4], Sakae Mukoyama[4], and Toshihiko Ichihara[5]

[1] Department of Earth Sciences, Chiba University, 1-33 Yayoi-cho, Inage-ku, Chiba 263-8522, Japan
[2] Department of Earth Science, Tohoku University, 6-3 Aoba, Aoba-ku, Sendai 980-8578, Japan
[3] Department of Environmental Systems Science, Doshisha University, 1-3 Tataramiyakodani, Kyotanabe, Kyoto 610-0394, Japan
[4] Department of Research & Development of Kokusai Kogyo Co., Ltd., 2-24-1 Harumi-cho, Fuchu, Tokyo 183-0057, Japan
[5] Department of Disaster Prevention & Geology of Hopedesign Co., Ltd., 3-5 Shuri-Akatacho, Naha, Okinawa 903-0813, Japan
[*]Corresponding author: ishimura@chiba-u.jp

Author ORCIDs

Daisuke Ishimura: 0000-0002-4798-3425
Naoya Takahashi: 0000-0003-4196-1409

Author contributions

Conceptualization: D. Ishimura
Data Curation: N. Takahashi, S. Homma, S. Mukoyama
Formal Analysis: D. Ishimura, S. Homma, S. Mukoyama
Funding Acquisition: D. Ishimura
Investigation: D. Ishimura, N. Takahashi, H. Tsutsumi, T. Ichihara
Methodology: D. Ishimura, S. Homma, S. Mukoyama
Project Administration: D. Ishimura
Resources: D. Ishimura
Software: S. Homma, S. Mukoyama
Supervision: H. Tsutsumi
Validation: D. Ishimura
Visualization: D. Ishimura, N. Takahashi
Writing – original draft: D. Ishimura
Writing – review & editing: N. Takahashi, H. Tsutsumi, S. Homma, S. Mukoyama

Abstract

Surface ruptures appear over a wide area in addition to the primary fault during a Large earthquake like the 2016 Kumamoto earthquake. Although the displacement of such distributed surface ruptures is small, information on their paleo activities provides clues for evaluating displacement hazard risk and whether they can be used as a paleoseismic history of the primary fault. We conducted LiDAR differencing analysis and trench excavation on the Idenokuchi fault, which was activated simultaneously with the primary Futagawa fault, during the 2016 Kumamoto earthquake, and where a slip partition occurred. First, we clarified the 3D displacement field by LiDAR differencing and discussed quantitatively how the slip partition occurred on both faults. We found that deep oblique slip is completely split into horizontal and vertical components at the ground surface and inferred that the Idenokuchi fault is structurally connected to the Futagawa fault. Then, we excavated a trench on the conjugate surface rupture of the Idenokuchi fault and identified eight faulting events since 15 ka. Finally, we revealed a reliable activity history since 7.3 ka. Our results indicate that the Futagawa fault has ruptured relatively periodically and many surface ruptures have appeared in the last few events, like the 2016 event.

Second language abstract: 要旨 (日本語)

2016 年熊本地震のような大地震の際に主断層周辺に加えて幅広い範囲に断層が出現することがある．そのような断層の変位は小さいが，その過去の活動の情報は変位ハザードリスクや主断層の活動履歴の復元に有用かどうかの評価に関して手がかりを与えてくれる．そこで我々は LiDAR 差分解析とトレンチ掘削調査を 2016 年熊本地震の際に布田川断層と同時に活動しスリップパーティションが生じたとされた出ノ口断層で実施した．まず，LiDAR 差分により 3 次元変位場を求め，定量的に両断層でスリップパーティションが生じたかどうかを議論した．その結果，深部の斜めすべりが地表では完全に水平と鉛直成分に分割されたことが明らかとなり，出ノ口断層は構造的に布田川断層と地下でつながっていることが推定された．また，出ノ口断層の共役断層上でトレンチ掘削した結果，15 ka 以降に 8 回のイベントを推定し，最終的に 7.3 ka 以降の信頼たる活動時期を明らかにした．この結果は布田川断層が比較的周期的に活動したことと，最近数回のイベントでは 2016 年同様に多くの断層が地表に出現したことを示唆する．

Third language abstract: NA

Non-technical summary

We conducted a geomorphological differencing analysis using pre- and post-earthquake topography and trench excavation on the Idenokuchi fault, which was activated simultaneously with the primary Futagawa fault, during the 2016 Kumamoto earthquake, Japan. First, we clarified the 3D displacement field by geomorphological differencing and quantitatively discussed how displacement was partitioned on active faults. We found that deep oblique slip is completely split into horizontal and vertical components at the ground surface and inferred that the Idenokuchi fault is structurally connected downdip to the Futagawa fault. Second, we excavated a trench on the surface rupture of the Idenokuchi fault and identified eight faulting events since about 15,000 years ago. Our results indicate that the Futagawa fault has ruptured relatively periodically and many surface ruptures have appeared in the last few events.

1. Introduction

Recent developments in remote sensing technology (e.g., SAR and optical correlation) have enabled the distribution and amount of ground surface displacement associated with earthquakes to be captured with high resolution and precision. As a result, it has become clear that the distribution of surface ruptures by earthquakes is not simple but complex when viewed in detail, and in some cases, they appeared over an extensive area (e.g., 2016 Kumamoto earthquake, 2016 Kaikoura earthquake, and 2019 Ridgecrest earthquake). Various terms, such as primary, secondary, and subsidiary surface ruptures/faults, have been used to describe ~~such~~ complex surface ruptures in previous studies. Recently, Nurminen et al. (2020, 2022) categorized principal, distributed, and sympathetic faults for hazard assessment. However, it is difficult to adopt the classification, and there are many cases in which it is not unambiguously determined. In any case, a hierarchical relationship between primary and secondary surface ruptures/faults (in the broader sense of the term) has been recognized in surface ruptures and active faults. While surface ruptures and active faults in such a secondary relationship are also important for evaluation when considering displacement hazard, it has not been sufficiently verified whether such surface ruptures and faults have repeatedly occurred in the past due to the activity of the primary fault.

InSAR analysis indicated that surface ruptures appeared over a wide area around the main (primary) fault in the 2016 Kumamoto earthquake (Fujiwara et al., 2016) as well as the 2016 Kaikoura earthquake (e.g., Hamling et al., 2017) and 2019 Ridgecrest earthquake (e.g., Barnhart et al., 2019; Xu et al., 2020). In Kumamoto's case, field surveys confirmed surface displacements and/or deformations at the InSAR

discontinuities (Goto et al., 2017; Ishimura et al., 2017; Okamura et al., 2018; Sato et al., 2021). The Idenokuchi and Miyaji faults ~~especially~~ represent ~~such characteristics of surface ruptures.~~ The Idenokuchi fault runs parallel to the Futagawa fault. Along this parallel running section, right-lateral displacement occurred on the Futagawa fault and vertical displacement occurred on the Idenokuchi fault, which Toda et al. (2016) inferred that the dextral and vertical components of the fault slip were partitioned into the two faults. Therefore, the Futagawa and Idenokuchi faults are considered to merge at ~~the deeper part; that is,~~ the Idenokuchi fault is structurally related to the Futagawa fault. On the other hand, the Miyaji faults (Fig. 1; Ishimura et al., 2021) have the same strike and displacement sense as the Futagawa fault but are not connected to the Futagawa fault according to the fault model inferred from the InSAR analysis (Fukushima and Ishimura, 2020), and are considered surface ruptures caused by triggered slip. This indicates that various factors may have contributed to the surface ruptures around the Futagawa fault during the 2016 Kumamoto earthquake.

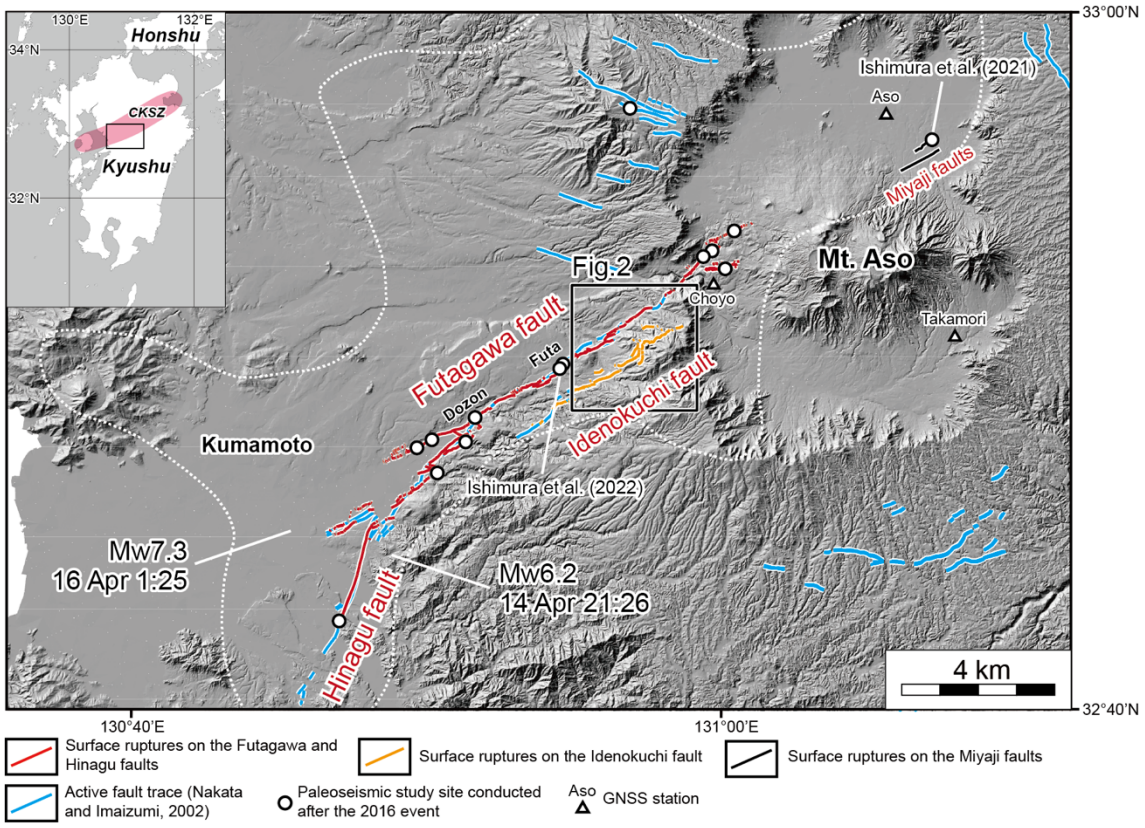

Figure 1. Spatial relationships among the primary Futagawa–Hinagu rupture zones and previously mapped active fault traces. Locations of the surface ruptures along the Futagawa, Hinagu, Idenokuchi, and Miyaji faults are from Kumahara et al. (2022). Previously mapped active fault traces are from Nakata and Imaizumi (2002). Red and orange lines indicate primary and subsidiary surface ruptures as defined in this study. The dotted line encloses the area where lineaments indicating secondary surface ruptures were identified by InSAR (Fujiwara et al., 2016). The Miyaji faults (Ishimura et al., 2021) are examples of the many secondary surface ruptures associated with the 2016 event. In this study, we defined the Kiyama, Futagawa, and Kitamukiyama faults, previously mapped by the Research Group for Active Faults of Japan (1991), as the Futagawa fault. CKSZ, Central Kyushu Shear Zone (Oohashi et al., 2020).

A paleoseismic survey conducted on the Miyaji faults revealed that the fault moved about 2,000 years ago, which coincides with the previous activity of the Futagawa fault (Ishimura et al., 2021). Their results suggest that the slip on the Miyaji faults was repeatedly triggered by the Futagawa fault in the past. In addition, trenching surveys on surface ruptures in the outer rim of the Aso caldera and on other short surface ruptures

also showed activity preceding the 2016 event (Inoue et al., 2020; Sato et al., 2021), suggesting that these surface ruptures appeared not only during the 2016 event but appeared repeatedly. Because the smaller displacement of such surface ruptures compared to that of the primary surface ruptures does not displace sediments much, they are expected to record paleoseismic history more clearly and for a more extended period in trench walls and outcrops if the sedimentation rate is sufficiently fast. In fact, on the Miyaji faults, the fast sedimentation rate and multiple tephra layers of distinct age and lithology due to its location downwind of the Aso volcano have allowed us to reveal the amount and timing of past vertical displacement of about 15 cm with high accuracy (Ishimura et al., 2021). Therefore, paleoseismic investigations on such surface ruptures could provide long-term and more accurate paleoseismic history information than on the primary fault and enable us to examine their simultaneity with it.

In this study, we conducted ~~a~~ paleoseismic trenching of the Idenokuchi fault, which has a strong structural relationship with the primary Futagawa fault. Using digital terrain models (DTMs) before and after the earthquake, we calculated the three-dimensional displacement across the Futagawa and Idenokuchi faults and examined whether slip partitioning occurred and, if so, what the distribution of displacement partitioning was like. We then discussed the slip partition on the Idenokuchi fault, clarified the relationship between the Futagawa and Idenokuchi faults, and revealed the paleofaulting history of the Idenokuchi fault. Finally, we compared the paleofaulting history of the Idenokuchi fault with that of the Futagawa and Miyaji faults and discussed the simultaneity of these faults' activity. This study ~~would~~ provide important insights into the past activities of secondary faults visualized by recent technological improvements

(especially relative to the activities of the primary fault) and their value as new paleoseismic survey sites and displacement hazards on secondary faults. In addition, there are few examples of slip partitions occurring in a single earthquake on inland active faults (King et al., 2005), and this study can provide a valuable case study on such a relationship on the faults.

2. Definition of primary, subsidiary, and secondary surface ruptures/faults in the 2016 Kumamoto earthquake

In this study, we defined primary, subsidiary, and secondary surface ruptures/faults in the 2016 Kumamoto earthquake according to the criteria by Ishimura et al. (2022). A surface rupture or fault that is clearly a branch of the primary fault (e.g., a surface rupture that occurs locally around the primary surface rupture) or that has been pointed out to be a branch of the primary fault (e.g., Idenokuchi fault; Toda et al., 2016) is defined as a subsidiary surface rupture/fault (Fig. 1). A surface rupture or fault that is located away from the primary and subsidiary surface ruptures is defined as a secondary surface rupture/fault (e.g., Miyaji faults, black lines in Fig. 1; Ishimura et al., 2021). Although it is difficult to define the threshold of distance from the primary and subsidiary surface ruptures for a fault to be considered secondary, most of the surface ruptures detected by InSAR (distributed within the area enclosed by the white dotted line in Fig. 1) are likely to be defined as secondary surface ruptures (Fujiwara et al., 2016), except those on the Futagawa, Hinagu, and Idenokuchi faults. These secondary surface ruptures characterized the 2016 Kumamoto earthquake. Some of them have also been confirmed in the field (Goto et al., 2017; Ishimura et al., 2017; Okamura et al., 2018; Sato et al., 2021).

3. Regional Settings

Central Kyushu, where a north-south extension has been ongoing since 6 Ma (Kamata and Kodama, 1994), is structurally characterized by the Beppu-Shimabara graben (Matsumoto, 1979). This area is characterized by many east-west-striking normal faults (Research Group for Active Faults of Japan, 1991) and high levels of volcanic activity. According to Oohashi et al. (2020), central Kyushu has been a transtensional tectonic zone, which they call the Central Kyushu Shear Zone, since 1 Ma (Fig. 1), characterized by dextral faults, rift zones, and volcanism.

The Futagawa fault (Fig. 1) is a ca. 25-km-long active dextral strike-slip fault (Watanabe and Ono, 1969; Research Group for Active Faults of Japan, 1980, 1991; Nakata and Imaizumi, 2002; Kumahara et al., 2017a; Suzuki et al., 2017) and generated the mainshock (Mw 7.0) of the 2016 Kumamoto earthquake sequence on April 16, 2016. Primary surface ruptures appeared during the mainshock along the previously mapped active fault traces (Fig. 1; Kumahara et al., 2022). A large dextral displacement (~2 m) was observed from Dozon to Futa along the central part of the Futagawa fault, and a maximum dextral displacement of 2.5 m was observed at Dozon (Fig. 1; Shirahama et al., 2016; Okamura et al., 2018; Kumahara et al., 2022). The slip rate of the Futagawa fault for the area around Futa is 1.5–3.7 mm/yr for the right lateral slip and 0.9–1.1 mm/yr for the vertical slip (Ishimura, 2019).

The Idenokuchi fault is a 10-km-long active dip-slip fault mainly up on the south (Research Group for Active Faults of Japan, 1980, 1991; Nakata and Imaizumi, 2002),

and moved during the mainshock of the 2016 Kumamoto earthquake (Fig. 1; Kumahara et al., 2022). Multiple surface ruptures, including conjugate faults, appeared along the fault. The maximum vertical displacement was 2 m (south up), and the average vertical displacement was about 1 m (Kaneda et al., 2022). Toda et al. (2016) assumed that the slip-partition was caused by the oblique slip on the deep part of the Futagawa fault between the parallel running section of the Futagawa and Idenokuchi faults because horizontal displacement occurred on the Futagawa fault and the vertical displacement occurred on the Idenokuchi fault. The slip rate of the Idenokuchi fault has not been determined.

The three-dimensional deformation caused by the 2016 event has been revealed by InSAR and differential light detection and ranging (LiDAR) analyses (Moya et al., 2017; Scott et al., 2018; He et al., 2019; Himematsu and Furuya, 2020; Aoyagi et al., 2021; Muroi et al., 2024). In particular, LiDAR differencing provides higher resolution and more accurate displacement information in areas with larger displacements than InSAR analysis. Although it has been conducted by Scott et al. (2018), Aoyagi et al. (2021), and Muroi et al. (2024) along the portion and extension of the Futagawa fault, it has not been obtained in the area where the slip partition occurred, which is the focus of this ~~study, and~~ how the amount of displacement due to the slip partition is distributed has not been obtained until now in the world.

4. Methods and Data

4.1 LiDAR differencing

We applied 3D-Geomorphic Image Velocimetry method (Kokusai Kogyo Co., Ltd., 2010) for LiDAR differencing. In this method, the particle image velocimetry method and pre- and post-event DTMs (Fig. 2) were used to calculate the surface displacement vectors according to Mukoyama (2011) and Ishimura et al. (2019). Aoyagi et al. (2021) and Muroi et al. (2024) used this method for the eastern extension of the Futagawa fault inside the Aso caldera. The method procedure is as follows. First, we prepared slope-shaded images using pre- and post-event DTMs. Next, we carried out a grid search by moving a pre-event image in a pixel-by-pixel manner in the scanning area on the post-event image and estimated the position that exhibits the highest value of the coefficient of correlation using subpixel interpolation. Additionally, we calculated the horizontal component of displacement and estimated the vertical component using the elevation values from DTMs with interpolation calculation around the head and tail of each horizontal vector. Subsequently, we slid the search area in steps and repeated the image matching and calculation of the 3D displacement. Finally, we plotted the complete 3D vectors on maps. In this study, the search area size, search area step size, and output grid size were set to be 64 x 64 pixels (128 x 128 m), 5 m, and 5 x 5 m, respectively. Additionally, the theoretical error of this analysis is 0.1 pixel (0.2 m) due to subpixel interpolation in the displacement calculation.

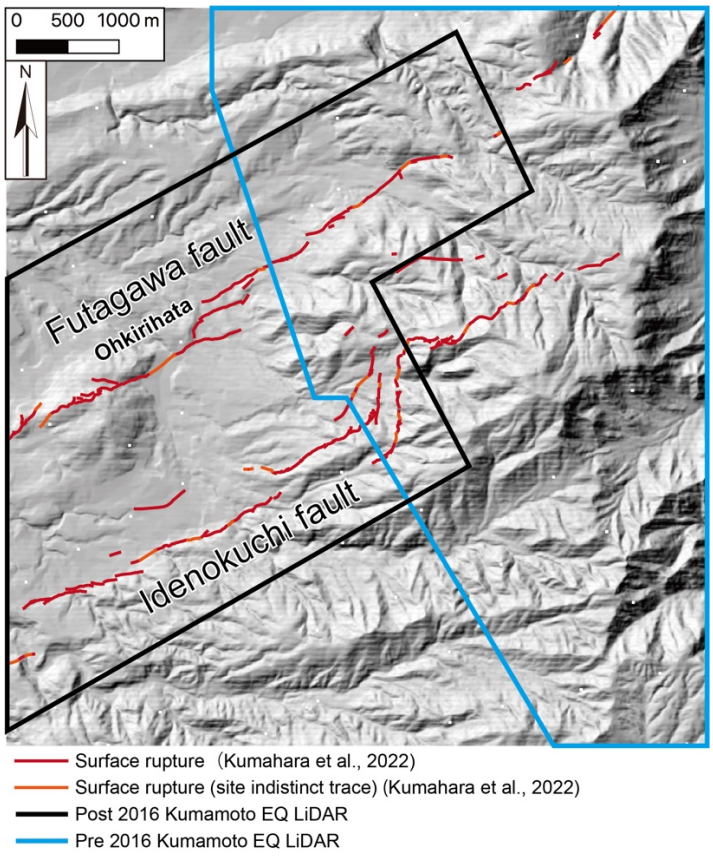

Figure 2. LiDAR measurement areas.

The DTMs we used were 2-m grid DTM taken from January 2013 to February 2014 and 2-m grid DTM taken on 8 May 2016. Although we do not possess the original point cloud data of pre- and post-earthquake datasets, nor have the details for constructing the DTMs from the original point cloud data, all the DTMs were tested and examined under the regulations required for a public LiDAR survey in Japan. We used the Japan plane rectangular coordinate system II (in meters) for the horizontal data and as the coordinate system for all data.

The expected ground motions during the measurement period are as follows: (1) the deformation associated with the 2016 Kumamoto earthquake, (2) the postseismic deformation (e.g., aftershocks and afterslip), (3) the background tectonic deformation, and (4) the artificial modification and present-day surface processes. We evaluate the deformation of items 2 and 3 using the GNSS observations in the study area. Based on the GNSS stations at the Choyo (960701), Aso (960703), and Takamori (960704) of GeoNET, the postseismic and background deformations (vertical, north-south, and east-west components) from April 2010 to May 2016 are nearly equal of the theoretical error level (0.2 m). Thus, the deformations associated with items 2 and 3 are negligible.

4.2 Trench survey

We looked for an appropriate site for a paleoseismic excavation survey along the Idenokuchi fault (Fig. 2). We selected possible survey sites based on the following criteria: 1) little artificial modification, 2) clear surface rupture traces, and 3) stable and continuous soil deposition. As a result, we selected a trench excavation site on a gentle slope between conjugate surface ruptures of the Idenokuchi fault, expecting trapped sediment and stable and continuous soil deposition (Fig. 3). The trench site is on a clear single surface rupture (north-up normal fault), and another surface rupture (south-up normal fault) runs parallel at its southeast side. Currently, the fields are cow ranches with few artificial modifications.

We excavated a 13-m-long, 5-m-wide, and 3.5-m-deep trench (Fig. 3; KMR trench) and established a grid system on the trench walls. We logged the walls and collected samples for tephra analyses and radiocarbon dating. To further examine the subsurface geology, we used a handy corer 50 cm long and 4 cm wide to obtain seven cores from the trench floor and upthrown side (Fig. S1). The Nikon Nivo5.SC total station was used to map the locations of surface ruptures, trench, and coring sites (Fig. 3b).

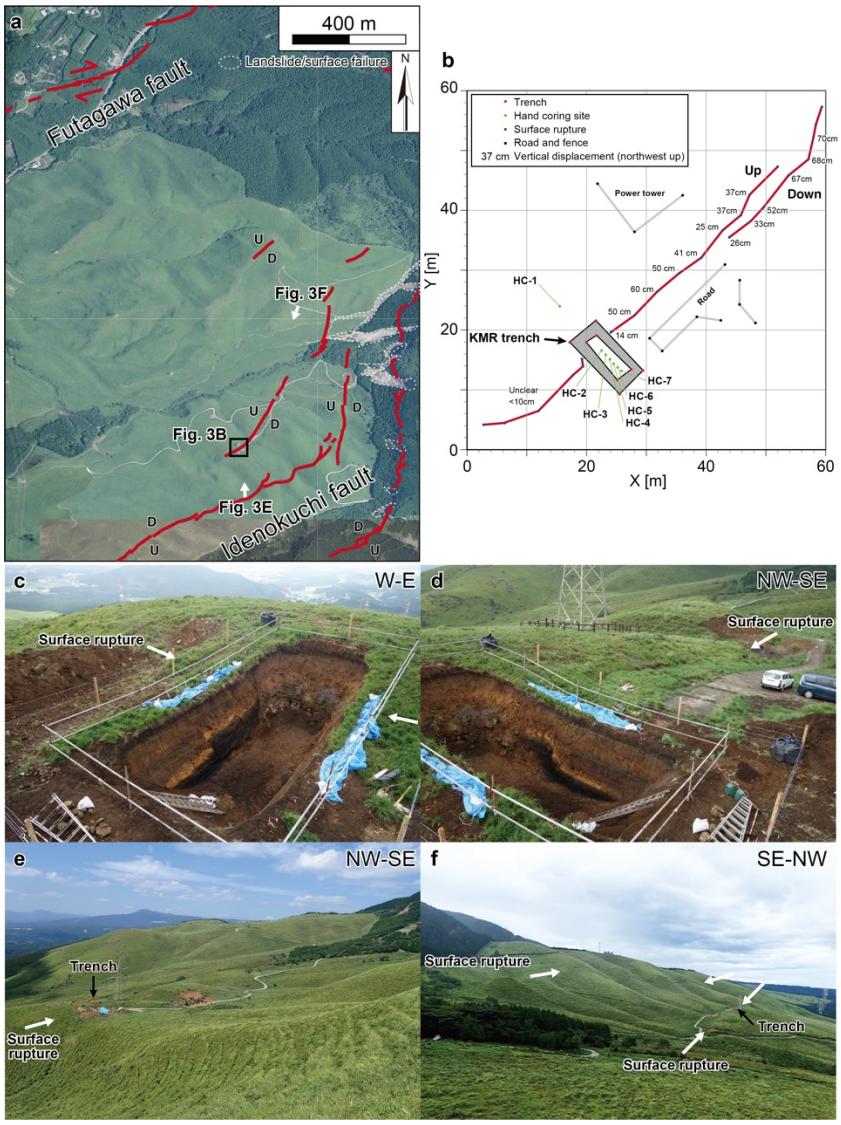

Figure 3. Geomorphic map and photographs around the trench site. (a) Red lines show the 2016 surface ruptures (Kumahara et al., 2022). Aerial photographs are from the Geospatial Information Authority of Japan. (b) Location map of the trench and surface ruptures. (c) West wall of the trench. (d) East wall of the trench. (e) (f) Geomorphology around the Idenokuchi fault. Photo locations are shown in Fig. 3a.

4.3 Laboratory analysis

We determined refractive indices and major element compositions of volcanic glass shards in sampled tephras. First, we sieved the samples with water through a 62-μm nylon mesh. Then, we oven-dried the samples at 50 ℃ and sieved the dried samples through a 120-μm nylon mesh. The refractive index of volcanic glass shards in the 62–120 μm fraction of each sample was measured with a RIMS 2000 refractive index measuring system (Kyoto Fission Track Co., Ltd.) with an accuracy of ±0.0002 (Danhara et al., 1992). The major element composition of volcanic glass shards was measured by energy-dispersive X-ray spectrometry (EDAX Genesis APEX2 and JEOL JSM-6390) following the method and analysis conditions described by Suzuki et al. (2014). Volcanic glass shards of the AT tephra sampled at Chigaki, Toyama Prefecture (Machida and Arai, 2003) were used as a working standard to check data reproducibility and instrument stability.

A total of 26 radiocarbon samples of charcoal and organic sediment were dated by accelerator mass spectrometry at the Laboratory of Radiocarbon Dating, the University Museum, the University of Tokyo, and the Institute of Accelerator Analysis Ltd., Japan. The obtained age data were calibrated using the OxCal 4.4 software (Bronk Ramsey, 2009) with the IntCal20 dataset (Reimer et al., 2020). The ages of paleofaulting events were calculated in the OxCal program by Bayesian analysis (Bronk Ramsey, 2008).

5. Results

5.1 3D displacement

Figure 4 shows the distribution of 3D displacement, and Figure 5 shows the cross-sections of the A-D lines. In the cross-sections (Fig. 5), the horizontal component is divided into two components: one parallel to the general strike of the Futagawa fault (N57°E) and the other perpendicular to it. The vertical component (Figs. 4B and 5) shows a displacement of 1.0–2.5 m at the southernmost part of the Idenokuchi fault and a vertical displacement of several tens of centimeters at the northern part of the fault. Compared to field measurements (Kaneda et al., 2022), a similar displacement was measured along the southernmost branch of the Idenokuchi fault, where a 2 m vertical displacement was observed. However, the amount of vertical displacement along the fault is noisy and subject to uncertainty because of slope failures in the surrounding area. Along the conjugate fault of the Idenokuchi fault, where we excavated the KMR trench, there is no significant difference between the calculated and field-measured displacements in the field. On the other hand, on the Futagawa fault, the amount of local vertical displacement associated with the dextral displacement is observed in a narrow section about 200 m wide. Still, almost no vertical displacement is observed when viewed over 200–400 m wide from the fault, ~~virtually no vertical displacement is observed~~. The vertical displacement along the long baseline (> 3 km) between both the Futagawa and Idenokuchi faults is south-up of about 1 m (Lines A and B in Fig. 5).

Regarding the fault-parallel component (Figs. 4B and 5), a large displacement was observed on the Futagawa fault, and 1.8–3.1 m of dextral displacement occurred on the

western part of the calculated area. Since the displacement measured in the field was about 1.5–2.0 m (Shirahama et al., 2016; Kumahara et al., 2022), the 3D displacement data can be used to determine the amount of off-fault displacement in addition to the on-fault displacement. This trend has also been discussed by Scott et al. (2018), and in the western part of the Futagawa fault, larger dextral displacements were obtained for the long baseline (1 km) than for the short baseline (35 m and 100 m). Although it is difficult to read from the 3D displacement distribution map (Fig. 4B), a slight sinistral displacement occurred on the Idenokuchi fault, which is consistent with the field measurements (Toda et al., 2016; Shirahama et al., 2016; Kaneda et al., 2022). In the eastern half of the calculation area, the contrast in displacement is smaller, the amount of displacement decreases, and there is greater variability because surface failures and other factors may have also occurred. The dextral displacement along the long baseline (> 3 km) between both faults is about 2–2.5 m.

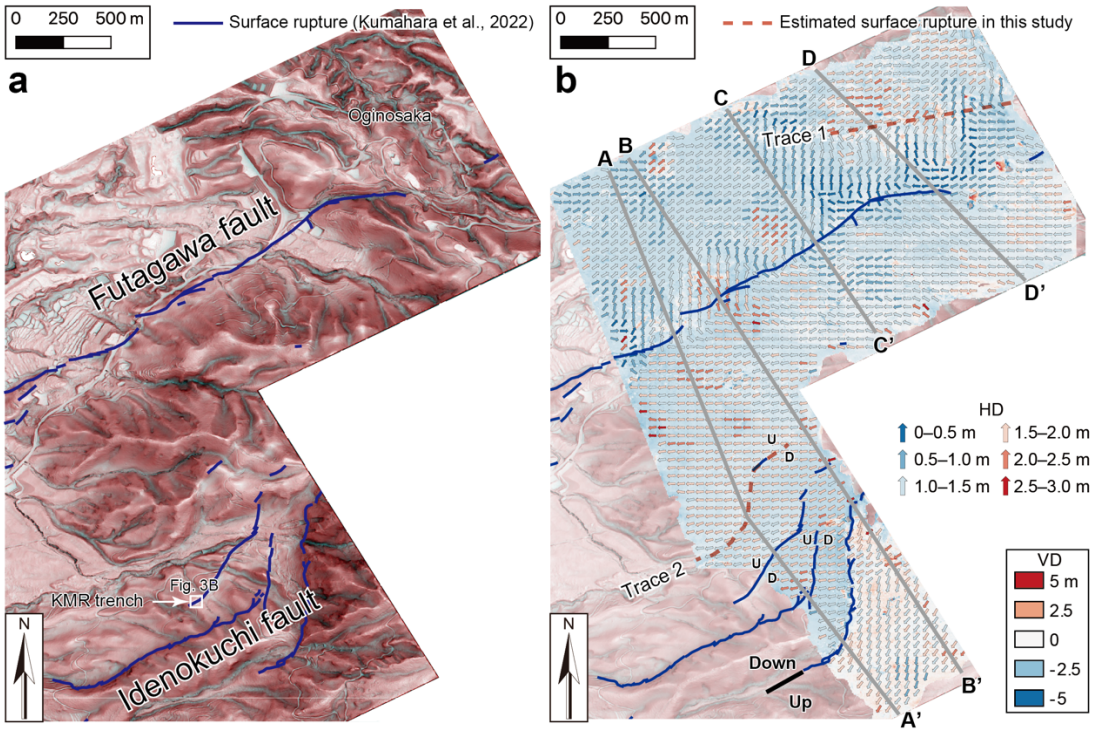

Figure 4. Results of the differential LiDAR analysis. (a) Red relief image map around the study area. The map was created based on Kaneda and Chiba (2019). Surface ruptures are after Kumahara et al. (2022). (b) 3D displacement fields. Vertical displacement is shown by the color map. Horizontal displacement is indicated by the arrow and color. HD: horizontal displacement, VD: vertical displacement.

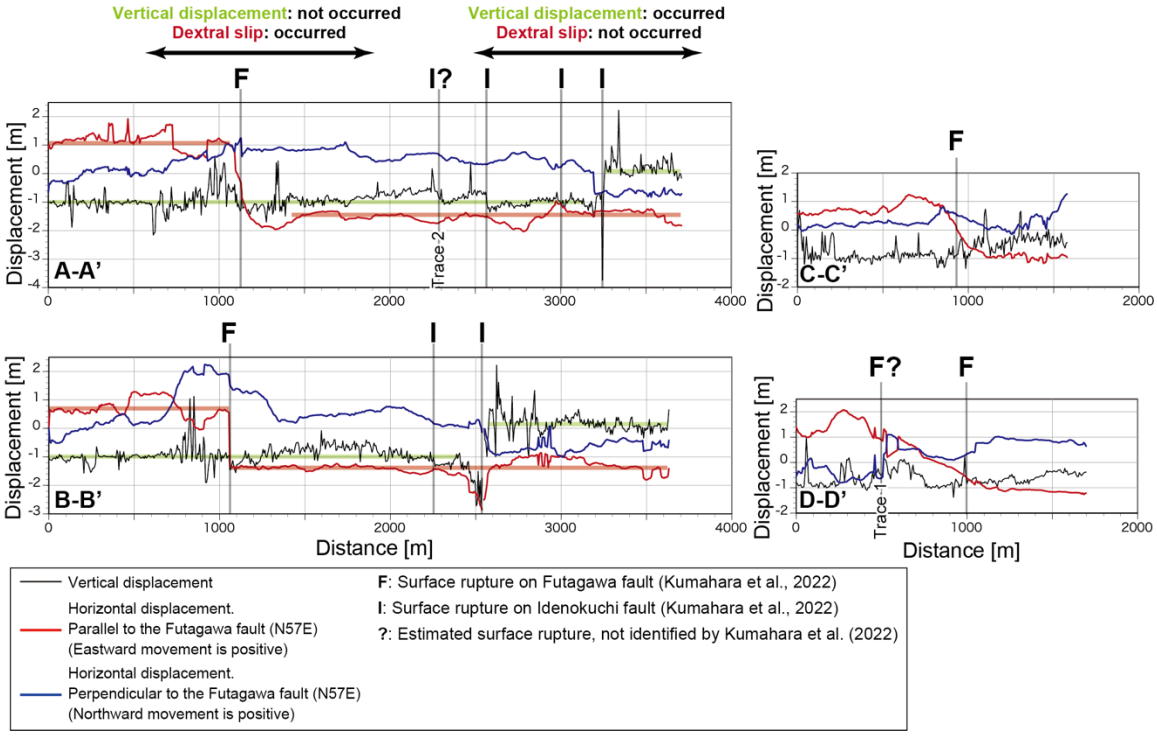

Figure 5. Vertical and horizontal displacement profiles. The profile lines are shown in Figure 4b.

Regarding the fault-perpendicular component (Figs. 4B and 5), an extension occurred locally on the Idenokuchi fault, and a contraction occurred locally on the Futagawa fault. The extension is large at the southernmost part of the Idenokuchi fault, with a displacement of about 1–1.5 m. The contraction of about <1 m occurred on the Futagawa fault. The displacement in the perpendicular direction of the fault along the long baseline (> 3 km) across both faults is about 1 m of extension.

The 3D displacement and field measurements generally agreed regarding the locations of surface ruptures and the amount and sense of displacements. On the other hand, two locations where surface ruptures were deduced in areas not confirmed in the field were recognized, and each trace was named Trace 1 and Trace 2 (Fig. 4B). Trace 1 is the eastern part of the Futagawa fault in the calculated area. Here, contrasts in fault parallel and perpendicular components are observed, although they are indistinct. Although it is unclear whether a well-defined fault has appeared, this eastern extension is connected to a surface rupture that continues into the caldera (Kumahara et al., 2022). It is also consistent with the 2 m shortening identified abutments in the bridge at Oginosaka (Fig. 4) (Shirahama et al., 2016). Trace 2 is an extension of the short displacement recognized at the northernmost part of the Idenokuchi fault. Here, a discontinuity in vertical displacement is recognized. However, it is consistent with the present valley topography and may have been affected by fluvial erosion and other factors during the DTM measurement period.

5.2 Trench

5.2.1 Sediments description (including tephra analysis)

Figure 6 shows photomosaics and sketches of the west, east, and north walls. In this trench, sediments with different sedimentary facies and ages are distributed on the north (up-thrown side) and south (down-thrown side) sides across the primary normal fault at W9/E9. For this reason, the north and south sides are assigned different unit numbers except for the topsoil (unit 00). The following describes the sediments from the upper part on the south side.

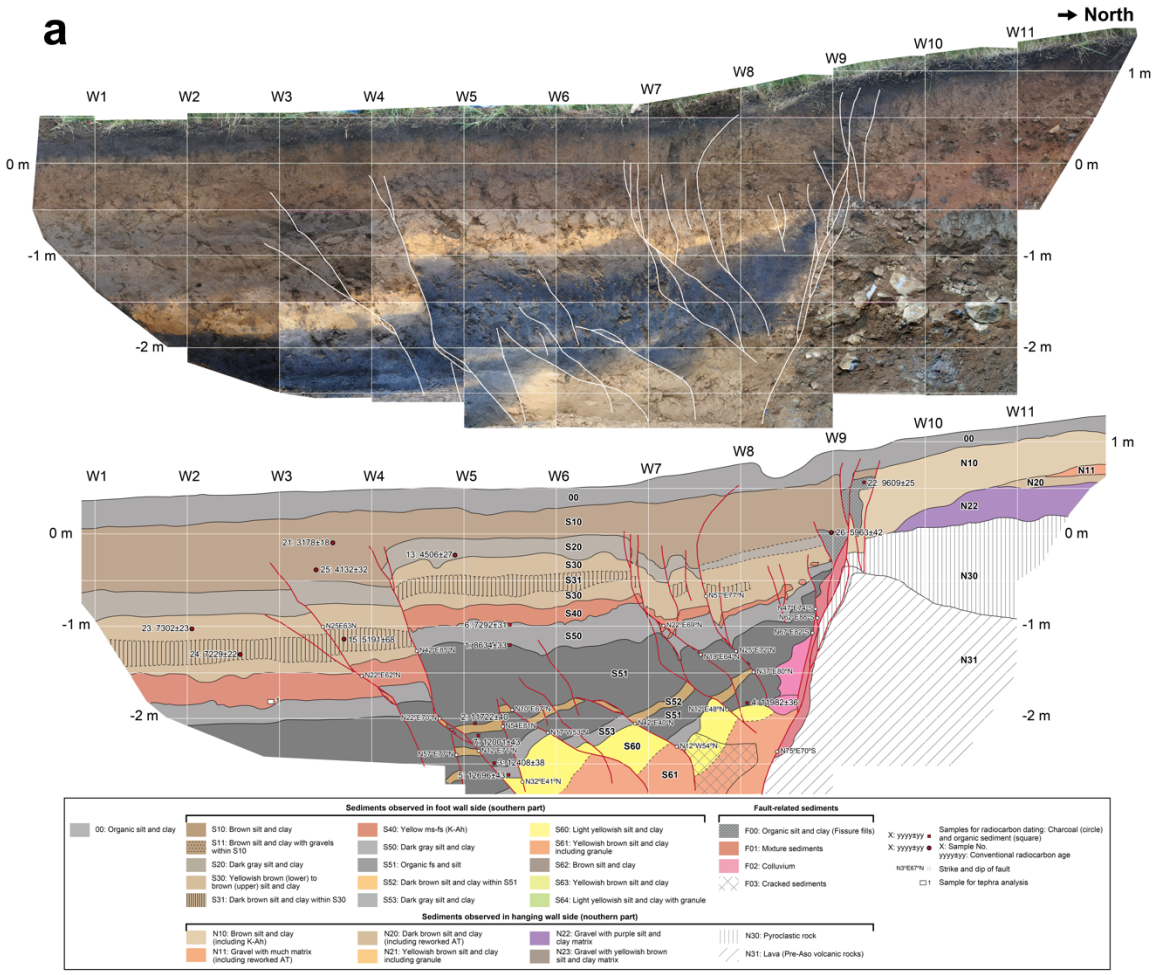
a
North
W1
W2
W3
W4
W5
W6
W7
W8
W9
W10
W11
0 m
-1 m
-2 m
1 m
00
S10
S20
S30
S31
S40
S50
S51
S52
S53
S60
S61
N10
N11
N20
N22
N30
N31
21: 3178±18
25: 4132±32
13: 4506±27
23: 7302±23
15: 5197±68
6: 7292±31
1: 8634±33
24: 7229±22
22: 9609±25
26: 5863±42
4: 11082±36
2: 11774±41
7: 12001±42
3: 12408±38
5: 12069±43
Sediments observed in foot wall side (southern part)
00: Organic silt and clay
S10: Brown silt and clay
S11: Brown silt and clay with gravels within S10
S20: Dark gray silt and clay
S30: Yellowish brown (lower) to brown (upper) silt and clay
S31: Dark brown silt and clay within S30
S40: Yellow ms-fs (K-Ah)
S50: Dark gray silt and clay
S51: Organic fs and silt
S52: Dark brown silt and clay within S51
S53: Dark gray silt and clay
S60: Light yellowish silt and clay
S61: Yellowish brown silt and clay including granule
S62: Brown silt and clay
S63: Yellowish brown silt and clay
S64: Light yellowish silt and clay with granule
Fault-related sediments
F00: Organic silt and clay (Fissure fills)
F01: Mixture sediments
F02: Colluvium
F03: Cracked sediments
Sediments observed in hanging wall side (nouthern part)
N10: Brown silt and clay (including K-Ah)
N11: Gravel with much matrix (including reworked AT)
N20: Dark brown silt and clay (including reworked AT)
N21: Yellowish brown silt and clay including granule
N22: Gravel with purple silt and clay matrix
N23: Gravel with yellowish brown silt and clay matrix
N30: Pyroclastic rock
N31: Lava (Pre-Aso volcanic rocks)
X: yyyyyyy
X: yyyyyyy
Samples for radiocarbon dating: Charcoal (circle) and organic sediment (square)
X: Sample No.
yyyyyyy: Conventional radiocarbon age
N3°E67°N
Strike and dip of fault
1
Sample for tephra analysis

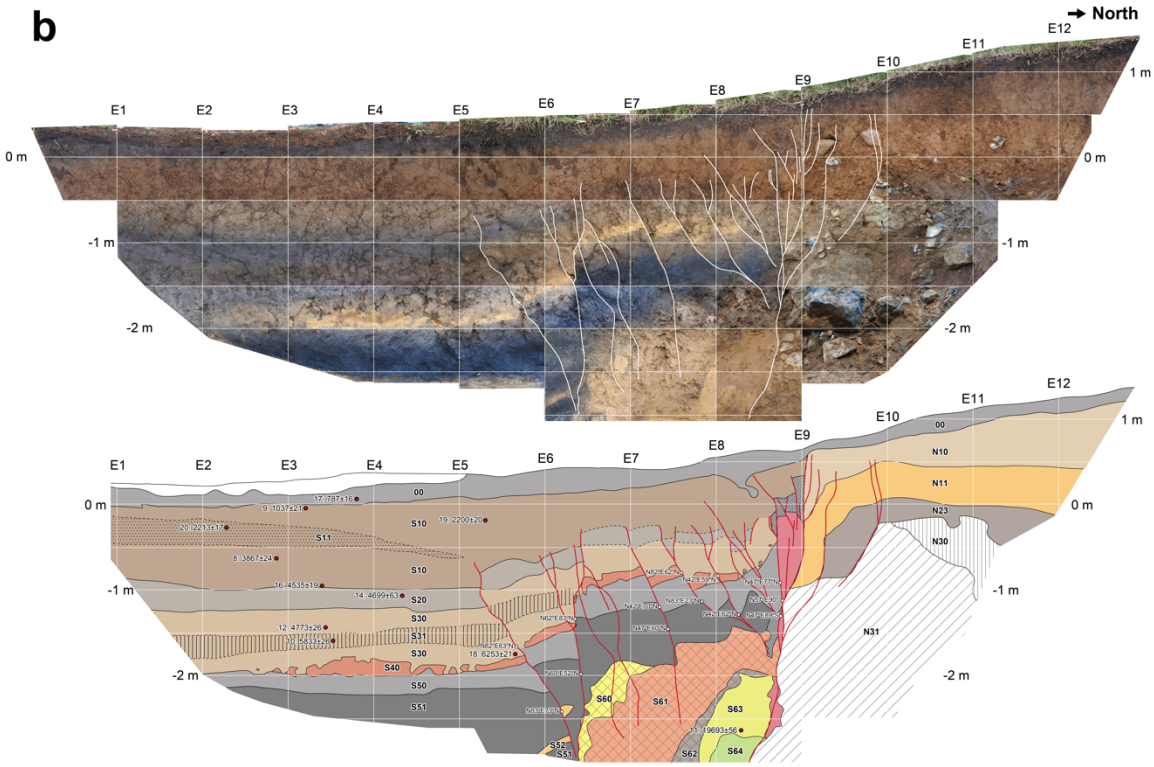
b
North
E1
E2
E3
E4
E5
E6
E7
E8
E9
E10
E11
E12
1 m
0 m
-1 m
-2 m
00
N10
N11
N23
N30
N31
S10
S11
S20
S30
S40
S50
S51
S52
S60
S61
S62
S63
S64

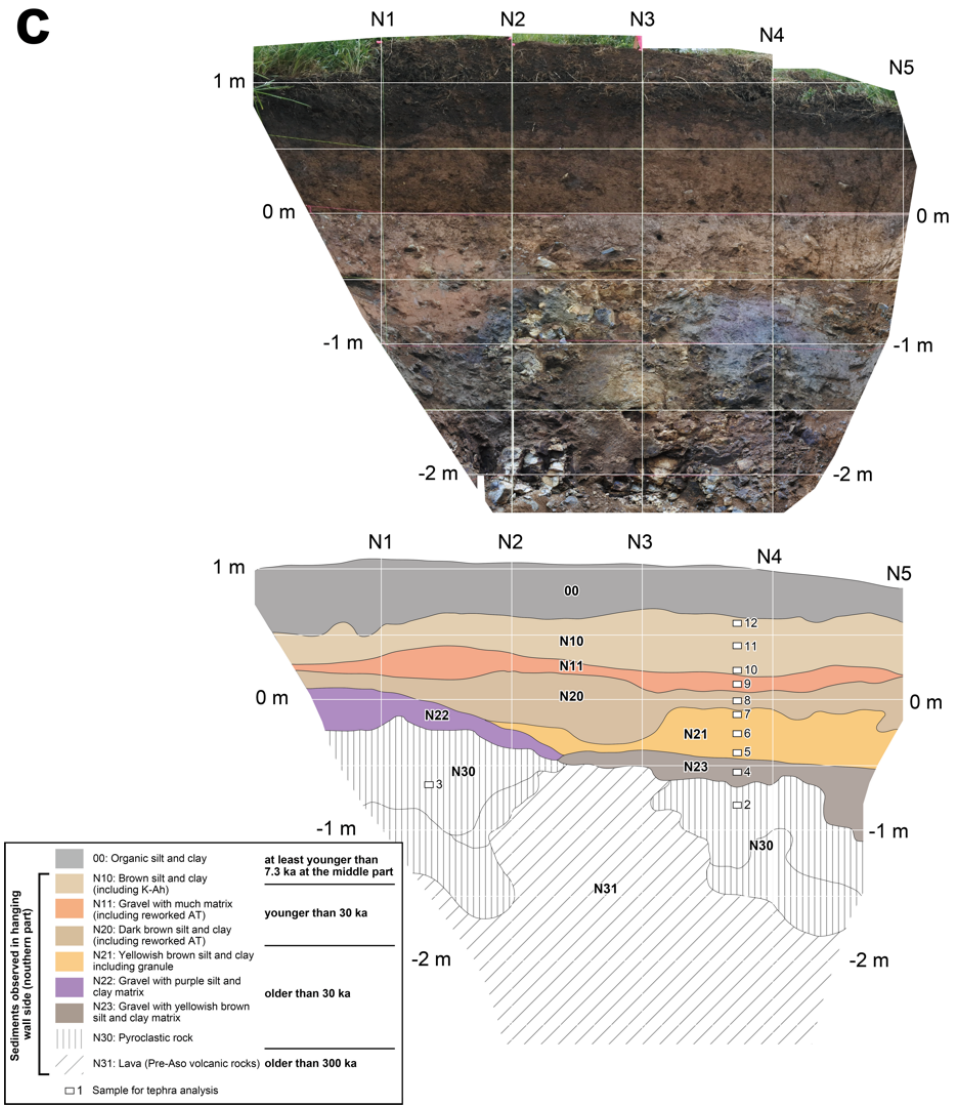

Figure 6. Photomosaics and sketches of the KMR trench walls. (a) West wall. The sketch of the west wall is flipped. (b) East wall. (c) North wall.

On the south side, the sediments were deposited continuously, mainly because it is on the down-thrown side of the fault (Fig. 6). Unit 00 is the topsoil and consists of black organic silt and clay. Unit S10 is a thick, brown silt and clay below unit 00. On the east wall, an unclear layer containing gravel within unit S10 was classified as unit S11. Unit S20 is a dark gray silt and clay and is considered an organic-rich paleosol. Unit S30 is a

yellowish brown to brown silt and clay with a slightly darker unit S31 within the thicker portion of unit S30 at the south side of the trench walls. Unit S31 is also considered an organic-rich paleosol like unit S20. Unit S40 is yellow fine to medium sand, mainly composed of volcanic glass. Unit S50 is dark gray silt and clay, and unit S51 is organic silt and fine sand, with unit S50 slightly lighter than unit S51. Unit S52 is yellowish brown to brown silt and clay, partially observed on the south side of the thicker part of unit S51. Unit S53, which is observed only in the west wall, is a slightly lighter gray silt and clay similar to unit S50. The base of unit S53 is undulating, and a time gap is inferred between units S53 and S60. Unit S60 is a bright yellowish silt and clay, and unit S61 is a yellowish brown silt and clay with granules. In the west wall, unit S61 is the lowest (oldest) sediments. Unit S62 is brown silt and clay, unit S63 is yellowish brown silt and clay, and unit S64 is light yellowish silt and clay with granules on the east wall.

On the north side, the sediments are thinner than on the south side and are composed of gravel and rock (Fig. 6c). Unit N10, consisting of brown silt and clay, shows a time gap with unit N11 and lower units (see west wall in Fig. 6a). Unit N11 is a matrix-rich gravel bed. Units N20 and N21 are dark brown and yellowish brown silt and clay, respectively. Both units N22 and N23 are gravel beds containing a lot of matrix with different colors. Unit N30 is pyroclastic rock, and its base shows undulating contact. Unit N31 is fragmented lava and is considered to be pre-Aso volcanic rock that forms the basement rock of the surrounding area (Hoshizumi et al., 2004).

The coring results (Fig. S1) showed that on the upthrown side (HC-1), the same stratigraphy is recognized at almost the same depth as on the north wall. Therefore, the sediments on the north wall are considered to be distributed widely and uniformly on the

northern side of the fault. On the downthrown side (HC-2 to HC-7), the black silt and clay and yellowish brown to brown silt and clay, corresponding to unit S51 and lower, were also observed as well as on the trench walls. No black soil, corresponding to units S51 to S53, was observed at depths greater than 1 m from the trench floor. Gravel and sand beds, not recognized in trench walls, were observed in some cores. However, no tephra layers were identified. On the other hand, sediments were in contact with high angles, and voids were observed in some cores, where we inferred faults. The primary normal fault was considered the boundary with the basement rock, so we inferred the normal fault at a depth where drilling was no longer possible.

5.2.2 Faults

In this trench, the primary normal fault is observed at W9/E9, and many other faults were rootless with bending in the lower part. Faults extending down to the trench bottom are the north-up normal faults at W9/E9 and the reverse faults at W3-W5 and E5-E6. Normal fault groups that form grabens develop at W7-W9 and E7-E10. The 2016 displacement was an open crack near W9/E9, which was already filled with sediments. Such 2016 open cracks and fissure fill sediments have also been identified in the Futa trench at Futa (Fig. 1; Ishimura et al., 2022). However, no other distinct 2016 displacement (e.g., apparent vertical displacement) was observed in the trench walls. This is likely because the trench is located in an area of decreasing vertical displacement from northeast to southwest (Fig. 3b), where the 2016 displacement is small and indistinct. Other fissure-fill sediments that may have been formed by the pre-2016 activity are also identified below the 2016 fissure-fill sediments. Measurements of the strike and dip of faults on the trench walls

indicate that the main strike is northeast to southwest, but some are north to south or east-northeast to west-southwest (Fig. 6). The northeast-southwest strike is consistent with the surface ruptures (Fig. 3b). The other strike directions suggest that subsidiary surface ruptures to the primary normal fault were present in the past events.

5.2.3 Tephra analysis

The results of the tephra analysis are shown in Table S1, and the major element composition of volcanic glass shards is shown in Tables S2 and S3. The results show that unit S40 is composed almost entirely of volcanic glass, with a refractive index of 1.510-1.512 (mode: 1.511), suggesting that it correlates with the widespread tephra, Kikai-Akahoya (K-Ah), by the eruption of southern Kyushu at 7.3 ka (Machida and Arai, 2003; Smith et al., 2013). The chemical compositions confirmed this correlation (Table S2), consistent with the existing studies in the vicinity (e.g., Ishimura et al., 2022). Volcanic ash analysis of the samples from the north wall revealed no tephra layers. Therefore, we examined the volcanic glass content and its refractive index to determine if the samples contain volcanic glass shards from Aira-Tn (AT) (30 ka; Smith et al., 2013) and K-Ah tephras, which are commonly identified widespread tephras in this area (Machida and Arai, 2003). The results show almost no volcanic glass below unit N21, while units N20 and N11 show very low volcanic glass content (2%). The refractive indices of volcanic glass are mainly 1.495-1.500, which correlates with AT tephra. In contrast, the volcanic glass content increases from the lower to the upper part of unit N10. The refractive indices show that while unit N10 contains 1.497-1.500 of AT origin, the percentage of volcanic glass of 1.508-1.512 of K-Ah origin increases toward the upper part of unit N10.

This suggests that the age of the middle part of unit N10 is after the K-Ah tephra. This mixing of AT and K-Ah volcanic glass is also observed in soils in other regions, and the K-Ah ash fall horizon is roughly estimated at the peak of K-Ah volcanic glass shard content (Ishimura and Kakiuchi, 2011). Such distribution of volcanic glass shard content may be due to bioturbation and secondary deposition of tephra-origin particles. Based on the presence of AT volcanic glass, unit N20 is at least younger than 30 ka, and unit N21 and below are older than 30 ka. Based on the K-Ah glass content, the upper to middle part of unit N10 is interpreted to be at least younger than 7.3 ka. The fact that K-Ah tephra is visible on the south side indicates that the sediments' deposition rate and preservation potential differ from north to south across the primary normal fault, as already mentioned.

5.2.4 Radiocarbon dating

Because the faulting events described below were identified on the down-thrown side of the primary normal fault, radiocarbon dating of samples collected from the south side of the trench walls was performed (Table S4). The youngest age was 787 ± 16 yr BP (charcoal) from unit 00, and the oldest was 19693 ± 56 yr BP (charcoal) from unit S63. For sediments older than unit S50, bulk samples (organic sediments) were used except for the sample from unit S63. As Ishimura et al. (2022) pointed out, the ages of the bulk samples in this region sometimes show younger than the actual ages. In this trench, we compared the bulk sample ages with the ages of the K-Ah tephra and the charcoal from unit S63. As a result, the bulk sample ages were consistent with the tephra and charcoal age, and there was no contradiction between the stratigraphy and age. Because we used

charcoal samples for radiocarbon dating to determine the ages above unit S30, it is possible that older charcoals were included by reworking, resulting in older ages. In such cases, charcoals with younger ages in the same unit were employed for further analyses. As a result, we did not use the ages of Nos. 23 and 24 samples (Table S4). Additionally, the ages of the open cracks were determined from the bulk samples, which are older than the surroundings. Therefore, the ages of these fissure-fill sediments are also not used.

6. Discussions

6.1 Slip partition based on 3D displacements

In this section, we discuss how the displacement is divided on both faults for the slip partition with line A (Fig. 5), where the influence of surface failure is small, and the Futagawa fault appeared as a single trace (Fig. 4). First, dextral displacement occurred only on the Futagawa fault, and local sinistral displacement is observed along the Idenokuchi fault. However, along the long baseline (> 3 km), no lateral displacement occurred on the Idenokuchi fault. On the other hand, the vertical displacement is the opposite of the lateral displacement. Vertical displacement of 1 m occurred only in the southernmost trace of the Idenokuchi fault along the long baseline, and little vertical displacement occurred in the 1 km width across the Futagawa fault. Vertical displacement of several tens of centimeters occurred on the conjugate faults of the Idenokuchi fault, but that decreased with distance from the fault. These suggest that extensional deformation and block rotation cause apparent vertical displacement on the conjugate faults.

Based on these observations, the slip partition on the Futagawa and Idenokuchi faults is considered to be the result of oblique lateral displacement at depth, which is

almost completely split into dextral and vertical displacement near the surface and accommodated by both faults, respectively, as shown schematically by Toda et al. (2016). In addition, our results show that the displacement is completely split, as mentioned in King et al. (2005). This may provide an important insight into the geometry (dip angle, distance of two faults, and amount of oblique displacement) of faults where slip partitioning can occur. In other words, the deeper part of the Idenokuchi fault is connected to the deeper part of the Futagawa fault, and the Idenokuchi fault is a branch fault of the Futagawa fault. The estimated depth at which they merge may be several kilometers, as shown by Toda et al. (2016), although it depends on their dip angles. This means that the two faults can be treated as a single source fault when assessing seismic hazards of active faults. Therefore, the paleoseismic history of the Idenokuchi fault should be consistent with that of the Futagawa fault, given its subsurface structure. In Scott et al. (2018) and Himematsu and Furuya (2020), large vertical displacement (1-2 m south-up) was observed on the Futagawa fault on the west side of the parallel section of the Futagawa and Idenokuchi faults. This indicates that the Futagawa fault has accommodated oblique slip on the west side of the Idenokuchi fault's parallel section. In addition, Himematsu and Furuya (2020) showed a sharp decrease in vertical displacement and nearly unchanged right lateral displacement along the Futagawa fault at the parallel section of the Idenokuchi fault, which is consistent with our results.

We discuss the relationship between slip partition and geology. King et al. (2005) mentioned the relationship between the slip partition and geology; the depth at which the fault branches into two could coincide with the bottom of surface sediments. Aoyagi et al. (2024) reported another slip partition on the western part of the Futagawa fault based on

the surface rupture distribution of the 2016 event, drilling cores, and seismic reflection survey. They reported that the subparallel surface ruptures/faults consumed oblique slip in the deeper part in the 2016 Kumamoto earthquake and converged at a depth of 350 m. The depth corresponds to that of the pre-Aso volcanic rocks and/or Kiyama metamorphic rocks (Kumamoto Prefecture Geological Map Compilation Committee, 2008) and there are unconsolidated sediments, including pyroclastic flow deposits from middle to late Pleistocene above these rocks. Thus, the upper end depth (convergent depth of both faults) of oblique slip ~~faults~~ seems to correspond to some geological (physical property) difference. In our study area, unlike the study area of Aoyagi et al. (2024), pre-Aso volcanic rocks are exposed on the surface around the Idenokuchi fault, deeper geology (e.g., Kiyama metamorphic rocks) may constrain the convergent depth of both faults.

6.2 Paleofaulting events on the Idenokuchi fault

We interpreted faulting events since unit S53 deposition by retrodeformation (Fig. 7 and S2) because soils develop continuously (Table S4). Ev0 is the 2016 event, and an open crack occurred directly above the primary normal fault near W9 (Fig. 6a). In the 2016 event, a further open crack was formed in the open crack formed by Ev1, which is described below, and was already filled with ~~the deposit.~~ Although no vertical displacement can be identified on the trench walls, it is clear from the mapping of surface ruptures that vertical displacement occurred here. Similarly, an open crack directly above the primary normal fault near E9 is recognized on the east wall (Fig. 6b).

Ev1, like Ev0, developed an open crack directly above the primary normal fault near W9 and was filled by fissure-fill deposits. This event is considered to have occurred during the deposition of unit S10. The bulk of this fissure-fill deposit was dated (Sample No. 22 (9609 ± 25 yr BP)), but this age is not used to estimate the age of the Ev1 because it is older than its surroundings.

In Ev2, an open crack, normal fault displacements near the primary normal fault (W7-W9), and reverse fault displacements on the southern faults (W3-W4) occurred. This event occurred after the deposition of unit S20 paleosol and during the deposition of unit S10. Similarly, on the east wall, normal fault displacements were observed near the primary normal fault (E7-E9), and the faults in the south (E5-E6) show reverse fault displacements. In addition, a gravel-rich unit S11 is recognized in unit S10 on the east wall, which is wedge-shaped and may be a deposit supplied from the southern slope due to surface failures. Therefore, unit S11 may be a post-earthquake deposit related to Ev2. Thus, the event horizon of Ev2 is estimated to be after unit S20 and before unit S11. This also confirms that the age of Ev1 is after unit S11 and during unit S10.

Ev3, like Ev2, shows normal fault displacements near the primary normal fault (W7-W9) and reverse fault displacements on the southern faults (W3-W4). The east wall similarly shows normal fault displacements at (E7-E9) and reverse fault displacements at the southern faults (E5-E6). The event horizon of Ev3 is estimated to be between units S20 and S31 since the fault at W3 displaces unit S31 but does not displace unit S20.

Ev4 is indistinct in the west wall, while it is distinct in the east wall, with reverse fault displacement on the lower surface of unit S50 near E6 and normal fault

displacements at E8-E9 (Fig. S2). The event horizon of Ev4 is estimated to be during the deposition of unit S50.

Ev5 and Ev6 are estimated after unit S52 deposition while the upper part of unit S51 is being deposited. During this period, reverse and normal fault displacements are observed in W4-W8. The reverse fault displacements occurred in Ev2-Ev4, and normal fault displacements occurred in Ev7, as described below. Considering the similarity of the displacement patterns, reverse fault motion was grouped as Ev5 and normal fault motion was grouped as Ev6. These normal and reverse fault displacements are considered to have occurred separately rather than simultaneously. Therefore, we interpreted that at least two events occurred during this period. Since the ages of Ev5 and Ev6 cannot be distinguished, both events are only constrained after unit S52 and during unit S51 deposition.

In Ev7, a normal fault displacement at W7-W8 occurred at the lowest part of the soil deposits in this trench. Its age is between unit S52 and S53 deposition.

From these interpretations, eight faulting events (including the 2016 event) were recognized in this study since unit S53 deposition. The ages of the faulting events were obtained using OxCal (Fig. S4). The results show that Ev1: 2190–940 cal BP, Ev2: 4760–4250 cal BP, Ev3: 6040–5360 cal BP, Ev4: 9550–7280 cal BP, Ev5-Ev6: 13500–9680 cal BP, Ev7: 14700–13840 cal BP in the 2σ range. The average recurrence interval is 1990–2110 years. Unit S53 is buried 4.5–5 m below the present ground surface, indicating that the average buried amount is about 0.6 m per event. This value is roughly consistent with a representative coseismic displacement of 60 cm along the surface rupture in the 2016

event in case the downthrown side is buried by the same amount as the coseismic vertical displacement in each event.

We also examined why the reverse fault displacement was observed in this normal fault trench. Such subsidiary reverse faults in the primary normal fault displacements are generally considered "pseudreverse faults" (McCalpin, 2009), and it is considered to be an apparent reverse fault when the normal fault exceeds 90°, that is, “overturns,” near the ground surface. In this study, such a reverse fault is also apparent, with little compression, and gravity is considered a contributing factor. A similar one is recognized in Ev0 (2016 event) in the west wall. However, deformation at Ev2-Ev4 is characterized by the formation of graben near the primary normal fault and the southern reverse faults, which differs from the aforementioned explanation by McCalpin (2009). Therefore, we attempted to explain the deformation by assuming a block diagram shown in Figure 8.

The 3D displacement results show that the displacement around the trench indicates that the ratio of vertical to extensional displacement is 2:1. Therefore, we considered this ratio of fault displacement and displaced blocks 1 to 3 (Fig. 8). We assumed the displacement of each block like this; The block 1 was displaced 100%, block 2 was displaced 50%, and Block 3 was displaced 0%. Then, block 2 collapses to the downthrown side, as shown in Fig. 8b. Block 3 then falls between Block 2 and the primary normal fault. This causes graben-like displacement near the primary normal fault and an apparent reverse fault between blocks 2 and 3. Furthermore, in this trench, some rootless faults are bent at depth, and this kind of bending can also be explained by this block model. In reality, the red area in Figure 8 is not void, so the fault bends, and the displacement is distributed by minor faults. A similar displacement was described in the

trench on the Wasatch fault (Machette et al., 1992). Their trench was excavated to a greater depth (8 m) than ours and showed a reverse fault branching from the primary normal fault to the downthrown side. This reverse fault is behind the primary normal fault and is different from an apparent reverse fault, which is the normal fault exceeding 90° near the ground surface, as suggested by McCalpin (2009).

Then, we considered why such displacement occurs and suggested that tephric soil and sediments may be a factor. Because soil and sediments near the ground surface including many tephric particles (e.g., volcanic glass and clay minerals) are very sticky, when normal fault displacement occurs, the shallow part (blocks 2 and 3) cannot fall as far as the deep part along the fault plane.

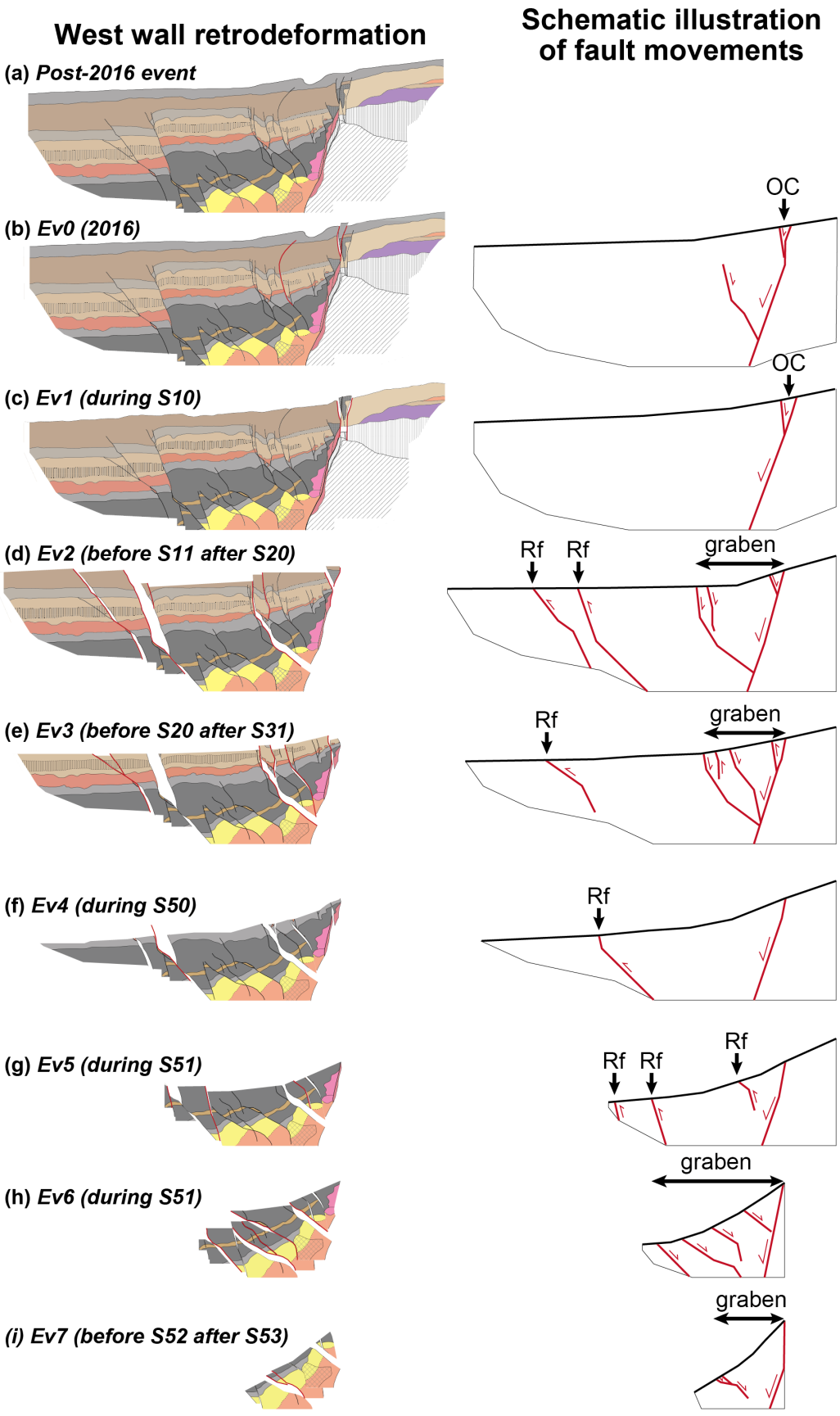
West wall retrodeformation
Schematic illustration of fault movements
(a) Post-2016 event
(b) Ev0 (2016)
(c) Ev1 (during S10)
(d) Ev2 (before S11 after S20)
(e) Ev3 (before S20 after S31)
(f) Ev4 (during S50)
(g) Ev5 (during S51)
(h) Ev6 (during S51)
(i) Ev7 (before S52 after S53)
OC
OC
Rf
Rf
graben
Rf
graben
Rf
Rf
Rf
graben
graben

Figure 7. Retrodeformation of the faults and schematic illustration of fault movements on the west wall. The left figures show reconstructions of the displacement for each event, and the right figures show the faults that were active during that event. Rf: reverse fault, OC: open crack.

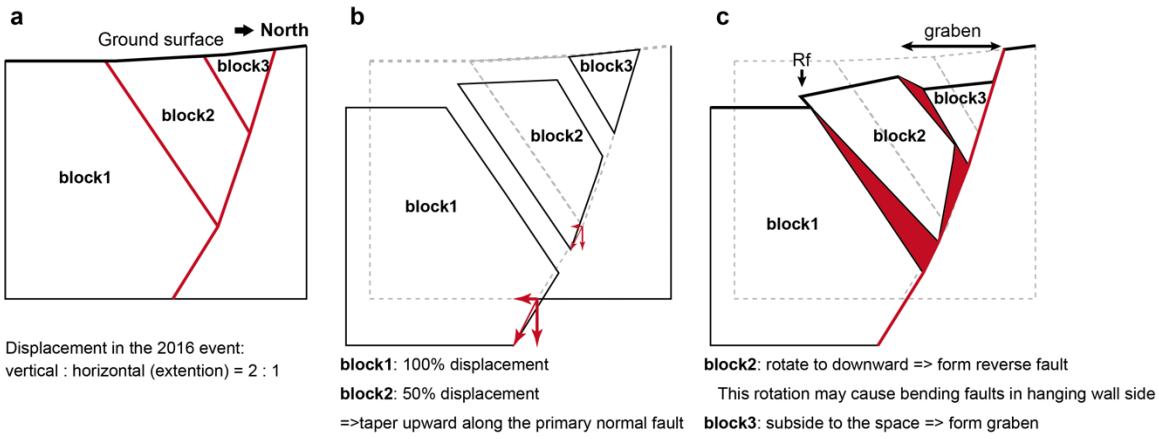

605

Figure 8. Schematic illustration explaining how the graben and apparent reverse faults were formed in the trench.

6.3 Comparison of paleoseismic events between the Futagawa and other faults

A summary of the paleofaulting history by the author's group (Fig. 9) shows that the ages of faulting events after the K-Ah tephra all overlap. This suggests that the Futagawa fault (Ishimura et al., 2022), Miyaji faults (Ishimura et al., 2021), and Idenokuchi fault have all moved simultaneously at least in the recent past. In particular, as shown in section 6.1, the Idenokuchi fault accommodates the vertical component of oblique slip in the deep part of the Futagawa fault, and the subsurface structure suggests that the Futagawa and Idenokuchi faults moved at the same time. The Miyaji faults that produced the 2016 surface rupture, which is distant from the Futagawa fault and seems structurally discontinuous (Fukushima and Ishimura, 2020), are also presumed to have been active in the past with the Futagawa fault. The relationship between the primary and secondary

faults has not been sufficiently discussed in paleoseismological studies for simultaneity. To analyze rupture process scenarios seen in the interlocking ruptures such as the 2016 Kaikoura earthquake and induced displacements such as the 2019 Ridgecrest earthquake, paleoseismic investigations focusing on such secondary and small displacements are also necessary.

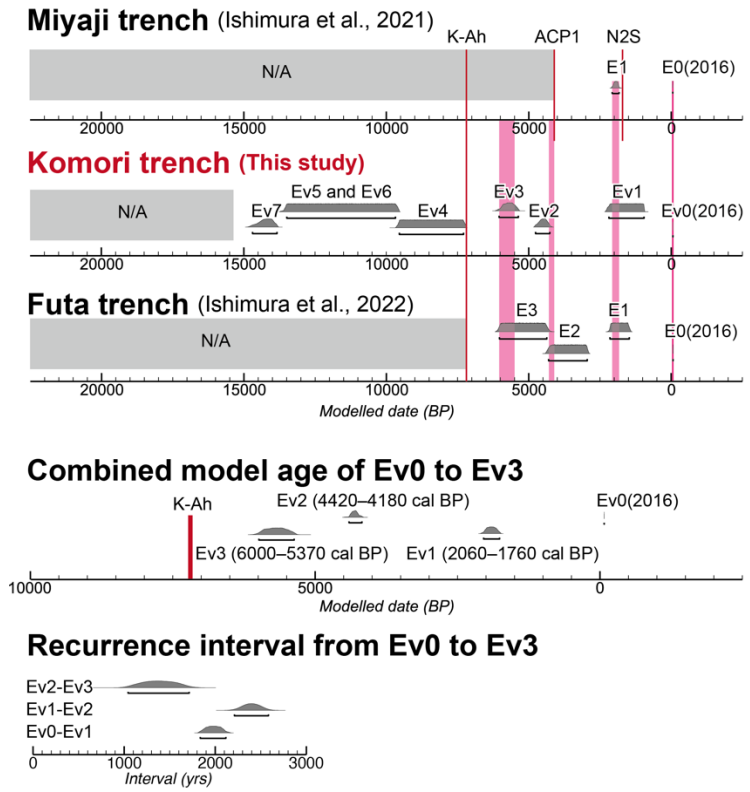

Figure 9. Modeled event ages and comparison to the author's previous paleoseismic studies. The underbars show the 2σ probability distribution ranges of the modeled ages. ACP1 and N2S are local tephras from the Aso volcano (Miyabuchi, 2009). ACP1 is Aso central cone pumice and its age is 4.1 ka (Miyabuchi, 2009). N2S is Nakadake N2 scoria and its age is 1490–1470 cal BP (68.2%) (Yamada et al., 2017).

Furthermore, assuming that the faulting events from Ev0 to Ev3 are the same among our three trenches, the calculated ages in OxCal modeling are Ev1: 2060–1760 cal

BP, Ev2: 4420–4180 cal BP, and Ev3: 6000–5370 cal BP (Fig. 9). Each recurrence intervals are Ev0/Ev1: 1830–2120 years, Ev1/Ev2: 2210–2590 years, and Ev2/Ev3: 1040–1720 years in the 2σ range. Based on the trench results, the average recurrence interval from Ev0 to Ev7 is 1990–2110 years, consistent with the interval from Ev0 to Ev3 mentioned above. This indicates that the Futagawa fault has ruptured relatively periodically. Despite the shallow depth of the trench, we could identify seven events, which were greater than those identified in trenches excavated on the primary Futagawa fault. This result emphasizes the importance of selecting a site with small displacement per event and relatively fast and continuous deposition.

The dextral slip rate from the recurrence interval (1990–2110 years) and single displacement (1.8–3.1 m) obtained in this study is 0.9–1.5 mm/yr for the Futagawa fault. For the Idenokuchi fault, vertical displacement is 1.0–2.5 m, so the vertical slip rate is estimated to be 0.5–1.3 mm/yr. On the west of this study area (Futa to Ohkirihata), across only the Futagawa fault, Ishimura (2019) calculated 0.9–1.1 mm/yr vertical slip rate and 1.5–3.7 mm/yr dextral slip rate from the vertical and dextral displacements of Takayubaru lava (K–Ar ages 81 ± 4 ka and 98 ± 18 ka; Miyoshi et al., 2013). The Idenokuchi fault runs parallel to the Futagawa fault, where these slip rates, i.e., the west of the study area, were calculated. However, the vertical displacement on the Idenokuchi fault in the 2016 event west of the study area is small (Kaneda et al., 2022). Therefore, the long-term slip rates can be regarded as representative values when oblique slip is accommodated only by the Futagawa fault. In considering this way, the long-term dextral and vertical slip rates are consistent with the results of this study. Oohashi (2020) pointed out that normal fault displacement was predominant on the Futagawa fault before Aso-4 pyroclastic flow

deposits (87 ka; Aoki, 2008), and dextral displacement became apparent later. Oohashi (2020) proposed the following possibilities for this change: 1) The stress field changed from a normal fault type with north-south extension to a dextral strike-slip fault type with predominant east-west compression, and 2) the normal fault component of the Futagawa fault was replaced by Idenokuchi fault and off-fault displacements, and the dextral displacement of the Futagawa fault became apparent. The fact that the long-term vertical slip rate coincides with that of the Idenokuchi fault from this study agrees with the second explanation. Therefore, the slip partition on the Idenokuchi fault must have occurred after the Aso-4 event.

Figure 10 summarizes the paleofaulting history since 7.3 ka based on the previous paleoseismic results, including archeological information, which is consistent with this study. The number of activities since 7.3 ka (including 2016) on the Futagawa fault is estimated to be four with considerable accuracy and precision based on the results of multiple trenches along the Futagawa fault and its vicinity. We believe that a series of studies by our group has provided ~~highly~~ accurate ages for the past three events because we studied the sites ~~where~~ minor artificial disturbance, continuous sediments, and good age markers (tephras). In addition, the paleofaulting history at the northwestern Aso caldera (Sato et al., 2021) and the western part of the Futagawa fault (Inoue et al., 2020), which are at secondary surface ruptures, indicate one of their events coincides with Ev1 in this study. Therefore, it is highly likely that the secondary faults were active simultaneously during at least the penultimate event of the Futagawa fault. Lateral spreading recognized at archaeological sites in the caldera (Kumamoto Prefectural Board of Education, 2010; Aso City Board of Education, 2011) was also approximately 2000

years ago, which also supports that secondary phenomena caused by earthquake similar to the 2016 event that occurred in the caldera. Thus, it is inferred that similar phenomena in the 2016 event (e.g., secondary surface rupture, liquefaction, and lateral spreading) also occurred during the previous activity. However, the age of the antepenultimate event in the northwestern part of the caldera does not match that of the Futagawa fault (Sato et al., 2021). In addition, no other secondary surface ruptures have been identified as having ~~fault events~~ older than the antepenultimate event, so it is unclear how the secondary fault behaved during the older events. Future accumulation of information on the presence or absence of older ~~activities~~ on such secondary faults and their histories will help us to better understand the secondary faults.

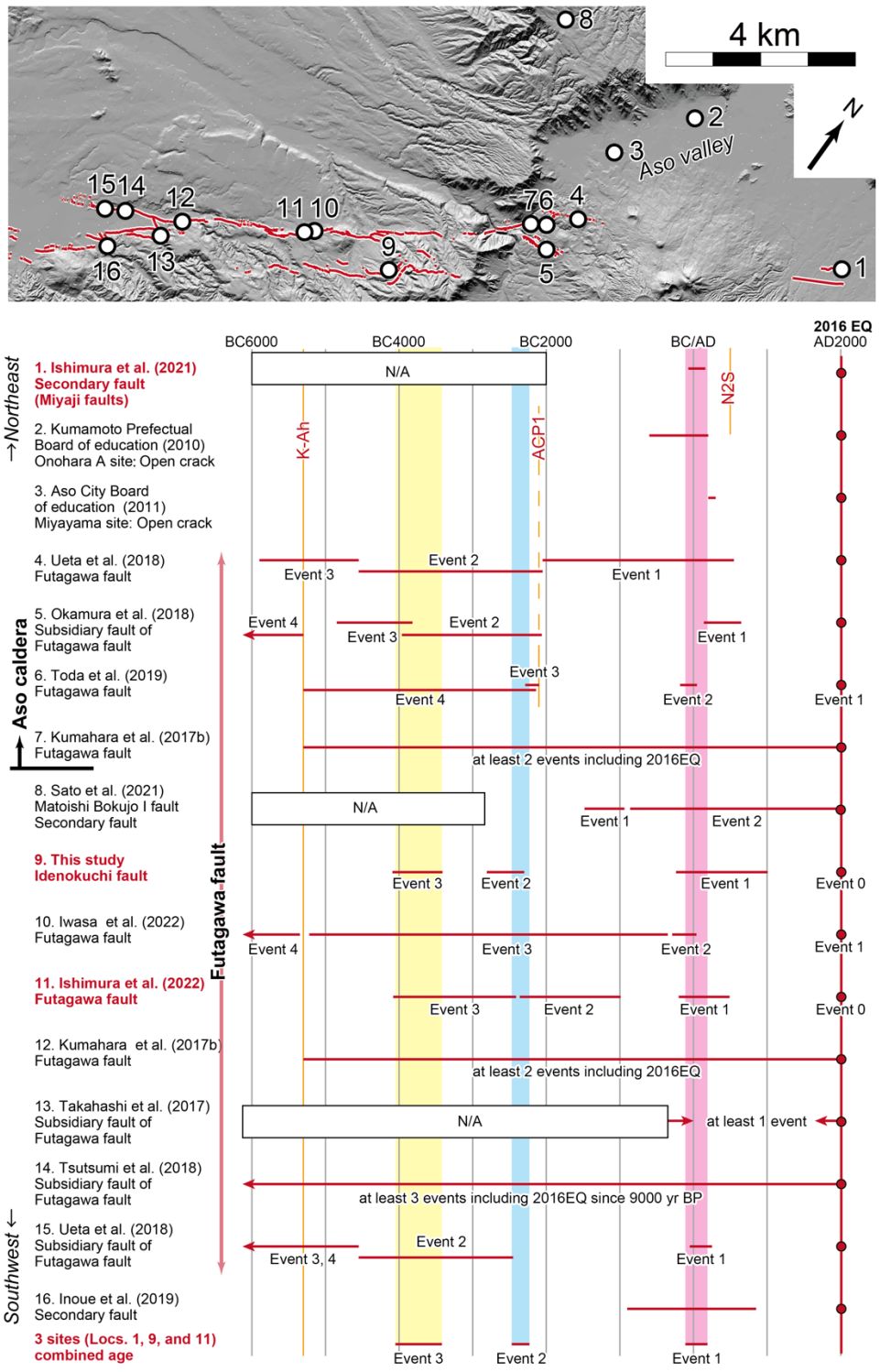

Figure 10. Compiled spatial-temporal age distribution of the paleofaulting events along the Futagawa and its subsidiary and secondary faults.

7. Conclusions

Using the 2016 Kumamoto earthquake as an example, we performed a DTM difference analysis in the area crossing the Futagawa and Idenokuchi faults where the slip partition occurred and conducted an excavation survey on the Idenokuchi fault. Based on the 3D displacement distribution, we discussed how the slip partition occurred on them and found that the oblique slip at depth was split entirely into vertical and horizontal displacements on the ground surface. This indicates that the Idenokuchi fault is structurally related to the Futagawa fault and that the paleofaulting history of the Idenokuchi fault is likely to correspond to that of the Futagawa fault.

The KMR trench at the Idenokuchi fault revealed continuous deposition of soil and tephra since 15 ka, and retrodeformation of the trench walls revealed at least eight faulting events (including 2016) during this period. Among them, the faulting events after K-Ah are consistent with paleoseismic surveys on the Futagawa fault (primary fault) and Miyaji faults (a secondary fault in the Aso caldera). This indicates that at least some surface ruptures that appeared around the Futagawa fault in the 2016 event are likely to have been active at the same time as the past activities of the Futagawa fault. The activity histories since 7.3 ka with the author's three trenches on the Futagawa, Miyaji, and Idenokuchi faults are E1: 2060–1760 cal BP, E2: 4420–4180 cal BP, and E3: 6000–5370 cal BP, indicating that they occurred relatively periodically. The mean recurrence interval since 15 ka is about 2000 years, supporting the periodic activity. The results of this study are also consistent with other trench investigations conducted after 2016. It is important to improve the accuracy and precision of the activity history of the Futagawa fault before 7.3 ka and to investigate the activity history of the Hinagu fault zone in the southern part

of the Futagawa fault zone to consider future seismic hazard and interlocking rupture. In addition, it will be important to clarify the subsurface structure and activity history of secondary faults in other earthquakes involving large amounts of surface ruptures, as well, to consider displacement hazards.

Acknowledgements

We thank Yasuhiro Kumahara, Ryuhei Oda, Jun Matsukaze, Motoya Kobayashi, Makoto Kobayashi, Yoshiya Iwasa, and Daichi Tomita for their help during the trench survey. We also thank Shinji Toda, Heitaro Kaneda, and Yasuo Miyabuchi for their discussions and constructive comments. This work was supported by KAKENHI Grant Number JP17H04730 from the Japan Society for the Promotion of Science.

Data and code availability

Supplementary figures (S1 to S2) and tables (S1 to S4) are available in the supplement material.

OxCal model codes are listed in the supplementary material.

Pre- and post-event DTMs used in this study were provided from Geospatial Information Authority of Japan (https://www.gsi.go.jp/ENGLISH/index.html).

Competing interests

The authors have no competing interests.

References

Aoki, K. (2008) Revised age and distribution of ca. 87 ka Aso-4 tephra based on new evidence from the Northwest Pacific Ocean. Quaternary International, 178, 100–118. doi: 10.1016/j.quaint.2007.02.005.

Aoyagi, Y., Higashi, S., Homma, S., Mukoyama S., Sugiyama, M., and Hijikata, K. (2021) Surface ruptures in the Aso campus of Tokai University caused by the 2016 Kumamoto Earthquake. Active Fault Research, 55, 1–18. (in Japanese with English abstract)

Aoyagi, Y., Ueta, K., Takemoto, T., Suehiro, M.,and Miyawaki, R. (2024) Seismic constraints on the subsurface extent of subparallel surface ruptures in Mashiki Town, Japan, associated with the 2016 Kumamoto Earthquake. Journal of the Seismological Society of Japan. 2nd ser., 77, 5–19. (in Japanese with English abstract)

Aso City Board of Education (2011) Miyayama ruinsII, Cultural Property Investigation Report of Aso City 2. Aso City Board of Education, Aso City. (in Japanese)

Barnhart, W.D., Hayes, G.P., and Gold, R.D. (2019) The July 2019 Ridgecrest, California, earthquake sequence: Kinematics of slip and stressing in cross-fault ruptures. Geophysical Research Letters, 46, 11859–11867. doi: 10.1029/2019GL084741.

Bronk Ramsey, C. (2008) Deposition models for chronological records. Quaternary Science Reviews, 27, 42–60. doi: 10.1016/j.quascirev.2007.01.019.

Bronk Ramsey, C. (2009) Bayesian analysis of radiocarbon dates. Radiocarbon, 51, 337–360. doi: 10.2458/azu_js_rc.v51i1.3494.

Danhara, T., Yamashita, T., Iwano, H., and Kasuya, M. (1992) An improved system for measuring refractive index using the thermal immersion method. Quaternary International, 13–14, 89–91. doi: 10.1016/1040-6182(92)90013-R.

Fujiwara, S., Yarai, H., Kobayashi, T., Morishita, Y., Nakano, T., Miyahara, B., Nakai, H., Miura, Y., Ueshiba, H., Kakiage, Y., and Une, H. (2016) Small-displacement linear surface ruptures of the 2016 Kumamoto earthquake sequence detected by ALOS-2 SAR interferometry. Earth, Planets and Space, 68, 160. doi: 10.1186/s40623-016-0534-x.

Fukushima, Y., and Ishimura, D. (2020) Characteristics of secondary-ruptured faults in the Aso Caldera triggered by the 2016 Mw 7.0 Kumamoto earthquake. Earth, Planets and Space, 72, 175. doi: 10.1186/s40623-020-01306-y.

Goto, H., Tsutsumi, H., Toda, S., and Kumahara, Y. (2017) Geomorphic features of surface ruptures associated with the 2016 Kumamoto earthquake in and around the downtown of Kumamoto City, and implications on triggered slip along active faults. Earth, Planets and Space, 69, 26. doi: 10.1186/s40623-017-0603-9.

Hamling, I.J., Hreinsdóttir, S., Clark, K., Elliott, J., Liang, C., Fielding, E., Litchfield, N., Villamor, P., Wallace, L., Wright, T.J., D'Anastasio, E., Bannister, S., Burbidge, D., Denys, P., Gentle, P., Howarth, J., Mueller, C., Palmer, N., Pearson, C., Power, W., Barnes, P., Barrell, D.J.A., Van Dissen, R., Langridge, R., Little, T., Nicol, A., Pettinga, J., Rowland, J., and Stirling, M. (2017). Complex multifault rupture during the 2016 Mw 7.8 Kaikōura earthquake, New Zealand. Science, 356, 6334. doi: 10.1126/science.aam7194.

He, P., Wen, Y., Xu, C., and Chen, Y. (2019) Complete three-dimensional near-field surface displacements from imaging geodesy techniques applied to the 2016 Kumamoto earthquake. Remote Sensing of Environment, 232, 111321. doi: 10.1016/j.rse.2019.111321.

Himematsu, Y., and Furuya, M. (2020) Coseismic and postseismic crustal deformation associated with the 2016 Kumamoto earthquake sequence revealed by PALSAR-2 pixel tracking and InSAR. Earth, Planets and Space, 7, 1–19. doi: 10.1029/2020EA001200.

Hoshizumi, H., Ozaki, M., Miyazaki, K., Matsuura, H., Toshimitsu, S., Uto, K., Uchiumi, S., Komazawa, M., Hiroshima, T., and Sudo, S. (2004) Geological Map of Japan 1:200,000, Kumamoto. Geological Survey of Japan, AIST.

Inoue, N., Kitada, N., Shibuya, N., Omata, M., Takahama, T., Tonagi, M., and Irikura, K. (2020) Probabilistic Evaluation of Off-Fault Displacements of the 2016 Kumamoto Earthquake. Pure and Applied Geophysics, 177, 2007–2019. doi: 10.1007/s00024-019-02345-7.

Ishimura, D., and Kakiuchi, Y. (2011) Chronology and processes of fluvial terrace formation in northeastern Kinki district, southwest Japan, based on cryptotephra analysis. Quaternary International, 246, 190–202. doi: 10.1016/j.quaint.2011.08.039.

Ishimura, D. (2019) Co-seismic vertical displacement associated with the 2016 Kumamoto earthquake (Mw7.0) and activity of the Futagawa fault around Futa, Nishihara Village, Kumamoto prefecture. Active Fault Resarch, 50, 33–32. (in Japanese with English abstract)

Ishimura, D., Toda, S., Ichihara, T., Takahashi, N., Konno, A., and Sato, H. (2017) A study on surface ruptures around Miyaji, Aso City, Kumamoto Prefecture, associated with the 2016 Kumamoto earthquake sequence and upward slip tapering on pit excavation walls. Active Fault Research, 47, 9–16. (in Japanese with English abstract)

Ishimura, D., Toda, S., Mukoyama, S., Homma, S., Yamaguchi, K., and Takahashi, N. (2019) 3D surface displacement and surface ruptures associated with the 2014 Mw 6.2 Nagano earthquake using differential lidar. Bulletin of the Seismological Society of America, 109, 780–796. doi: 10.1785/0120180020.

Ishimura, D., Tsutsumi, H., Toda, S., Fukushima, Y., Kumahara, Y., Takahashi, N., Ichihara, T., and Takada, K. (2021) Repeated triggered ruptures on a distributed secondary fault system: an example from the 2016 Kumamoto earthquake, Southwest Japan. Earth, Planets and Space, 73 doi: 10.1186/s40623-021-01371-x.

Ishimura, D., Iwasa, Y., Takahashi, N., Tadokoro, R. and Oda, R. (2022) Paleoseismic events and shallow subsurface structure of the central part of the Futagawa fault, which generated the 2016 Mw 7.0 Kumamoto earthquake. Geomorphology, 414, 108387. doi: 10.1016/j.geomorph.2022.108387.

Iwasa, Y., Kumahara, Y., Goto, H., Ishimura, D., and Hosoya, T. (2022) Faulting history of the Futagawa fault zone based on trenching survey at Komori, Nishihara Village, Kumamoto Prefecture. Active Fault Research, 56, 47–58. (in Japanese with English abstract)

Kamata, H., and Kodama, K. (1994) Tectonics of an arc-arc junction: an example from Kyushu Island at the junction of the Southwest Japan Arc and the Ryukyu Arc. Tectonophysics, 233, 69–81. doi: 10.1016/0040-1951(94)90220-8.

Kaneda, H., and Chiba, T. (2019) Stereopaired morphometric protection index red relief image maps (Stereo MPI-RRIMs): Effective visualization of high-resolution digital elevation models for interpreting and mapping small tectonic geomorphic features. Bulletin of the Seismological Society of America, 109, 99–109. doi: 10.1785/0120180166.

Kaneda, H., Toda, S., Ishimura, D., Kumahara, Y., Goto, H., Okada, S., and Kobayashi, M. (2022) Surface Ruptures and Tectonic Geomorphology Along and Around the Idenokuchi Fault. In: Kumahara, Y., Kaneda, H., Tsutsumi, H. (eds) Surface Ruptures Associated with the 2016 Kumamoto Earthquake Sequence in Southwest Japan. Advances in Geological Science. Springer, Singapore. doi: 10.1007/978-981-19-1150-7_12.

King, G., Klinger, Y., Bowman, D., and Tapponnier, P. (2005) Slip-Partitioned Surface Breaks for the Mw 7.8 2001 Kokoxili Earthquake, China. Bulletin of the Seismological Society of America, 95 (2), 731–738. doi: 10.1785/0120040101.

Kokusai Kogyo C o.,Ltd. (2010) 3D-Geomorphic Image Velocimetry. JP Patent No. 4545219.

Kumahara, Y., Okada, S., Kagohara, K., Kaneda, H., Goto, H., and Tsutsumi, H. (2017a) 1:25,000 Active Fault Map, Futagawa-Hinagu Fault Zone and its Vicinity “Kumamoto (Revision)”. Geospatial Information Authority of Japan, Ibaraki. (in Japanese)

Kumahara, Y., Torii, M., Nakata, T., Goto, H., Iwasa, Y., Suzuki, Y., Watanabe, M., Toda, S., Takahashi, N., and Okuno, M. (2017b) Fault History of the Northern Part of Futagawa-Hinagu Fault Zone Based on Trench Survey at Dozon, Mashiki Town and at Kawayo, Minami-Aso Village, Programme and Abstracts JSAF 2017 Fall Meeting, 24–25. (in Japanese)

Kumahara, Y., Kaneda, H., and Tsutsumi, H. (2022) Surface Ruptures Associated with the 2016 Kumamoto Earthquake Sequence in Southwest Japan. Advances in Geological Science. Springer, Singapore. doi: 10.1007/978-981-19-1150-7.

Kumamoto Prefectural Board of Education (2010) Earthquake traces in Onobaru-A site. Onobaru ruins group. In: Cultural Property Investigation Report of Kumamoto Prefecture, 257 (2), 147–149. (in Japanese)

Kumamoto Prefecture Geological Map Compilation Committee (2008) Geological Map of the Kumamoto Prefecture (1:100,000). Kumamoto Prefecture Geotechnical Consultants Association, Kumamoto.

Machette, M.N., Personius, S.F., and Nelson, A.R. (1992) Paleoseismology of the Wasatch fault zone: a summary of recent investigations, interpretations, and conclusions. in Gori, P.L., and Hays, W.W., eds., Assessment of Regional Earthquake Hazards and

Risk Along the Wasatch Front, Utah: U.S. Geological Survey Professional Paper 1500, A1–A71.

Machida, H., and Arai, F. (2003) Atlas of Tephra in and around Japan [revised edition]. University of Tokyo Press, Tokyo.

Matsumoto, Y. (1979) Some problems on volcanic activities and depression structures in Kyushu, Japan. Memoirs of the Geological Society of Japan, 16, 127–139. (in Japanese with English abstract)

McCalpin, J.P. (2009) Paleoseismology. 2nd Edition, Academic Press, Amsterdam-London.

Miyabuchi, Y. (2009) A 90,000-year tephrostratigraphic framework of Aso Volcano, Japan. Sedimentary Geology, 220, 169–189. doi: 10.1016/j.sedgeo.2009.04.018.

Miyoshi, M., Shinmura, T., Sumino, H., Sano, T., Miyabuchi, Y., Mori, Y., Inakura, H., Furukawa, K., Uno, K., Hasenaka, T., Nagao, K., Arakawa, Y., and Yamamoto, J. (2013) Lateral magma intrusion from a caldera-forming magma chamber: Constraints from geochronology and geochemistry of volcanic products from lateral cones around the Aso caldera, SW Japan. Chemical Geology, 352, 202–210. doi: 10.1016/j.chemgeo.2013.06.003.

Moya, L., Yamazaki, F., Liu, W., and Chiba, T. (2017) Calculation of coseismic displacement from lidar data in the 2016 Kumamoto, Japan, earthquake. Natural Hazards and Earth System Sciences, 17, 143–156. doi: 10.5194/nhess-17-143-2017.

Nakata, T., and Imaizumi, T. (2002) Digital Active Fault Map of Japan. University of Tokyo Press, Tokyo. (in Japanese)

Mukoyama, S. (2011) Estimation of ground deformation caused by the earthquake (M 7.2) in Japan, 2008, from the geomorphic image analysis of high resolution LiDAR DEMs. Journal of Mountain Science, 8, 239–245. doi: 10.1007/s11629-011-2106-7.

Muroi, S., Suzuki, Y., Mukoyama, S., Iwasa, Y., Yamashita, H., Muraki, M., Yamashita, K., Fukuba, T. (2024) Surface displacement vector discontinuity in the easternmost part of the Futagawa-Hinagu fault zone analyzed by using airborne laser scanning data at two different timings. Active Fault Research, 60, 11–25. (in Japanese with English abstract)

Nurminen, F., Baize, S., Boncio, P., Blumetti, A.M., Cinti, F.R., Civico, R., and Guerrieri, L. (2022) SURE 2.0 – New release of the worldwide database of surface ruptures for fault displacement hazard analyses. Scientific Data 9, 729. doi: 10.1038/s41597-022-01835-z.

Nurminen, F., Boncio, P., Visini, F., Pace, B., Valentini, A., Baize, S., and Scotti, O. (2020) Probability of Occurrence and Displacement Regression of Distributed Surface Rupturing for Reverse Earthquakes. Frontiers in Earth Science, 8, 581605. doi: 10.3389/feart.2020.581605.

Okamura, Y., Abe, S., Miyashita, Y., Azuma, T., Togo, T., Shirahama, Y., Awata, Y., Maruyama, T., Ogami, T., Imura, R., Tsutsumi, H., Goto, H., and Kumahara, Y. (2018) 3.1 Survey of detailed position and shape of active faults to understand the fault segments and observation to reveal the paleoseismic history and slip rates. In: Research Report of a

Comprehensive Active Fault Survey After the 2016 Kumamoto Earthquake, 2017 Fiscal Year. Ministry of Education, Culture, Sports, Science and Technology and Kyushu University. (in Japanese)

Oohashi, K., Otsubo, M., Matsumoto, S., Kobayashi, K., Sato, K., and Nishimura, T. (2020) The Quaternary tectonics of Central Kyushu and the 2016 Kumamoto Earthquake: from a multifaceted viewpoint combining geology, seismology, and geodesy. Journal of the Geological Society of Japan, 129, 565–589. (in Japanese with English abstract)

Reimer, P.J., Austin, W.E.N., Bard, E., Bayliss, A., Blackwell, P.G., Bronk Ramsey, C., Butzin, M., Cheng, H., Edwards, R.L., Friedrich, M., Grootes, P.M., Guilderson, T.P., Hajdas, I., Heaton, T.J., Hogg, A.G., Hughen, K.A., Kromer, B., Manning, S.W., Muscheler, R., Palmer, J.G., Pearson, C., Van Der Plicht, J., Reimer, R.W., Richards, D.A., Scott, E.M., Southon, J.R., Turney, C.S.M., Wacker, L., Adolphi, F., Büntgen, U., Capano, M., Fahrni, S.M., Fogtmann-Schulz, A., Friedrich, R., K¨ohler, P., Kudsk, S., Miyake, F., Olsen, J., Reinig, F., Sakamoto, M., Sookdeo, A., and Talamo, S. (2020) The IntCal20 Northern Hemisphere radiocarbon age calibration curve (0–55 cal kBP). Radiocarbon, 62, 725–757. doi: 10.1017/RDC.2020.41.

Research Group for Active Faults of Japan, 1980. Active Faults in Japan, Sheet Maps and Inventories. University of Tokyo Press, Tokyo. (in Japanese)

Research Group for Active Faults of Japan, 1991. Active Faults in Japan, Sheet Maps and Inventories, Rev. Ed. University of Tokyo Press, Tokyo. (in Japanese)

Sato, P.H., Komura, K., Une, H., Nakano, T., and Yagi, K. (2021) Study on Cumulative Activities of Passively Ruptured Faults through a Trenching Survey at the Matoishi Bokujo I Fault, Northwest Side of the Aso Caldera, Southwestern Japan. Geographical Review of Japan Series A, 94, 250–264. doi: 10.4157/grj.94.250. (in Japanese with English abstract)

Scott, C.P., Arrowsmith, J.R., Nissen, E., Lajoie, L., Maruyama, T., and Chiba, T. (2018) The M7 2016 Kumamoto, Japan, earthquake: 3-D Deformation along the Fault and within the damage Zone Constrained from Differential Lidar Topography. Journal of Geophysical Research: Solid Earth, 123, 6138–6155. doi: 10.1029/2018JB015581.

Shirahama, Y., Yoshimi, M., Awata, Y., Maruyama, T., Azuma, T., Miyashita, Y., Mori, H., Imanishi, K., Takeda, N., Ochi, T., Otsubo, M., Asahina, D., and Miyakawa, A. (2016) Characteristics of the surface ruptures associated with the 2016 Kumamoto earthquake sequence, Central Kyushu, Japan. Earth, Planets and Space, 68, 191. doi: 10.1186/s40623-016-0559-1.

Smith, V.C., Staff, R.A., Blockley, S.P.E., Bronk Ramsey, C., Nakagawa, T., Mark, D.F., Takemura, K., and Danhara, T. (2013) Identification and correlation of visible tephras in the Lake Suigetsu SG06 sedimentary archive, Japan: chronostratigraphic markers for synchronising of east Asian/west Pacific palaeoclimatic records across the last 150 ka. Quaternary Science Reviews, 67, 121–137. doi: 10.1016/j.quascirev.2013.01.026.

Suzuki, T., Kasahara, A., Nishizawa, F., and Saito, H. (2014) Chemical characterization of volcanic glass shards by energy dispersive X-ray spectrometry with EDAX Genesis

APEX2 and JEOL JSM-6390. Geographical reports of Tokyo Metropolitan University, 49, 1–12.

Suzuki, Y., Ishimura, D., Kumaki, Y., Kumahara, Y., Chida, N., Nakata, T., and Nakano, T. (2017) 1:25,000 Active Fault Map, Futagawa-Hinagu Fault Zone and its Vicinity "Aso". Geospatial Information Authority of Japan, Ibaraki. (in Japanese)

Takahashi, N., Ishimura, D., Toda, S., Nakata, T., and Watanabe, M. (2017) Vertical slip rate on a normal fault co-ruptured with the Futagawa fault at the 2016 Kumamoto earthquake. Active Fault Research, 46, 27–32. (in Japanese with English abstract).

Toda, S., Kaneda, H., Okada, S., Ishimura, D., and Mildon, Z.K. (2016) Slip-partitioned surface ruptures for the Mw 7.0 16 April 2016 Kumamoto, Japan, earthquake. Earth, Planets and Space, 68, 188. doi: 10.1186/s40623-016-0560-8.

Toda, S., Torii, M., Okuno, M., Konno, A., Ono, H., and Takahashi, N. (2019) Evidence for Holocene paleoseismic events on the 2016 Kumamoto earthquake rupture zone within the Aso caldera: a trench excavation survey at Kurokawa, the town of Minami-Aso, Southwest Japan. Active Fault Research, 51, 13–25. (in Japanese with English abstract)

Tsutsumi, H., Toda, S., Goto, H., Kumahara, Y., Ishimura, D., Takahashi, N., Taniguchi, K., Omata, M., Kohriya, Y., Gomi, M., Asano, K., and Iwata, T. (2018) Paleoseismic trenching across the surface rupture of the 2016 Kumamoto earthquake at Jichu, Mashiki Town, Kumamoto Prefecture. Active Fault Research, 49, 31–39. (in Japanese with English abstract)

Ueta, K., Miyawaki, R., Iemura, K., Yokoyama, T., and Miyawaki, A. (2018) Paleoseismological study on surface fault ruptures produced by the 2016 Kumamoto earthquake. In: Abstracts of Japan Geoscience Union Meeting 2018, Makuhari Messe, Chiba. (in Japanese with English abstract).

Watanabe, K. and Ono, K. (1969) Geology of the vicinity of Omine on the western flank of the Aso caldera. Journal of the Geological Society of Japan, 75, 365–374. (in Japanese with English abstract)

Xu, X., Sandwell, D.T., and Smith-Konter, B. (2020) Coseismic Displacements and Surface Fractures from Sentinel-1 InSAR: 2019 Ridgecrest Earthquakes. Seismological Research Letters, 91, 1979–1985. doi: 10.1785/0220190275.

Yamada, K., Takemura, K., Kuwae, M., Yamamoto, M., and Danhara, T. (2017) Revised ages of late Holocene tephras in Beppu Bay, central Kyushu, southwest Japan. Quaternary International, 452, 33–42. doi: 10.1016/j.quain t.2017.01.024.

Editor's Round Two Decision Letter:

Subject: [Seismica] Editor Decision

Dear Daisuke Ishimura, Naoya O Takahashi, Hiroyuki Tsutsumi, Shin'ichi Homma, Sakae Mukoyama, Toshihiko Ichihara:

I hope this email finds you well. I have reached a decision regarding your submission to Seismica, "Paleoseismic trenching on slip-partitioned surface ruptures associated with the 2016 Kumamoto earthquake: Implications for simultaneous rupturing of the primary, subsidiary, and secondary active faults ". Thank you once again for submitting your work to Seismica.

Based on reviews I have received, your manuscript may be suitable for publication after some revisions.

Thank you for your diligent attempts to address the reviewer comments. As you will see from the second round of comments below, the reviewers are generally satisfied that there concerns have been addressed. Both reviewers are recommending minor revisions prior to proceeding forward with publication. For my part, I would describe the sum total of the requested changes as somewhere between minor and moderate revisions. As such, whether the manuscript will need to receive additional, external peer review will depend in part on your responses to the comments below. Thank you again for choosing Seismica for your work. I think we will be able to proceed forward with publication relatively soon.

PLEASE NOTE: Reviewer 2 also provided comments on an annotated Word document. You can find that document uploaded with the other files in your OJS submission. Please let me know if you are unable to locate it.

When you are ready to resubmit the revised version of your manuscript, please upload:

A 'cleaned' version of the revised manuscript, without any markup/changes highlighted.
A pdf version of the revised manuscript clearly highlighting changes/markup/edits.
A 'response-to-reviewers' letter that shows your response to each of the reviewers' points, together with a summary of the resulting changes made to the manuscript.

Once I have read your revised manuscript and rebuttal, I will then decide whether the manuscript either needs to be sent to reviewers again, requires further minor changes, or can be accepted.

If you deem it appropriate, please check that the revised version of your manuscript recognises the work of the reviewers in the Acknowledgements section.

Please note that Seismica does not have any strict deadlines for submitting revisions, but naturally, it is likely to be in your best interest to submit these fairly promptly, and please let me know of any expected delays.

I wish you the best with working on the revisions. Please don't hesitate to contact me with any questions or comments about your submission, or if you have any feedback about your experience with Seismica.

Kind regards,

Randy Williams

Reviewer 1 Round 2 Comments:

Dear authors and editor.

This paper provides data on the surface ruptures of the 2016 Kumamoto earthquake, the patterns of displacement and amounts of slip partitioning inferred from lidar differencing, and a record of past events inferred from a paleoseismic trench.

This is my second review of this paper and I find it much improved. In fact I commend you on your fantastic consideration of my previous comments. It is now clearly written and presented. The figures are all very nice.

In my view there are just a few minor items to clear up prior to publication. I appreciate your clarification of the evidence for the individual earthquake events, however there are a few more points of uncertainty that I think should be addressed. these include:

1) I think the evidence supports at least six clear events but up to 8 events is posssible. This should be updated in the abstract and conclusions.

2) Evidence to separate earthquakes Ev5 and Ev6 into separate events is weak. Attributing one event to one fault strand and another event to a different fault strand at the same

stratigraphic level is not very compelling evidence for two events. Could be possible. However, it is critical to acknowledge that is could be one event. Event Ev5/6.

3) Evidence for earthquake Ev7 is also weak. A small remaining vertical displacement on one trace (post retrodeforming) is not very compelling evidence. Could be but should be considered uncertain. A small amount of remaining offset after retrodeformation could be related to thickness (facies) changes in the deposit, variable deformation related to later events, and/or a component of oblique slip and not necessarily require an additional earthquake.

These points do not really affect the overall conclusions but really need to be emphasized to stay true to the stratigraphic relations presented on the logs.

I do appreciate you separating the events into 'certain' and 'uncertain' categories. I just feel that needs to be modified slightly to reflect the presented data. I came up with a sentence to begin section 5.2 to highlight this as follows:

"Based on evidence for paleofaulting events, we infer six certain faulting events including Ev0–Ev4 and a single event (combined Ev5/Ev6) that occurred since the deposition of unit S53. We also interpret several additional less certain events including Ev7 and the possibility that two events occurred after the deposition of S52 (Ev5 and Ev6 as separate events)."

In addition to the comments above, I have also added a few very minor text suggestions as well as a few comments for labeling the logs (adding the ages and tephra names directly to the log, etc). The log suggestions are annotated on the attached jpg.

Overall. Great job. After considerations of the minor revisions included on the annotated manuscript, this will make a valuable contribution to paleoseismology.

Sincerely,

Rich Koehler

Associate Prof

University of Nevada, Reno

Reviewer 2 Round 2 Comments:

Re-review of Ishimura et al for Seismica.

The revised version of the manuscript is much improved over the first version, especially with regard to English language and grammar. The authors have also significantly improved the introduction, regional/tectonic setting, and evidence for paleo earthquake sections. However, despite the general improvements, there are a few comments that still need to be addressed prior to publication. I provide general comments below, and minor detailed comments in the attached Word document.

The authors seemed to have missed the general comments I provided in the first round of review, responding only to the line comments I left in the PDF. Here are the general comments I submitted in the first review:

"It is difficult to follow the evidence that supports the rich earthquake history described in section 6.2. A table or a section in the results describing the evidence used to interpret each earthquake would be useful.

Additionally, the authors present a single version of the earthquake history from the trench. However, their interpretations seem to support the option that earthquakes 5 and 6 were one earthquake. While this would not change the conclusions of the study, it would be good to acknowledge more of the uncertainty in the interpreted earthquake history in the text and perhaps offer another version(s) of earthquake history that are is supported by the data.

The interpretation of Trace 2 as a surface rupture trace does not seem supported by the horizontal differencing (vectors seem continuous across it in Figure 4). I cannot tell if there is vertical across it because it is difficult to see the vertical differencing results in Figure 4 (see comment in the attached PDF for Figure 4). The vertical difference across it shown in Figure 5, line A-A' is minimal, and could be interpreted as noise, so more evidence is likely necessary to include it as a surface rupture trace."

The authors do seem to have addressed the first two comments, but the third one, about the (un)certainty of the interpretation of Trace 2 remains.

The study is very, very local in focus, and while is of course the choice of the authors, it would likely be more engaging to a broader audience if it included discussion of and relevance to other fault systems. There are a few angles that could be interesting to place in broader context: (1) the small displacements with detailed stratigraphy that enable the interpretation of up to 8 earthquakes in a shallow trench; (2) the behavior of other fault systems that are structurally linked at depth and/or (3) the behavior of other slip-partitioned fault systems, including their paleoseismic history. Some discussion of at least one of these points (slip partitioning seems the most interesting to me) in global context and how this study might help to understand other fault systems would certainly broaden the impact of this work.

How the vertical displacements are calculated is not described in the methods. Is it a simple DTM difference (subtraction)?

Paleoseismic trenching on slip-partitioned surface ruptures associated with the 2016 Kumamoto earthquake

Daisuke Ishimura[1,*], Naoya O. Takahashi [2], Hiroyuki Tsutsumi[3], Shin'ichi Homma[4], Sakae Mukoyama[4], and Toshihiko Ichihara[5]

[1] Department of Earth Sciences, Chiba University, 1-33 Yayoi-cho, Inage-ku, Chiba 263-8522, Japan
[2] Department of Earth Science, Tohoku University, 6-3 Aoba, Aoba-ku, Sendai 980-8578, Japan
[3] Department of Environmental Systems Science, Doshisha University, 1-3 Tataramiyakodani, Kyotanabe, Kyoto 610-0394, Japan
[4] Department of Research & Development of Kokusai Kogyo Co., Ltd., 2-24-1 Harumi-cho, Fuchu, Tokyo 183-0057, Japan
[5] Department of Disaster Prevention & Geology of Hopedesign Co., Ltd., 3-5 Shuri-Akatacho, Naha, Okinawa 903-0813, Japan
[*]Corresponding author: ishimura@chiba-u.jp

Author ORCIDs

Daisuke Ishimura: 0000-0002-4798-3425
Naoya Takahashi: 0000-0003-4196-1409

Author contributions

Conceptualization: D. Ishimura
Data Curation: N. O. Takahashi, S. Homma, S. Mukoyama
Formal Analysis: D. Ishimura, S. Homma, S. Mukoyama
Funding Acquisition: D. Ishimura
Investigation: D. Ishimura, N. O. Takahashi, H. Tsutsumi, T. Ichihara
Methodology: D. Ishimura, S. Homma, S. Mukoyama
Project Administration: D. Ishimura
Resources: D. Ishimura
Software: S. Homma, S. Mukoyama
Supervision: H. Tsutsumi
Validation: D. Ishimura
Visualization: D. Ishimura, N. O. Takahashi
Writing – original draft: D. Ishimura
Writing – review & editing: N. O. Takahashi, H. Tsutsumi, S. Homma, S. Mukoyama

Abstract

Surface ruptures can appear over a wide area, in addition to the primary fault, during ~~a~~ large earthquakes, such as the 2016 Kumamoto earthquake. Although the displacement of such distributed surface ruptures is small, information on their paleo activities may provide clues for evaluating displacement hazard risk and whether they can offer a paleoseismic history of the primary fault. We conducted lidar differencing analysis and trench excavation on the Idenokuchi fault, which was activated simultaneously with the primary Futagawa fault during the 2016 Kumamoto earthquake, as a result of slip partitioning and ~~of the~~ oblique slip. First, we clarified the 3D displacement field by lidar differencing and discussed quantitatively how the slip partition occurred on both faults. We found that deep oblique slip is completely split into horizontal and vertical components at the ground surface and inferred that the Idenokuchi fault is structurally connected to the Futagawa fault. Then, we excavated a trench on a subparallel surface rupture of the Idenokuchi fault and identified at least six and up to eight faulting events since 15 ka. Finally, we revealed a reliable faulting history since 7.3 ka. Combined with the results of other paleoseismic trenches, our findings on the Idenokuchi fault indirectly suggest that the Futagawa fault has ruptured relatively periodically. We conclude that many surface ruptures appeared in the last few events, as was the case during the 2016 event.

Second language abstract: 要旨 (日本語)

2016 年熊本地震のような大地震の際に主断層周辺に加えて幅広い範囲に断層が出現することがある．そのような断層の変位は小さいが，その過去の活動の情報は変位ハザードリスクや主断層の活動履歴の復元に有用かどうかの評価に関して手がかりを与えてくれる．そこで我々は lidar 差分解析とトレンチ掘削調査を 2016 年熊本地震の際に布田川断層と同時に活動しスリップパーティションが生じたとされた出ノ口断層で実施した．まず，lidar 差分により 3 次元変位場を求め，両断層でスリップパーティションが生じたかどうかを定量的に議論した．その結果，深部の斜めすべりが地表では完全に水平と鉛直成分に分割されたことが明らかとなり，出ノ口断層は構造的に布田川断層と地下でつながっていることが推定された．また，出ノ口断層に並走する断層上でトレンチ掘削した結果，15 ka 以降に最大 8 回のイベントを推定し，最終的に 7.3 ka 以降の信頼たる活動時期が得られた．この結果は布田川断層が比較的周期的に活動したことと，最近数回のイベントでは 2016 年同様に多くの断層が地表に出現したことを示唆する．

Third language abstract: NA

Non-technical summary

We conducted a study on the Idenokuchi fault, which moved together with the main Futagawa fault during the 2016 Kumamoto earthquake, Japan. By comparing the topography before and after the earthquake, and by digging a trench, we were able to understand how the fault moved during the 2016 earthquake and during the prehistoric earthquakes. Our findings indicate that the oblique displacement on the fault at depth is split into horizontal and vertical movements at the surface. This suggests that the Idenokuchi fault merges with the Futagawa fault at depth. By digging a trench on the Idenokuchi fault, we found evidence for at least six and ~~of~~ up to eight

past earthquakes over the last 15,000 years. The recurrence interval revealed on the Idenokuchi fault indirectly indicates that the Futagawa fault has ruptured at somewhat regular intervals.

1. Introduction

Recent developments in remote sensing technology (e.g., SAR and optical correlation) have enabled the capture of ground surface displacement associated with earthquakes with high resolution and precision, including the distribution and amount of displacement. As a result, it has become clear that the distribution of coseismic surface ruptures is complex when viewed in detail, and in some cases, ruptures are distributed over extensive areas (e.g., the 2016 Kumamoto earthquake, the 2016 Kaikoura earthquake, and the 2019 Ridgecrest earthquake). Such complex ruptures have involved contemporaneous slip on the primary faults and other related faults, which are variably referred to as secondary, subsidiary, sympathetic, and distributed faults (e.g., Nurminen et al., 2020, 2022). Understanding the history and distribution of complex ruptures is important for assessing displacement hazards; however, few studies have evaluated the relative synchronicity of past ruptures along primary faults and their associated nearby faults.

The epicentral area of the Mw7.0 2016 Kumamoto earthquake provides a rare opportunity to study such co-rupturing events. InSAR analyses and field surveys have shown that the surface ruptures were widely distributed around the main (primary) fault of the 2016 Kumamoto earthquake (Fujiwara et al., 2016). Detailed field reconnaissance studies confirmed surface displacements and/or deformation at discontinuities observed in the InSAR data (Goto et al., 2017; Ishimura et al., 2017; Okamura et al., 2018; Sato et al., 2021). In addition to the ruptures along the primary Futagawa and Hinagu faults, surface displacements were observed along the Idenokuchi and Miyaji faults (Fig. 1). The Idenokuchi fault extends for approximately 10 km parallel to and within 2 km southeast

of the Futagawa fault. Along this parallel section of the rupture, right-lateral displacement occurred on the Futagawa fault and vertical displacement occurred on the Idenokuchi fault, from which Toda et al. (2016) inferred that the slip was partitioned between the two faults. This suggests that the Futagawa and Idenokuchi faults merge at depth and are structurally connected. The Miyaji faults (Fig. 1; Ishimura et al., 2021) have the same strike and displacement sense as the Futagawa fault. However, the fault model based on the InSAR analysis (Fukushima and Ishimura, 2020) has revealed that the Miyaji faults are not connected to the Futagawa fault, suggesting that the 2016 surface ruptures on the Miyaji faults were triggered slip. These observations indicate that various mechanisms may have contributed to the surface ruptures around the Futagawa fault during the 2016 Kumamoto earthquake.

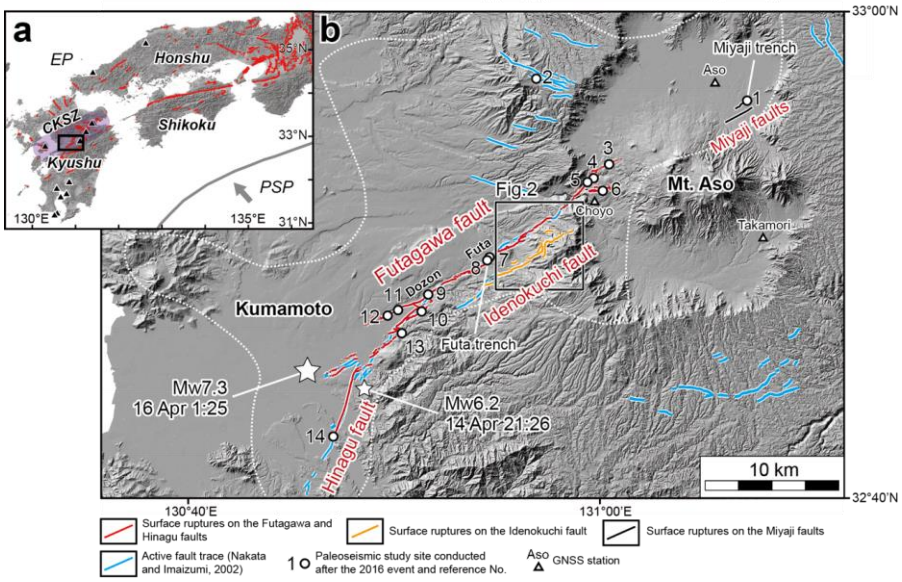

Figure 1. Spatial relationships among the primary Futagawa–Hinagu rupture zones and previously mapped active fault traces. (a) Tectonic setting, active volcanoes, and active faults in southwest Japan. CKSZ, Central Kyushu Shear Zone. (b) Locations of the surface ruptures along the Futagawa, Hinagu, Idenokuchi, and Miyaji faults. The surface rupture traces are from Kumahara et al. (2022). Previously mapped active fault traces are from Nakata and Imaizumi (2002). Red and orange lines indicate primary and subsidiary surface ruptures, respectively, as defined in this study. The dotted line encloses the area where secondary surface ruptures were identified by InSAR (Fujiwara et al., 2016). The Miyaji faults (Ishimura et al., 2021) are examples of the many secondary surface ruptures associated with the 2016 event. In this study, we defined the Kiyama, Futagawa, and Kitamukiyama faults, previously mapped by the Research Group for Active Faults of Japan (1991), as the Futagawa fault. CKSZ, Central Kyushu Shear Zone (Oohashi et al., 2020). 1: Ishimura et al. (2021), 2: Sato et al. (2021), 3: Ueta et al. (2018), 4: Toda et al. (2019), 5: Kumahara et al. (2017b), 6: Okamura et al. (2018), 7: Iwasa et al. (2022), 8: Ishimura et al. (2022), 9: Kumahara et al. (2017b), 10: Takahashi et al. (2017), 11: Tsutsumi et al. (2018), 12: Ueta et al. (2018), 13: Inoue et al. (2019), 14: Shirahama et al. (2021).

In addition to field measurements of fault displacements (Shirahama et al., 2016; Okamura et al., 2018; Kumahara et al., 2022), the three-dimensional deformation caused by the 2016 event has been revealed by InSAR and differential light detection and ranging (lidar) analyses (Moya et al., 2017; Scott et al., 2018; He et al., 2019; Himematsu and Furuya, 2020; Aoyagi et al., 2021; Muroi et al., 2024). In particular, lidar differencing provides higher resolution and more accurate displacement information in areas with larger displacements than InSAR analysis. These types of analyses have been conducted along some parts of the 2016 rupture (Scott et al., 2018; Aoyagi et al., 2021; Muroi et al., 2024), revealing the details of three-dimensional deformation.

After the 2016 Kumamoto earthquake, more than 10 paleoseismic trenches were excavated on the Futagawa and surrounding faults (Fig. 1). A paleoseismic survey (Miyaji trench in Fig. 1) conducted on the Miyaji faults revealed that the fault moved about 2,000 years ago, which ~~overlapped~~ is consistent with the age range of the penultimate event of the Futagawa fault revealed by paleoseismic trenches (Ishimura et al., 2021). This suggests that the slip on the Miyaji faults has been repeatedly triggered by

the slip on the Futagawa fault in the past. In addition, trenching surveys on other short surface ruptures of the 2016 event within the Aso caldera also revealed activity preceding the 2016 event (Sato et al., 2021), suggesting the possibility of repeated synchronous ruptures. The interpretation of these trenches benefited from site conditions characterized by rapid sedimentation rates and multiple thin tephra layers (downwind of the Aso volcano), which enabled the identification of displacements as small as approximately 15 cm (Ishimura et al., 2021). The success of these efforts prompted us to search for sites along other faults near the Futagawa fault to examine the~~ir~~ timing of events and potential contemporaneous rupture ~~in relation to~~with the Futagawa fault.

In this study, we use lidar-based digital terrain models (DTMs) before and after the earthquake to calculate the three-dimensional displacement fields across the Futagawa and Idenokuchi faults, examining the amount of slip partitioning during the 2016 Kumamoto earthquake. Although Scott et al. (2018), Aoyagi et al. (2021), and Muroi et al. (2024) conducted differential lidar analyses along other sections of the 2016 rupture, there has been no study to estimate the amount of displacement in the area of slip partitioning between the Futagawa and Idenokuchi faults. Then, we conduct a paleoseismic trenching investigation of the Idenokuchi fault. We document the paleoseismic history of the Idenokuchi fault and compare our results with those of the Futagawa and Miyaji faults. The results indicate that all three faults have ruptured together multiple times in the past, providing insight into understanding the interaction of multiple faults in complex ruptures. The results also have implications for assessing displacement hazards associated with slip partitioning on secondary faults.

2. Regional Setting

Kyushu Island is part of the Southwest Japan arc and is the southernmost of the four main islands of the Japanese archipelago (Fig. 1). It is located on the Eurasian Plate, beneath which the Philippine Sea Plate is subducting northwestward at an oblique angle (Seno et al., 1993). Kyushu is characterized by many active volcanoes that have produced numerous tephra layers with well-established ages (Machida and Arai, 2003). Active faults are primarily concentrated in the central and northern regions of Kyushu (Research Group for Active Faults of Japan, 1980, 1991).

The central Kyushu region has been deformed by north-south extension since 6 Ma (Kamata and Kodama, 1994), and is structurally characterized by the Beppu-Shimabara graben (Matsumoto, 1979). This area is characterized by many east-west-striking normal faults (Research Group for Active Faults of Japan, 1991) and high levels of volcanic activity. According to Oohashi et al. (2020), central Kyushu has been a transtensional tectonic zone since approximately 1 Ma, referred to as the Central Kyushu Shear Zone (Fig. 1), characterized by dextral faults, rift zones, and volcanism.

2.1 Futagawa fault zone

The Futagawa fault (Fig. 1) is a ca. 25-km-long active dextral strike-slip fault (Watanabe and Ono, 1969; Research Group for Active Faults of Japan, 1980, 1991; Nakata and Imaizumi, 2002; Kumahara et al., 2017a; Suzuki et al., 2017) and generated the mainshock (Mw 7.0) of the 2016 Kumamoto earthquake sequence on April 16, 2016. Primary surface ruptures appeared during the mainshock along the previously mapped

active fault traces (Fig. 1; Kumahara et al., 2022). Dextral displacements of about 2 m were observed between Dozon and Futa along the central part of the Futagawa fault, with a maximum dextral displacement of 2.5 m at Dozon (Fig. 1; Shirahama et al., 2016; Okamura et al., 2018; Kumahara et al., 2022). Vertical displacement of about 1 m (south up) was observed along the central ~~to~~ and western parts of the Futagawa fault (Shirahama et al., 2016; Okamura et al., 2018; Kumahara et al., 2022). The right-lateral and vertical slip rates ~~of~~ for the Futagawa fault ~~around~~ determined near Futa ~~is~~ are 1.5–3.7 mm/yr ~~for the right lateral slip~~ and 0.9–1.1 mm/yr, respectively ~~for the vertical slip~~ (Ishimura, 2019).

The Idenokuchi fault is a 10-km-long active dip-slip fault primarily up on the south (Research Group for Active Faults of Japan, 1980, 1991; Nakata and Imaizumi, 2002), and also ruptured the surface during the mainshock of the 2016 Kumamoto earthquake (Fig. 1; Kumahara et al., 2022). ~~Multiple s~~Surface ruptures ~~appeared~~ occurred along ~~the~~ multiple subparallel faults. The maximum vertical displacement was 2 m (south up), and the average vertical displacement was about 1 m (Kaneda et al., 2022). Toda et al (2016) inferred that the vertical slip on the Idenokuchi fault was related to the slip partitioning of the oblique lateral slip on the Futagawa fault. There is no data on the slip rate of the Idenokuchi fault.

2.2 Previous paleoseismic survey along the Futagawa fault

Extensive paleoseismic trenching has been conducted along the Futagawa fault and its vicinity since the 2016 event (Fig. 1). They are divided into three types: 1) on the

surface ruptures along the primary Futagawa fault (Kumahara et al., 2017b; Takahashi et al., 2017; Okamura et al., 2018; Tsutsumi et al., 2018; Ueta et al., 2018; Toda et al., 2019; Ishimura et al., 2022; Iwasa et al., 2022), 2) on the surface ruptures along the Hinagu fault (Shirahama et al., 2021), and 3) on other secondary surface ruptures (Inoue et al., 2019; Ishimura et al., 2021; Sato et al., 2021). Almost all of them identified multiple events in the Holocene. Some studies estimated the age of the penultimate event on the primary Futagawa fault to be about 2 ka (Ueta et al., 2018; Toda et al., 2019; Iwasa et al., 2022; Ishimura et al., 2022). Comparison of paleoseismic information obtained after the earthquake with that before the earthquake (Headquarters for Earthquake Research Promotion, 2013) suggests that the Futagawa fault has been more active than previously assessed before 2016.

3. Methods and Data

3.1 Lidar differencing

We used a 2-m grid DTM ~~taken~~ surveyed from January 2013 to February 2014 and a 2-m grid DTM ~~taken~~ surveyed on 8 May 2016. Although we do not possess the original point cloud data of pre- and post-earthquake datasets, nor have the details for constructing the DTMs from the original point cloud data, all the DTMs were prepared under the regulations required for a public lidar survey in Japan. We used the Japan plane rectangular coordinate system II (in meters) as the coordinate system for all data.

We applied the 3D-Geomorphic Image Velocimetry method (Kokusai Kogyo Co., Ltd., 2010) for lidar differencing. The particle image velocimetry method and pre- and post-event DTMs (Fig. 2) were used to calculate the surface displacement vectors

following the methods of Mukoyama (2011) and Ishimura et al. (2019). Aoyagi et al. (2021) and Muroi et al. (2024) used this method for the eastern extension of the Futagawa fault inside the Aso caldera. The method procedure is as follows. First, we prepared slope-shaded images using pre- and post-event DTMs. We then carried out a grid search by moving a pre-event image in a pixel-by-pixel manner in the scanning area on the post-event image and estimated the position that exhibited the highest value of the coefficient of correlation using subpixel interpolation. Additionally, we calculated the horizontal and vertical components of displacement. Subsequently, we slid the search area in steps and repeated the image matching and calculation of the 3D displacement. Finally, we plotted the complete 3D vectors on maps. In this study, the search area size, search area step size, and output grid size were set to be 64 x 64 pixels (128 x 128 m), 5 m, and 5 x 5 m, respectively. Additionally, the theoretical error of this analysis is 0.1 pixel (0.2 m) due to subpixel interpolation in the displacement calculation.

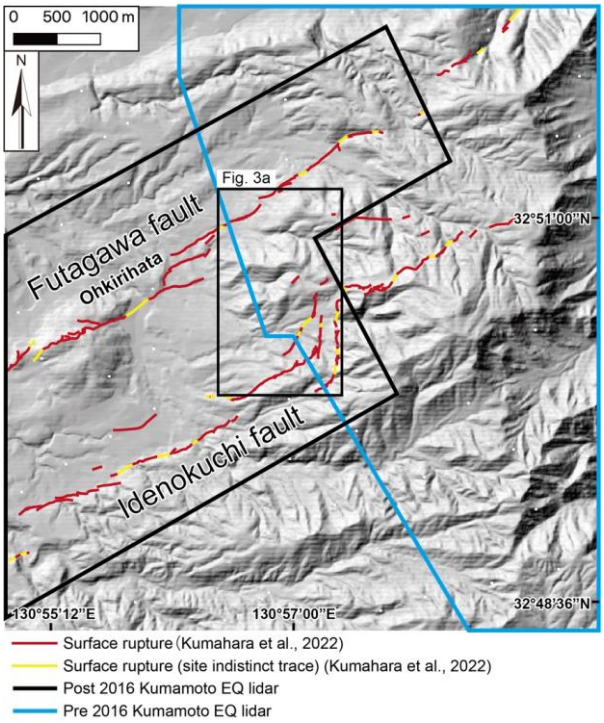

Figure 2. Extent of lidar data used to measure displacements and surface ruptures. ~~Lidar measurement areas~~. Lidar survey areas include the post-2016 Kumamoto earthquake (black polygon) and pre-2016 Kumamoto earthquake (blue polygon).

The expected ground motions during the measurement period are as follows: (1) the deformation associated with the 2016 Kumamoto earthquake, (2) the postseismic deformation (e.g., aftershocks and afterslip), (3) the background tectonic deformation, and (4) the artificial modification and present-day surface processes. We evaluate the deformation of items 2 and 3 using the GNSS observations in the study area. Based on the GNSS stations at the Choyo (960701), Aso (960703), and Takamori (960704) of GeoNET, the postseismic and background deformations (vertical, north-south, and east-

west components) from April 2010 to May 2016 are nearly equal to the theoretical error level (0.2 m). Thus, the deformations associated with items 2 and 3 are negligible.

3.2 Trench survey

We looked for an appropriate site for a paleoseismic excavation along the Idenokuchi fault (Figs. 2 and 3). We selected possible sites based on the following criteria: 1) minor artificial modification, 2) clear surface rupture traces, and 3) stable and continuous sediment deposition. As a result, we selected a trench site on a gentle slope characterized by parallel fault traces of the Idenokuchi fault, expecting trapped sediment and stable and continuous soil deposition (Fig. 3). The trench site is on an apparent single surface rupture (north-up normal fault), and another surface rupture (south-up normal fault) runs parallel on its southeast side. Currently, the fields are cow ranches with minor artificial modification.

We excavated a 13-m-long, 5-m-wide, and 3.5-m-deep trench (Fig. 3; KMR trench) and established a grid system on the trench walls. We logged the walls and collected samples for tephra analyses and radiocarbon dating. To further examine the subsurface geology, we used a 50 cm long and 4 cm wide corer to obtain seven cores from the trench floor and the upthrown side (Fig. S1). We used a Nikon Nivo5.SC total station to map the locations of the surface ruptures, trench, and coring sites (Fig. 3b).

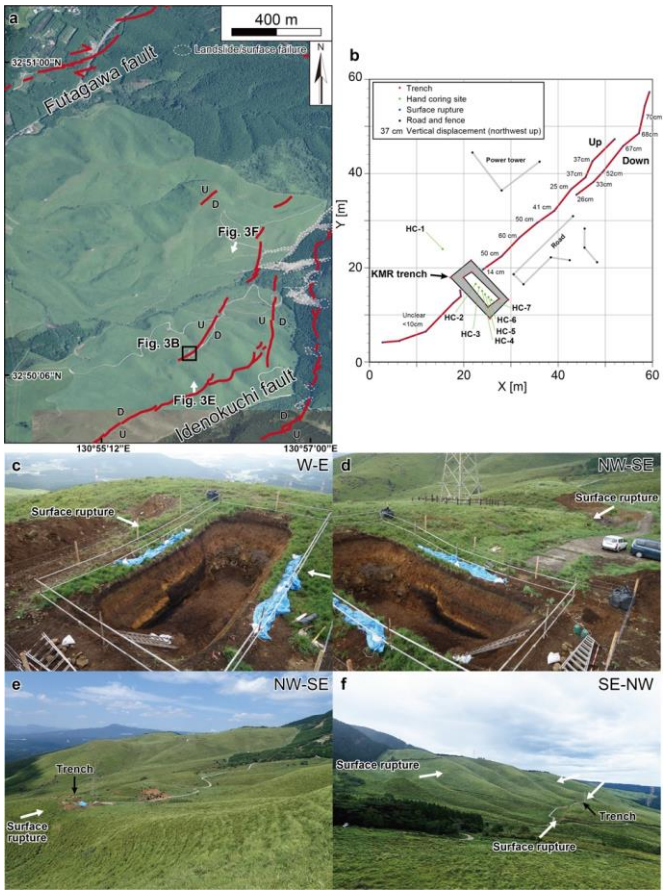

Figure 3. Geomorphic map and photographs around the trench site. (a) Red lines show the 2016 surface ruptures (Kumahara et al., 2022). Aerial photograph from the Geospatial Information Authority of Japan. (b) Location map of the trench and surface ruptures. Numbers indicate vertical displacement measurements. (c) Photo of the west wall of the trench. (d) Photo of the east wall of the trench. (e) (f) Photos of geomorphic conditions around the Idenokuchi fault trench site. Photo locations are shown in Fig. 3a.

260

3.3 Laboratory analysis

We determined refractive indices and major element compositions of volcanic glass shards in the sampled tephras. First, we sieved the samples with water through a 62-

μm nylon mesh. Then, we oven-dried the samples at 50 ℃ and sieved the dried samples through a 120-μm nylon mesh. The refractive index of volcanic glass shards in the 62–120 μm fraction of each sample was measured with a RIMS 2000 refractive index measuring system (Kyoto Fission Track Co., Ltd.) with an accuracy of ±0.0002 (Danhara et al., 1992). The major element composition of volcanic glass shards was measured by an energy-dispersive X-ray spectrometry (EDAX Genesis APEX2 and JEOL JSM-6390) following the method and analysis conditions described by Suzuki et al. (2014). Volcanic glass shards of the AT tephra sampled at Chigaki, Toyama Prefecture (Machida and Arai, 2003) were used as a working standard to check data reproducibility and instrument stability. A total of 12 tephra samples from the trench walls were analyzed and compared to two reference samples (Tables S1, S2, and S3).

A total of 26 radiocarbon samples, including charcoal and organic sediment (Table S4), were dated by accelerator mass spectrometry at the Laboratory of Radiocarbon Dating, University Museum, University of Tokyo, and the Institute of Accelerator Analysis Ltd., Japan. The obtained ages were calibrated using the OxCal 4.4 software (Bronk Ramsey, 2009) with the IntCal20 dataset (Reimer et al., 2020). The ages of paleofaulting events were calculated in the OxCal program by Bayesian analysis (Bronk Ramsey, 2008).

4. Results

4.1 3D displacement analysis

Figure 4 shows the distribution of 3D displacements during the 2016 earthquake, and Figure 5 shows topographic displacement profile lines A-D. In the profile lines (Fig.

5), the horizontal component is divided into two parts: parallel to the general strike of the Futagawa fault (N57°E) and perpendicular to it. The vertical component (Figs. 4c and 5) shows a displacement of 1.0–2.5 m at the southernmost part of the Idenokuchi fault and a vertical displacement of several tens of centimeters at the northern part of the fault. Compared to field measurements (Kaneda et al., 2022), a similar displacement was observed along the southernmost branch of the Idenokuchi fault, where a 2 m vertical displacement was recorded. However, the amount of vertical displacement along the fault is noisy and subject to uncertainty because of slope failures in the surrounding area. Along the parallel splay of the Idenokuchi fault, where we excavated the KMR trench, there is no significant difference between the calculated and field-measured displacements. On the other hand, on the Futagawa fault, the amount of local vertical displacement associated with the dextral displacement is observed in a narrow section about 200 m wide. When viewed over a 200–400 m wide zone from the fault, virtually no vertical displacement is observed. The vertical displacement along the long baseline (> 3 km) extending across both the Futagawa and Idenokuchi faults is about 1 m south-up (Lines A and B in Fig. 5).

A large fault-parallel displacement was observed on the Futagawa fault, and 1.8–3.1 m of dextral displacement occurred on the western part of the calculated area (Figs. 4b and 5). Since the displacement measured in the field was approximately 1.5–2.0 m (Shirahama et al., 2016; Kumahara et al., 2022), the 3D displacement data can be used to determine both the amount of off-fault displacement and on-fault displacement. This trend has also been discussed by Scott et al. (2018). In the western part of the Futagawa fault, larger dextral displacements were obtained for the long baseline (1 km) compared

310 to the short baselines (35 m and 100 m). Although it is difficult to identify from the 3D displacement distribution map (Fig. 4b), a slight sinistral displacement occurred on the Idenokuchi fault, which is consistent with the field measurements (Toda et al., 2016; Shirahama et al., 2016; Kaneda et al., 2022). In the eastern half of the calculation area, the contrast in displacement is smaller, the amount of displacement decreases, and there
315 is greater variability because surface failures and other factors may have also occurred. The dextral displacement along the long baseline (> 3 km) between both faults is about 2–2.5 m.

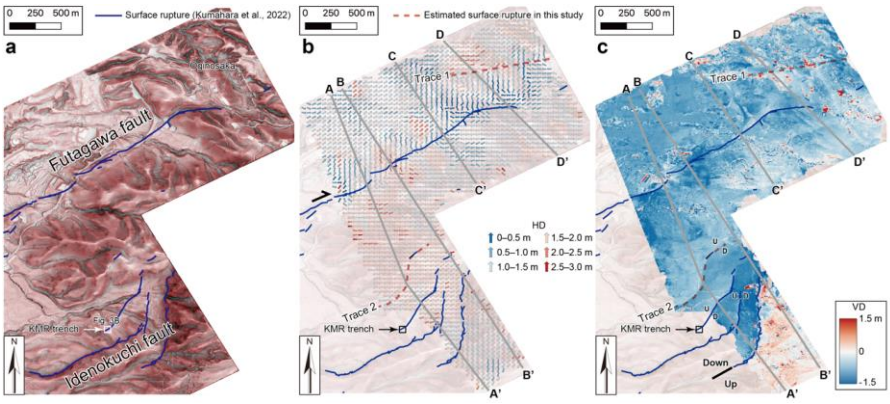

Figure 4. Results of the differential lidar analysis. (a) Red relief image map around the study area. The map was created following the methods of Kaneda and Chiba (2019). Surface ruptures are after Kumahara et al. (2022). (b) Horizontal displacement field. Horizontal displacement is indicated by the arrow and color. (c) Vertical displacement field. Vertical displacement is shown by the color map. HD: horizontal displacement, VD: vertical displacement. Letters (i.e., A-A') indicate endpoints of displacement profiles shown in Figure 5.

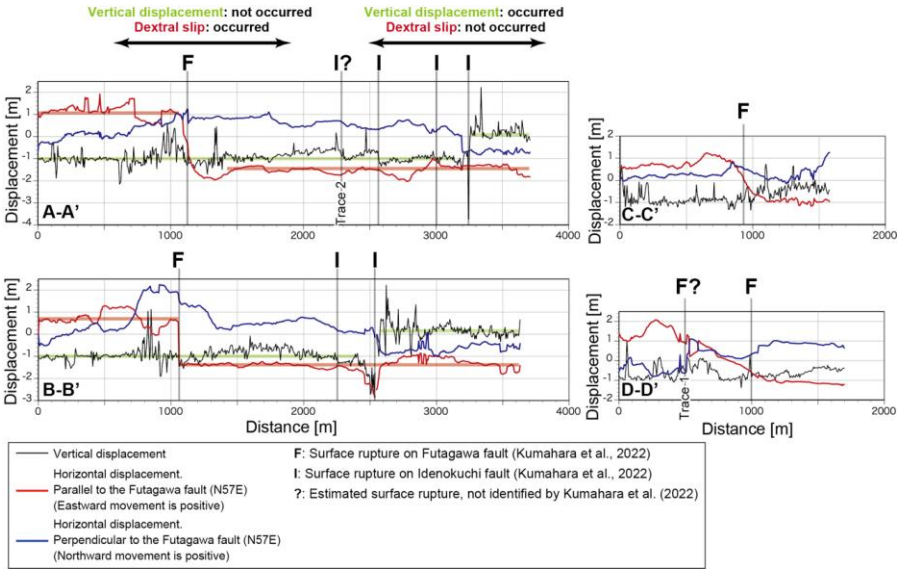

Figure 5. Vertical and horizontal displacement profiles. The profile lines are shown in Figure 4.

Regarding the fault-perpendicular component (Fig. 4b and A-A' and B-B' in Fig. 5), extension occurred locally on the Idenokuchi fault, and contraction occurred locally on the Futagawa fault. The extension is large at the southernmost part of the Idenokuchi fault, with a displacement of about 1–1.5 m. A contraction of about <1 m occurred on the Futagawa fault. The displacement in the perpendicular direction of the fault along the long baseline (> 3 km) across both faults is approximately 1 m of extension.

The 3D displacement observations and field measurements ~~generally agreed~~are generally in agreement in terms of ~~on~~ the locations of surface ruptures and the amount and sense of displacements. However, in two locations, surface ruptures were inferred from the displacement data but have not been confirmed in the field (Trace 1 and Trace 2;

Figs. 4b and 4c). Trace 1 occurs north of the Futagawa fault in the eastern part of the calculated area. Here, slight contrasts in fault parallel and perpendicular components are observed. Although it is unclear whether these displacements are associated with a well-defined fault, the discontinuity projects towards a surface rupture that continues eastward into the caldera (Kumahara et al., 2022). It also coincides with a 2 m shortening identified at a bridge abutment near Oginosaka (Fig. 4) (Shirahama et al., 2016). Trace 2 is a north-up displacement recognized along the northernmost splay of the Idenokuchi fault. Here, a short surface rupture was recognized (Kaneda et al., 2022), and it is likely to extend further to the southwest. However, it coincides with the present valley topography and may have been affected by fluvial erosion and other factors during the DTM measurement period.

4.2 Paleoseismic trench

4.2.1 Trench stratigraphy (including tephra analysis)

The trench exposed a package of silts, clays, and paleosols, separated from gravels and bedrock, across the primary normal fault. Figure 6 shows photomosaics and sketches of the west, east, and north walls. In this trench, sediments with different sedimentary facies and ages accumulated on the north (footwall, upthrown side) and south (hanging wall, downthrown side) sides across the primary normal fault at W9/E9. For this reason, the footwall and hanging wall sediments are assigned different unit numbers except for the topsoil (unit 00), which extends across the entire exposure.

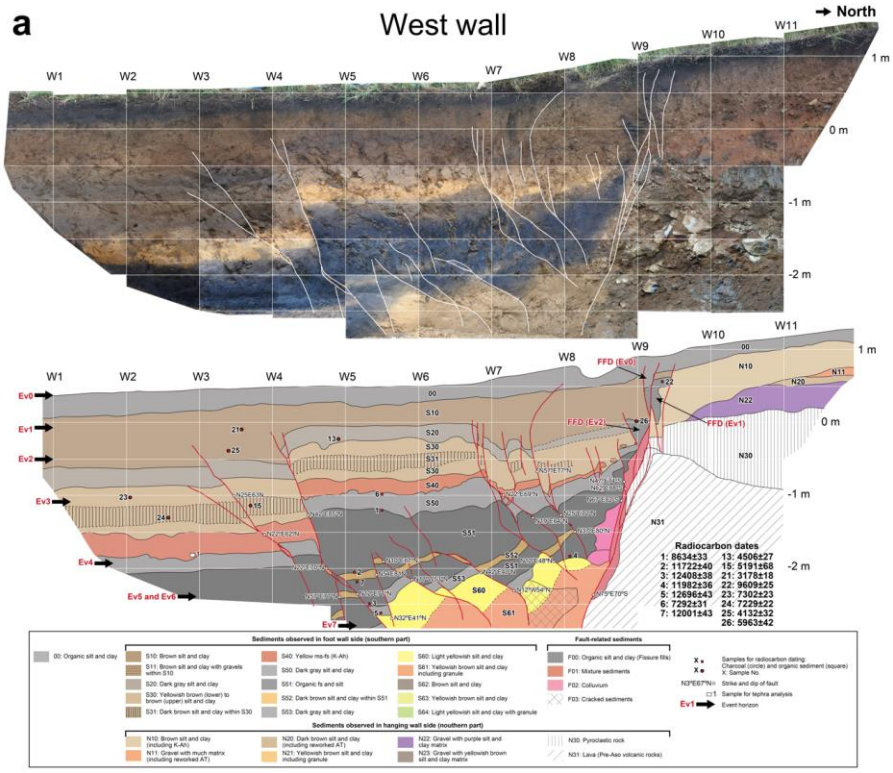
a
West wall
North
W1
W2
W3
W4
W5
W6
W7
W8
W9
W10
W11
1 m
0 m
-1 m
-2 m
FFD (Ev0)
FFD (Ev1)
FFD (Ev2)
Ev0
Ev1
Ev2
Ev3
Ev4
Ev5 and Ev6
Ev7
Radiocarbon dates
1: 8634±33
2: 11722±40
3: 12408±38
4: 11982±36
5: 12696±43
6: 7292±31
7: 12001±43
13: 4506±27
15: 5191±68
21: 3178±18
22: 9609±25
23: 7302±23
24: 7229±22
25: 4132±32
26: 5963±42
Sediments observed in foot wall side (southern part)
Fault-related sediments
Sediments observed in hanging wall side (southern part)

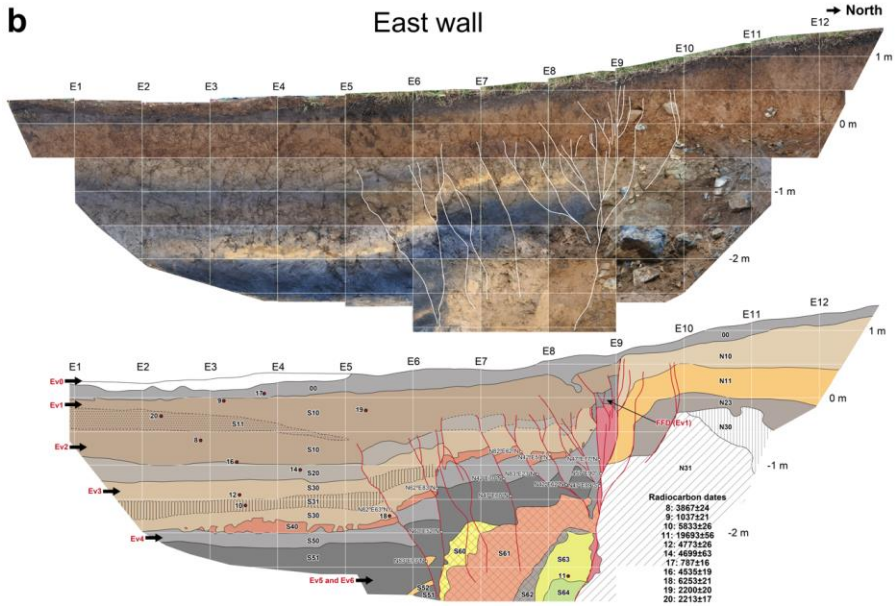
b
East wall
North
E1
E2
E3
E4
E5
E6
E7
E8
E9
E10
E11
E12
1 m
0 m
-1 m
-2 m
Ev0
Ev1
Ev2
Ev3
Ev4
Ev5 and Ev6
N10
N11
N23
N30
N31
S10
S20
S30
S40
S50
S51
S61
S63
S64
Radiocarbon dates
8: 3867±24
9: 1037±21
10: 5833±26
11: 19693±56
12: 4773±26
14: 4699±63
17: 787±16
16: 4635±19
18: 6253±21
19: 2200±20
20: 2213±17

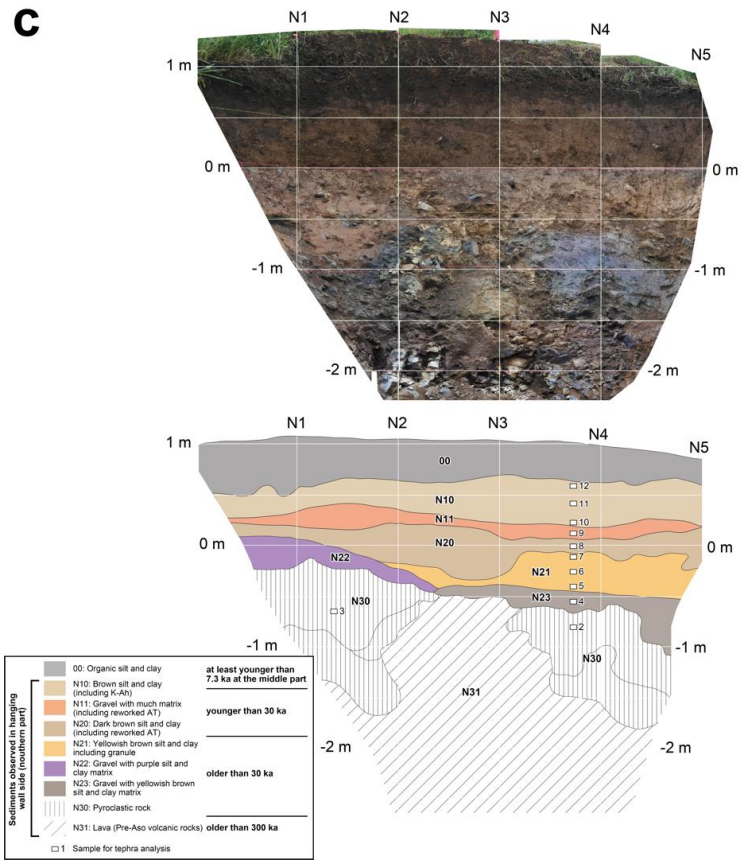

355

Figure 6. Photomosaics and sketches of the stratigraphic and structural relations exposed in the KMR trench walls. (a) West wall. The sketch of the west wall is flipped. (b) East wall. Legend shown in (a) applies to both the west and east walls. (c) North wall. FFD: fissure-fill deposits.

Commented [RDK1]: Headings on the legend are switched. Should say "Sediments observed in the hanging wall (southern part)". And "Sediments observed in the foot wall (northern part). Please correct. Also it would be nice to add the definition of "FFD" to the legend.

~~The following describes the sediments from the upper part of the south side.~~

Sediments exposed in the south side of the trench (hanging wall) were deposited relatively continuously (Fig. 6a and 6b) and are described from ~~the~~ youngest to oldest.

360 Unit 00 is the topsoil, consisting of black, organic silt and clay. Unit S10 is a thick, brown

silt and clay below unit 00. On the east wall, an interbed within unit S10 consisting of gravelly clay was classified as unit S11. Unit S20 is a dark gray silt and clay and is considered an organic-rich paleosol. Unit S30 is a yellowish brown to brown silt and clay with a slightly darker interbed (unit S31), which is an organic-rich paleosol similar to unit S20. Both Units S30 and S31 slightly thicken to the south away from the primary normal fault. Unit S40 is composed of fine to medium yellow sand, mainly composed of volcanic glass that is bioturbated and discontinuous in places. Units S50 and S51 are organic-rich paleosols. Unit S50 is dark gray silt and clay, and unit S51 is organic silt and fine sand, with unit S50 slightly lighter in color than unit S51. Unit S52 is yellowish brown to brown silt and clay interbedded within unit S51. Unit S53, which is observed only on the west wall, is a slightly lighter gray silt and clay similar to unit S50. ~~The base of u~~Unit S53 ~~is~~ has an undulating basal contact suggesting an unconformity with unit ~~between units S53 and~~ S60 on the ~~east~~ west wall~~, indicating an unconformity between them~~. Unit S60 is a bright yellowish silt and clay, and unit S61 is a yellowish-brown silt and clay with granules. On the west wall, unit S61 is the lowest (oldest) deposit. On the east wall, unit S61 is underlain by brown to yellowish brown silt and clay (units S62 and S63). The basal deposit (unit S64) is a light yellowish silt and clay with granules.

Sediments exposed in the north side of the trench ~~on the(~~-footwall) are thinner than those on the hanging wall and are primarily composed of gravel and rock (Fig. 6). The footwall sediments are slightly different between the east and west walls, and are thus described from the north trench wall which exposed the entire footwall package (Fig. 6c). Unit N10, consisting of brown silt and clay, has an erosional relationship with the underlying unit N11 and lower units (see west wall in Fig. 6a). Unit N11 is a matrix-

supported gravel bed. Units N20 and N21 are dark brown and yellowish-brown silt and clay, respectively. Both units N22 and N23 are matrix-supported gravel beds that vary in color from purple to yellowish brown. Unit N30 is a pyroclastic rock unit with an undulating and irregular basal contact. Unit N31 is composed of fragmented lava from pre-Aso volcanic rock, which forms the basement rock of the surrounding area (Hoshizumi et al., 2004).

To further explore the site stratigraphy, a transect of cores was advanced into the floor of the trench on the hanging wall (cores HC-2 to HC-7) and beyond the limits of the trench on the footwall (core HC-1) (Fig. S1). Core HC-1 revealed nearly identical stratigraphy and thicknesses as that exposed on the trench walls, from which we infer that the sediments exposed on the north wall are distributed widely and uniformly on the northern side of the fault. On the downthrown side (HC-2 to HC-7), the black silt and clay and yellowish brown to brown silt and clay, corresponding to unit S51 and lower, were observed. No black soil, corresponding to units S51 to S53, was observed at depths greater than 1 m from the trench floor. Gravel and sand beds, not recognized on trench walls, were observed in some cores. However, no tephra layers were identified. On the other hand, sediments were in contact with high angles, and voids were observed in some cores, which we inferred to be faults. The primary normal fault was considered the boundary with the basement rock, so we inferred the normal fault at a depth where drilling was no longer possible.

405 4.2.2 Faults

In this trench, we identified faults, rootless faults, and cracks. Faults refer to discontinuities with apparent displacement that extend downward to the bottom of the trench. Rootless faults are those with apparent displacement but do not extend downward to the trench bottom. Cracks are those without displacement. Although we observed many 410 cracks on the trench walls, we did not show them in the figures because they were interpreted to be related to drying of the walls and did not affect the paleoseismic interpretations. The primary normal fault is observed at W9/E9, and many other faults are rootless with bending in the lower part. Faults extending down to the trench bottom are the north-up normal faults at W9/E9 and the reverse faults at W3-W5 and E5-E6. Normal 415 faults that form grabens develop at W7-W9 and E7-E10. The 2016 displacement was an open crack near W9/E9, which was already filled with sediments at the time of trench excavation. Similar open cracks and fissure fill deposits have been identified in the Futa trench at Futa (Fig. 1; Ishimura et al., 2022). However, no other distinct 2016 displacement (e.g., apparent vertical displacement) was observed on the trench walls. 420 This is likely because the trench is located in an area of decreasing vertical displacement from northeast to southwest, where the 2016 displacement is small (<14 cm) and indistinct (Fig. 3b). Other fissure-fill deposits that may have formed prior to the 2016 event were also identified below the 2016 fissure-fill deposits. Measurements of the strike and dip of the faults on the trench walls indicate that the predominant strike is 425 northeast to southwest, but some are north to south or east-northeast to west-southwest (Fig. 6). The northeast-southwest strike is consistent with the surface ruptures (Fig. 3b). The other strike directions suggest that subsidiary surface ruptures to the primary normal fault may have occurred in the past events.

4.2.3 Tephra analysis

We completed tephra analysis for unit S40 (sample No. 1) on the hanging wall as well as a suite of 11 samples (Sample No. 2 to No. 12) from the footwall (Table S1 and Fig. 6). The results of the tephra analysis are shown in Table S1, and the major element composition of volcanic glass shards is shown in Tables S2 and S3. The results show that unit S40 is composed almost entirely of volcanic glass, with a refractive index of 1.510-1.512 (mode: 1.511), suggesting that it correlates with the widespread tephra, Kikai-Akahoya (K-Ah), by the eruption of southern Kyushu at 7.3 ka (Machida and Arai, 2003; Smith et al., 2013). The chemical compositions confirmed this correlation (Table S2), consistent with the existing studies in the vicinity (e.g., Ishimura et al., 2022). Volcanic ash analysis of the samples from the north wall (Samples No. 2 to No. 12) revealed no tephra layers. Therefore, we examined the volcanic glass content and refractive indices to determine if the samples contained volcanic glass shards of Aira-Tn (AT) (30 ka; Smith et al., 2013) and K-Ah tephras, which are commonly identified tephras in this area (Machida and Arai, 2003). The results (Table S1) show that there is almost no volcanic glass below unit N21, while units N20 and N11 exhibit very low volcanic glass content (2%). The refractive indices of volcanic glass are mainly 1.495-1.500, which correlates with AT tephra. In contrast, the volcanic glass content increases from the lower to the upper part of unit N10. The refractive indices show that while unit N10 contains glass with a refractive index of 1.497-1.500 of AT origin, the percentage of volcanic glass of 1.508-1.512 of K-Ah origin increases toward the upper part of unit N10. This suggests that the age of the middle part of unit N10 ~~is after~~postdates the K-Ah tephra. This mixing

Commented [RDK2]: It would be more clear and help the reader if this could be annotated on the trench logs. For the west wall a label could be added directly to the log within S40 "7.3 ka K-AH tephra". For the east wall, it's a little tight so I suggest labeling it below the log with a tag line to S40. I have added this to a mocked up version (attached to this review). You can decide how to best clearly show this.

of AT and K-Ah volcanic glass is also observed in soils in other regions, and the K-Ah ash fall horizon is roughly estimated at the peak of K-Ah volcanic glass shard content (Ishimura and Kakiuchi, 2011). Such distribution of volcanic glass shard content may be due to bioturbation and secondary deposition of tephra-origin particles. Based on the presence of AT volcanic glass, unit N20 is at least younger than 30 ka, and unit N21 and below are older than 30 ka. Based on the K-Ah glass content, the upper to middle part of unit N10 is interpreted to be at least younger than 7.3 ka. The fact that K-Ah tephra is exposed in the hanging wall indicates that sediment preservation potential is better on the downthrown side of the fault.

4.2.4 Radiocarbon dating

Because the faulting events described below were identified on the downthrown side of the primary normal fault, we performed radiocarbon dating of samples collected from the south side of ~~the~~ both trench walls. A total of 26 samples were analyzed. Sample locations and ages are shown on the trench logs (Fig. 6) and radiocarbon data is summarized in ~~(~~Table S4~~)~~. The youngest age was 787 ± 16 yr BP (charcoal; Sample 17) from unit 00, and the oldest was 19693 ± 56 yr BP (charcoal; Sample 11) from unit S63. In general, the radiocarbon results are stratigraphically consistent (progressively older ages with depth, with only several exceptions explained below. For sediments older than unit S50, bulk samples (organic sediments) were dated except for the sample from unit S63. As Ishimura et al. (2022) pointed out, the ages of bulk samples in this region are sometimes younger than the actual ages. In this trench, we compared the bulk sample ages with the ages of the K-Ah tephra and the charcoal from unit S63. As a result, the

Commented [RDK3]: It is nice to see the sample ages listed on the side of the logs, however it would be more clear if the ages were also shown on the logs. It makes it easier for readers to evaluate the trench. I realize this will get a little cluttered in places so you will have to be creative on how to best show this. I have annotated them on the logs attached, but you can decide how to best show this.

Commented [RDK4]: Trench logs show 26 samples, but table S4 only shows 24. Need to add samples #25 and #26 to table S4.

bulk sample ages were consistent with the tephra and charcoal age, with no contradiction between the stratigraphy and age. Because we used charcoal samples above unit S30, it is possible that older charcoals were included by reworking, resulting in older ages. In such cases, charcoals with younger ages in the same unit were employed for further analyses. As a result, we did not use the ages, 7302 ± 23 yr BP and 7229 ± 22 yr BP from samples 23 and 24, respectively (Table S4). Additionally, the ages of bulk samples collected within the fissure-fill deposits (samples 22 and 26) ~~using the bulk samples~~ were significantly older than the surrounding sediments. The specific organic matter responsible for the cause is unknown because they are bulk samples. One possibility is that the trench site is located on an uphill−facing scarp, acting as a trap for sediments, allowing old organic matter to deposit along faults and open fractures. In any case, it is thought that the fissure-fill deposits contained old organic matter. Therefore, the ages of these fissure-fill deposits are also not used.

4.3 Evidence for paleofaultings

We identified geologic evidence for faulting events since the deposition of unit S53 by stratigraphic evidence (Fig. 6) and retrodeformation (Fig. 7 and S2). Ev0 is the 2016 event, and an open crack occurred directly above the primary normal fault near W9/E9 (Fig. 6a and 6b). In Ev0, a further open crack was formed in the pre-existing open crack created by Ev1 (the penultimate event), which is described in the following paragraph. This pre-existing crack was already filled with sediment at the time of our survey. Similarly, an open crack directly above the primary normal fault, located near E9, is recognized on the east wall (Fig. 6b). The surface rupture runs between W8-W9 and

E8-E9, corresponding to the locations of open cracks. These observations confirm that the 2016 event formed these open cracks.

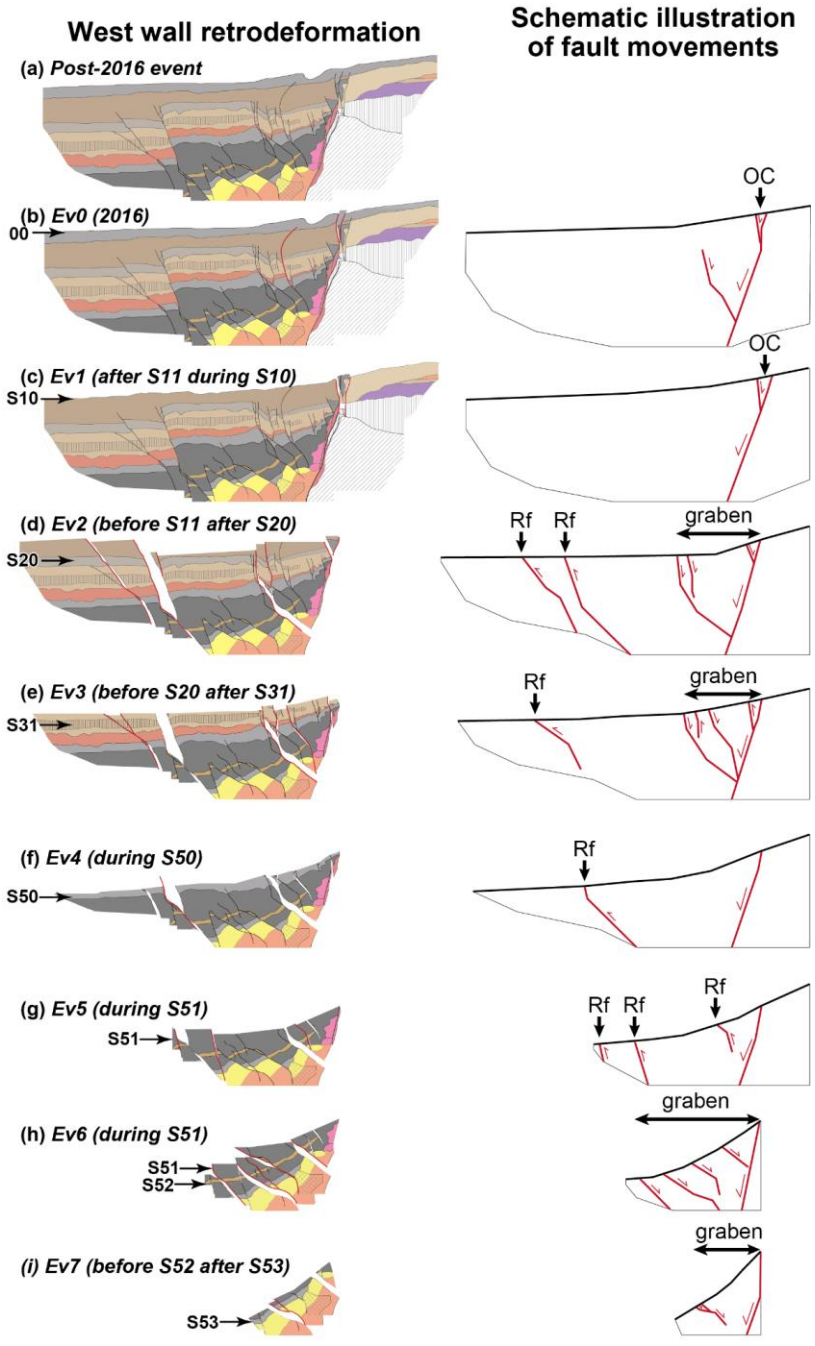
West wall retrodeformation
Schematic illustration of fault movements
(a) Post-2016 event
(b) Ev0 (2016)
00
(c) Ev1 (after S11 during S10)
S10
(d) Ev2 (before S11 after S20)
S20
(e) Ev3 (before S20 after S31)
S31
(f) Ev4 (during S50)
S50
(g) Ev5 (during S51)
S51
(h) Ev6 (during S51)
S51
S52
(i) Ev7 (before S52 after S53)
S53
OC
OC
Rf
Rf
graben
Rf
graben
Rf
Rf
Rf
Rf
graben
graben

500

Figure 7. Retrodeformation of the faults and deformed strata, and schematic illustration of fault movements on the west wall. The left figures show reconstructions of the displacement for each event, and the right figures show the faults that were active during each event. Rf: reverse fault, OC: open crack.

Ev1, like Ev0, developed an open crack directly above the primary normal fault near W9, which was immediately next to the open crack of Ev0 and filled by fissure-fill deposits. On the west wall, this fissure-fill deposit was formed in unit S10 during Ev1 and was displaced at the southern part by Ev0 event. Unit S10, displaced by Ev1, is stratigraphically positioned above unit S11, which ~~was probably~~may have been deposited by a slope failure in Ev2 as described in the following paragraph. Therefore, Ev1 is interpreted to have occurred during the deposition of unit S10, ~~especially~~ particularly after unit S11 deposition.

In Ev2, an open crack, normal fault displacements near the primary normal fault (W7-W9), and reverse fault displacements on the southern faults (W3-W4) occurred. Subsidiary normal and reverse faults displaced unit S20 and the lower part of unit S10, and a fissure-fill deposit was identified on the west wall (W9, 0 m). Therefore, this event occurred after the deposition of unit S20 paleosol and during the deposition of unit S10. Similarly, on the east wall, unit S20 was deformed by normal fault displacements ~~were observed~~ near the primary normal fault (E7-E9), and reverse fault displacements across ~~the~~ faults ~~in~~ to the south (E5-E6) ~~show reverse fault displacements~~. In addition, the gravel-rich unit S11 is recognized in unit S10 on the east wall, which is wedge-shaped and may be a deposit supplied from the southern slope, rather than from the main normal fault in the trench. A similar surface failure occurred in the southern slope along the

Idenokuchi fault during the 2016 earthquake (Fig. 3a). Unit S11 is stratigraphically above the basal part of unit S10 and the faulted S20 deposit. Therefore, unit S11 may be a post-earthquake deposit related to Ev2. Thus, the event horizon of Ev2 is ~~estimated~~ inferred to be after unit S20 and before unit S11.

Ev3, like Ev2, involved normal fault displacements near the primary normal fault (W7-W9) and reverse fault displacements on the southern faults (W3-W4). The east wall similarly shows normal fault displacements at E7-E9 and reverse fault displacements of the southern faults (E5-E6). On the east wall, even after restoring the fault displacement of Ev2, vertical displacement was still observed in faults at E6-E8 (Fig. S2). This indicates cumulative displacement, suggesting fault activity between units S20 and S40. The fault at W3 displaces unit S31, but does not displace unit S20. Therefore, the event horizon of Ev3 is ~~estimated~~ inferred to be between units S20 and S31.

Ev4 is indistinct on the west wall, while it is distinct on the east wall. On the east wall, even after restoring the fault displacement of Ev2 and Ev3, vertical displacement was still observed for the reverse fault at E6 and normal fault at E8-E9 (Fig. S2). This indicates cumulative displacement, suggesting fault activity between units S40 and S51. Therefore, the event horizon of Ev4 is ~~estimated~~ inferred to be during the deposition of unit S50.

Ev5 and Ev6 occurred after the deposition of unit S52 and during unit S51 deposition. During this period, reverse and normal subsidiary fault displacements are observed in W4-W8 even after restoring the fault displacement of Ev2 to Ev4 (Fig. 7). Although it is possible that both displacements occurred during a single event, we

estimate two separate events (Ev5 and Ev6). From the retrodeformation (Figs. 7 and S2), we found that the displacement patterns tended to be similar in consecutive events. In other words, Ev0 and Ev1 created open cracks along the primary normal fault (W8-W9), and Ev2 to Ev4 caused reverse fault displacement in the southern part and normal fault displacement on the primary normal fault. Additionally, Ev7 involves only normal fault displacement as described in the following paragraph. Considering the similarity of the displacement patterns in consecutive events, reverse fault motions could be related to Ev5, and normal fault motion could be related to Ev6 (Fig. 7). Therefore, we interpreted that there could have been two events during this period, however ~~,~~ we recognize that the observed deformation can also be attributed to a single event. Since the ages of Ev5 and Ev6 cannot be distinguished, both events are only constrained as after unit S52 and during unit S51 deposition.

In Ev7, a normal fault displacement at W7-W8 occurred at the lowest part of the soil deposits in this trench. On the west wall, even after restoring the fault displacement of Ev2 to Ev6, vertical displacement was still observed in the normal fault at W6 (Fig. 7) from which we infer the occurrence of Ev7. Its age is estimated to be between units S52 and S53 deposition. We recognize that the small amount of remaining offset after retrodeformation could be related to thickness (facies) changes in the deposit, variable deformation related to later events, and/or a component of oblique slip and not necessarily require an additional earthquake.

Units 60-64 may represent sediments downdropped in earlier events. ~~The~~, however, the available exposure is complicated and precludes clear identification of additional events.

Commented [RDK5]: Attributing one event to one fault strand and another event to a different fault strand at the same stratigraphic level is not very compelling evidence for two events. Could be possible. However, it is critical to acknowledge that is could be one event. Event Ev5/6.

Commented [RDK6]: A small remaining vertical displacement on one trace is not very compelling evidence. Could be but should be considered uncertain.

Commented [RDK7]: Probably worth adding a final paragraph here that indicates potential older events that are not resolvable.

~~However~~Thus, an unknown number of events may have occurred prior to about 12 ka. Deeper excavations would be required to test this possibility.

Commented [RDK8]: Added this as a suggestion.

5. Discussion

5.1 Slip partition based on 3D displacements

In this section, we discuss how the displacement is divided on the Futagawa and Idenokuchi faults for the slip partition along line A (Fig. 5), where the influence of surface failure is small and the Futagawa fault appeared as a single trace (Fig. 4). First, dextral displacement occurred only on the Futagawa fault. Local sinistral displacement was observed along the Idenokuchi fault in the field (Toda et al., 2016; Shirahama et al., 2016). However, along the long baseline (> 3 km), the amount of lateral displacement was similar across the Idenokuchi fault. On the other hand, the vertical displacement is the opposite of the lateral displacement. Vertical displacement of 1 m occurred only in the southernmost trace of the Idenokuchi fault along the long baseline, and little vertical displacement occurred within a 1 km width across the Futagawa fault. Vertical displacement of several tens of centimeters occurred on the subparallel faults of the Idenokuchi fault, but that decreased immediately within a short distance from the fault, indicating that the deformation was localized to a shallow depth. These observations suggest that extensional deformation and block rotation cause apparent vertical displacement on the subparallel faults.

Scott et al. (2018) and Himematsu and Furuya (2020) observed a large vertical displacement (1-2 m south-up) on the Futagawa fault on the west side of the parallel section of the Futagawa and Idenokuchi faults. This indicates that the Futagawa fault accommodated oblique slip on the west side of the Idenokuchi fault's parallel section. In

addition, Himematsu and Furuya (2020) showed a sharp decrease in vertical displacement and nearly constant right lateral displacement along the Futagawa fault at the parallel section of the Idenokuchi fault, which is consistent with our results.

Our observations suggest that the slip partition on the Futagawa and Idenokuchi faults is the result of oblique lateral displacement at depth, which is almost completely split into dextral and vertical displacement near the surface and accommodated by both faults, respectively, as shown schematically by Toda et al. (2016). In addition, our results show that the displacement is completely split, as shown in King et al. (2005). This may provide an important insight into the geometry (dip angle, distance of two faults, and amount of oblique displacement) of faults where slip partitioning can occur. We interpret that the deeper part of the Idenokuchi fault is connected to the deeper part of the Futagawa fault, and the Idenokuchi fault is a branch fault of the Futagawa fault. The estimated depth at which they merge may be several kilometers, as shown by Toda et al. (2016), although it depends on their dip angles.

We discuss the relationship between slip partition and geology. According to King et al. (2005), the depth at which the fault branches upwards may coincide with the bottom of surface sediments. Aoyagi et al. (2024) reported another slip partition on the western part of the Futagawa fault based on the surface rupture distribution of the 2016 event, drilling cores, and seismic reflection survey. They reported that the short (<2 km) subparallel surface ruptures/faults accommodated oblique slip in the deeper part of the 2016 Kumamoto earthquake and converged at a depth of 350 m. The depth corresponds to the top of the pre-Aso volcanic rocks and/or Kiyama metamorphic rocks (Kumamoto Prefecture Geological Map Compilation Committee, 2008). Unconsolidated sediments,

including pyroclastic flow deposits of middle to late Pleistocene age, overlie these rocks. Thus, the upper end depth (convergent depth of both faults) of oblique slip seems to correspond to some geological (physical property) difference. There is no data on the deep subsurface geology of our study area. Since there is no surface sediment (unconsolidated) and pre-Aso volcanic rocks are exposed on the surface around the trench site, the situation differs from that in King et al. (2005) and Aoyagi et al. (2024).

Commented [RDK9]: So if the situation differs, can you offer a final concluding statement here that summarizes what it means.

5.2 Age of paleofaulting events on the Idenokuchi fault

Based on evidence for paleofaulting events, we ~~estimated~~ infer six certain faulting events including ~~(~~Ev0–Ev4~~,~~ and a single event (combined Ev5/Ev6) that occurred since the deposition of unit S53. ~~Ev7) and two~~We also interpret several additional less certain events including Ev7 and the possibility that two events occurred after the deposition of S52 (Ev5 and Ev6 as separate events~~) faulting events since the deposition of unit S53~~. The ages of the faulting events were obtained using OxCal (Fig. S4). The results show that the ages of each event are as follows: Ev1: 2190–940 cal BP, Ev2: 4760–4250 cal BP, Ev3: 6040–5360 cal BP, Ev4: 9550–7280 cal BP, Ev5-Ev6: 13500–9680 cal BP, Ev7: 14700–13840 cal BP with the 2σ range. The average recurrence interval of the maximum of eight interpreted events is 1990–2110 years. Unit S53 is buried 4.5–5 m below the present ground surface, indicating that the strata dropped an average of 0.6–0.7 m per event relative to the ground surface. This value is roughly consistent with a representative 2016 coseismic displacement of 60 cm along the surface rupture, where the KMR trench was excavated. Despite the shallow depth of the trench, we could identify up to eight events, significantly more than those identified in trenches excavated on the primary

Commented [RDK10]: I my inspection of the trench logs the largest uncertainties are 1) whether or not Ev5 and Ev6 are two separate events as they are at the same stratigraphic level and it seems unlikely that just one strand would rupture. They likely represent one event as is shown by the oxcal model.
And 2) the existence of Ev7. The evidence is pretty weak (just a little bit of deformation left after retrodeformation). There could just be variable slip on individual strands in later events, thickness variations in the deposit (facies changes), oblique slip……all of which could result in slightly variable slip on an individual strand. It does not require another earthquake.

Futagawa fault. This result emphasizes the importance of selecting a site with small displacement per event and relatively fast and continuous deposition.

5.3 Comparison of paleoseismic events between the Futagawa and other faults

A summary of the paleofaulting history constructed by the author's group (Fig. 8) shows that the ages of faulting events after the K-Ah tephra (7.3 ka), which is widely identified in the paleoseismic trenches around the Futagawa fault, all overlap. This suggests that the Futagawa fault (Ishimura et al., 2022), Miyaji faults (Ishimura et al., 2021), and Idenokuchi fault have all moved simultaneously at least in the past several earthquakes. Notably, the simultaneity of the Futagawa and Idenokuchi faults is consistent with the idea that they are connected at a deeper level, as described in Section 5.1. Therefore, the paleoseismic history of the Idenokuchi fault is likely to represent that of the Futagawa fault, given its subsurface structure. The Miyaji faults, which produced the 2016 surface rupture and are distant from the Futagawa fault and structurally discontinuous (Fukushima and Ishimura, 2020), are also presumed to have been active in the past, together with the Futagawa fault. Given inherent uncertainties in dating techniques, it is technically challenging to prove the simultaneous rupture of faults. Nevertheless, further studies are necessary to determine whether the simultaneous rupture of the primary and secondary faults is common or if it is worthwhile to incorporate small displacements relative to those on the primary fault into seismic hazard assessment.

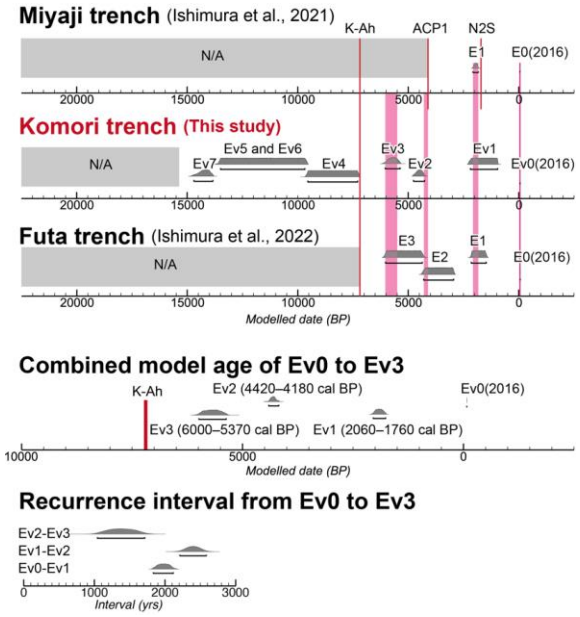

Figure 8. Modeled event ages and comparison to the authors' previous paleoseismic studies. The underbars show the 2σ probability distribution ranges of the modeled ages. ACP1 and N2S are local tephras from the Aso volcano (Miyabuchi, 2009). ACP1 is Aso central cone pumice and its age is 4.1 ka (Miyabuchi, 2009). N2S is Nakadake N2 scoria, and its age is 1490–1470 cal BP (68.2%) (Yamada et al., 2017).

Furthermore, assuming that the faulting events from Ev1 to Ev3 are the same among our three trenches (Komori, Miyaji, and Futa trenches), the calculated ages in OxCal modeling are Ev1: 2060–1760 cal BP, Ev2: 4420–4180 cal BP, and Ev3: 6000–5370 cal BP (Fig. 8). The recurrence intervals of each event are Ev0/Ev1: 1830–2120 years, Ev1/Ev2: 2210–2590 years, and Ev2/Ev3: 1040–1720 years with the 2σ range. Based on the trenching results, the average recurrence interval from Ev0 to Ev7 is 1990–2110 years, consistent with the modeled recurrence interval from Ev0 to Ev3. This indicates that the Futagawa fault has ruptured relatively periodically.

The dextral slip rate, calculated from the recurrence interval (1990–2110 years) and single displacement (1.8–3.1 m) obtained in this study, is 0.9–1.5 mm/yr for the Futagawa fault. For the Idenokuchi fault, the vertical displacement ranges from 1.0 to 2.5 m, indicating an estimated vertical slip rate of 0.5 to 1.3 mm/yr. ~~On the west~~West of the study area (Futa to Ohkirihata), Ishimura (2019) calculated ~~0.9–1.1 mm/yr~~ a vertical slip rate (0.9–1.1 mm/yr) and ~~1.5–3.7 mm/yr~~ dextral slip rate (1.5–3.7 mm/yr) for the Futagawa fault from the vertical and dextral displacements of Takayubaru lava (K–Ar ages 81 ± 4 ka and 98 ± 18 ka; Miyoshi et al., 2013). The Idenokuchi fault runs parallel to the Futagawa fault, where these slip rates, i.e., the west of the study area, were calculated. However, the vertical displacement on the Idenokuchi fault in the 2016 event west of the study area is small (Kaneda et al., 2022). Therefore, the long-term slip rates can be regarded as representative values when oblique slip is accommodated only by the Futagawa fault. Therefore, the long-term dextral and vertical slip rates are consistent with the results of this study. Oohashi (2020) pointed out that normal fault displacement was predominant on the Futagawa fault before Aso-4 pyroclastic flow deposits (87 ka; Aoki, 2008), and dextral displacement became apparent later. Oohashi (2020) proposed the following possibilities for this change: 1) The stress field changed from a normal fault type with north-south extension to a dextral strike-slip fault type with predominant east-west compression, and 2) the normal fault component of the Futagawa fault was replaced by the Idenokuchi fault and off-fault displacements, and the dextral displacement of the Futagawa fault became apparent. The fact that the long-term vertical slip rate coincides with that of the Idenokuchi fault from this study agrees with the second explanation.

Therefore, the slip partition on the Idenokuchi fault must have ~~occurred~~ commenced after the Aso-4 event (ca. 87 ka).

Figure 9 summarizes the paleofaulting history of the Kumamoto earthquake area since 7.3 ka, based on previous paleoseismic results, including archaeological information. The number of earthquakes since 7.3 ka (including 2016) on the Futagawa fault is estimated to be four with considerable accuracy and precision, based on the results of multiple trenches along the Futagawa fault and its vicinity. We believe that a series of trenching studies by our group has provided accurate ages for the past three events because we studied the sites with minor artificial disturbance, continuous sediments, and good age markers (tephras). In addition, the paleofaulting history at the northwestern Aso caldera (Sato et al., 2021) and the western part of the Futagawa fault (Inoue et al., 2020), which are at secondary surface ruptures, indicates that one of their events coincides with Ev1 in this study. Therefore, it is highly likely that the secondary faults were activated simultaneously during at least the penultimate event of the Futagawa fault. Lateral spreading recognized at archaeological sites within the caldera (Kumamoto Prefectural Board of Education, 2010; Aso City Board of Education, 2011) was also approximately 2000 years ago, which also supports that secondary phenomena caused by an earthquake similar to the 2016 event occurred repeatedly in the caldera. Thus, it is inferred that similar phenomena in the 2016 event (e.g., secondary surface rupture, liquefaction, and lateral spreading) also occurred during the previous activity. However, the age of the antepenultimate event in the northwestern part of the caldera does not match that of the Futagawa fault (Sato et al., 2021). In addition, no other secondary surface ruptures have been identified as having earthquakes older than the

antepenultimate event, so it is unclear how the secondary fault behaved during the older events. Future information on the presence or absence of older earthquakes on such secondary faults and their histories will help us to better understand the secondary faults and how frequently they rupture simultaneously with the Futagawa fault.

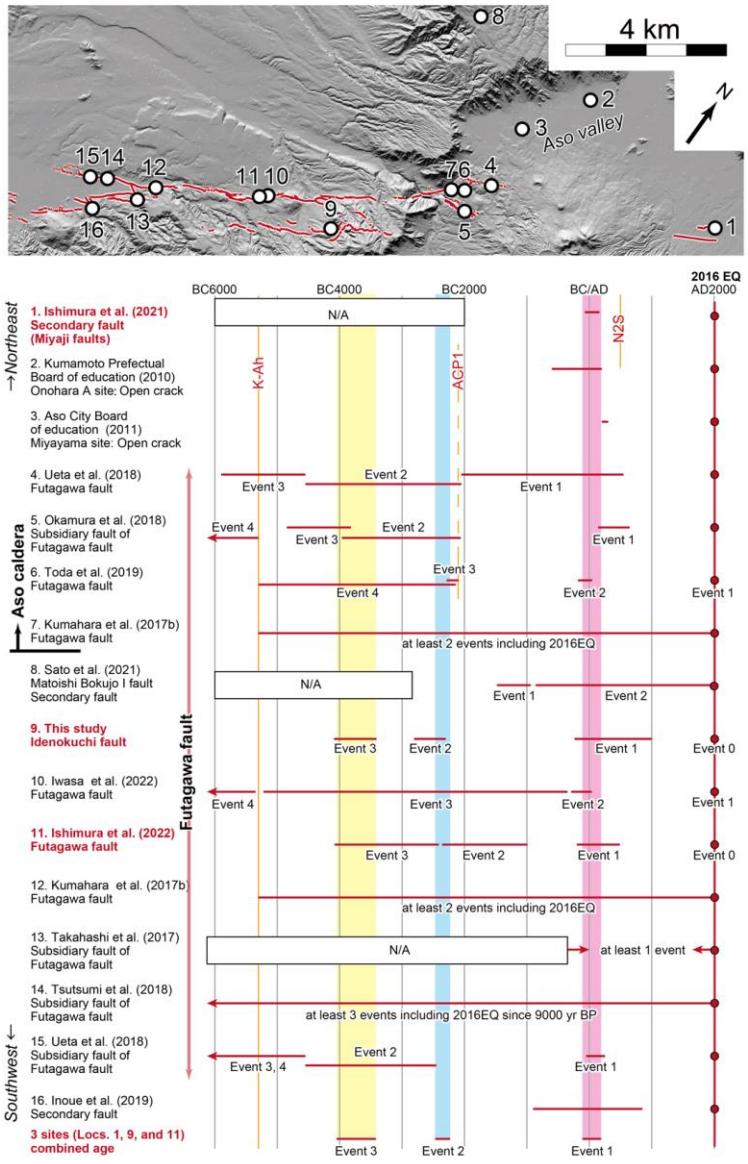

Figure 9. Compilation of paleofaulting events. The upper panel shows the locations of the lower panel data. The lower panel shows the compiled spatial-temporal age distribution of the paleofaulting events along the Futagawa and its subsidiary and secondary faults. Event chronologies correspond to studies referenced on the left side of the panel. The red bar represents the event age range in each study. The

red arrow indicates that the age is estimated to be outside the range shown in the figure. The pink, blue, and yellow shading represent the combined model age ranges of Ev1, Ev2, and Ev3, respectively. Details of K-Ah, ACP1, and N2S tephras were described in the caption of Figure 8.

6. Conclusions

Using the 2016 Kumamoto earthquake as an example, we performed a DTM difference analysis in the area where the Futagawa and Idenokuchi faults interact, and conducted an excavation survey on the Idenokuchi fault. Based on the 3D displacement distribution, we discussed how the slip partition occurred on them and found that the oblique slip at depth was split entirely into vertical and horizontal displacements on the ground surface. This indicates that the Idenokuchi fault is structurally related to the Futagawa fault and that the paleofaulting history of the Idenokuchi fault is likely to correspond to that of the Futagawa fault.

The KMR trench at the Idenokuchi fault revealed continuous deposition of soil and tephra since 15 ka, and retrodeformation of the trench walls revealed at least six and up to eight faulting events (including 2016) during this period. Among them, the faulting events after Kikai-Akahoya tephra (7.3 ka) are consistent with paleoseismic surveys on the Futagawa fault (the primary fault) and Miyaji faults (secondary faults in the Aso caldera). This suggests that at least some surface ruptures that occurred around the Futagawa fault during the 2016 event were likely active at the same time as past activities of the Futagawa fault. The activity histories since 7.3 ka with the authors' three trenches on the Futagawa, Miyaji, and Idenokuchi faults are E1: 2060–1760 cal BP, E2: 4420–4180 cal BP, and E3: 6000–5370 cal BP, indicating that they occurred relatively periodically. The mean recurrence interval since 15 ka is about 2000 years, supporting the periodic activity. The results of this study are also consistent with other trench

investigations conducted after 2016. It is important to improve the accuracy and precision of the activity history of the Futagawa fault before 7.3 ka and to investigate the activity history of the Hinagu fault zone in the southern part of the Futagawa fault zone to consider future seismic hazard and interlocking rupture. In addition, it will be important to clarify the subsurface structure and activity history of secondary faults in other earthquakes to consider displacement hazards.

Acknowledgements

We thank Yasuhiro Kumahara, Ryuhei Oda, Jun Matsukaze, Motoya Kobayashi, Makoto Kobayashi, Yoshiya Iwasa, and Daichi Tomita for their help during the trench survey. We also thank Shinji Toda, Heitaro Kaneda, and Yasuo Miyabuchi for their discussions and constructive comments. The thoughtful comments from the reviewer Rich Koehler, and the anonymous reviewer improved the article. This work was supported by KAKENHI Grant Number JP17H04730 from the Japan Society for the Promotion of Science.

Data and code availability

Supplementary figures (S1 to S2) and tables (S1 to S4) are available in the supplement material.

OxCal model codes are listed in the supplementary material.

Pre- and post-event DTMs used in this study were provided by the Geospatial Information Authority of Japan (https://www.gsi.go.jp/ENGLISH/index.html).

Competing interests

The authors have no competing interests.

References

Aoki, K. (2008) Revised age and distribution of ca. 87 ka Aso-4 tephra based on new evidence from the Northwest Pacific Ocean. Quaternary International, 178, 100–118. doi: 10.1016/j.quaint.2007.02.005.

Aoyagi, Y., Higashi, S., Homma, S., Mukoyama S., Sugiyama, M., and Hijikata, K. (2021) Surface ruptures in the Aso campus of Tokai University caused by the 2016 Kumamoto Earthquake. Active Fault Research, 55, 1–18. (in Japanese with English abstract)

Aoyagi, Y., Ueta, K., Takemoto, T., Suehiro, M.,and Miyawaki, R. (2024) Seismic constraints on the subsurface extent of subparallel surface ruptures in Mashiki Town, Japan, associated with the 2016 Kumamoto Earthquake. Journal of the Seismological Society of Japan. 2nd ser., 77, 5–19. (in Japanese with English abstract)

Aso City Board of Education (2011) Miyayama ruinsII, Cultural Property Investigation Report of Aso City 2. Aso City Board of Education, Aso City. (in Japanese)

Barnhart, W.D., Hayes, G.P., and Gold, R.D. (2019) The July 2019 Ridgecrest, California, earthquake sequence: Kinematics of slip and stressing in cross-fault ruptures. Geophysical Research Letters, 46, 11859–11867. doi: 10.1029/2019GL084741.

Bronk Ramsey, C. (2008) Deposition models for chronological records. Quaternary Science Reviews, 27, 42–60. doi: 10.1016/j.quascirev.2007.01.019.

Bronk Ramsey, C. (2009) Bayesian analysis of radiocarbon dates. Radiocarbon, 51, 337–360. doi: 10.2458/azu_js_rc.v51i1.3494.

Danhara, T., Yamashita, T., Iwano, H., and Kasuya, M. (1992) An improved system for measuring refractive index using the thermal immersion method. Quaternary International, 13–14, 89–91. doi: 10.1016/1040-6182(92)90013-R.

Fujiwara, S., Yarai, H., Kobayashi, T., Morishita, Y., Nakano, T., Miyahara, B., Nakai, H., Miura, Y., Ueshiba, H., Kakiage, Y., and Une, H. (2016) Small-displacement linear surface ruptures of the 2016 Kumamoto earthquake sequence detected by ALOS-2 SAR interferometry. Earth, Planets and Space, 68, 160. doi: 10.1186/s40623-016-0534-x.

Fukushima, Y., and Ishimura, D. (2020) Characteristics of secondary-ruptured faults in the Aso Caldera triggered by the 2016 Mw 7.0 Kumamoto earthquake. Earth, Planets and Space, 72, 175. doi: 10.1186/s40623-020-01306-y.

Goto, H., Tsutsumi, H., Toda, S., and Kumahara, Y. (2017) Geomorphic features of surface ruptures associated with the 2016 Kumamoto earthquake in and around the downtown of Kumamoto City, and implications on triggered slip along active faults. Earth, Planets and Space, 69, 26. doi: 10.1186/s40623-017-0603-9.

Hamling, I.J., Hreinsdóttir, S., Clark, K., Elliott, J., Liang, C., Fielding, E., Litchfield, N., Villamor, P., Wallace, L., Wright, T.J., D'Anastasio, E., Bannister, S., Burbidge, D., Denys, P., Gentle, P., Howarth, J., Mueller, C., Palmer, N., Pearson, C., Power, W., Barnes, P., Barrell, D.J.A., Van Dissen, R., Langridge, R., Little, T., Nicol, A., Pettinga, J., Rowland, J., and Stirling, M. (2017). Complex multifault rupture during the 2016 Mw 7.8 Kaikōura earthquake, New Zealand. Science, 356, 6334. doi: 10.1126/science.aam7194.

He, P., Wen, Y., Xu, C., and Chen, Y. (2019) Complete three-dimensional near-field surface displacements from imaging geodesy techniques applied to the 2016 Kumamoto earthquake. Remote Sensing of Environment, 232, 111321. doi: 10.1016/j.rse.2019.111321.

Headquarters for Earthquake Research Promotion (2013) Long-term evaluation of the Futagawa and Hinagu fault zones (partial revision version) (in Japanese). http://www.jishin.go.jp/main/chousa/13feb_chi_kyushu/k_11.pdf. (Accessed 17 August 2025).

Himematsu, Y., and Furuya, M. (2020) Coseismic and postseismic crustal deformation associated with the 2016 Kumamoto earthquake sequence revealed by PALSAR-2 pixel tracking and InSAR. Earth, Planets and Space, 7, 1–19. doi: 10.1029/2020EA001200.

Hoshizumi, H., Ozaki, M., Miyazaki, K., Matsuura, H., Toshimitsu, S., Uto, K., Uchiumi, S., Komazawa, M., Hiroshima, T., and Sudo, S. (2004) Geological Map of Japan 1:200,000, Kumamoto. Geological Survey of Japan, AIST.

Inoue, N., Kitada, N., Shibuya, N., Omata, M., Takahama, T., Tonagi, M., and Irikura, K. (2020) Probabilistic Evaluation of Off-Fault Displacements of the 2016 Kumamoto Earthquake. Pure and Applied Geophysics, 177, 2007–2019. doi: 10.1007/s00024-019-02345-7.

Ishimura, D., and Kakiuchi, Y. (2011) Chronology and processes of fluvial terrace formation in northeastern Kinki district, southwest Japan, based on cryptotephra analysis. Quaternary International, 246, 190–202. doi: 10.1016/j.quaint.2011.08.039.

Ishimura, D. (2019) Coseismic vertical displacement associated with the 2016 Kumamoto earthquake (Mw7.0) and activity of the Futagawa fault around Futa, Nishihara Village, Kumamoto prefecture. Active Fault Resarch, 50, 33–32. (in Japanese with English abstract)

Ishimura, D., Toda, S., Ichihara, T., Takahashi, N., Konno, A., and Sato, H. (2017) A study on surface ruptures around Miyaji, Aso City, Kumamoto Prefecture, associated with the 2016 Kumamoto earthquake sequence and upward slip tapering on pit excavation walls. Active Fault Research, 47, 9–16. (in Japanese with English abstract)

Ishimura, D., Toda, S., Mukoyama, S., Homma, S., Yamaguchi, K., and Takahashi, N. (2019) 3D surface displacement and surface ruptures associated with the 2014 Mw 6.2 Nagano earthquake using differential lidar. Bulletin of the Seismological Society of America, 109, 780–796. doi: 10.1785/0120180020.

Ishimura, D., Tsutsumi, H., Toda, S., Fukushima, Y., Kumahara, Y., Takahashi, N., Ichihara, T., and Takada, K. (2021) Repeated triggered ruptures on a distributed secondary fault system: an example from the 2016 Kumamoto earthquake, Southwest Japan. Earth, Planets and Space, 73 doi: 10.1186/s40623-021-01371-x.

Ishimura, D., Iwasa, Y., Takahashi, N., Tadokoro, R. and Oda, R. (2022) Paleoseismic events and shallow subsurface structure of the central part of the Futagawa fault, which generated the 2016 Mw 7.0 Kumamoto earthquake. Geomorphology, 414, 108387. doi: 10.1016/j.geomorph.2022.108387.

Iwasa, Y., Kumahara, Y., Goto, H., Ishimura, D., and Hosoya, T. (2022) Faulting history of the Futagawa fault zone based on trenching survey at Komori, Nishihara Village, Kumamoto Prefecture. Active Fault Research, 56, 47–58. (in Japanese with English abstract)

Kamata, H., and Kodama, K. (1994) Tectonics of an arc-arc junction: an example from Kyushu Island at the junction of the Southwest Japan Arc and the Ryukyu Arc. Tectonophysics, 233, 69–81. doi: 10.1016/0040-1951(94)90220-8.

Kaneda, H., and Chiba, T. (2019) Stereopaired morphometric protection index red relief image maps (Stereo MPI-RRIMs): Effective visualization of high-resolution digital elevation models for interpreting and mapping small tectonic geomorphic features. Bulletin of the Seismological Society of America, 109, 99–109. doi: 10.1785/0120180166.

Kaneda, H., Toda, S., Ishimura, D., Kumahara, Y., Goto, H., Okada, S., and Kobayashi, M. (2022) Surface Ruptures and Tectonic Geomorphology Along and Around the Idenokuchi Fault. In: Kumahara, Y., Kaneda, H., Tsutsumi, H. (eds) Surface Ruptures Associated with the 2016 Kumamoto Earthquake Sequence in Southwest Japan. Advances in Geological Science. Springer, Singapore. doi: 10.1007/978-981-19-1150-7_12.

King, G., Klinger, Y., Bowman, D., and Tapponnier, P. (2005) Slip-Partitioned Surface Breaks for the Mw 7.8 2001 Kokoxili Earthquake, China. Bulletin of the Seismological Society of America, 95 (2), 731–738. doi: 10.1785/0120040101.

Kokusai Kogyo C o.,Ltd. (2010) 3D-Geomorphic Image Velocimetry. JP Patent No. 4545219.

Kumahara, Y., Okada, S., Kagohara, K., Kaneda, H., Goto, H., and Tsutsumi, H. (2017a) 1:25,000 Active Fault Map, Futagawa-Hinagu Fault Zone and its Vicinity “Kumamoto (Revision)”. Geospatial Information Authority of Japan, Ibaraki. (in Japanese)

Kumahara, Y., Torii, M., Nakata, T., Goto, H., Iwasa, Y., Suzuki, Y., Watanabe, M., Toda, S., Takahashi, N., and Okuno, M. (2017b) Fault History of the Northern Part of Futagawa-Hinagu Fault Zone Based on Trench Survey at Dozon, Mashiki Town and at Kawayo, Minami-Aso Village, Programme and Abstracts JSAF 2017 Fall Meeting, 24–25. (in Japanese)

Kumahara, Y., Kaneda, H., and Tsutsumi, H. (2022) Surface Ruptures Associated with the 2016 Kumamoto Earthquake Sequence in Southwest Japan. Advances in Geological Science. Springer, Singapore. doi: 10.1007/978-981-19-1150-7.

Kumamoto Prefectural Board of Education (2010) Earthquake traces in Onobaru-A site. Onobaru ruins group. In: Cultural Property Investigation Report of Kumamoto Prefecture, 257 (2), 147–149. (in Japanese)

Kumamoto Prefecture Geological Map Compilation Committee (2008) Geological Map of the Kumamoto Prefecture (1:100,000). Kumamoto Prefecture Geotechnical Consultants Association, Kumamoto.

Machida, H., and Arai, F. (2003) Atlas of Tephra in and around Japan [revised edition]. University of Tokyo Press, Tokyo.

Matsumoto, Y. (1979) Some problems on volcanic activities and depression structures in Kyushu, Japan. Memoirs of the Geological Society of Japan, 16, 127–139. (in Japanese with English abstract)

Miyabuchi, Y. (2009) A 90,000-year tephrostratigraphic framework of Aso Volcano, Japan. Sedimentary Geology, 220, 169–189. doi: 10.1016/j.sedgeo.2009.04.018.

Miyoshi, M., Shinmura, T., Sumino, H., Sano, T., Miyabuchi, Y., Mori, Y., Inakura, H., Furukawa, K., Uno, K., Hasenaka, T., Nagao, K., Arakawa, Y., and Yamamoto, J. (2013) Lateral magma intrusion from a caldera-forming magma chamber: Constraints from geochronology and geochemistry of volcanic products from lateral cones around the Aso caldera, SW Japan. Chemical Geology, 352, 202–210. doi: 10.1016/j.chemgeo.2013.06.003.

Moya, L., Yamazaki, F., Liu, W., and Chiba, T. (2017) Calculation of coseismic displacement from lidar data in the 2016 Kumamoto, Japan, earthquake. Natural Hazards and Earth System Sciences, 17, 143–156. doi: 10.5194/nhess-17-143-2017.

Mukoyama, S. (2011) Estimation of ground deformation caused by the earthquake (M 7.2) in Japan, 2008, from the geomorphic image analysis of high resolution LiDAR DEMs. Journal of Mountain Science, 8, 239–245. doi: 10.1007/s11629-011-2106-7.

Muroi, S., Suzuki, Y., Mukoyama, S., Iwasa, Y., Yamashita, H., Muraki, M., Yamashita, K., Fukuba, T. (2024) Surface displacement vector discontinuity in the easternmost part of the Futagawa-Hinagu fault zone analyzed by using airborne laser scanning data at two different timings. Active Fault Research, 60, 11–25. (in Japanese with English abstract)

Nakata, T., and Imaizumi, T. (2002) Digital Active Fault Map of Japan. University of Tokyo Press, Tokyo. (in Japanese)

Nurminen, F., Baize, S., Boncio, P., Blumetti, A.M., Cinti, F.R., Civico, R., and Guerrieri, L. (2022) SURE 2.0 – New release of the worldwide database of surface ruptures for fault displacement hazard analyses. Scientific Data 9, 729. doi: 10.1038/s41597-022-01835-z.

Nurminen, F., Boncio, P., Visini, F., Pace, B., Valentini, A., Baize, S., and Scotti, O. (2020) Probability of Occurrence and Displacement Regression of Distributed Surface Rupturing for Reverse Earthquakes. Frontiers in Earth Science, 8, 581605. doi: 10.3389/feart.2020.581605.

Okamura, Y., Abe, S., Miyashita, Y., Azuma, T., Togo, T., Shirahama, Y., Awata, Y., Maruyama, T., Ogami, T., Imura, R., Tsutsumi, H., Goto, H., and Kumahara, Y. (2018) 3.1 Survey of detailed position and shape of active faults to understand the fault segments and observation to reveal the paleoseismic history and slip rates. In: Research Report of a Comprehensive Active Fault Survey After the 2016 Kumamoto Earthquake, 2017 Fiscal Year. Ministry of Education, Culture, Sports, Science and Technology and Kyushu University. (in Japanese)

Oohashi, K., Otsubo, M., Matsumoto, S., Kobayashi, K., Sato, K., and Nishimura, T. (2020) The Quaternary tectonics of Central Kyushu and the 2016 Kumamoto Earthquake: from a multifaceted viewpoint combining geology, seismology, and geodesy. Journal of the Geological Society of Japan, 129, 565–589. (in Japanese with English abstract)

Reimer, P.J., Austin, W.E.N., Bard, E., Bayliss, A., Blackwell, P.G., Bronk Ramsey, C., Butzin, M., Cheng, H., Edwards, R.L., Friedrich, M., Grootes, P.M., Guilderson, T.P., Hajdas, I., Heaton, T.J., Hogg, A.G., Hughen, K.A., Kromer, B., Manning, S.W., Muscheler, R., Palmer, J.G., Pearson, C., Van Der Plicht, J., Reimer, R.W., Richards, D.A., Scott, E.M., Southon, J.R., Turney, C.S.M., Wacker, L., Adolphi, F., Büntgen, U., Capano, M., Fahrni, S.M., Fogtmann-Schulz, A., Friedrich, R., K¨ohler, P., Kudsk, S., Miyake, F., Olsen, J., Reinig, F., Sakamoto, M., Sookdeo, A., and Talamo, S. (2020) The IntCal20 Northern Hemisphere radiocarbon age calibration curve (0–55 cal kBP). Radiocarbon, 62, 725–757. doi: 10.1017/RDC.2020.41.

Research Group for Active Faults of Japan, 1980. Active Faults in Japan, Sheet Maps and Inventories. University of Tokyo Press, Tokyo. (in Japanese)

Research Group for Active Faults of Japan, 1991. Active Faults in Japan, Sheet Maps and Inventories, Rev. Ed. University of Tokyo Press, Tokyo. (in Japanese)

Sato, P.H., Komura, K., Une, H., Nakano, T., and Yagi, K. (2021) Study on Cumulative Activities of Passively Ruptured Faults through a Trenching Survey at the Matoishi Bokujo I Fault, Northwest Side of the Aso Caldera, Southwestern Japan. Geographical Review of Japan Series A, 94, 250–264. doi: 10.4157/grj.94.250. (in Japanese with English abstract)

Scott, C.P., Arrowsmith, J.R., Nissen, E., Lajoie, L., Maruyama, T., and Chiba, T. (2018) The M7 2016 Kumamoto, Japan, earthquake: 3-D Deformation along the Fault and within the damage Zone Constrained from Differential Lidar Topography. Journal of Geophysical Research: Solid Earth, 123, 6138–6155. doi: 10.1029/2018JB015581.

Seno, T., Stein, S. and Gripp, A.E.（1993）A model for the motion of the Philippine Sea Plate consistent with NUVEL-1 and geological data. Journal of Geophysical Research: Solid Earth, 98, 17941–17948. doi: 10.1029/93JB00782.

Shirahama, Y., Yoshimi, M., Awata, Y., Maruyama, T., Azuma, T., Miyashita, Y., Mori, H., Imanishi, K., Takeda, N., Ochi, T., Otsubo, M., Asahina, D., and Miyakawa, A. (2016) Characteristics of the surface ruptures associated with the 2016 Kumamoto earthquake sequence, Central Kyushu, Japan. Earth, Planets and Space, 68, 191. doi: 10.1186/s40623-016-0559-1.

Shirahama, Y., Miyashita, Y., Kametaka, M., Suzuki, Y., Miyairi, Y., and Yokoyama, Y. (2021) Detailed paleoseismic history of the Hinagu fault zone revealed by the high-density radiocarbon dating and trenching survey across a surface rupture of the 2016 Kumamoto earthquake, Kyushu, Japan. Island Arc, 30, e12376. doi: 10.1111./iar.12376.

Smith, V.C., Staff, R.A., Blockley, S.P.E., Bronk Ramsey, C., Nakagawa, T., Mark, D.F., Takemura, K., and Danhara, T. (2013) Identification and correlation of visible tephras in the Lake Suigetsu SG06 sedimentary archive, Japan: chronostratigraphic markers for synchronising of east Asian/west Pacific palaeoclimatic records across the last 150 ka. Quaternary Science Reviews, 67, 121–137. doi: 10.1016/j.quascirev.2013.01.026.

Suzuki, T., Kasahara, A., Nishizawa, F., and Saito, H. (2014) Chemical characterization of volcanic glass shards by energy dispersive X-ray spectrometry with EDAX Genesis APEX2 and JEOL JSM-6390. Geographical reports of Tokyo Metropolitan University, 49, 1–12.

Suzuki, Y., Ishimura, D., Kumaki, Y., Kumahara, Y., Chida, N., Nakata, T., and Nakano, T. (2017) 1:25,000 Active Fault Map, Futagawa-Hinagu Fault Zone and its Vicinity "Aso". Geospatial Information Authority of Japan, Ibaraki. (in Japanese)

Takahashi, N., Ishimura, D., Toda, S., Nakata, T., and Watanabe, M. (2017) Vertical slip rate on a normal fault co-ruptured with the Futagawa fault at the 2016 Kumamoto earthquake. Active Fault Research, 46, 27–32. (in Japanese with English abstract).

Toda, S., Kaneda, H., Okada, S., Ishimura, D., and Mildon, Z.K. (2016) Slip-partitioned surface ruptures for the Mw 7.0 16 April 2016 Kumamoto, Japan, earthquake. Earth, Planets and Space, 68, 188. doi: 10.1186/s40623-016-0560-8.

Toda, S., Torii, M., Okuno, M., Konno, A., Ono, H., and Takahashi, N. (2019) Evidence for Holocene paleoseismic events on the 2016 Kumamoto earthquake rupture zone within the Aso caldera: a trench excavation survey at Kurokawa, the town of Minami-Aso, Southwest Japan. Active Fault Research, 51, 13–25. (in Japanese with English abstract)

Tsutsumi, H., Toda, S., Goto, H., Kumahara, Y., Ishimura, D., Takahashi, N., Taniguchi, K., Omata, M., Kohriya, Y., Gomi, M., Asano, K., and Iwata, T. (2018) Paleoseismic trenching across the surface rupture of the 2016 Kumamoto earthquake at Jichu, Mashiki Town, Kumamoto Prefecture. Active Fault Research, 49, 31–39. (in Japanese with English abstract)

Ueta, K., Miyawaki, R., Iemura, K., Yokoyama, T., and Miyawaki, A. (2018) Paleoseismological study on surface fault ruptures produced by the 2016 Kumamoto

earthquake. In: Abstracts of Japan Geoscience Union Meeting 2018, Makuhari Messe, Chiba. (in Japanese with English abstract).

Watanabe, K. and Ono, K. (1969) Geology of the vicinity of Omine on the western flank of the Aso caldera. Journal of the Geological Society of Japan, 75, 365–374. (in Japanese with English abstract)

Xu, X., Sandwell, D.T., and Smith-Konter, B. (2020) Coseismic Displacements and Surface Fractures from Sentinel-1 InSAR: 2019 Ridgecrest Earthquakes. Seismological Research Letters, 91, 1979–1985. doi: 10.1785/0220190275.

Yamada, K., Takemura, K., Kuwae, M., Yamamoto, M., and Danhara, T. (2017) Revised ages of late Holocene tephras in Beppu Bay, central Kyushu, southwest Japan. Quaternary International, 452, 33–42. doi: 10.1016/j.quain t.2017.01.024.

Paleoseismic trenching on slip-partitioned surface ruptures associated with the 2016 Kumamoto earthquake

Daisuke Ishimura[1,*], Naoya O. Takahashi [2], Hiroyuki Tsutsumi[3], Shin'ichi Homma[4], Sakae Mukoyama[4], and Toshihiko Ichihara[5]

[1] Department of Earth Sciences, Chiba University, 1-33 Yayoi-cho, Inage-ku, Chiba 263-8522, Japan
[2] Department of Earth Science, Tohoku University, 6-3 Aoba, Aoba-ku, Sendai 980-8578, Japan
[3] Department of Environmental Systems Science, Doshisha University, 1-3 Tataramiyakodani, Kyotanabe, Kyoto 610-0394, Japan
[4] Department of Research & Development of Kokusai Kogyo Co., Ltd., 2-24-1 Harumi-cho, Fuchu, Tokyo 183-0057, Japan
[5] Department of Disaster Prevention & Geology of Hopedesign Co., Ltd., 3-5 Shuri-Akatacho, Naha, Okinawa 903-0813, Japan
[*]Corresponding author: ishimura@chiba-u.jp

Author ORCIDs

Daisuke Ishimura: 0000-0002-4798-3425
Naoya Takahashi: 0000-0003-4196-1409

Author contributions

Conceptualization: D. Ishimura
Data Curation: N. O. Takahashi, S. Homma, S. Mukoyama
Formal Analysis: D. Ishimura, S. Homma, S. Mukoyama
Funding Acquisition: D. Ishimura
Investigation: D. Ishimura, N. O. Takahashi, H. Tsutsumi, T. Ichihara
Methodology: D. Ishimura, S. Homma, S. Mukoyama
Project Administration: D. Ishimura
Resources: D. Ishimura
Software: S. Homma, S. Mukoyama
Supervision: H. Tsutsumi
Validation: D. Ishimura
Visualization: D. Ishimura, N. O. Takahashi
Writing – original draft: D. Ishimura
Writing – review & editing: N. O. Takahashi, H. Tsutsumi, S. Homma, S. Mukoyama

Abstract

Surface ruptures appear over a wide area, in addition to the primary fault, during a large earthquake, such as the 2016 Kumamoto earthquake. Although the displacement of such distributed surface ruptures is small, information on their paleo activities may provide clues for evaluating displacement hazard risk and whether they can offer a paleoseismic history of the primary fault. We conducted lidar differencing analysis and trench excavation on the Idenokuchi fault, which was activated simultaneously with the primary Futagawa fault during the 2016 Kumamoto earthquake, as a result of slip partition of the oblique slip. First, we clarified the 3D displacement field by lidar differencing and discussed quantitatively how the slip partition occurred on both faults. We found that deep oblique slip is completely split into horizontal and vertical components at the ground surface and inferred that the Idenokuchi fault is structurally connected to the Futagawa fault. Then, we excavated a trench on a subparallel surface rupture of the Idenokuchi fault and identified up to eight faulting events since 15 ka. Finally, we revealed a reliable faulting history since 7.3 ka. Combined with the results of other paleoseismic trenches, our findings on the Idenokuchi fault indirectly suggest that the Futagawa fault has ruptured relatively periodically. We conclude that many surface ruptures appeared in the last few events, as was the case during the 2016 event.

Commented [A1]: This is possible, though not guaranteed. Suggest revise to: In large earthquakes, surface ruptures of secondary faults may appear in addition to the primary fault rupture, such as in the 2016 Kumamoto earthquake.

Commented [A2]: delete "risk". Risk depends on population exposure to hazard

Commented [A3]: Suggest convert to present tense

Commented [A4]: clarify - meaning of the secondary fault?

Second language abstract: 要旨 (日本語)

2016 年熊本地震のような大地震の際に主断層周辺に加えて幅広い範囲に断層が出現することがある．そのような断層の変位は小さいが，その過去の活動の情報は変位ハザードリスクや主断層の活動履歴の復元に有用かどうかの評価に関して手がかりを与えてくれる．そこで我々は lidar 差分解析とトレンチ掘削調査を 2016 年熊本地震の際に布田川断層と同時に活動しスリップパーティションが生じたとされた出ノ口断層で実施した．まず，lidar 差分により 3 次元変位場を求め，両断層でスリップパーティションが生じたかどうかを定量的に議論した．その結果，深部の斜めすべりが地表では完全に水平と鉛直成分に分割されたことが明らかとなり，出ノ口断層は構造的に布田川断層と地下でつながっていることが推定された．また，出ノ口断層に並走する断層上でトレンチ掘削した結果，15 ka 以降に最大 8 回のイベントを推定し，最終的に 7.3 ka 以降の信頼たる活動時期が得られた．この結果は布田川断層が比較的周期的に活動したことと，最近数回のイベントでは 2016 年同様に多くの断層が地表に出現したことを示唆する．

Third language abstract: NA

Non-technical summary

We conducted a study on the Idenokuchi fault, which moved together with the main Futagawa fault during the 2016 Kumamoto earthquake, Japan. By comparing the topography before and after the earthquake, and by digging a trench, we were able to understand how the fault moved during the 2016 earthquake and during the prehistoric earthquakes. Our findings indicate that the oblique displacement on the fault at depth is split into horizontal and vertical movements at the surface. This suggests that the Idenokuchi fault merges with the Futagawa fault at depth. By digging a trench on the Idenokuchi fault, we found evidence of up to eight past earthquakes over

the last 15,000 years. The recurrence interval revealed on the Idenokuchi fault indirectly indicates that the Futagawa fault has ruptured at somewhat regular intervals.

1. Introduction

Recent developments in remote sensing technology (e.g., SAR and optical correlation) have enabled the capture of ground surface displacement associated with earthquakes with high resolution and precision, including the distribution and amount of displacement. As a result, it has become clear that the distribution of coseismic surface ruptures is complex when viewed in detail, and in some cases, ruptures are distributed over extensive areas (e.g., the 2016 Kumamoto earthquake, the 2016 Kaikoura earthquake, and the 2019 Ridgecrest earthquake). Such complex ruptures have involved contemporaneous slip on the primary faults and other related faults, which are variably referred to as secondary, subsidiary, sympathetic, and distributed faults (e.g., Nurminen et al., 2020, 2022). Understanding the history and distribution of complex ruptures is important for assessing displacement hazards; however, few studies have evaluated the relative synchronicity of past ruptures along primary faults and their associated nearby faults.

Commented [A5]: add citations

The epicentral area of the Mw7.0 2016 Kumamoto earthquake provides a rare opportunity to study such co-rupturing events. InSAR analyses and field surveys have shown that the surface ruptures were widely distributed around the main (primary) fault of the 2016 Kumamoto earthquake (Fujiwara et al., 2016). Detailed field reconnaissance studies confirmed surface displacements and/or deformation at discontinuities observed in the InSAR data (Goto et al., 2017; Ishimura et al., 2017; Okamura et al., 2018; Sato et al., 2021). In addition to the ruptures along the primary Futagawa and Hinagu faults, surface displacements were observed along the Idenokuchi and Miyaji faults (Fig. 1). The Idenokuchi fault extends for approximately 10 km parallel to and within 2 km southeast

of the Futagawa fault. Along this parallel section of the rupture, right-lateral displacement occurred on the Futagawa fault and vertical displacement occurred on the Idenokuchi fault, from which Toda et al. (2016) inferred that the slip was partitioned between the two faults. This suggests that the Futagawa and Idenokuchi faults merge at depth and are structurally connected. The Miyaji faults (Fig. 1; Ishimura et al., 2021) have the same strike and displacement sense as the Futagawa fault. However, the fault model based on the InSAR analysis (Fukushima and Ishimura, 2020) has revealed that the Miyaji faults are not connected to the Futagawa fault, suggesting that the 2016 surface ruptures on the Miyaji faults were triggered slip. These observations indicate that various mechanisms may have contributed to the surface ruptures around the Futagawa fault during the 2016 Kumamoto earthquake.

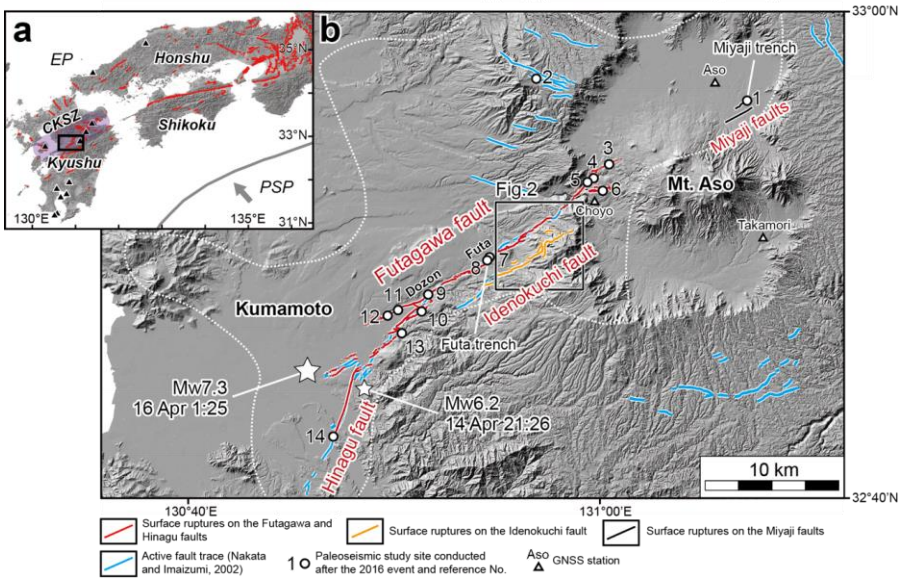

Figure 1. Spatial relationships among the primary Futagawa–Hinagu rupture zones and previously mapped active fault traces. (a) Tectonic setting, active volcanoes, and active faults in southwest Japan. (b) Locations of the surface ruptures along the Futagawa, Hinagu, Idenokuchi, and Miyaji faults. The surface rupture traces are from Kumahara et al. (2022). Previously mapped active fault traces are from Nakata and Imaizumi (2002). Red and orange lines indicate primary and subsidiary surface ruptures, respectively, as defined in this study. The dotted line encloses the area where secondary surface ruptures were identified by InSAR (Fujiwara et al., 2016). The Miyaji faults (Ishimura et al., 2021) are examples of the many secondary surface ruptures associated with the 2016 event. In this study, we defined the Kiyama, Futagawa, and Kitamukiyama faults, previously mapped by the Research Group for Active Faults of Japan (1991), as the Futagawa fault. CKSZ, Central Kyushu Shear Zone (Oohashi et al., 2020). 1: Ishimura et al. (2021), 2: Sato et al. (2021), 3: Ueta et al. (2018), 4: Toda et al. (2019), 5: Kumahara et al. (2017b), 6: Okamura et al. (2018), 7: Iwasa et al. (2022), 8: Ishimura et al. (2022), 9: Kumahara et al. (2017b), 10: Takahashi et al. (2017), 11: Tsutsumi et al. (2018), 12: Ueta et al. (2018), 13: Inoue et al. (2019), 14: Shirahama et al. (2021).

In addition to field measurements of fault displacements (Shirahama et al., 2016; Okamura et al., 2018; Kumahara et al., 2022), the three-dimensional deformation caused by the 2016 event has been revealed by InSAR and differential light detection and ranging (lidar) analyses (Moya et al., 2017; Scott et al., 2018; He et al., 2019; Himematsu and Furuya, 2020; Aoyagi et al., 2021; Muroi et al., 2024). In particular, lidar differencing provides higher resolution and more accurate displacement information in areas with larger displacements than InSAR analysis. These types of analyses have been conducted along some parts of the 2016 rupture (Scott et al., 2018; Aoyagi et al., 2021; Muroi et al., 2024), revealing the details of three-dimensional deformation.

After the 2016 Kumamoto earthquake, more than 10 paleoseismic trenches were excavated on the Futagawa and surrounding faults (Fig. 1). A paleoseismic survey (Miyaji trench in Fig. 1) conducted on the Miyaji faults revealed that the fault moved about 2,000 years ago, which overlapped with the age range of the penultimate event of the Futagawa fault revealed by paleoseismic trenches (Ishimura et al., 2021). This suggests that the slip on the Miyaji faults has been repeatedly triggered by the slip on the

Futagawa fault in the past. In addition, trenching surveys on other short surface ruptures of the 2016 event within the Aso caldera also revealed activity preceding the 2016 event (Sato et al., 2021), suggesting repeated synchronous ruptures. The interpretation of these trenches benefited from site conditions characterized by rapid sedimentation rates and multiple thin tephra layers (downwind of the Aso volcano), which enabled the identification of displacements as small as approximately 15 cm (Ishimura et al., 2021). The success of these efforts prompted us to search for sites along other faults near the Futagawa fault to examine their contemporaneous rupture in relation to the Futagawa fault.

In this study, we use lidar-based digital terrain models (DTMs) before and after the earthquake to calculate the three-dimensional displacement fields across the Futagawa and Idenokuchi faults, examining the amount of slip partitioning during the 2016 Kumamoto earthquake. Although Scott et al. (2018), Aoyagi et al. (2021), and Muroi et al. (2024) conducted differential lidar analyses along other sections of the 2016 rupture, there has been no study to estimate the amount of displacement in the area of slip partitioning between the Futagawa and Idenokuchi faults. Then, we conduct a paleoseismic trenching investigation of the Idenokuchi fault. We document the paleoseismic history of the Idenokuchi fault and compare our results with those of the Futagawa and Miyaji faults. The results indicate that all three faults have ruptured together multiple times in the past, providing insight into understanding the interaction of multiple faults in complex ruptures. The results also have implications for assessing displacement hazards associated with slip partitioning on secondary faults.

Commented [A6]: Could it also be the other way around? That slip on the Miyaji faults triggered slip on the Futagawa fault 2000 years ago?

Commented [A7]: could have ruptured together

2. Regional Setting

Kyushu Island is part of the Southwest Japan arc and is the southernmost of the four main islands of the Japanese archipelago (Fig. 1). It is located on the Eurasian Plate, beneath which the Philippine Sea Plate is subducting northwestward at an oblique angle (Seno et al., 1993). Kyushu is characterized by many active volcanoes that have produced numerous tephra layers with well-established ages (Machida and Arai, 2003). Active faults are primarily concentrated in the central and northern regions of Kyushu (Research Group for Active Faults of Japan, 1980, 1991).

The central Kyushu region has been deformed by north-south extension since 6 Ma (Kamata and Kodama, 1994), and is structurally characterized by the Beppu-Shimabara graben (Matsumoto, 1979). This area is characterized by many east-west-striking normal faults (Research Group for Active Faults of Japan, 1991) and high levels of volcanic activity. According to Oohashi et al. (2020), central Kyushu has been a transtensional tectonic zone since approximately 1 Ma, referred to as the Central Kyushu Shear Zone (Fig. 1), characterized by dextral faults, rift zones, and volcanism.

2.1 Futagawa fault zone

The Futagawa fault (Fig. 1) is a ca. 25-km-long active dextral strike-slip fault (Watanabe and Ono, 1969; Research Group for Active Faults of Japan, 1980, 1991; Nakata and Imaizumi, 2002; Kumahara et al., 2017a; Suzuki et al., 2017) and generated the mainshock (Mw 7.0) of the 2016 Kumamoto earthquake sequence on April 16, 2016. Primary surface ruptures appeared during the mainshock along the previously mapped

active fault traces (Fig. 1; Kumahara et al., 2022). Dextral displacements of about 2 m were observed between Dozon and Futa along the central part of the Futagawa fault, with a maximum dextral displacement of 2.5 m at Dozon (Fig. 1; Shirahama et al., 2016; Okamura et al., 2018; Kumahara et al., 2022). Vertical displacement of about 1 m (south up) was observed along the central to west part of the Futagawa fault (Shirahama et al., 2016; Okamura et al., 2018; Kumahara et al., 2022). The slip rate of the Futagawa fault around Futa is 1.5–3.7 mm/yr for the right lateral slip and 0.9–1.1 mm/yr for the vertical slip (Ishimura, 2019).

The Idenokuchi fault is a 10-km-long active dip-slip fault primarily up on the south (Research Group for Active Faults of Japan, 1980, 1991; Nakata and Imaizumi, 2002), and also ruptured the surface during the mainshock of the 2016 Kumamoto earthquake (Fig. 1; Kumahara et al., 2022). Multiple surface ruptures appeared along the subparallel faults. The maximum vertical displacement was 2 m (south up), and the average vertical displacement was about 1 m (Kaneda et al., 2022). Toda et al (2016) inferred that the vertical slip on the Idenokuchi fault was related to the slip partitioning of the oblique lateral slip on the Futagawa fault. There is no data on the slip rate of the Idenokuchi fault.

Commented [A8]: Is this over the entire 10 km of the Idenokuchi fault?

2.2 Previous paleoseismic survey along the Futagawa fault

Extensive paleoseismic trenching has been conducted along the Futagawa fault and its vicinity since the 2016 event (Fig. 1). They are divided into three types: 1) on the surface ruptures along the primary Futagawa fault (Kumahara et al., 2017b; Takahashi et

al., 2017; Okamura et al., 2018; Tsutsumi et al., 2018; Ueta et al., 2018; Toda et al., 2019; Ishimura et al., 2022; Iwasa et al., 2022), 2) on the surface ruptures along the Hinagu fault (Shirahama et al., 2021), and 3) on other secondary surface ruptures (Inoue et al., 2019; Ishimura et al., 2021; Sato et al., 2021). Almost all of them identified multiple events in the Holocene. Some studies estimated the age of the penultimate event on the primary Futagawa fault to be about 2 ka (Ueta et al., 2018; Toda et al., 2019; Iwasa et al., 2022; Ishimura et al., 2022). Comparison of paleoseismic information obtained after the earthquake with that before the earthquake (Headquarters for Earthquake Research Promotion, 2013) suggests that the Futagawa fault has been more active than previously assessed before 2016.

Commented [A9]: over what time period?

3. Methods and Data

3.1 Lidar differencing

We used a 2-m grid DTM taken from January 2013 to February 2014 and a 2-m grid DTM taken on 8 May 2016. Although we do not possess the original point cloud data of pre- and post-earthquake datasets, nor have the details for constructing the DTMs from the original point cloud data, all the DTMs were prepared under the regulations required for a public lidar survey in Japan. We used the Japan plane rectangular coordinate system II (in meters) as the coordinate system for all data.

Commented [A10]: delete

We applied the 3D-Geomorphic Image Velocimetry method (Kokusai Kogyo Co., Ltd., 2010) for lidar differencing. The particle image velocimetry method and pre- and post-event DTMs (Fig. 2) were used to calculate the surface displacement vectors following the methods of Mukoyama (2011) and Ishimura et al. (2019). Aoyagi et al.

(2021) and Muroi et al. (2024) used this method for the eastern extension of the Futagawa fault inside the Aso caldera. The method procedure is as follows. First, we prepared slope-shaded images using pre- and post-event DTMs. We then carried out a grid search by moving a pre-event image in a pixel-by-pixel manner in the scanning area on the post-event image and estimated the position that exhibited the highest value of the coefficient of correlation using subpixel interpolation. Additionally, we calculated the horizontal and vertical components of displacement. Subsequently, we slid the search area in steps and repeated the image matching and calculation of the 3D displacement. Finally, we plotted the complete 3D vectors on maps. In this study, the search area size, search area step size, and output grid size were set to be 64 x 64 pixels (128 x 128 m), 5 m, and 5 x 5 m, respectively. Additionally, the theoretical error of this analysis is 0.1 pixel (0.2 m) due to subpixel interpolation in the displacement calculation.

Commented [A11]: Please elaborate on how the vertical component was calculated from the horizontal grid search method described here.

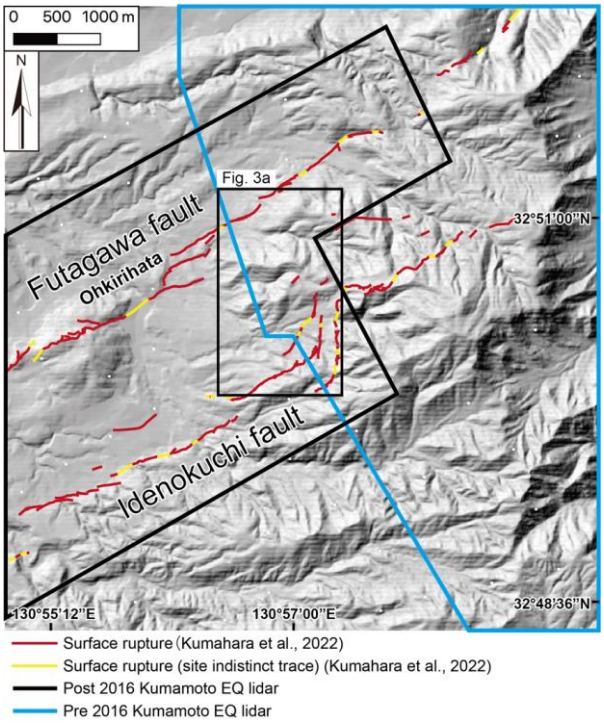

Figure 2. Lidar measurement areas. Lidar survey areas include the post-2016 Kumamoto earthquake (black polygon) and pre-2016 Kumamoto earthquake (blue polygon).

The expected ground motions during the measurement period are as follows: (1) the deformation associated with the 2016 Kumamoto earthquake, (2) the postseismic deformation (e.g., aftershocks and afterslip), (3) the background tectonic deformation, and (4) the artificial modification and present-day surface processes. We evaluate the deformation of items 2 and 3 using the GNSS observations in the study area. Based on the GNSS stations at the Choyo (960701), Aso (960703), and Takamori (960704) of GeoNET, the postseismic and background deformations (vertical, north-south, and east-west components) from April 2010 to May 2016 are nearly equal to the theoretical error level (0.2 m). Thus, the deformations associated with items 2 and 3 are negligible.

Commented [A12]: Please comment on the expected magnitude of the anthropogenic signal within the study area.

3.2 Trench survey

We looked for an appropriate site for a paleoseismic excavation along the Idenokuchi fault (Fig. 2). We selected possible sites based on the following criteria: 1) minor artificial modification, 2) clear surface rupture traces, and 3) stable and continuous sediment deposition. As a result, we selected a trench site on a gentle slope characterized by parallel fault traces of the Idenokuchi fault, expecting trapped sediment and stable and continuous soil deposition (Fig. 3). The trench site is on an apparent single surface rupture (north-up normal fault), and another surface rupture (south-up normal fault) runs parallel on its southeast side. Currently, the fields are cow ranches with minor artificial modification.

We excavated a 13-m-long, 5-m-wide, and 3.5-m-deep trench (Fig. 3; KMR trench) and established a grid system on the trench walls. We logged the walls and collected samples for tephra analyses and radiocarbon dating. To further examine the subsurface geology, we used a 50 cm long and 4 cm wide corer to obtain seven cores from the trench floor and the upthrown side (Fig. S1). We used a Nikon Nivo5.SC total station to map the locations of the surface ruptures, trench, and coring sites (Fig. 3b).

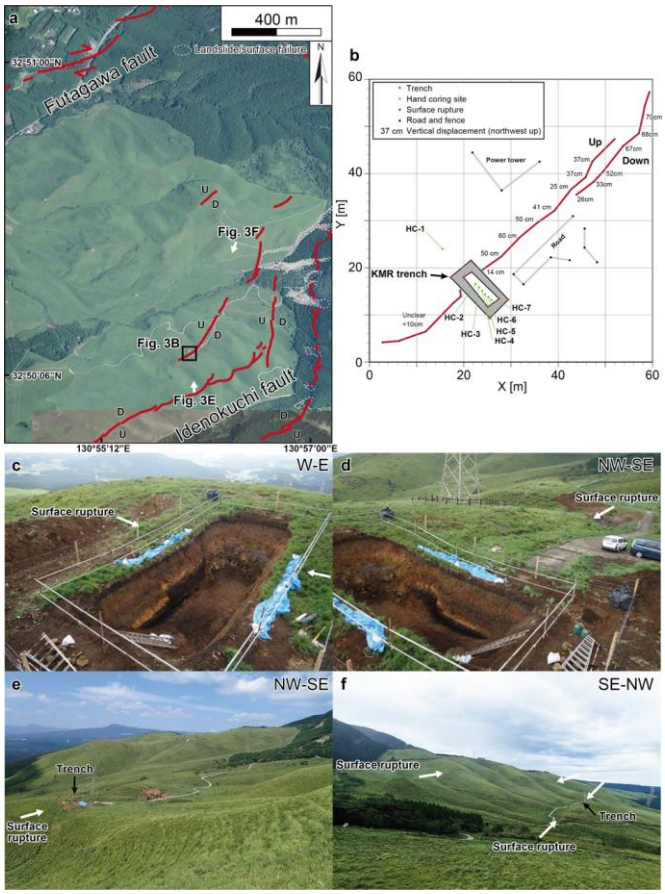

Figure 3. Geomorphic map and photographs around the trench site. (a) Red lines show the 2016 surface ruptures (Kumahara et al., 2022). Aerial photograph from the Geospatial Information Authority of Japan. (b) Location map of the trench and surface ruptures. Numbers indicate vertical displacement measurements. (c) Photo of the west wall of the trench. (d) Photo of the east wall of the trench. (e) (f) Photos of geomorphic conditions around the Idenokuchi fault trench site. Photo locations are shown in Fig. 3a.

260 *3.3 Laboratory analysis*

We determined refractive indices and major element compositions of volcanic glass shards in the sampled tephras. First, we sieved the samples with water through a 62-

μm nylon mesh. Then, we oven-dried the samples at 50 ℃ and sieved the dried samples through a 120-μm nylon mesh. The refractive index of volcanic glass shards in the 62–120 μm fraction of each sample was measured with a RIMS 2000 refractive index measuring system (Kyoto Fission Track Co., Ltd.) with an accuracy of ±0.0002 (Danhara et al., 1992). The major element composition of volcanic glass shards was measured by an energy-dispersive X-ray spectrometry (EDAX Genesis APEX2 and JEOL JSM-6390) following the method and analysis conditions described by Suzuki et al. (2014). Volcanic glass shards of the AT tephra sampled at Chigaki, Toyama Prefecture (Machida and Arai, 2003) were used as a working standard to check data reproducibility and instrument stability. A total of 12 tephra samples from the trench walls were analyzed and compared to two reference samples (Tables S1, S2, and S3).

A total of 26 radiocarbon samples, including charcoal and organic sediment (Table S4), were dated by accelerator mass spectrometry at the Laboratory of Radiocarbon Dating, University Museum, University of Tokyo, and the Institute of Accelerator Analysis Ltd., Japan. The obtained ages were calibrated using the OxCal 4.4 software (Bronk Ramsey, 2009) with the IntCal20 dataset (Reimer et al., 2020). The ages of paleofaulting events were calculated in the OxCal program by Bayesian analysis (Bronk Ramsey, 2008).

4. Results

4.1 3D displacement analysis

Figure 4 shows the distribution of 3D displacements during the 2016 earthquake, and Figure 5 shows topographic displacement profile lines A-D. In the profile lines (Fig.

5), the horizontal component is divided into two: parallel to the general strike of the Futagawa fault (N57°E) and perpendicular to it. The vertical component (Figs. 4c and 5) shows a displacement of 1.0–2.5 m at the southernmost part of the Idenokuchi fault and a vertical displacement of several tens of centimeters at the northern part of the fault. Compared to field measurements (Kaneda et al., 2022), a similar displacement was observed along the southernmost branch of the Idenokuchi fault, where a 2 m vertical displacement was recorded. However, the amount of vertical displacement along the fault is noisy and subject to uncertainty because of slope failures in the surrounding area. Along the parallel splay of the Idenokuchi fault, where we excavated the KMR trench, there is no significant difference between the calculated and field-measured displacements. On the other hand, on the Futagawa fault, the amount of local vertical displacement associated with the dextral displacement is observed in a narrow section about 200 m wide. When viewed over a 200–400 m wide zone from the fault, virtually no vertical displacement is observed. The vertical displacement along the long baseline (> 3 km) extending across both the Futagawa and Idenokuchi faults is about 1 m south-up (Lines A and B in Fig. 5).

A large fault-parallel displacement was observed on the Futagawa fault, and 1.8–3.1 m of dextral displacement occurred on the western part of the calculated area (Figs. 4b and 5). Since the displacement measured in the field was approximately 1.5–2.0 m (Shirahama et al., 2016; Kumahara et al., 2022), the 3D displacement data can be used to determine both the amount of off-fault displacement and on-fault displacement. This trend has also been discussed by Scott et al. (2018). In the western part of the Futagawa fault, larger dextral displacements were obtained for the long baseline (1 km) compared

to the short baselines (35 m and 100 m). Although it is difficult to identify from the 3D displacement distribution map (Fig. 4b), a slight sinistral displacement occurred on the Idenokuchi fault, which is consistent with the field measurements (Toda et al., 2016; Shirahama et al., 2016; Kaneda et al., 2022). In the eastern half of the calculation area, the contrast in displacement is smaller, the amount of displacement decreases, and there is greater variability because surface failures and other factors may have also occurred. The dextral displacement along the long baseline (> 3 km) between both faults is about 2–2.5 m.

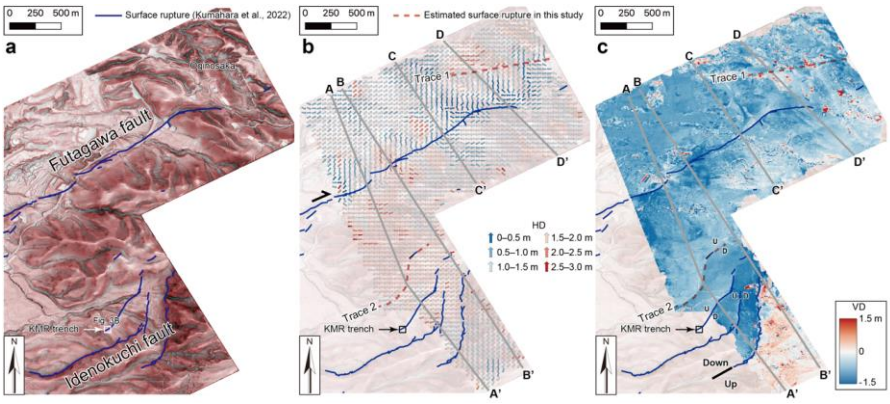

Figure 4. Results of the differential lidar analysis. (a) Red relief image map around the study area. The map was created following the methods of Kaneda and Chiba (2019). Surface ruptures are after Kumahara et al. (2022). (b) Horizontal displacement field. Horizontal displacement is indicated by the arrow and color. (c) Vertical displacement field. Vertical displacement is shown by the color map. HD: horizontal displacement, VD: vertical displacement. Letters (i.e., A-A') indicate endpoints of displacement profiles shown in Figure 5.

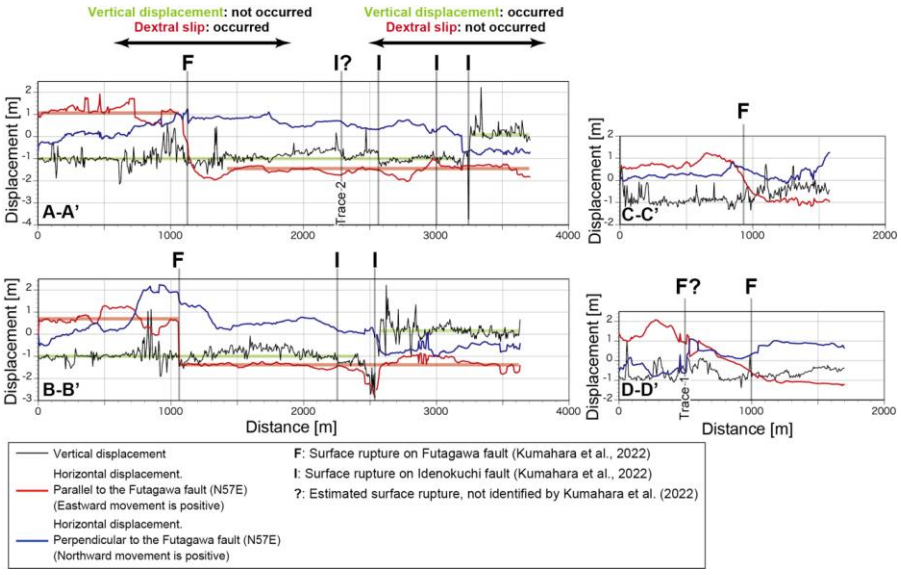

Figure 5. Vertical and horizontal displacement profiles. The profile lines are shown in Figure 4.

Regarding the fault-perpendicular component (Fig. 4b and A-A' and B-B' in Fig. 5), extension occurred locally on the Idenokuchi fault, and contraction occurred locally on the Futagawa fault. The extension is large at the southernmost part of the Idenokuchi fault, with a displacement of about 1–1.5 m. A contraction of about <1 m occurred on the Futagawa fault. The displacement in the perpendicular direction of the fault along the long baseline (> 3 km) across both faults is approximately 1 m of extension.

The 3D displacement and field measurements generally agreed on the locations of surface ruptures and the amount and sense of displacements. However, in two locations, surface ruptures were inferred from the displacement data but have not been confirmed in the field (Trace 1 and Trace 2; Figs. 4b and 4c). Trace 1 occurs north of the Futagawa

fault in the eastern part of the calculated area. Here, slight contrasts in fault parallel and perpendicular components are observed. Although it is unclear whether these displacements are associated with a well-defined fault, the discontinuity projects towards a surface rupture that continues eastward into the caldera (Kumahara et al., 2022). It also coincides with a 2 m shortening identified at a bridge abutment near Oginosaka (Fig. 4) (Shirahama et al., 2016). Trace 2 is a north-up displacement recognized along the northernmost splay of the Idenokuchi fault. Here, a short surface rupture was recognized (Kaneda et al., 2022), and it is likely to extend further to the southwest. However, it coincides with the present valley topography and may have been affected by fluvial erosion and other factors during the DTM measurement period.

4.2 Paleoseismic trench

4.2.1 Trench stratigraphy (including tephra analysis)

The trench exposed a package of silts, clays, and paleosols, separated from gravels and bedrock, across the primary normal fault. Figure 6 shows photomosaics and sketches of the west, east, and north walls. In this trench, sediments with different sedimentary facies and ages accumulated on the north (footwall, upthrown side) and south (hanging wall, downthrown side) sides across the primary normal fault at W9/E9. For this reason, the footwall and hanging wall sediments are assigned different unit numbers except for the topsoil (unit 00), which extends across the entire exposure.

350

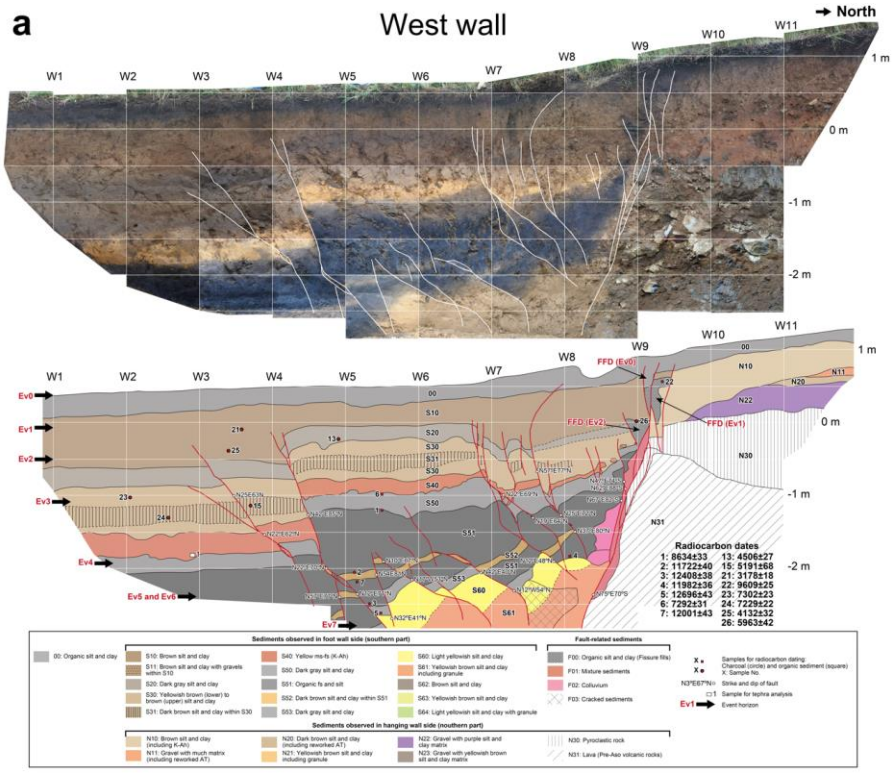
a
West wall
North
W1
W2
W3
W4
W5
W6
W7
W8
W9
W10
W11
1 m
0 m
-1 m
-2 m
FFD (Ev0)
FFD (Ev1)
FFD (Ev2)
Ev0
Ev1
Ev2
Ev3
Ev4
Ev5 and Ev6
Ev7
Radiocarbon dates
1: 8634±33
2: 11722±40
3: 12408±38
4: 11982±36
5: 12696±43
6: 7292±31
7: 12001±43
13: 4506±27
15: 5191±68
21: 3178±18
22: 9609±25
23: 7302±23
24: 7229±22
25: 4132±32
26: 5963±42
Sediments observed in foot wall side (southern part)
Fault-related sediments
Sediments observed in hanging wall side (southern part)

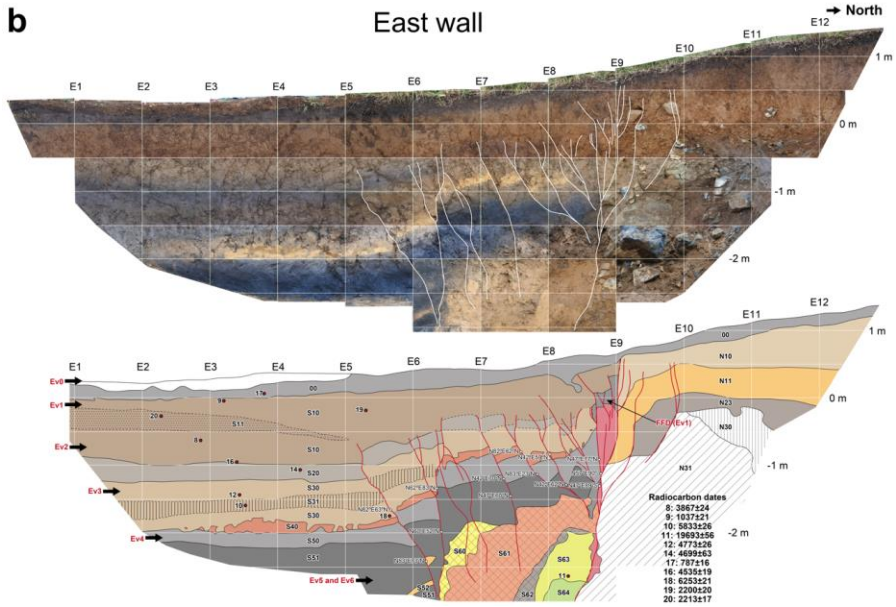
b
East wall
North
E1
E2
E3
E4
E5
E6
E7
E8
E9
E10
E11
E12
1 m
0 m
-1 m
-2 m
Ev0
Ev1
Ev2
Ev3
Ev4
Ev5 and Ev6
N10
N11
N23
N30
N31
S10
S20
S30
S40
S50
S51
S61
S63
S64
Radiocarbon dates
8: 3867±24
9: 1037±21
10: 5833±26
11: 19693±56
12: 4773±26
14: 4699±63
17: 787±16
16: 4635±19
18: 6253±21
19: 2200±20
20: 2213±17

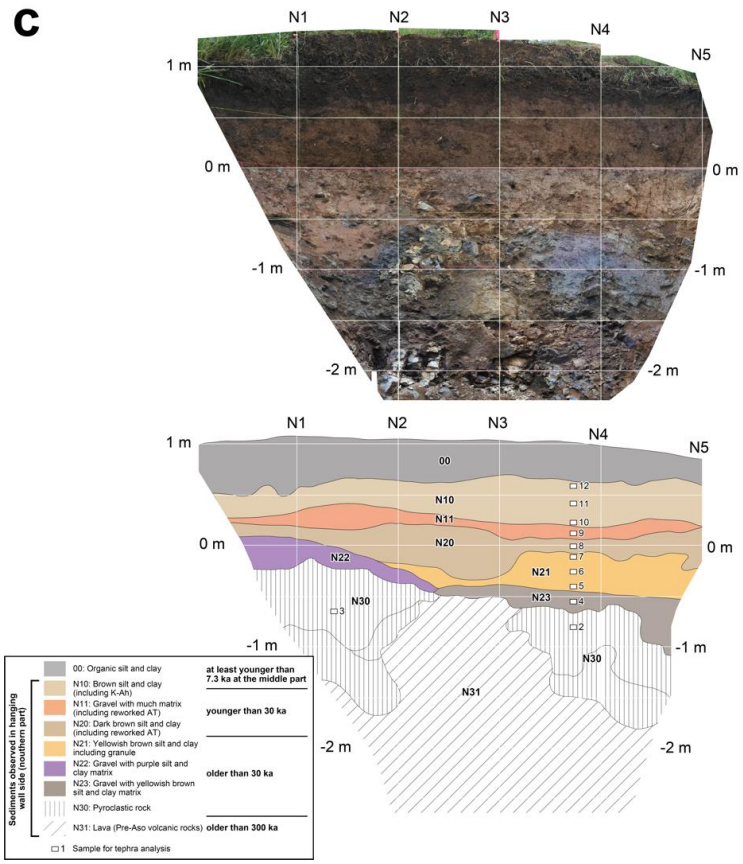

Figure 6. Photomosaics and sketches of the stratigraphic and structural relations exposed in the KMR trench walls. (a) West wall. The sketch of the west wall is flipped. (b) East wall. (c) North wall. FFD: fissure-fill deposits.

355 The following describes the sediments from the upper part of the south side. Sediments exposed in the hanging wall were deposited relatively continuously (Fig. 6a and 6b) and are described from the youngest to oldest. Unit 00 is the topsoil, consisting of black, organic silt and clay. Unit S10 is a thick, brown silt and clay below unit 00. On the

east wall, an interbed within unit S10 consisting of gravelly clay was classified as unit S11. Unit S20 is a dark gray silt and clay and is considered an organic-rich paleosol. Unit S30 is a yellowish brown to brown silt and clay with a slightly darker interbed (unit S31), which is an organic-rich paleosol similar to unit S20. Both Units S30 and S31 slightly thicken to the south away from the primary normal fault. Unit S40 is composed of fine to medium yellow sand, mainly composed of volcanic glass that is bioturbated and discontinuous in places. Units S50 and S51 are organic-rich paleosols. Unit S50 is dark gray silt and clay, and unit S51 is organic silt and fine sand, with unit S50 slightly lighter in color than unit S51. Unit S52 is yellowish brown to brown silt and clay interbedded within unit S51. Unit S53, which is observed only on the west wall, is a slightly lighter gray silt and clay similar to unit S50. The base of unit S53 is undulating between units S53 and S60 on the east wall, indicating an unconformity between them. Unit S60 is a bright yellowish silt and clay, and unit S61 is a yellowish-brown silt and clay with granules. On the west wall, unit S61 is the lowest (oldest) deposit. On the east wall, unit S61 is underlain by brown to yellowish brown silt and clay (units S62 and S63). The basal deposit (unit S64) is a light yellowish silt and clay with granules.

Sediments exposed on the footwall are thinner than those on the hanging wall and are primarily composed of gravel and rock (Fig. 6). The footwall sediments are slightly different between the east and west walls, and are thus described from the north trench wall which exposed the entire footwall package (Fig. 6c). Unit N10, consisting of brown silt and clay, has an erosional relationship with the underlying unit N11 and lower units (see west wall in Fig. 6a). Unit N11 is a matrix-supported gravel bed. Units N20 and N21 are dark brown and yellowish-brown silt and clay, respectively. Both units N22 and N23

are matrix-supported gravel beds that vary in color from purple to yellowish brown. Unit N30 is a pyroclastic rock unit with an undulating and irregular basal contact. Unit N31 is composed of fragmented lava from pre-Aso volcanic rock, which forms the basement rock of the surrounding area (Hoshizumi et al., 2004).

To further explore the site stratigraphy, a transect of cores was advanced into the floor of the trench on the hanging wall (cores HC-2 to HC-7) and beyond the limits of the trench on the footwall (core HC-1) (Fig. S1). Core HC-1 revealed nearly identical stratigraphy and thicknesses as that exposed on the trench walls, from which we infer that the sediments exposed on the north wall are distributed widely and uniformly on the northern side of the fault. On the downthrown side (HC-2 to HC-7), the black silt and clay and yellowish brown to brown silt and clay, corresponding to unit S51 and lower, were observed. No black soil, corresponding to units S51 to S53, was observed at depths greater than 1 m from the trench floor. Gravel and sand beds, not recognized on trench walls, were observed in some cores. However, no tephra layers were identified. On the other hand, sediments were in contact with high angles, and voids were observed in some cores, which we inferred to be faults. The primary normal fault was considered the boundary with the basement rock, so we inferred the normal fault at a depth where drilling was no longer possible.

4.2.2 Faults

In this trench, we identified faults, rootless faults, and cracks. Faults refer to discontinuities with apparent displacement that extend downward to the bottom of the

trench. Rootless faults are those with apparent displacement but do not extend downward to the trench bottom. Cracks are those without displacement. Although we observed many cracks on the trench walls, we did not show them in the figures because they did not affect the paleoseismic interpretations. The primary normal fault is observed at W9/E9, and many other faults are rootless with bending in the lower part. Faults extending down to the trench bottom are the north-up normal faults at W9/E9 and the reverse faults at W3-W5 and E5-E6. Normal faults that form grabens develop at W7-W9 and E7-E10. The 2016 displacement was an open crack near W9/E9, which was already filled with sediments at the time of trench excavation. Similar open cracks and fissure fill deposits have been identified in the Futa trench at Futa (Fig. 1; Ishimura et al., 2022). However, no other distinct 2016 displacement (e.g., apparent vertical displacement) was observed on the trench walls. This is likely because the trench is located in an area of decreasing vertical displacement from northeast to southwest, where the 2016 displacement is small (<14 cm) and indistinct (Fig. 3b). Other fissure-fill deposits that may have formed prior to the 2016 event were also identified below the 2016 fissure-fill deposits. Measurements of the strike and dip of the faults on the trench walls indicate that the predominant strike is northeast to southwest, but some are north to south or east-northeast to west-southwest (Fig. 6). The northeast-southwest strike is consistent with the surface ruptures (Fig. 3b). The other strike directions suggest that subsidiary surface ruptures to the primary normal fault may have occurred in the past events.

4.2.3 Tephra analysis

We completed tephra analysis for unit S40 (sample No. 1) on the hanging wall as well as a suite of 11 samples (Sample No. 2 to No. 12) from the footwall (Table S1). The results of the tephra analysis are shown in Table S1, and the major element composition of volcanic glass shards is shown in Tables S2 and S3. The results show that unit S40 is composed almost entirely of volcanic glass, with a refractive index of 1.510-1.512 (mode: 1.511), suggesting that it correlates with the widespread tephra, Kikai-Akahoya (K-Ah), by the eruption of southern Kyushu at 7.3 ka (Machida and Arai, 2003; Smith et al., 2013). The chemical compositions confirmed this correlation (Table S2), consistent with the existing studies in the vicinity (e.g., Ishimura et al., 2022). Volcanic ash analysis of the samples from the north wall (Samples No. 2 to No. 12) revealed no tephra layers. Therefore, we examined the volcanic glass content and refractive indices to determine if the samples contained volcanic glass shards of Aira-Tn (AT) (30 ka; Smith et al., 2013) and K-Ah tephras, which are commonly identified tephras in this area (Machida and Arai, 2003). The results (Table S1) show that there is almost no volcanic glass below unit N21, while units N20 and N11 exhibit very low volcanic glass content (2%). The refractive indices of volcanic glass are mainly 1.495-1.500, which correlates with AT tephra. In contrast, the volcanic glass content increases from the lower to the upper part of unit N10. The refractive indices show that while unit N10 contains glass with a refractive index of 1.497-1.500 of AT origin, the percentage of volcanic glass of 1.508-1.512 of K-Ah origin increases toward the upper part of unit N10. This suggests that the age of the middle part of unit N10 is after the K-Ah tephra. This mixing of AT and K-Ah volcanic glass is also observed in soils in other regions, and the K-Ah ash fall horizon is roughly estimated at the peak of K-Ah volcanic glass shard content (Ishimura and Kakiuchi,

2011). Such distribution of volcanic glass shard content may be due to bioturbation and secondary deposition of tephra-origin particles. Based on the presence of AT volcanic glass, unit N20 is at least younger than 30 ka, and unit N21 and below are older than 30 ka. Based on the K-Ah glass content, the upper to middle part of unit N10 is interpreted to be at least younger than 7.3 ka. The fact that K-Ah tephra is exposed in the hanging wall indicates that sediment preservation potential is better on the downthrown side of the fault.

4.2.4 Radiocarbon dating

Because the faulting events described below were identified on the downthrown side of the primary normal fault, we performed radiocarbon dating of samples collected from the south side of the trench walls (Table S4). The youngest age was 787 ± 16 yr BP (charcoal; Sample 17) from unit 00, and the oldest was 19693 ± 56 yr BP (charcoal; Sample 11) from unit S63. For sediments older than unit S50, bulk samples (organic sediments) were dated except for the sample from unit S63. As Ishimura et al. (2022) pointed out, the ages of bulk samples in this region are sometimes younger than the actual ages. In this trench, we compared the bulk sample ages with the ages of the K-Ah tephra and the charcoal from unit S63. As a result, the bulk sample ages were consistent with the tephra and charcoal age, with no contradiction between the stratigraphy and age. Because we used charcoal samples above unit S30, it is possible that older charcoals were included by reworking, resulting in older ages. In such cases, charcoals with younger ages in the same unit were employed for further analyses. As a result, we did not use the ages, 7302 ± 23 yr BP and 7229 ± 22 yr BP from samples 23 and 24, respectively (Table

S4). Additionally, the ages of the fissure-fill deposits (samples 22 and 26) using the bulk samples were significantly older than the surrounding sediments. The specific organic matter responsible for the cause is unknown because they are bulk samples. One possibility is that the trench site is located on an uphill−facing scarp, acting as a trap for sediments, allowing old organic matter to deposit along faults and open fractures. In any case, it is thought that the fissure-fill deposits contained old organic matter. Therefore, the ages of these fissure-fill deposits are also not used.

4.3 Evidence for paleofaultings

We identified geologic evidence for faulting events since the deposition of unit S53 by stratigraphic evidence (Fig. 6) and retrodeformation (Fig. 7 and S2). Ev0 is the 2016 event, and an open crack occurred directly above the primary normal fault near W9/E9 (Fig. 6a and 6b). In Ev0, a further open crack was formed in the pre-existing open crack created by Ev1 (the penultimate event), which is described in the following paragraph. This pre-existing crack was already filled with sediment at the time of our survey. Similarly, an open crack directly above the primary normal fault, located near E9, is recognized on the east wall (Fig. 6b). The surface rupture runs between W8-W9 and E8-E9, corresponding to the locations of open cracks. These observations confirm that the 2016 event formed these open cracks.

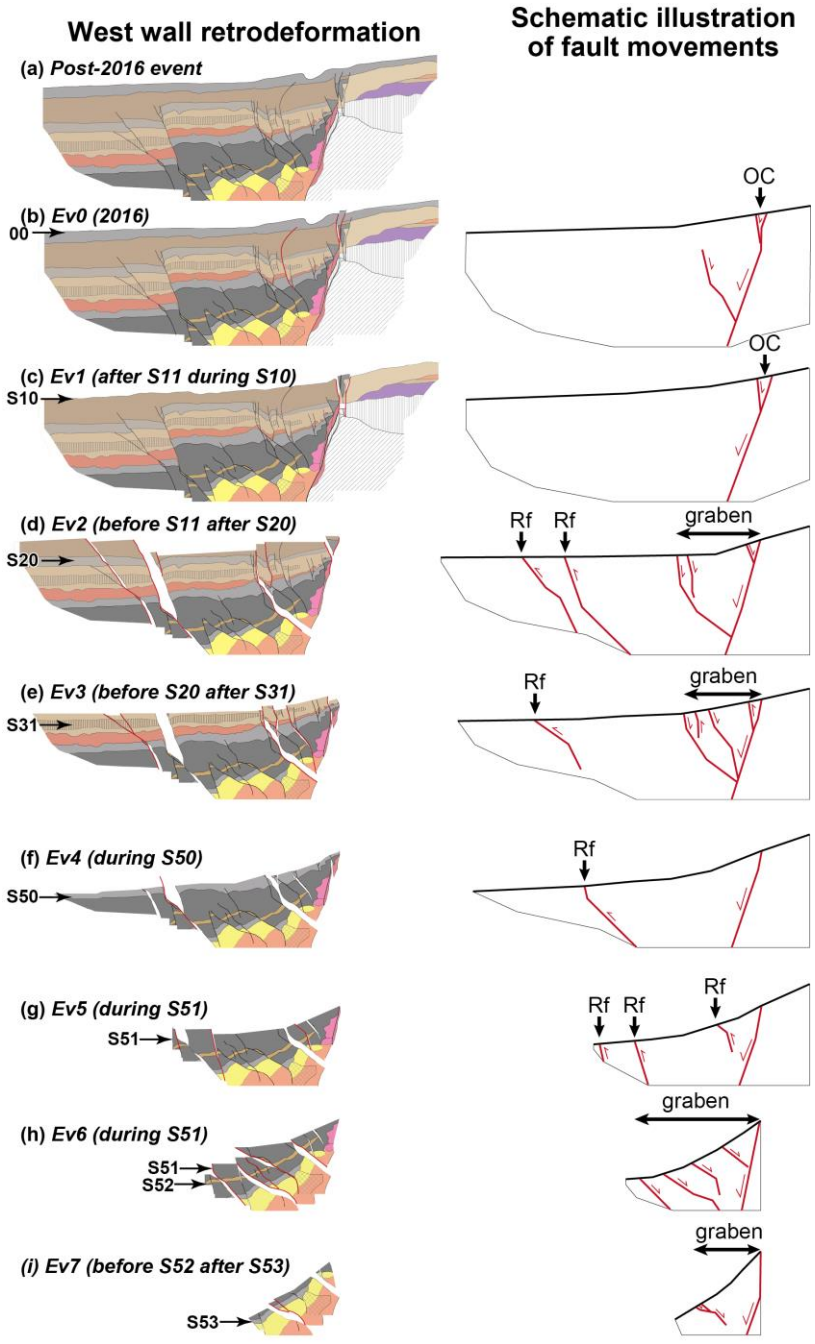
West wall retrodeformation
Schematic illustration of fault movements
(a) Post-2016 event
(b) Ev0 (2016)
00
(c) Ev1 (after S11 during S10)
S10
(d) Ev2 (before S11 after S20)
S20
(e) Ev3 (before S20 after S31)
S31
(f) Ev4 (during S50)
S50
(g) Ev5 (during S51)
S51
(h) Ev6 (during S51)
S51
S52
(i) Ev7 (before S52 after S53)
S53
OC
OC
Rf
Rf
graben
Rf
graben
Rf
Rf
Rf
Rf
graben
graben

Figure 7. Retrodeformation of the faults and deformed strata, and schematic illustration of fault movements on the west wall. The left figures show reconstructions of the displacement for each event, and the right figures show the faults that were active during each event. Rf: reverse fault, OC: open crack.

Ev1, like Ev0, developed an open crack directly above the primary normal fault near W9, which was immediately next to the open crack of Ev0 and filled by fissure-fill deposits. On the west wall, this fissure-fill deposit was formed in unit S10 during Ev1 and was displaced at the southern part by Ev0 event. Unit S10, displaced by Ev1, is stratigraphically positioned above unit S11, which was probably deposited by a slope failure in Ev2 as described in the following paragraph. Therefore, Ev1 is interpreted to have occurred during the deposition of unit S10, especially after unit S11 deposition.

In Ev2, an open crack, normal fault displacements near the primary normal fault (W7-W9), and reverse fault displacements on the southern faults (W3-W4) occurred. Subsidiary normal and reverse faults displaced unit S20 and the lower part of unit S10, and a fissure-fill deposit was identified on the west wall (W9, 0 m). Therefore, this event occurred after the deposition of unit S20 paleosol and during the deposition of unit S10. Similarly, on the east wall, normal fault displacements were observed near the primary normal fault (E7-E9), and the faults in the south (E5-E6) show reverse fault displacements. In addition, the gravel-rich unit S11 is recognized in unit S10 on the east wall, which is wedge-shaped and may be a deposit supplied from the southern slope, rather than from the main normal fault in the trench. A similar surface failure occurred in the southern slope along the Idenokuchi fault during the 2016 earthquake (Fig. 3a).

Therefore, unit S11 may be a post-earthquake deposit related to Ev2. Thus, the event horizon of Ev2 is estimated to be after unit S20 and before unit S11.

Ev3, like Ev2, involved normal fault displacements near the primary normal fault (W7-W9) and reverse fault displacements on the southern faults (W3-W4). The east wall similarly shows normal fault displacements at E7-E9 and reverse fault displacements of the southern faults (E5-E6). On the east wall, even after restoring the fault displacement of Ev2, vertical displacement was still observed in faults at E6-E8 (Fig. S2). This indicates cumulative displacement, suggesting fault activity between units S20 and S40. The fault at W3 displaces unit S31, but does not displace unit S20. Therefore, the event horizon of Ev3 is estimated to be between units S20 and S31.

Ev4 is indistinct on the west wall, while it is distinct on the east wall. On the east wall, even after restoring the fault displacement of Ev2 and Ev3, vertical displacement was still observed for the reverse fault at E6 and normal fault at E8-E9 (Fig. S2). This indicates cumulative displacement, suggesting fault activity between units S40 and S51. Therefore, the event horizon of Ev4 is estimated to be during the deposition of unit S50.

Ev5 and Ev6 occurred after the deposition of unit S52 and during unit S51 deposition. During this period, reverse and normal subsidiary fault displacements are observed in W4-W8 even after restoring the fault displacement of Ev2 to Ev4 (Fig. 7). Although it is possible that both displacements occurred during a single event, we estimate two separate events (Ev5 and Ev6). From the retrodeformation (Figs. 7 and S2), we found that the displacement patterns tended to be similar in consecutive events. In other words, Ev0 and Ev1 created open cracks along the primary normal fault (W8-W9),

and Ev2 to Ev4 caused reverse fault displacement in the southern part and normal fault displacement on the primary normal fault. Additionally, Ev7 involves only normal fault displacement as described in the following paragraph. Considering the similarity of the displacement patterns in consecutive events, reverse fault motions could be related to Ev5, and normal fault motion could be related to Ev6 (Fig. 7). Therefore, we interpreted that there could have been two events during this period. Since the ages of Ev5 and Ev6 cannot be distinguished, both events are only constrained as after unit S52 and during unit S51 deposition.

In Ev7, a normal fault displacement at W7-W8 occurred at the lowest part of the soil deposits in this trench. On the west wall, even after restoring the fault displacement of Ev2 to Ev6, vertical displacement was still observed in the normal fault at W6 (Fig. 7). Its age is estimated to be between units S52 and S53 deposition.

5. Discussion

5.1 Slip partition based on 3D displacements

In this section, we discuss how the displacement is divided on the Futagawa and Idenokuchi faults for the slip partition along line A (Fig. 5), where the influence of surface failure is small and the Futagawa fault appeared as a single trace (Fig. 4). First, dextral displacement occurred only on the Futagawa fault. Local sinistral displacement was observed along the Idenokuchi fault in the field (Toda et al., 2016; Shirahama et al., 2016). However, along the long baseline (> 3 km), the amount of lateral displacement was similar across the Idenokuchi fault. On the other hand, the vertical displacement is the opposite of the lateral displacement. Vertical displacement of 1 m occurred only in the

southernmost trace of the Idenokuchi fault along the long baseline, and little vertical displacement occurred within a 1 km width across the Futagawa fault. Vertical displacement of several tens of centimeters occurred on the subparallel faults of the Idenokuchi fault, but that decreased immediately within a short distance from the fault, indicating that the deformation was localized to a shallow depth. These observations suggest that extensional deformation and block rotation cause apparent vertical displacement on the subparallel faults.

Scott et al. (2018) and Himematsu and Furuya (2020) observed a large vertical displacement (1-2 m south-up) on the Futagawa fault on the west side of the parallel section of the Futagawa and Idenokuchi faults. This indicates that the Futagawa fault accommodated oblique slip on the west side of the Idenokuchi fault's parallel section. In addition, Himematsu and Furuya (2020) showed a sharp decrease in vertical displacement and nearly constant right lateral displacement along the Futagawa fault at the parallel section of the Idenokuchi fault, which is consistent with our results.

Our observations suggest that the slip partition on the Futagawa and Idenokuchi faults is the result of oblique lateral displacement at depth, which is almost completely split into dextral and vertical displacement near the surface and accommodated by both faults, respectively, as shown schematically by Toda et al. (2016). In addition, our results show that the displacement is completely split, as shown in King et al. (2005). This may provide an important insight into the geometry (dip angle, distance of two faults, and amount of oblique displacement) of faults where slip partitioning can occur. We interpret that the deeper part of the Idenokuchi fault is connected to the deeper part of the Futagawa fault, and the Idenokuchi fault is a branch fault of the Futagawa fault. The

estimated depth at which they merge may be several kilometers, as shown by Toda et al. (2016), although it depends on their dip angles.

Commented [A13]: please add the range of expected dip angles for both faults

We discuss the relationship between slip partition and geology. According to King et al. (2005), the depth at which the fault branches upwards may coincide with the bottom of surface sediments. Aoyagi et al. (2024) reported another slip partition on the western part of the Futagawa fault based on the surface rupture distribution of the 2016 event, drilling cores, and seismic reflection survey. They reported that the short (<2 km) subparallel surface ruptures/faults accommodated oblique slip in the deeper part of the 2016 Kumamoto earthquake and converged at a depth of 350 m. The depth corresponds to the top of the pre-Aso volcanic rocks and/or Kiyama metamorphic rocks (Kumamoto Prefecture Geological Map Compilation Committee, 2008). Unconsolidated sediments, including pyroclastic flow deposits of middle to late Pleistocene age, overlie these rocks. Thus, the upper end depth (convergent depth of both faults) of oblique slip seems to correspond to some geological (physical property) difference. There is no data on the deep subsurface geology of our study area. Since there is no surface sediment (unconsolidated) and pre-Aso volcanic rocks are exposed on the surface around the trench site, the situation differs from that in King et al. (2005) and Aoyagi et al. (2024).

5.2 Age of paleofaulting events on the Idenokuchi fault

Based on evidence for paleofaulting events, we estimated six certain (Ev0–Ev4, and Ev7) and two less certain (Ev5 and Ev6) faulting events since the deposition of unit S53. The ages of the faulting events were obtained using OxCal (Fig. S4). The results

show that the ages of each event are as follows: Ev1: 2190–940 cal BP, Ev2: 4760–4250 cal BP, Ev3: 6040–5360 cal BP, Ev4: 9550–7280 cal BP, Ev5-Ev6: 13500–9680 cal BP, Ev7: 14700–13840 cal BP with the 2σ range. The average recurrence interval of the maximum of eight interpreted events is 1990–2110 years. Unit S53 is buried 4.5–5 m below the present ground surface, indicating that the strata dropped an average of 0.6–0.7 m per event relative to the ground surface. This value is roughly consistent with a representative 2016 coseismic displacement of 60 cm along the surface rupture, where the KMR trench was excavated. Despite the shallow depth of the trench, we could identify up to eight events, significantly more than those identified in trenches excavated on the primary Futagawa fault. This result emphasizes the importance of selecting a site with small displacement per event and relatively fast and continuous deposition.

Commented [A14]: Please add the average recurrence interval for the minimum number of earthquakes or discuss how different it is.

Commented [A15]: Any comment on why this is true? Is the trench in this study in finer sediments or have better ash fall correlations?

5.3 Comparison of paleoseismic events between the Futagawa and other faults

A summary of the paleofaulting history constructed by the author's group (Fig. 8) shows that the ages of faulting events after the K-Ah tephra (7.3 ka), which is widely identified in the paleoseismic trenches around the Futagawa fault, all overlap. This suggests that the Futagawa fault (Ishimura et al., 2022), Miyaji faults (Ishimura et al., 2021), and Idenokuchi fault have all moved simultaneously at least in the past several earthquakes. Notably, the simultaneity of the Futagawa and Idenokuchi faults is consistent with the idea that they are connected at a deeper level, as described in Section 5.1. Therefore, the paleoseismic history of the Idenokuchi fault is likely to represent that of the Futagawa fault, given its subsurface structure. The Miyaji faults, which produced the 2016 surface rupture and are distant from the Futagawa fault and structurally

Commented [A16]: could omit

Commented [A17]: Please re-phrase with more nuance. This is possible given the overlapping age ranges, but not required, as triggered earthquakes could happen days, weeks, months, or years after earthquakes on nearby faults, timescales that are indistinguishable with the available dating uncertainties.

Commented [A18]: Are there other case studies of faults that are connected at depth that definitively rupture together or separately that the authors can bring into this discussion to bolster the idea that the paleoseismic history of the Idenokuchi fault can represent that of the Futagawa fault? Currently the data supporting this idea is rather weak.

discontinuous (Fukushima and Ishimura, 2020), are also presumed to have been active in the past, together with the Futagawa fault. Given inherent uncertainties in dating techniques, it is technically challenging to prove the simultaneous rupture of faults. Nevertheless, further studies are necessary to determine whether the simultaneous rupture of the primary and secondary faults is common or if it is worthwhile to incorporate small displacements relative to those on the primary fault into seismic hazard assessment.

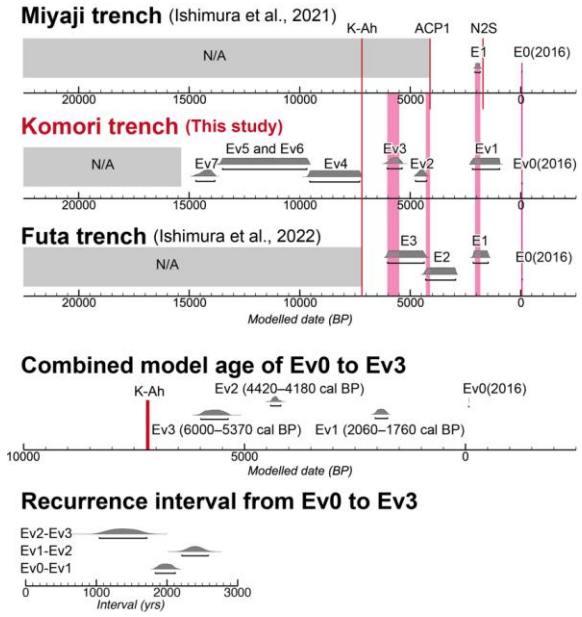

Figure 8. Modeled event ages and comparison to the authors' previous paleoseismic studies. The underbars show the 2σ probability distribution ranges of the modeled ages. ACP1 and N2S are local tephras from the Aso volcano (Miyabuchi, 2009). ACP1 is Aso central cone pumice and its age is 4.1 ka (Miyabuchi, 2009). N2S is Nakadake N2 scoria, and its age is 1490–1470 cal BP (68.2%) (Yamada et al., 2017).

Furthermore, assuming that the faulting events from Ev1 to Ev3 are the same among our three trenches (Komori, Miyaji, and Futa trenches), the calculated ages in OxCal modeling are Ev1: 2060–1760 cal BP, Ev2: 4420–4180 cal BP, and Ev3: 6000–5370 cal BP (Fig. 8). The recurrence intervals of each event are Ev0/Ev1: 1830–2120 years, Ev1/Ev2: 2210–2590 years, and Ev2/Ev3: 1040–1720 years with the 2σ range. Based on the trenching results, the average recurrence interval from Ev0 to Ev7 is 1990–2110 years, consistent with the modeled recurrence interval from Ev0 to Ev3. This indicates that the Futagawa fault has ruptured relatively periodically.

The dextral slip rate, calculated from the recurrence interval (1990–2110 years) and single displacement (1.8–3.1 m) obtained in this study, is 0.9–1.5 mm/yr for the Futagawa fault. For the Idenokuchi fault, the vertical displacement ranges from 1.0 to 2.5 m, indicating an estimated vertical slip rate of 0.5 to 1.3 mm/yr. On the west of the study area (Futa to Ohkirihata), Ishimura (2019) calculated 0.9–1.1 mm/yr vertical slip rate and 1.5–3.7 mm/yr dextral slip rate for the Futagawa fault from the vertical and dextral displacements of Takayubaru lava (K–Ar ages 81 ± 4 ka and 98 ± 18 ka; Miyoshi et al., 2013). The Idenokuchi fault runs parallel to the Futagawa fault, where these slip rates, i.e., the west of the study area, were calculated. However, the vertical displacement on the Idenokuchi fault in the 2016 event west of the study area is small (Kaneda et al., 2022). Therefore, the long-term slip rates can be regarded as representative values when oblique slip is accommodated only by the Futagawa fault. Therefore, the long-term dextral and vertical slip rates are consistent with the results of this study. Oohashi (2020) pointed out that normal fault displacement was predominant on the Futagawa fault before Aso-4 pyroclastic flow deposits (87 ka; Aoki, 2008), and dextral displacement became

apparent later. Oohashi (2020) proposed the following possibilities for this change: 1) The stress field changed from a normal fault type with north-south extension to a dextral strike-slip fault type with predominant east-west compression, and 2) the normal fault component of the Futagawa fault was replaced by the Idenokuchi fault and off-fault displacements, and the dextral displacement of the Futagawa fault became apparent. The fact that the long-term vertical slip rate coincides with that of the Idenokuchi fault from this study agrees with the second explanation. Therefore, the slip partition on the Idenokuchi fault must have occurred after the Aso-4 event (ca. 87 ka).

Figure 9 summarizes the paleofaulting history of the Kumamoto earthquake area since 7.3 ka, based on previous paleoseismic results, including archaeological information. The number of earthquakes since 7.3 ka (including 2016) on the Futagawa fault is estimated to be four with considerable accuracy and precision, based on the results of multiple trenches along the Futagawa fault and its vicinity. We believe that a series of trenching studies by our group has provided accurate ages for the past three events because we studied the sites with minor artificial disturbance, continuous sediments, and good age markers (tephras). In addition, the paleofaulting history at the northwestern Aso caldera (Sato et al., 2021) and the western part of the Futagawa fault (Inoue et al., 2020), which are at secondary surface ruptures, indicates that one of their events coincides with Ev1 in this study. Therefore, it is highly likely that the secondary faults were activated simultaneously during at least the penultimate event of the Futagawa fault. Lateral spreading recognized at archaeological sites within the caldera (Kumamoto Prefectural Board of Education, 2010; Aso City Board of Education, 2011) was also approximately 2000 years ago, which also supports that secondary phenomena

caused by an earthquake similar to the 2016 event occurred repeatedly in the caldera. Thus, it is inferred that similar phenomena in the 2016 event (e.g., secondary surface rupture, liquefaction, and lateral spreading) also occurred during the previous activity. However, the age of the antepenultimate event in the northwestern part of the caldera does not match that of the Futagawa fault (Sato et al., 2021). In addition, no other secondary surface ruptures have been identified as having earthquakes older than the antepenultimate event, so it is unclear how the secondary fault behaved during the older events. Future information on the presence or absence of older earthquakes on such secondary faults and their histories will help us to better understand the secondary faults and how frequently they rupture simultaneously with the Futagawa fault.

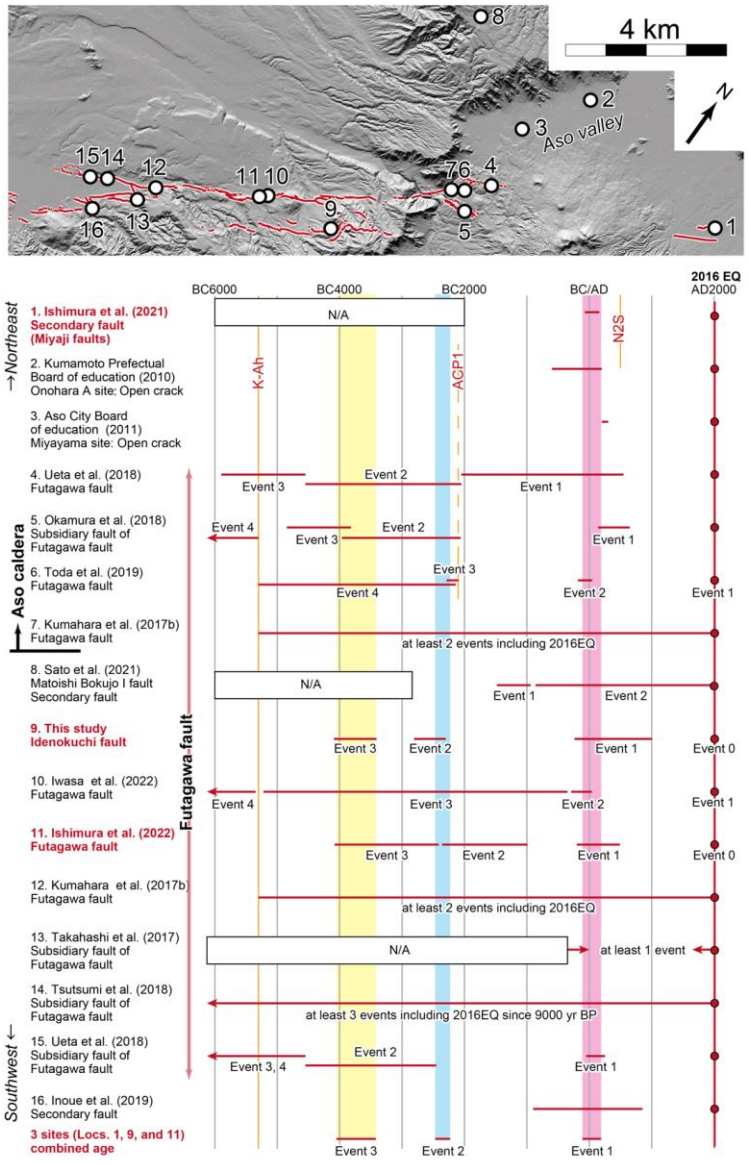

Figure 9. Compilation of paleofaulting events. The upper panel shows the locations of the lower panel data. The lower panel shows the compiled spatial-temporal age distribution of the paleofaulting events along the Futagawa and its subsidiary and secondary faults. Event chronologies correspond to studies referenced on the left side of the panel. The red bar represents the event age range in each study. The

Commented [A19]: In the above figure, the Event numbers for the Sato et al study (2021) are reversed compared to the other studies (event 2 comes more recently than event 1)

red arrow indicates that the age is estimated to be outside the range shown in the figure. The pink, blue, and yellow shading represent the combined model age ranges of Ev1, Ev2, and Ev3, respectively. Details of K-Ah, ACP1, and N2S tephras were described in the caption of Figure 8.

6. Conclusions

Using the 2016 Kumamoto earthquake as an example, we performed a DTM difference analysis in the area where the Futagawa and Idenokuchi faults interact, and conducted an excavation survey on the Idenokuchi fault. Based on the 3D displacement distribution, we discussed how the slip partition occurred on them and found that the oblique slip at depth was split entirely into vertical and horizontal displacements on the ground surface. This indicates that the Idenokuchi fault is structurally related to the Futagawa fault and that the paleofaulting history of the Idenokuchi fault is likely to correspond to that of the Futagawa fault.

The KMR trench at the Idenokuchi fault revealed continuous deposition of soil and tephra since 15 ka, and retrodeformation of the trench walls revealed up to eight faulting events (including 2016) during this period. Among them, the faulting events after Kikai-Akahoya tephra (7.3 ka) are consistent with paleoseismic surveys on the Futagawa fault (the primary fault) and Miyaji faults (secondary faults in the Aso caldera). This suggests that at least some surface ruptures that occurred around the Futagawa fault during the 2016 event were likely active at the same time as past activities of the Futagawa fault. The activity histories since 7.3 ka with the authors' three trenches on the Futagawa, Miyaji, and Idenokuchi faults are E1: 2060–1760 cal BP, E2: 4420–4180 cal BP, and E3: 6000–5370 cal BP, indicating that they occurred relatively periodically. The mean recurrence interval since 15 ka is about 2000 years, supporting the periodic activity. The results of this study are also consistent with other trench investigations conducted

after 2016. It is important to improve the accuracy and precision of the activity history of the Futagawa fault before 7.3 ka and to investigate the activity history of the Hinagu fault zone in the southern part of the Futagawa fault zone to consider future seismic hazard and interlocking rupture. In addition, it will be important to clarify the subsurface structure and activity history of secondary faults in other earthquakes to consider displacement hazards.

Acknowledgements

We thank Yasuhiro Kumahara, Ryuhei Oda, Jun Matsukaze, Motoya Kobayashi, Makoto Kobayashi, Yoshiya Iwasa, and Daichi Tomita for their help during the trench survey. We also thank Shinji Toda, Heitaro Kaneda, and Yasuo Miyabuchi for their discussions and constructive comments. The thoughtful comments from the reviewer Rich Koehler, and the anonymous reviewer improved the article. This work was supported by KAKENHI Grant Number JP17H04730 from the Japan Society for the Promotion of Science.

Data and code availability

Supplementary figures (S1 to S2) and tables (S1 to S4) are available in the supplement material.

OxCal model codes are listed in the supplementary material.

Pre- and post-event DTMs used in this study were provided by the Geospatial Information Authority of Japan (https://www.gsi.go.jp/ENGLISH/index.html).

Competing interests

The authors have no competing interests.

References

Aoki, K. (2008) Revised age and distribution of ca. 87 ka Aso-4 tephra based on new evidence from the Northwest Pacific Ocean. Quaternary International, 178, 100–118. doi: 10.1016/j.quaint.2007.02.005.

Aoyagi, Y., Higashi, S., Homma, S., Mukoyama S., Sugiyama, M., and Hijikata, K. (2021) Surface ruptures in the Aso campus of Tokai University caused by the 2016 Kumamoto Earthquake. Active Fault Research, 55, 1–18. (in Japanese with English abstract)

Aoyagi, Y., Ueta, K., Takemoto, T., Suehiro, M.,and Miyawaki, R. (2024) Seismic constraints on the subsurface extent of subparallel surface ruptures in Mashiki Town, Japan, associated with the 2016 Kumamoto Earthquake. Journal of the Seismological Society of Japan. 2nd ser., 77, 5–19. (in Japanese with English abstract)

Aso City Board of Education (2011) Miyayama ruinsII, Cultural Property Investigation Report of Aso City 2. Aso City Board of Education, Aso City. (in Japanese)

Barnhart, W.D., Hayes, G.P., and Gold, R.D. (2019) The July 2019 Ridgecrest, California, earthquake sequence: Kinematics of slip and stressing in cross-fault ruptures. Geophysical Research Letters, 46, 11859–11867. doi: 10.1029/2019GL084741.

Bronk Ramsey, C. (2008) Deposition models for chronological records. Quaternary Science Reviews, 27, 42–60. doi: 10.1016/j.quascirev.2007.01.019.

Bronk Ramsey, C. (2009) Bayesian analysis of radiocarbon dates. Radiocarbon, 51, 337–360. doi: 10.2458/azu_js_rc.v51i1.3494.

Danhara, T., Yamashita, T., Iwano, H., and Kasuya, M. (1992) An improved system for measuring refractive index using the thermal immersion method. Quaternary International, 13–14, 89–91. doi: 10.1016/1040-6182(92)90013-R.

Fujiwara, S., Yarai, H., Kobayashi, T., Morishita, Y., Nakano, T., Miyahara, B., Nakai, H., Miura, Y., Ueshiba, H., Kakiage, Y., and Une, H. (2016) Small-displacement linear surface ruptures of the 2016 Kumamoto earthquake sequence detected by ALOS-2 SAR interferometry. Earth, Planets and Space, 68, 160. doi: 10.1186/s40623-016-0534-x.

Fukushima, Y., and Ishimura, D. (2020) Characteristics of secondary-ruptured faults in the Aso Caldera triggered by the 2016 Mw 7.0 Kumamoto earthquake. Earth, Planets and Space, 72, 175. doi: 10.1186/s40623-020-01306-y.

Goto, H., Tsutsumi, H., Toda, S., and Kumahara, Y. (2017) Geomorphic features of surface ruptures associated with the 2016 Kumamoto earthquake in and around the downtown of Kumamoto City, and implications on triggered slip along active faults. Earth, Planets and Space, 69, 26. doi: 10.1186/s40623-017-0603-9.

Hamling, I.J., Hreinsdóttir, S., Clark, K., Elliott, J., Liang, C., Fielding, E., Litchfield, N., Villamor, P., Wallace, L., Wright, T.J., D'Anastasio, E., Bannister, S., Burbidge, D., Denys, P., Gentle, P., Howarth, J., Mueller, C., Palmer, N., Pearson, C., Power, W., Barnes, P., Barrell, D.J.A., Van Dissen, R., Langridge, R., Little, T., Nicol, A., Pettinga, J., Rowland, J., and Stirling, M. (2017). Complex multifault rupture during the 2016 Mw 7.8 Kaikōura earthquake, New Zealand. Science, 356, 6334. doi: 10.1126/science.aam7194.

He, P., Wen, Y., Xu, C., and Chen, Y. (2019) Complete three-dimensional near-field surface displacements from imaging geodesy techniques applied to the 2016 Kumamoto earthquake. Remote Sensing of Environment, 232, 111321. doi: 10.1016/j.rse.2019.111321.

Headquarters for Earthquake Research Promotion (2013) Long-term evaluation of the Futagawa and Hinagu fault zones (partial revision version) (in Japanese). http://www.jishin.go.jp/main/chousa/13feb_chi_kyushu/k_11.pdf. (Accessed 17 August 2025).

Himematsu, Y., and Furuya, M. (2020) Coseismic and postseismic crustal deformation associated with the 2016 Kumamoto earthquake sequence revealed by PALSAR-2 pixel tracking and InSAR. Earth, Planets and Space, 7, 1–19. doi: 10.1029/2020EA001200.

Hoshizumi, H., Ozaki, M., Miyazaki, K., Matsuura, H., Toshimitsu, S., Uto, K., Uchiumi, S., Komazawa, M., Hiroshima, T., and Sudo, S. (2004) Geological Map of Japan 1:200,000, Kumamoto. Geological Survey of Japan, AIST.

Inoue, N., Kitada, N., Shibuya, N., Omata, M., Takahama, T., Tonagi, M., and Irikura, K. (2020) Probabilistic Evaluation of Off-Fault Displacements of the 2016 Kumamoto Earthquake. Pure and Applied Geophysics, 177, 2007–2019. doi: 10.1007/s00024-019-02345-7.

Ishimura, D., and Kakiuchi, Y. (2011) Chronology and processes of fluvial terrace formation in northeastern Kinki district, southwest Japan, based on cryptotephra analysis. Quaternary International, 246, 190–202. doi: 10.1016/j.quaint.2011.08.039.

Ishimura, D. (2019) Coseismic vertical displacement associated with the 2016 Kumamoto earthquake (Mw7.0) and activity of the Futagawa fault around Futa, Nishihara Village, Kumamoto prefecture. Active Fault Resarch, 50, 33–32. (in Japanese with English abstract)

Ishimura, D., Toda, S., Ichihara, T., Takahashi, N., Konno, A., and Sato, H. (2017) A study on surface ruptures around Miyaji, Aso City, Kumamoto Prefecture, associated with the 2016 Kumamoto earthquake sequence and upward slip tapering on pit excavation walls. Active Fault Research, 47, 9–16. (in Japanese with English abstract)

Ishimura, D., Toda, S., Mukoyama, S., Homma, S., Yamaguchi, K., and Takahashi, N. (2019) 3D surface displacement and surface ruptures associated with the 2014 Mw 6.2 Nagano earthquake using differential lidar. Bulletin of the Seismological Society of America, 109, 780–796. doi: 10.1785/0120180020.

Ishimura, D., Tsutsumi, H., Toda, S., Fukushima, Y., Kumahara, Y., Takahashi, N., Ichihara, T., and Takada, K. (2021) Repeated triggered ruptures on a distributed secondary fault system: an example from the 2016 Kumamoto earthquake, Southwest Japan. Earth, Planets and Space, 73 doi: 10.1186/s40623-021-01371-x.

Ishimura, D., Iwasa, Y., Takahashi, N., Tadokoro, R. and Oda, R. (2022) Paleoseismic events and shallow subsurface structure of the central part of the Futagawa fault, which generated the 2016 Mw 7.0 Kumamoto earthquake. Geomorphology, 414, 108387. doi: 10.1016/j.geomorph.2022.108387.

Iwasa, Y., Kumahara, Y., Goto, H., Ishimura, D., and Hosoya, T. (2022) Faulting history of the Futagawa fault zone based on trenching survey at Komori, Nishihara Village, Kumamoto Prefecture. Active Fault Research, 56, 47–58. (in Japanese with English abstract)

Kamata, H., and Kodama, K. (1994) Tectonics of an arc-arc junction: an example from Kyushu Island at the junction of the Southwest Japan Arc and the Ryukyu Arc. Tectonophysics, 233, 69–81. doi: 10.1016/0040-1951(94)90220-8.

Kaneda, H., and Chiba, T. (2019) Stereopaired morphometric protection index red relief image maps (Stereo MPI-RRIMs): Effective visualization of high-resolution digital elevation models for interpreting and mapping small tectonic geomorphic features. Bulletin of the Seismological Society of America, 109, 99–109. doi: 10.1785/0120180166.

Kaneda, H., Toda, S., Ishimura, D., Kumahara, Y., Goto, H., Okada, S., and Kobayashi, M. (2022) Surface Ruptures and Tectonic Geomorphology Along and Around the Idenokuchi Fault. In: Kumahara, Y., Kaneda, H., Tsutsumi, H. (eds) Surface Ruptures Associated with the 2016 Kumamoto Earthquake Sequence in Southwest Japan. Advances in Geological Science. Springer, Singapore. doi: 10.1007/978-981-19-1150-7_12.

King, G., Klinger, Y., Bowman, D., and Tapponnier, P. (2005) Slip-Partitioned Surface Breaks for the Mw 7.8 2001 Kokoxili Earthquake, China. Bulletin of the Seismological Society of America, 95 (2), 731–738. doi: 10.1785/0120040101.

Kokusai Kogyo C o.,Ltd. (2010) 3D-Geomorphic Image Velocimetry. JP Patent No. 4545219.

Kumahara, Y., Okada, S., Kagohara, K., Kaneda, H., Goto, H., and Tsutsumi, H. (2017a) 1:25,000 Active Fault Map, Futagawa-Hinagu Fault Zone and its Vicinity “Kumamoto (Revision)”. Geospatial Information Authority of Japan, Ibaraki. (in Japanese)

Kumahara, Y., Torii, M., Nakata, T., Goto, H., Iwasa, Y., Suzuki, Y., Watanabe, M., Toda, S., Takahashi, N., and Okuno, M. (2017b) Fault History of the Northern Part of Futagawa-Hinagu Fault Zone Based on Trench Survey at Dozon, Mashiki Town and at Kawayo, Minami-Aso Village, Programme and Abstracts JSAF 2017 Fall Meeting, 24–25. (in Japanese)

Kumahara, Y., Kaneda, H., and Tsutsumi, H. (2022) Surface Ruptures Associated with the 2016 Kumamoto Earthquake Sequence in Southwest Japan. Advances in Geological Science. Springer, Singapore. doi: 10.1007/978-981-19-1150-7.

Kumamoto Prefectural Board of Education (2010) Earthquake traces in Onobaru-A site. Onobaru ruins group. In: Cultural Property Investigation Report of Kumamoto Prefecture, 257 (2), 147–149. (in Japanese)

Kumamoto Prefecture Geological Map Compilation Committee (2008) Geological Map of the Kumamoto Prefecture (1:100,000). Kumamoto Prefecture Geotechnical Consultants Association, Kumamoto.

Machida, H., and Arai, F. (2003) Atlas of Tephra in and around Japan [revised edition]. University of Tokyo Press, Tokyo.

Matsumoto, Y. (1979) Some problems on volcanic activities and depression structures in Kyushu, Japan. Memoirs of the Geological Society of Japan, 16, 127–139. (in Japanese with English abstract)

Miyabuchi, Y. (2009) A 90,000-year tephrostratigraphic framework of Aso Volcano, Japan. Sedimentary Geology, 220, 169–189. doi: 10.1016/j.sedgeo.2009.04.018.

Miyoshi, M., Shinmura, T., Sumino, H., Sano, T., Miyabuchi, Y., Mori, Y., Inakura, H., Furukawa, K., Uno, K., Hasenaka, T., Nagao, K., Arakawa, Y., and Yamamoto, J. (2013) Lateral magma intrusion from a caldera-forming magma chamber: Constraints from geochronology and geochemistry of volcanic products from lateral cones around the Aso caldera, SW Japan. Chemical Geology, 352, 202–210. doi: 10.1016/j.chemgeo.2013.06.003.

Moya, L., Yamazaki, F., Liu, W., and Chiba, T. (2017) Calculation of coseismic displacement from lidar data in the 2016 Kumamoto, Japan, earthquake. Natural Hazards and Earth System Sciences, 17, 143–156. doi: 10.5194/nhess-17-143-2017.

Mukoyama, S. (2011) Estimation of ground deformation caused by the earthquake (M 7.2) in Japan, 2008, from the geomorphic image analysis of high resolution LiDAR DEMs. Journal of Mountain Science, 8, 239–245. doi: 10.1007/s11629-011-2106-7.

Muroi, S., Suzuki, Y., Mukoyama, S., Iwasa, Y., Yamashita, H., Muraki, M., Yamashita, K., Fukuba, T. (2024) Surface displacement vector discontinuity in the easternmost part of the Futagawa-Hinagu fault zone analyzed by using airborne laser scanning data at two different timings. Active Fault Research, 60, 11–25. (in Japanese with English abstract)

Nakata, T., and Imaizumi, T. (2002) Digital Active Fault Map of Japan. University of Tokyo Press, Tokyo. (in Japanese)

Nurminen, F., Baize, S., Boncio, P., Blumetti, A.M., Cinti, F.R., Civico, R., and Guerrieri, L. (2022) SURE 2.0 – New release of the worldwide database of surface ruptures for fault displacement hazard analyses. Scientific Data 9, 729. doi: 10.1038/s41597-022-01835-z.

Nurminen, F., Boncio, P., Visini, F., Pace, B., Valentini, A., Baize, S., and Scotti, O. (2020) Probability of Occurrence and Displacement Regression of Distributed Surface Rupturing for Reverse Earthquakes. Frontiers in Earth Science, 8, 581605. doi: 10.3389/feart.2020.581605.

Okamura, Y., Abe, S., Miyashita, Y., Azuma, T., Togo, T., Shirahama, Y., Awata, Y., Maruyama, T., Ogami, T., Imura, R., Tsutsumi, H., Goto, H., and Kumahara, Y. (2018) 3.1 Survey of detailed position and shape of active faults to understand the fault segments and observation to reveal the paleoseismic history and slip rates. In: Research Report of a Comprehensive Active Fault Survey After the 2016 Kumamoto Earthquake, 2017 Fiscal Year. Ministry of Education, Culture, Sports, Science and Technology and Kyushu University. (in Japanese)

Oohashi, K., Otsubo, M., Matsumoto, S., Kobayashi, K., Sato, K., and Nishimura, T. (2020) The Quaternary tectonics of Central Kyushu and the 2016 Kumamoto Earthquake: from a multifaceted viewpoint combining geology, seismology, and geodesy. Journal of the Geological Society of Japan, 129, 565–589. (in Japanese with English abstract)

Reimer, P.J., Austin, W.E.N., Bard, E., Bayliss, A., Blackwell, P.G., Bronk Ramsey, C., Butzin, M., Cheng, H., Edwards, R.L., Friedrich, M., Grootes, P.M., Guilderson, T.P., Hajdas, I., Heaton, T.J., Hogg, A.G., Hughen, K.A., Kromer, B., Manning, S.W., Muscheler, R., Palmer, J.G., Pearson, C., Van Der Plicht, J., Reimer, R.W., Richards, D.A., Scott, E.M., Southon, J.R., Turney, C.S.M., Wacker, L., Adolphi, F., Büntgen, U., Capano, M., Fahrni, S.M., Fogtmann-Schulz, A., Friedrich, R., K¨ohler, P., Kudsk, S., Miyake, F., Olsen, J., Reinig, F., Sakamoto, M., Sookdeo, A., and Talamo, S. (2020) The IntCal20 Northern Hemisphere radiocarbon age calibration curve (0–55 cal kBP). Radiocarbon, 62, 725–757. doi: 10.1017/RDC.2020.41.

Research Group for Active Faults of Japan, 1980. Active Faults in Japan, Sheet Maps and Inventories. University of Tokyo Press, Tokyo. (in Japanese)

Research Group for Active Faults of Japan, 1991. Active Faults in Japan, Sheet Maps and Inventories, Rev. Ed. University of Tokyo Press, Tokyo. (in Japanese)

Sato, P.H., Komura, K., Une, H., Nakano, T., and Yagi, K. (2021) Study on Cumulative Activities of Passively Ruptured Faults through a Trenching Survey at the Matoishi Bokujo I Fault, Northwest Side of the Aso Caldera, Southwestern Japan. Geographical Review of Japan Series A, 94, 250–264. doi: 10.4157/grj.94.250. (in Japanese with English abstract)

Scott, C.P., Arrowsmith, J.R., Nissen, E., Lajoie, L., Maruyama, T., and Chiba, T. (2018) The M7 2016 Kumamoto, Japan, earthquake: 3-D Deformation along the Fault and within the damage Zone Constrained from Differential Lidar Topography. Journal of Geophysical Research: Solid Earth, 123, 6138–6155. doi: 10.1029/2018JB015581.

Seno, T., Stein, S. and Gripp, A.E.（1993）A model for the motion of the Philippine Sea Plate consistent with NUVEL-1 and geological data. Journal of Geophysical Research: Solid Earth, 98, 17941–17948. doi: 10.1029/93JB00782.

Shirahama, Y., Yoshimi, M., Awata, Y., Maruyama, T., Azuma, T., Miyashita, Y., Mori, H., Imanishi, K., Takeda, N., Ochi, T., Otsubo, M., Asahina, D., and Miyakawa, A. (2016) Characteristics of the surface ruptures associated with the 2016 Kumamoto earthquake sequence, Central Kyushu, Japan. Earth, Planets and Space, 68, 191. doi: 10.1186/s40623-016-0559-1.

Shirahama, Y., Miyashita, Y., Kametaka, M., Suzuki, Y., Miyairi, Y., and Yokoyama, Y. (2021) Detailed paleoseismic history of the Hinagu fault zone revealed by the high-density radiocarbon dating and trenching survey across a surface rupture of the 2016 Kumamoto earthquake, Kyushu, Japan. Island Arc, 30, e12376. doi: 10.1111./iar.12376.

Smith, V.C., Staff, R.A., Blockley, S.P.E., Bronk Ramsey, C., Nakagawa, T., Mark, D.F., Takemura, K., and Danhara, T. (2013) Identification and correlation of visible tephras in the Lake Suigetsu SG06 sedimentary archive, Japan: chronostratigraphic markers for synchronising of east Asian/west Pacific palaeoclimatic records across the last 150 ka. Quaternary Science Reviews, 67, 121–137. doi: 10.1016/j.quascirev.2013.01.026.

Suzuki, T., Kasahara, A., Nishizawa, F., and Saito, H. (2014) Chemical characterization of volcanic glass shards by energy dispersive X-ray spectrometry with EDAX Genesis APEX2 and JEOL JSM-6390. Geographical reports of Tokyo Metropolitan University, 49, 1–12.

Suzuki, Y., Ishimura, D., Kumaki, Y., Kumahara, Y., Chida, N., Nakata, T., and Nakano, T. (2017) 1:25,000 Active Fault Map, Futagawa-Hinagu Fault Zone and its Vicinity "Aso". Geospatial Information Authority of Japan, Ibaraki. (in Japanese)

Takahashi, N., Ishimura, D., Toda, S., Nakata, T., and Watanabe, M. (2017) Vertical slip rate on a normal fault co-ruptured with the Futagawa fault at the 2016 Kumamoto earthquake. Active Fault Research, 46, 27–32. (in Japanese with English abstract).

Toda, S., Kaneda, H., Okada, S., Ishimura, D., and Mildon, Z.K. (2016) Slip-partitioned surface ruptures for the Mw 7.0 16 April 2016 Kumamoto, Japan, earthquake. Earth, Planets and Space, 68, 188. doi: 10.1186/s40623-016-0560-8.

Toda, S., Torii, M., Okuno, M., Konno, A., Ono, H., and Takahashi, N. (2019) Evidence for Holocene paleoseismic events on the 2016 Kumamoto earthquake rupture zone within the Aso caldera: a trench excavation survey at Kurokawa, the town of Minami-Aso, Southwest Japan. Active Fault Research, 51, 13–25. (in Japanese with English abstract)

Tsutsumi, H., Toda, S., Goto, H., Kumahara, Y., Ishimura, D., Takahashi, N., Taniguchi, K., Omata, M., Kohriya, Y., Gomi, M., Asano, K., and Iwata, T. (2018) Paleoseismic trenching across the surface rupture of the 2016 Kumamoto earthquake at Jichu, Mashiki Town, Kumamoto Prefecture. Active Fault Research, 49, 31–39. (in Japanese with English abstract)

Ueta, K., Miyawaki, R., Iemura, K., Yokoyama, T., and Miyawaki, A. (2018) Paleoseismological study on surface fault ruptures produced by the 2016 Kumamoto

earthquake. In: Abstracts of Japan Geoscience Union Meeting 2018, Makuhari Messe, Chiba. (in Japanese with English abstract).

Watanabe, K. and Ono, K. (1969) Geology of the vicinity of Omine on the western flank of the Aso caldera. Journal of the Geological Society of Japan, 75, 365–374. (in Japanese with English abstract)

Xu, X., Sandwell, D.T., and Smith-Konter, B. (2020) Coseismic Displacements and Surface Fractures from Sentinel-1 InSAR: 2019 Ridgecrest Earthquakes. Seismological Research Letters, 91, 1979–1985. doi: 10.1785/0220190275.

Yamada, K., Takemura, K., Kuwae, M., Yamamoto, M., and Danhara, T. (2017) Revised ages of late Holocene tephras in Beppu Bay, central Kyushu, southwest Japan. Quaternary International, 452, 33–42. doi: 10.1016/j.quain t.2017.01.024.